

Time-resolved size and element analysis of gas-borne nanoparticles

THÈSE N° 6988 (2016)

PRÉSENTÉE LE 11 AVRIL 2016

À LA FACULTÉ DE L'ENVIRONNEMENT NATUREL, ARCHITECTURAL ET CONSTRUIT

GROUPE LUDWIG

PROGRAMME DOCTORAL EN SCIENCE ET GÉNIE DES MATÉRIAUX

ÉCOLE POLYTECHNIQUE FÉDÉRALE DE LAUSANNE

POUR L'OBTENTION DU GRADE DE DOCTEUR ÈS SCIENCES

PAR

Adrian HESS

acceptée sur proposition du jury:

Prof. A. Fontcuberta i Morral, présidente du jury

Prof. C. Ludwig, directeur de thèse

Dr M. Kasper, rapporteur

Prof. D. Martuzevičius, rapporteur

Prof. S. Takahama, rapporteur



ÉCOLE POLYTECHNIQUE
FÉDÉRALE DE LAUSANNE

Suisse
2016

« On rencontre sa destinée souvent par les chemins
qu'on prend pour l'éviter. »

Jean de la Fontaine

Acknowledgements

If you once at night sit on a shabby old bicycle, riding along a closed railway line in the forest, pondering over your actual situation and plans for the future, it could be that five years later you are hurrying to finally get your work published, in order to finish your PhD thesis. You probably would not expect this, as I did, but it might happen.

It was Andrea Ulrich, who offered an interesting PhD project to me. She said: “This is a tinker project, Adrian. This is the right thing for you.” You were right, Andrea, it was like tailored for me. Thank you, and rest in peace.

The project started in the Analytical Chemistry Lab at Empa. I met a colorful, friendly, and cooperative crew there. Adi, Heinz, Noémie, Renato, Andi, Lukas, Markus, Regula, Oliver, Norbert, Jing, Julian, Claudia, Aron, Peter, Pascal, Beni, and Conny are just a part of all the people who made this time interesting. I never had to wait but could count on their immediate technical or organizational assistance or scientific advice, and it was always a pleasure to have discussions on professional and private topics on the floor, in the lab, or in the coffee room. Thank you.

My office mate over these years at Empa was Sabrina. Before I met her, I was not conscious of the tragedy of not finding a pink yoga mat. On the other hand, she managed to transport a huge exhaust silencer for my motorbike in her hand baggage, when she came back to Switzerland by plane, which was then lying about two years in our office. It is installed now. Thank you, Sabrina, for going this way together. It was never boring with you.

After Andrea’s accident, Christian Ludwig and Mohamed Tarik at PSI took over, although they had initially been intended just as co-supervisor and project collaborator. Thank you both for your invaluable support! When my contract at Empa expired, I could move to the Bioenergy and Catalysis Laboratory at PSI, where I was quickly integrated in another great team. I had interesting discussions about trivial and more complex issues, related to the private and scientific life, with Rolf, Marica, Frank, Gisela, Ajay, Florentina, and Ruud. To resolve technical problems with our TGA, Debora and Albert were doing repair works and performing measurements for me, even during my holidays. Thank you for your highly appreciated help.

I am also grateful for a lot of assistance from people outside my units at both institutions. Some of these were Silvio Harndt, Franz Stebler, Daniel Ebersold, Harald Hagendorfer, Dani Schreiber, Gabriele Ilari, and José Quinsaat at Empa, and Jörg Schneebeli, Dominik Gschwend, Martin Gysel, and Philip Edinger at PSI. Besides, I could rely on the advice of Heinz Burtscher and Martin Fierz at the University of Applied Science in Windisch. When I had technical problems with my equipment, I received support from Wolfgang Völker at TSI Germany and from my former

colleagues at Matter Aerosol, especially Andy Knecht, Pascal Winistörfer, Pascal Brand, and David Imhof.

However, the progress of my work was not only depending on professional support. During this period, my wife Martina gave birth to our two marvelous sons, Malvin and Tamaro. Although employed herself, she cared the children when I was away, and she kept them occupied in order that I could work at home, even on numerous weekends. Besides, we were assisted by our parents and siblings, who cared our sons so many days, especially in emergency situations when they became ill and could not go to the daycare facility. Thank you all for your efforts!

Zusammenfassung

Die physikalische und chemische Charakterisierung von gasgetragenen Partikeln im Nanometer- bis Sub-Mikrometer-Grössenbereich ist von grosser Bedeutung, z.B. in medizinischen Studien mit Bezug zu Nanopartikeln, in Untersuchungen zu Verteilungsvorgängen von Pulvern und Stäuben, zur Freisetzung von künstlich erzeugten Nanopartikeln („Engineered Nanoparticles“, ENP) aus nanopartikelverstärkten Werkstoffen als Abrieb oder bei deren Verbrennung, oder in Studien zur Partikelexposition, bezogen auf Sprayprodukte. Solche Beurteilungen sind auch wichtig für die Entwicklung technischer Prozesse, z.B. um chemische Elemente oder deren Isotope in gewissen Partikelgrössenfraktionen zu bestimmen, im Umgang mit radioaktiven Abfällen oder in der Analyse von Prozessgasen und Emissionen aus der thermischen Abfallbehandlung, aus Gasturbinen oder Verbrennungsmotoren. Um solche Aerosole beurteilen zu können, müssen Eigenschaften wie die Partikelgrössenverteilung und die chemische Zusammensetzung bekannt sein, wenn möglich mit hoher zeitlicher Auflösung. Die meisten verfügbaren Techniken können jedoch solche physikalische und chemische Information nicht gleichzeitig und online bieten. Der „Scanning Mobility Particle Sizer“ (SMPS) ist weit verbreitet und dient dazu, die Grössenverteilung und Konzentration solcher Partikel innert weniger Minuten zu bestimmen. Mit der induktiv gekoppelten Plasma-Massenspektrometrie (ICPMS) wird normalerweise die Elementarzusammensetzung flüssiger Proben mit hervorragenden Nachweisgrenzen und einem grossen dynamischen Messbereich bestimmt. In dieser Arbeit werden ein SMPS und ein ICPMS zu einem System gekoppelt. Ein Rotationsverdünner („Rotating Disk Diluter“, RDD) erlaubt es, der nachgeschalteten Messtechnik einen definierten Aerosolfluss zuzuführen, der zudem aufgrund der Verdünnung mehrheitlich auf Argon basiert. Ein RDD wird als Schnittstelle zwischen Proben-Aerosol und Messtechnik verwendet, und das SMPS-Flusskonzept wird überarbeitet, um den unterschiedlichen Analysemethoden gerecht zu werden. Die Kopplung erlaubt es, die Partikelgrössenverteilung und die Elementarzusammensetzung gleichzeitig zu messen, mit zeitlichen Auflösungen von wenigen Minuten. Sie bietet grosse Flexibilität bezüglich der zu messenden Aerosole mit Partikeln im Nanometer- bis Sub-Mikrometerbereich. Die korrekte Funktion des SMPS mit Argon anstelle von Luft wird überprüft. Die Messtechnik wird getestet an einem Modellaerosol aus luftgetragenen Silberpartikeln. Dann wird deren Potential demonstriert, an Metallaerosolen mit Partikeln gleicher Zusammensetzung und einem Misch-aerosol, das kleinere Gold- und grössere Silberpartikel enthält. Empfindlichkeit und Nachweisgrenze, bezogen auf die Partikelanzahl- und -massenkonzentration, werden für einige Elemente und Partikeldurchmesser bestimmt. Anschliessend wird die Messtechnik in zwei Forschungsanwendungen eingesetzt, zunächst für die Untersuchung von Aerosolpartikeln, freigesetzt durch kommerziell erhältliche Sprayprodukte, danach werden partikelförmige Metallemissionen aus der thermischen Behandlung von unterschiedlich imprägnierten Holzproben untersucht, mit dem Hauptaugenmerk auf Alkalimetallen.

Stichwörter

SMPS, ICPMS, Rotationsverdünner, Thermogravimetrie, Nanopartikel, Aerosol, Prozessgas, Elementanalyse, Wärmebehandlung, Verbrennung.

Abstract

Physical and chemical characterization of gas-borne particles in the nanometer to sub-micrometer size range is important in many applications, such as nanoparticle related health studies, the monitoring of powder or dust distribution processes, assessing the release of engineered nanoparticles (ENP) from ENP reinforced materials due to abrasion or combustion, or exposure studies related to ENP containing spray products. Such investigations are also highly valuable in the development of technical processes, e.g. to determine distinct size fractions containing specific elements or isotopes in terms of dealing with nuclear waste, or to evaluate particulate matter in process gases and emissions from thermal waste treatment, gas turbines, or other combustion engines. Such particle speciation includes knowledge about particle size distribution and chemical composition, and if possible obtained with a high time resolution. However, most of the available techniques are offline methods and/or not able to provide such physical and chemical information simultaneously. The Scanning Mobility Particle Sizer (SMPS) is a well-established and widely used equipment for determining size distribution and number concentration of such particles, within scan durations of a few minutes. Inductively Coupled Plasma Mass Spectrometry (ICPMS) is a highly sensitive multi-element technique, which allows determining the elemental composition of normally liquid samples, with excellent detection limits and a wide dynamic concentration range. In this work, SMPS and ICPMS are coupled to one hyphenated system. A Rotating Disk Diluter (RDD) allows directing a well-defined flow of a diluted aerosol into subsequent measuring equipment, which besides is mainly argon based, due to the dilution effect. Therefore an RDD is implemented as sample introduction interface, and the SMPS flow concept is re-designed to fulfil the requirements of both different analytical methods. This coupling strategy allows achieving simultaneous information on particle size and elemental composition, with SMPS-typical time resolutions of a few minutes, and offers high flexibility in terms of dealing with different aerosols, loaded with particles in the nanometer to sub-micrometer size range. Proper SMPS operation under argon atmosphere instead of air is validated. The developed setup is tested with a model aerosol containing air-borne silver nanoparticles. The capabilities are then demonstrated on uniformly composited metal aerosols, as well as an aerosol mixture containing smaller gold and larger silver nanoparticles. Sensitivity and limit of detection, related to particle number and mass concentration, are determined for several elements and particle diameters. After the successful characterization, the instrumentation is applied in two research applications. The first is a study on aerosol particles, released by commercial consumer spray products. In the second application, particulate metal emissions from the thermal treatment of differently impregnated wood samples are investigated, with the focus on alkali metals.

Keywords

SMPS, ICPMS, Rotating Disk Diluter, Thermogravimetric Analyzer, Nanoparticle, Aerosol, Process Gas, Element analysis, Thermal treatment, Combustion.

Table of contents

Acknowledgements	i
Zusammenfassung	iii
Stichwörter	iv
Abstract	v
Keywords	vi
Table of contents	vii
List of abbreviations and symbols	xi
1 Introduction	1
1.1 Background, motivation	1
1.2 Current practice	2
1.2.1 Common aerosol characterization techniques	2
1.2.2 Example of an established particle characterization procedure	3
1.2.3 Functional principle of SMPS	5
1.2.4 Functional Principle of ICPMS	7
1.3 Hyphenation of SMPS-ICPMS	8
1.3.1 Principle and limitations	8
1.3.2 Former coupling attempts of mobility analysis and atomic spectroscopy	8
1.3.3 Comparison of former coupling attempts	12
1.3.4 Aim of the actual work	15
2 Setting up the instrumentation	17
2.1 Preliminary tests and calculations	17
2.1.1 Recommissioning of an old SMPS	17
2.1.2 Particle size range covered by argon operated DMA	18
2.1.3 Argon operation validation measurements	20
2.2 SMPS modifications and first coupling	21
2.2.1 Instrument arrangement and flow concept	21
2.2.2 First RDD-SMPS-ICPMS coupling	21
2.3. Aerosol neutralizer	25
2.4 Data analysis	26
2.4.1 Data processing with MS Excel	26
2.4.2 Data processing with Matlab	28
3 Final setup	29
3.1 Instrumentation	29
3.1.1 Rotating Disk Diluter	29
3.1.2 Scanning Mobility Particle Sizer	30

3.1.3 Inductively Coupled Plasma Mass Spectrometer	31
3.1.4 SMPS-ICPMS hyphenation	31
3.1.5 Measuring arrangement	33
3.1.6 Data processing	34
3.1.7 Generation of example aerosol	36
3.2 Results from measuring the example silver aerosol	36
4 Instrument characterization	41
4.1 Model aerosol generation	41
4.1.1 Magnetite aerosol	41
4.1.2 20 nm gold aerosol – high concentration	42
4.1.3 20 nm gold aerosol – low concentration	43
4.1.4 Mixed gold/silver aerosol	43
4.2 Calculations	43
4.2.1 Signal calculations	43
4.2.2 Instrument performance calculations	44
4.3 Results and discussion of characterization measurements	46
4.3.1 Magnetite Aerosol	46
4.3.2 20 nm gold aerosol – high concentration	50
4.3.3 20 nm gold aerosol – low concentration	52
4.3.4 Mixed gold/silver aerosol	54
4.3.5 Instrument performance	56
5 Consumer spray aerosol particle assessment	59
6 Heat treatment of impregnated wood pellets	61
6.1 Experimental details	62
6.1.1 Instrumental arrangement	62
6.1.2 Gas flows	62
6.1.3 Instrument settings	64
6.1.4 Sample Preparation	65
6.1.5 Weight information obtained by TGA	67
6.2 Results of the heat treatment experiments	67
6.2.1 TGA data	67
6.2.2 SMPS-ICPMS results	69
6.3 Analysis of residues from the TGA experiments	79
7 Conclusions and outlook	83
7.1 Setting up the instrumentation	83
7.2 Instrumental setup	84
7.3 Instrument characterization	84
7.4 Heat treatment of impregnated wood pellets	85
7.5 General Conclusions	85
7.6 Outlook	86

7.6.1 Particle charge corrections	86
7.6.2 Gas recirculation	86
7.6.3 Distinguish between particulate and gaseous matter	87
7.6.4 Considering particle shape	88
7.6.5 Applications	88
Appendix	91
A.1 Observation of suspension aging	91
A.2 Thermodynamic equilibrium calculations	93
A.3 Characterization of ENP containing sprays	95
A.3.1 Introduction	95
A.3.2 Experimental section	97
A.3.3 Results	101
A.3.4 Discussion	109
A.3.5 Conclusion and outlook	112
A.4 Instrument and sample manufacturers	114
A.5 References	115
A.6 Outreach and publications	123
A.6.1 Peer-reviewed journal publications	123
A.6.2 Conference contributions	123
A.6.3 Media	125
A.7 Curriculum Vitae	126

List of abbreviations and symbols

AMS	Aerosol Mass Spectrometry	m/z	mass-to-charge ratio
APM	Aerosol Particle Mass analyzer	NAA	Neutron Activation Analysis
CPC	Condensation Particle Counter	nES	nano Electrospray
DF	dilution factor	PMP	European Particle Measurement Programme
DMA	Differential Mobility Analyzer	PSD	particle size distribution
EDX	Energy Dispersive X-ray spectroscopy	PSD _N	number weighted PSD
ENP	engineered nanoparticles	PSD _V	Volume weighted PSD
GC-FID	Gas Chromatography Flame Ionization Detector	PSL	polystyrene latex
GED	Gas Exchange Device	RDD	Rotating Disk Diluter
ICPMS	Inductively Coupled Plasma Mass Spectrometry	RF	radio frequency
ICPOES	Inductively Coupled Plasma Optical Emission Spectrometry	SMPS	Scanning Mobility Particle Sizer
LA-ICPMS	Laser Ablation-ICPMS	sp-ICPMS	single particle ICPMS
LoD	limit of detection	STEM	Scanning Transmission Electron Microscopy
macro IMS	macro Ion Mobility Spectrometry	TEM	Transmission Electron Microscopy
MFC	Mass Flow Controller	TRA	time-resolved analysis
		VSET	VERT Secondary Emission Test

1 Introduction

1.1 Background, motivation

A detailed characterization of gas-borne particles in the nanometer to sub-micrometer size range is mandatory in various fields. These include health related particle exposure studies (Limbach, Wick et al., 2007; Meier, Eeftens et al., 2015; Steiner, Czerwinski et al., 2015), environmental aerosol investigations (Mohr, DeCarlo et al., 2015; Setyan, Song et al., 2014), monitoring of powder and dust distribution processes (Schmid, 2010; Sun, Huang, & Wang, 2007; Z. M. Wang, Wagner, & Wall, 2011), the assessment of nanomaterials during end-of-life waste treatment (Buha, Mueller et al., 2014), or investigations on the release of Engineered Nanoparticles (ENP) from spray products (Hagendorfer, Lorenz et al., 2010; Lorenz, Hagendorfer et al., 2011; Losert, von Goetz et al., 2014), or from abrasion processes (Schlagenhauf, Chu et al., 2012). Such particle characterization is also important for developing technical processes, e.g. dealing with nuclear waste containing specific elements or isotopes in distinct particle size fractions (Wochele, Ludwig et al., 2006) or evaluating particulate matter in process gases (Wellinger, Biollaz et al., 2011) and emissions from gas turbines (Brem, Durdina et al., 2015) and other combustion engines (Mayer, Czerwinski et al., 2012). Such aerosol characterization may include physical information on the size-dependent particle concentration, i.e. the size distribution, as well as on the chemical composition of the investigated particles.

The Scanning Mobility Particle Sizer (SMPS) basically consists of a Differential Mobility Analyzer (DMA), to classify gas-borne particles according to their diameter, and a Condensation Particle Counter (CPC), to determine the number concentration of the prior classified particles. SMPS is one of the few established techniques for determining online the size distribution and concentration of air-borne particles, covering the size range from a few to some hundreds of nanometers, with scan durations of a few minutes. Inductively Coupled Plasma Mass Spectrometry (ICPMS) is a powerful technique in elemental chemical analysis with low limits of detection (*LoD*) and a large dynamic measuring range.

The characterization of gas-borne nanoparticles concerning elemental composition is usually performed by particle sampling and subsequent offline analysis. However, these analytical strategies are highly time-consuming and do not provide elemental information with temporal resolutions as they are needed to assess the development of aerosols, emitted by dynamic processes, or to study the transient behavior of gas-borne particles. Additionally, possible contamination during sample preparation cannot be completely prevented, and alteration in the morphology of the sampled particles cannot be excluded.

The coupling of SMPS and ICPMS allows achieving size and chemical information at the same time. SMPS scan durations of a few minutes for covering the whole accessible particle size range, or even shorter scan times for measuring within a narrower spectrum, enable transient particle observation, and open the possibility to chemically characterize an aerosol in its original condition instead of first particle sampling and subsequent offline chemical analysis.

1.2 Current practice

1.2.1 Common aerosol characterization techniques

Several analytical techniques are available for the characterization of size distribution, mass, and number concentration of gas-borne particles. A comprehensive summary of state-of-the-art aerosol measurement techniques and analysis principles is given, e.g. in review articles (Burtcher, 2005; Petrović, Janković et al., 2011), or in books on aerosol measuring techniques (Hinds, 1999; Kulkarni, Baron, & Willeke, 2011). Fig. 1 gives an overview of existing aerosol measurement techniques and the covered size ranges. Baron (Baron & Willeke, 2001)

Nevertheless, only a few techniques are available for the detection of such particles in the nanometer size range, and SMPS is one of the most common online techniques, covering the particle size range below 500 nm (S. C. Wang & Flagan, 1990). This combination of a DMA and a CPC allows a detailed determination of the particle size distribution (PSD) and number concentration, with a temporal resolution of a few minutes, down to particle diameters of 5 nm or

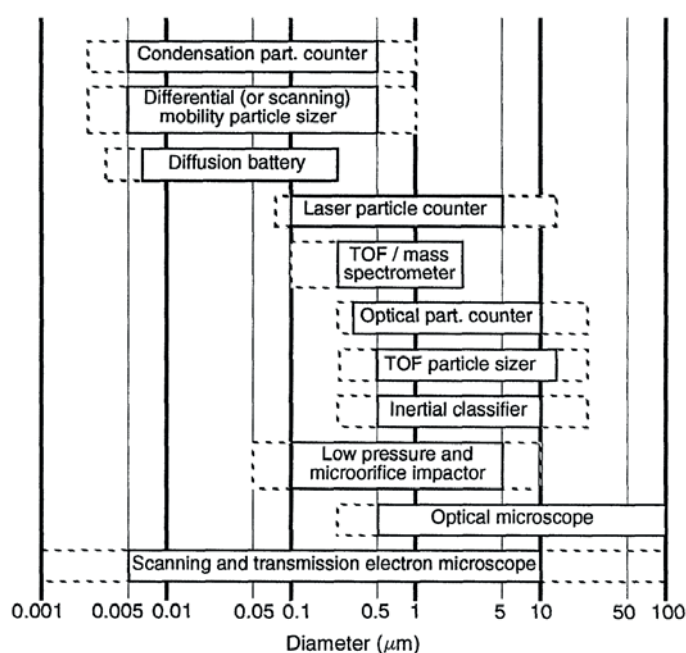


Fig. 1: Particle size range, covered by different aerosol particle measuring principles (from: Baron & Willeke, 2001)

even smaller, depending on the DMA geometry, flow settings, and CPC type. The SMPS technique is well established in most of the fields dealing with gas-borne nanoparticles, e.g. in emission control of vehicles or combustion processes in general (Zhang & Morawska, 2002). It is even implemented in standardized procedures such as homologation tests for diesel particulate filter systems.

Particles can be sampled on grids, e.g. using electrostatic or thermophoretic particle samplers, for subsequent electron microscopy investigation (Gehrig, Hill et al., 2007). Qualitative chemical information of the main components is accessible via the usually coupled x-ray spectrometry, whereas size distribution and morphology information are achievable via image analysis. Another method is particle collection on filters (Gianini, Gehrig et al., 2012; Hueglin, Gehrig et al., 2005; Solomon, Fraser, & Herckes, 2011), or using a single or multi stage impactor, followed by appropriate digestion and atomic spectroscopy investigations. However, these procedures are highly time-consuming and entail the risk of sample contamination and other alterations during particle collection, storage, transport, and preparation for analysis.

A method to characterize gas-borne particles even below 100 nm online and size resolved is Aerosol Mass Spectrometry (AMS). Particles are decomposed on a hot (600 °C) tungsten surface, the resulting gas molecules are ionized by electron impact, classified for their mass-to-charge ratio (m/z), and finally counted. The technique allows detecting organic compounds, their fragments, and some inorganic salts (Heringa, DeCarlo et al., 2012; Pratt & Prather, 2012). However, AMS does not provide information on the elemental composition of particles. Alternatively, ICPMS allows determining the elemental composition of aerosols directly introduced to the plasma (Suzuki, Sato et al., 2012), but such online aerosol characterization techniques commonly do not provide size information on the investigated particles. These problems can be overcome by coupling SMPS to ICPMS, offering online simultaneous achievement of size and chemical information.

1.2.2 Example of an established particle characterization procedure

The VERT Secondary Emission Test (VSET) procedure (Heeb, Ulrich et al., 2005), is an example for an established aerosol particle characterization method. This part of the Swiss sustainability test for diesel particulate filter systems is regulated in the Swiss national standard SN 277 206 (SN277206, 2011). The VSET test includes detailed monitoring of particulate matter, as well as chemical analysis of the fuel fired during the filter tests, and determination of the major gaseous pollutants and toxic trace components in the engine exhaust. Fig. 2 gives an overview of the VSET procedure and the current practice for size fractionated sampling and elemental analysis of particles.

The particle characterization includes separate physical and chemical analyses. Aerosol dilution and conditioning is needed for physical particle measurements, i.e. the determination of size distribution and number concentration. These are obtained by SMPS and a separate sensor providing real time particle surface concentration information. The additional chemical

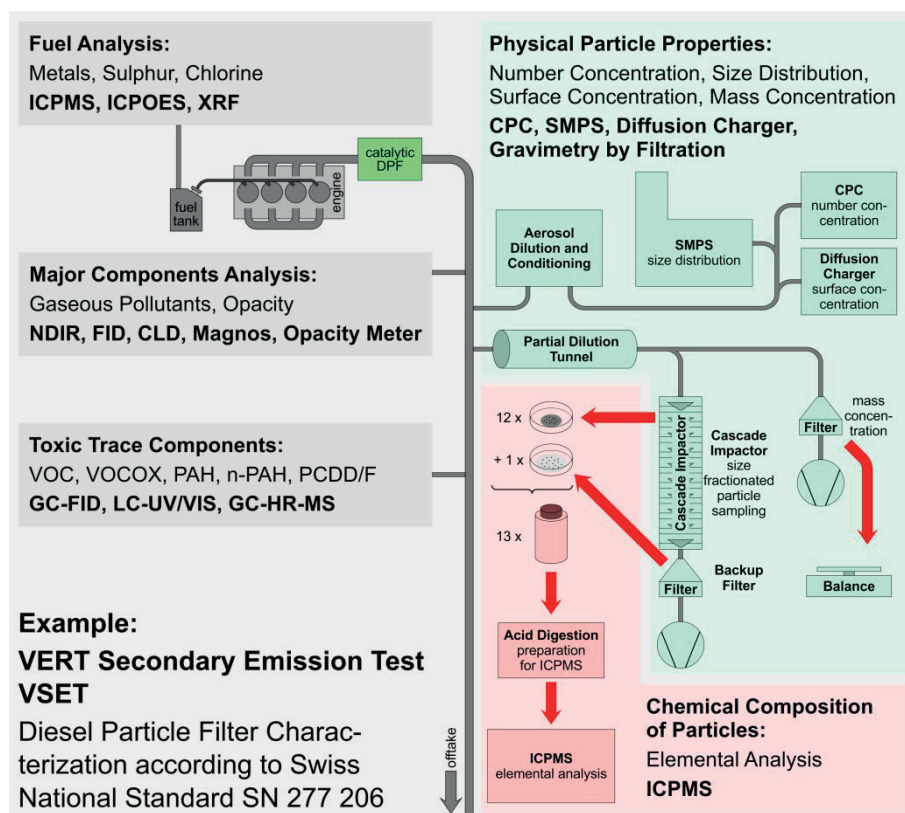


Fig. 2: Current practice example for the characterization of aerosol particles. Major gaseous engine exhaust components and size resolved particle concentrations are measured online. Organic compounds and element analysis of particulate matter are determined by offline analysis methods (adapted from: Ulrich & Wichser, 2003).

characterization of particulate matter in different size fractions requires size-classified sampling with subsequent chemical analysis. Behind a separate dilution tunnel, the particles are sampled on a filter, for subsequent weighing to determine the total particulate mass concentration. Size fractionated particle collection is performed in a cascade impactor for later ICPMS analysis, providing information on the elemental composition (Ulrich & Wichser, 2003). An example of such data is presented in Fig. 3.

The chemical analysis requires an acid digestion of every particle size fraction sample. The resulting liquid samples can then be nebulized and introduced as small droplets into an argon atmosphere, before being ionized in an argon plasma and finally analyzed in the mass spectrometer of the ICPMS. This analysis procedure allows determining the overall composition of particles which have been collected during a certain sampling period, i.e. usually during one driving test cycle. It has the following disadvantages:

- Time-consuming procedure due to the separate particle sampling and the different steps of sample preparation for chemical ICPMS analysis.
- Risk of contamination due to transport, storage, and preparation for analysis.

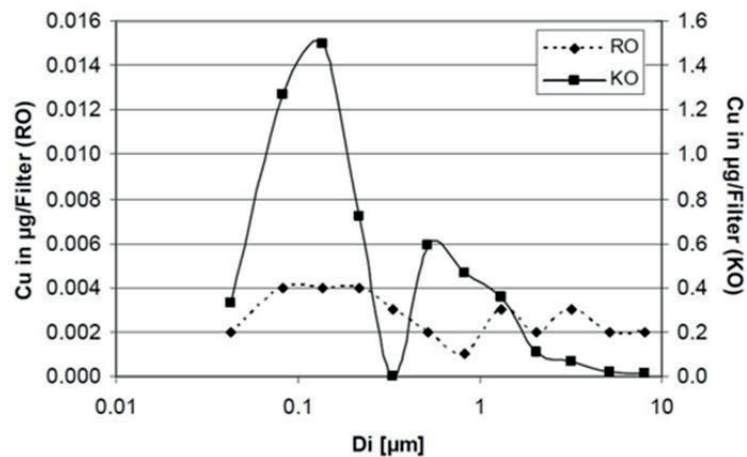


Fig. 3: Example for size resolved element information, obtained by offline ICPMS analysis. Copper (Cu), found in exhaust particles from a diesel engine, operated with reference fuel without (RO), and with a catalytic additive (KO). (from: Heeb, Ulrich et al., 2005)

- No online information about chemical composition.
- Particle size resolution of chemical analysis limited by number and properties of cascade impactor stages.

1.2.3 Functional principle of SMPS

The functional principles of SMPS and its components have been described by Richard Flagan in a helpful tutorial (Flagan, 2008). In the so called aerosol neutralizer, a radioactive source generates an ion cloud, wherein the elemental electric charges on the surface of the particles achieve the known Boltzmann equilibrium state. Subsequently, a distinct particle size fraction is separated in the DMA (Hewitt, 1957; Knutson & Whitby, 1975). Finally, the CPC determines the number concentration of the particles prior classified by the DMA (Agarwal & Sem, 1980; Sinclair & Hoopes, 1975). A PSD is obtained by collecting number concentration data while the DMA is scanning a certain size range, typically within a few minutes. The SMPS instrumentation is sketched in Fig. 4.

The DMA basically consists of a cylinder capacitor. The non-classified, polydisperse sample aerosol enters on one end into the volume between inner and outer electrode. A sheath gas layer is introduced and separates the polydisperse aerosol, located very close to the outer tube wall, from the inner electrode. These two gas flows travel along the capacitor in axial direction. They have to be highly laminar to minimize mixing of the polydisperse aerosol into the sheath gas layer. In standard operation, ambient air is used as sheath gas. In terms of the coupling to ICPMS, the sheath air was replaced by argon, necessitating a modified DMA flow concept.

High voltage applied between the inner and outer electrodes allows attracting positively charged particles from the incident outer gas layer, through the sheath gas, towards the inner electrode. A circular outlet slit is located at the end of the inner electrode of the capacitor. By applying a certain

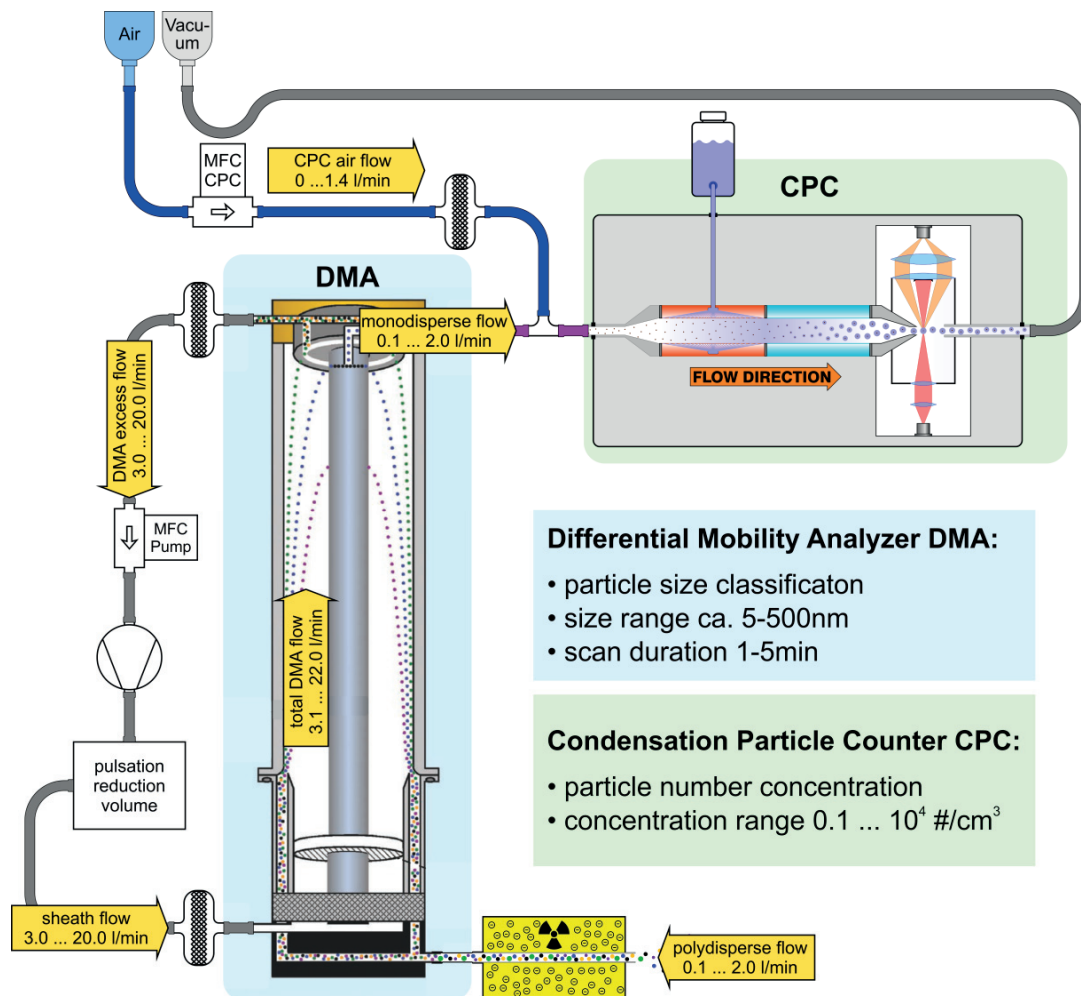


Fig. 4: Schematic of an SMPS. A radioactive source generates an ion cloud wherein the elemental charge distribution on the particles achieves a known equilibrium state. Positively charged particles are fractionated in the DMA, and their number concentration is determined in the CPC. (DMA scheme adapted from: Scanning Mobility Particle Sizer Brochure of TSI, available on www.tsi.com).

voltage, the charged particles experience a force due to the electric field and are selected, featuring a specific mobility diameter, which is the equivalent diameter of a sphere with equal diffusion dominated migration behavior in the surrounding gas as the particle of interest (DeCarlo, Slowik et al., 2004). Scanning a certain particle size range means sequentially scanning a DMA voltage range. The mobility diameter is often used in aerosol science, since it is the relevant measuring quantity considering the mobility and separation characteristics of nanoparticles in the environment or in the respiratory ducts of animals and humans.

DMA and CPC can basically also be operated as stand-alone instruments. A CPC operated as stand-alone device allows determining the particle number concentration every second, but without providing any information about the size of the detected particles.

1.2.4 Functional Principle of ICPMS

ICPMS has been described very well in text books, e.g. by Robert Thomas (Thomas, 2013). The main components of a common ICPMS instrument are illustrated in Fig. 5. Argon borne acid solution droplets, containing the dissolved sample, are introduced as an aerosol into the torch. Radio frequency AC voltage is applied to a coil surrounding the end of the torch, inducing an argon plasma. The sample is decomposed at 5000 to 10000 °C in this plasma into atomic ions. A fraction of these ions is then introduced into the high vacuum chamber via two tapered orifices, called sample and skimmer cones. Ion lenses are focusing and deflecting the ion beam, in order to get rid of uncharged elementary particles, like e.g. photons. Ions featuring a specific mass-to-charge ratio (m/z) are selected in the quadrupole analyzer.

The classified ions strike a photomultiplier and are finally counted by a detector, resulting in an intensity which is proportional to the introduced mass and often given in counts per second (cps). The correlation between the mass and the induced intensity is called sensitivity, and is depending on operating conditions, such as staining and alignment of the cones, gas flows, and detector lifetime. The sensitivity has to be individually determined for different elements and their isotopes. ICPMS signals often suffer from interferences, e.g. caused by molecular or other atomic ions, featuring the same m/z as the element or isotope of interest. Such interferences can be reduced by introducing a collision cell in the high vacuum chamber, wherein molecular ions can be deflected by collisions with gas atoms, e.g. helium, or the m/z ratio of interfering ions can be changed by chemical reactions, e.g. with hydrogen.

The sensitivity of ICPMS even allows determining mass information on single particles (sp-ICPMS) in the nanometer size range, if the analyzed particles are suspended in liquids and can be diluted and introduced to the plasma as a liquid spray (Laborda, Jimenez-Lamana et al., 2011; Lee, Bi et al., 2014; Mitrano, Dasilva, & Nowack, 2015).

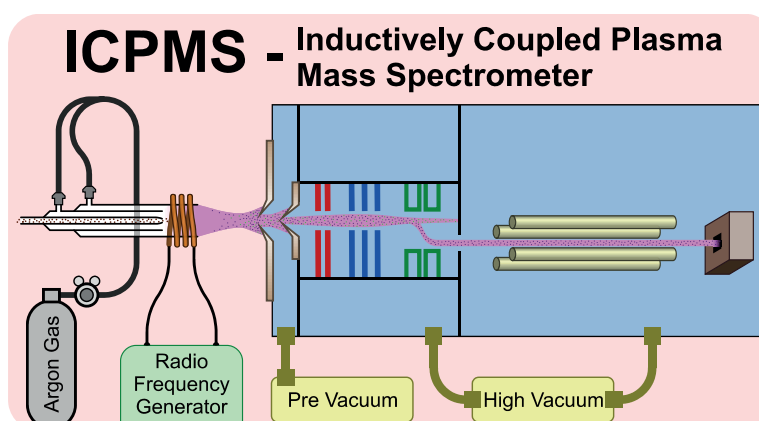


Fig. 5: Schematic of an Inductively Coupled Plasma Mass Spectrometer (ICPMS). Components from left to right: Torch with the radio frequency coil maintaining the plasma (pink). Sampler and skimmer cones as high vacuum interface. Ion lenses focusing and deflecting the ion beam. Quadrupole analyzer followed by the photomultiplier.

1.3 Hyphenation of SMPS-ICPMS

1.3.1 Principle and limitations

By hyphenating SMPS and ICPMS, the benefits of these two techniques can be combined and the established setup provides both information online and simultaneously, i.e. PSD and elemental composition of introduced aerosol particles. The DMA serves to select one particle size fraction from the original aerosol. The number concentration is then measured by the CPC, as in standard SMPS configuration, while the ICPMS, connected in parallel to the CPC, determines the elemental composition. This can be done for the whole particle size range.

Since aerosol particles are already dispersed in gas, they can be directly introduced to the plasma of the ICPMS, without the need of additional sampling, digestion and re-dispersion. This novel setup provides the following benefits:

- Simultaneous information on particle size and elemental composition
- Short scan durations of some minutes, allowing online measurements
- Size distribution and multi element information
- Direct monitoring of transient processes
- Elemental analysis of aerosols in their original conditions, without separate sampling and sample preparation

Due to the low oxygen tolerance of the inductively coupled argon plasma, the size fractionated particles have to be mainly argon borne when entering into the ICPMS. This means that a gas exchange has to be maintained if other process gases than argon are investigated, and the DMA is therefore operated using argon as sheath gas instead of air. Due to the lower dielectric strength of argon compared to air, the DMA voltage cannot utilize the full technically possible range of the instrument, since arcing would occur at very high voltage levels. This limits the particle size range which can be covered, since larger particles are selected by applying higher voltages.

Unlike the CPC, the ICPMS does not actively attract a certain sample flow rate. There is a need to actively control the flow towards the ICPMS plasma. This means that either a pump has to be introduced between DMA and ICPMS, or the sample inlet flow of the DMA has to be externally controlled.

1.3.2 Former coupling attempts of mobility analysis and atomic spectroscopy

A few research groups recognized the need for analysis techniques, providing online information on the chemical composition of nanoparticles, dispersed in air or another gaseous matrix. Several attempts were published, heading size fractionated and elemental analysis of gas-borne nanoparticles.

First coupling approach: DMA-ICPOES

The first reported approach for coupling a DMA to an Inductively Coupled Plasma Optical Emission Spectrometer (ICPOES) was carried out by Weber et al. at the Paul Scherrer Institut in Switzerland (Weber, 1992; Weber, Baltensperger et al., 1991; Weber, Keil et al., 1992). A standard SMPS was modified to adapt the instrument to the ICP: The sheath air flow in the DMA was replaced by argon as sheath gas, the aerosol flow through the DMA was no longer defined by the classified, monodisperse aerosol amount consumed by the CPC, but by a Mass Flow Controller (MFC), maintaining the argon flow through a spark discharge chamber, where primary silver (Ag) particles were generated into this predefined argon flow. The argon borne particles were then introduced to the DMA, to be classified concerning their diameter in a range between about 5.5 and 300 nm. The monodisperse DMA outlet flow was not completely introduced to the CPC but split into fractions going to several instruments.

One flow fraction was introduced to the ICPOES where the emission spectrum of Ag was measured to identify the chemical composition. The ICPOES signal was calibrated by using Neutron Activation Analysis (NAA) of Ag particles, sampled on nuclepore filters. The CPC and an epiphaniometer (Baltensperger, Gaggeler, & Jost, 1988; Gaggeler, Baltensperger et al., 1989) were connected in parallel to the ICPOES. The CPC provided the particle number concentration, the epiphaniometer the total particle surface concentration. Some particulate matter was sampled by electrostatic deposition on carbon foils for subsequent transmission electron microscopy (TEM) analysis, in order to precisely measure offline the size and shape of collected particles.

“Aerosol Spectrometer”: DMA-Electrometer-ICPMS

Okada et al. at the RIKEN Institute of Physical and Chemical Research, Japan, developed a setup which they called “Aerosol Spectrometer”, in 2001. This setup is explained in Fig. 6. It basically

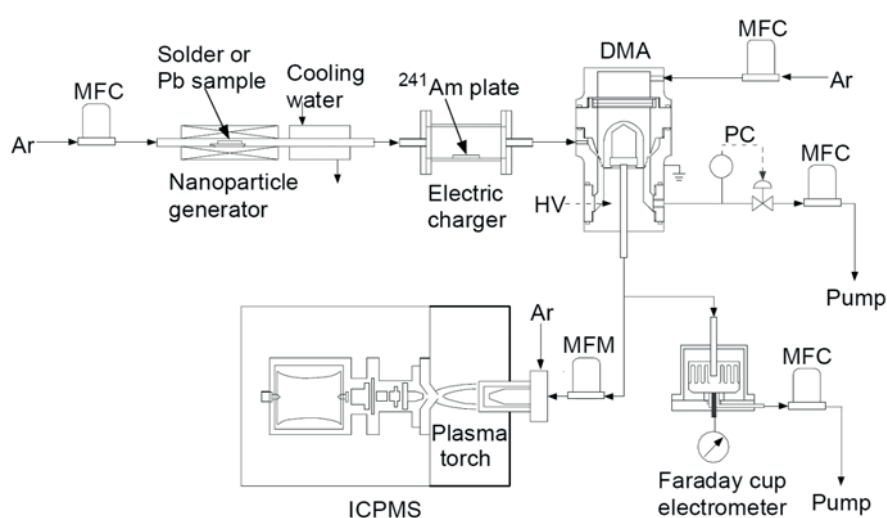


Fig. 6: Particle generator and all components of the “Aerosol Spectrometer”. The particles are directly generated into a defined argon flow and introduced to the DMA. The monodisperse aerosol flow is analyzed by an ICPMS and an electrometer, arranged in parallel (from: Okada, Yabumoto, & Takeuchi, 2002).

consisted of a DMA, connected to an ICPMS and an electrometer, operated in parallel (Okada, Yabumoto, & Takeuchi, 2002). The electrometer allows measuring the net charge on aerosol particles and therewith determining the particle concentration if the charge distribution is known. Using a Wyckoff type DMA, they focused on 2 to 40 nm particles, containing mainly lead (Pb) and tin (Sb), which usually emerge from soldering processes and are highly undesired in the semiconductor manufacturing industry. The nanoparticles of interest were generated directly into a defined argon flow, which was then fed into the DMA. The monodisperse aerosol at the outlet of the DMA was split into two portions, one being attracted by the electrometer, the other fed to the ICPMS. The ICPMS intensity and number concentration detected by the electrometer were compared. However, a detailed calibration concept was not proposed.

DMA as converter from aerosol to “argonsol”

A similar setup was adapted independently by Myojo et al. at the National Institute of Industrial Health, Japan (Myojo, Takaya, & Ono-Ogasawara, 2002; Takaya, 2004). A test aerosol was generated by nebulizing a lead nitrate ($\text{Pb}(\text{NO}_3)_2$) solution into a defined air flow. However, the authors were the first who reported the use of air as particle carrier gas in the primary aerosol. The setup was basing on a self-designed DMA from the Kanazawa University, used as gas exchanger, transporting the entering particles from originally air into an argon atmosphere, while scanning a particle size range between 30 and 150 nm. The DMA inlet flows consisted of the polydisperse particles, carried in 0.6 L min^{-1} air, and the sheath argon flow of 10.0 L min^{-1} .

Due to the use of argon as sheath gas, the classified particles at the monodisperse outlet of the DMA were then mainly carried by argon. They introduced the expression “argonsol” to distinguish between the particles dispersed in argon from those in air (“aerosol”). The mixing of the entering particle carrier and sheath gases was investigated by introducing different gases to the polydisperse sample inlet of the DMA. The used gases were carbon monoxide (CO) and carbon dioxide (CO_2) in nitrogen (N_2) and cyclohexane (C_6H_{12}). The gas concentrations at the monodisperse DMA outlet were then determined applying an infrared gas analyzer and a Gas Chromatography Flame Ionization Detector (GC-FID).

They found a nearly perfect gas mixing, even if the gas flows in the DMA are highly laminar, while the incoming particles were not mixed into the gas volume inside the DMA. This is explained by the much higher diffusion coefficients of the gas molecules, compared to those of the classified particles. The monodisperse “argonsol” flow was again divided into two fractions. One was consumed by a CPC, measuring the particle number concentration, the other was fed to ICPMS for determining the elemental composition.

Laser Ablation ICPMS with an introduced DMA for particle fractionation

Laser-Ablation-ICPMS (LA-ICPMS) is a widely established technique for chemically characterizing the surface layers of bulk material (Koch, Walle et al., 2008; Pisonero, Fernandez, & Gunther, 2009). The laser ablated aerosol was introduced to a DMA, to select specific particle size fractions, before they were analyzed in an ICPMS, by the Houk group at the Iowa State University,

USA (Perdian, Bajic et al., 2008; Saetveit, Bajic et al., 2008). The DMA was operated using argon as particle carrier and sheath gas. Further DMA operation details were not reported. The goal was to identify size dependent properties of ablated material, for different ablation parameters and samples, and to get hints on possible fractionation effects during the ablation process.

Another group at the Lawrence Berkeley National Laboratory, USA, used a DMA for the characterization of laser ablated material, but proposed a split flow whereof one stream was introduced to SMPS and the second directly into the ICPMS (Gonzalez, Liu et al., 2007). However, this setup gives size-information and chemical information, independent of each other, but does not allow the chemical speciation of defined size classes.

Classification of biological macromolecular ions

The SMPS principle has also been applied in the classification of biological macromolecular ions concerning their masses. In this context, the technique is known as Macro Ion Mobility Spectrometry (macro IMS). The instrumental setup is the same as that of SMPS, just another scanning voltage curve is applied, and the data calculations are different to those in SMPS. Macro IMS is usually operated in combination with a Nano-Electrospray (nES), where a suspension of dispersed macromolecules is sprayed into air and then dried, resulting in single air-borne macromolecules. These are then classified in a DMA, and subsequently counted in a CPC. Such a system was coupled to ICPMS at the University of Crete by the group around Pergantis (Carazzone, Rami, & Pergantis, 2008). With this coupling, they were able not only to determine the size and therewith the approximate mass of biological macromolecules in the size range between 3 and 16 nm, but also to qualitatively analyze metallic compounds of these macromolecules.

Another attempt was made in the same group, to characterize aqueous suspended ENP (Kapellios & Pergantis, 2012). These particles were first brought to aerosol arrangement, using nES. The aerosol particles were then classified in a DMA, and single size fractions of these particles were re-suspended in water by electrostatic precipitation, before being analyzed by sp-ICPMS.

Air operated DMA, followed by a Gas Exchange Device

The benefits of SMPS and those of ICPMS were also combined by Suzuki et al. at the Chuo University, Japan (Suzuki, Sato et al., 2010). A DMA and an Aerosol Particle Mass analyzer (APM) were serially arranged, to select only particles with 90 nm mobility diameter and 0.458 fg mass, i.e. with a density of 1.2 g cm^{-3} . This setup enabled a simultaneous classification of particles in terms of size and particle density. Subsequently, this classified, but still air based aerosol was partially passed through a Gas Exchange Device (GED), where the air was replaced by argon (Nishiguchi, Utani, & Fujimori, 2008). The resulting argon borne nanoparticles were then aspirated by a pneumatic concentric nebulizer, and introduced to ICPMS for determining the lead content of the measured particles. In Fig. 7, the GED (A), the APM (B), and the general arrangement (C), are sketched. The aerosol amount whereof the carrier air can be replaced by argon is limited by the GED, lowering the amount of particles, available for ICPMS analysis. A particle detector like a CPC or an electrometer was not implemented. However, the ICPMS could be calibrated using an

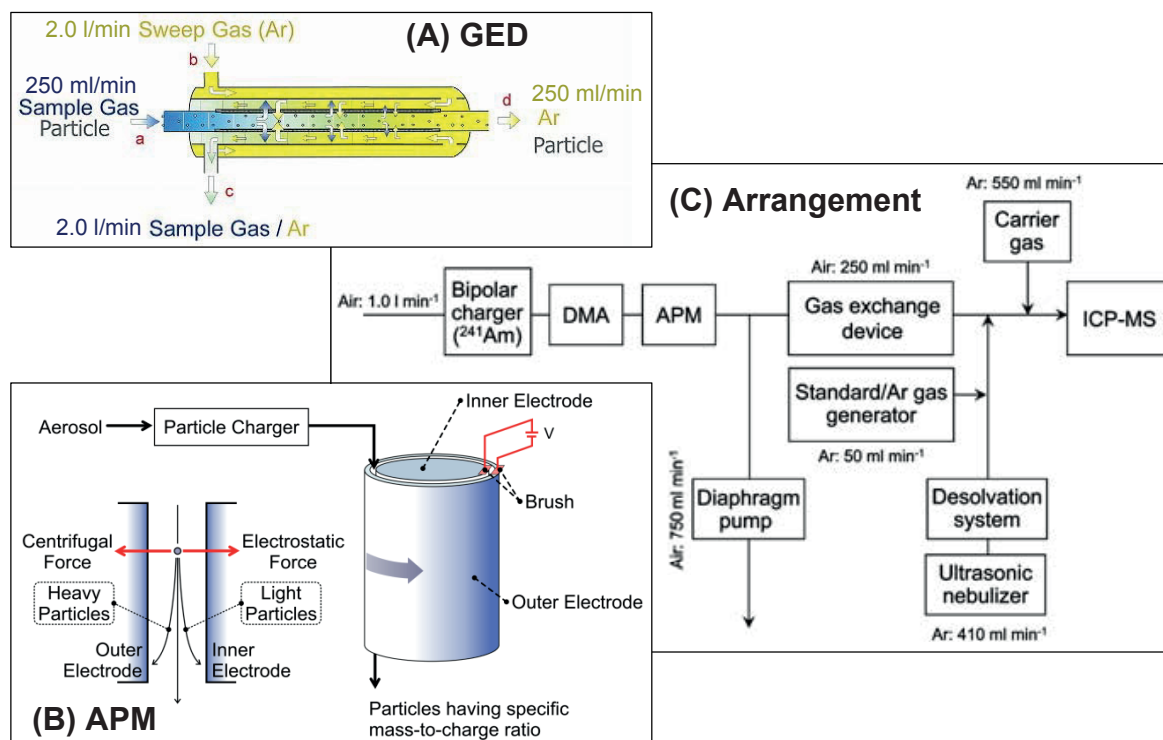


Fig. 7: Experimental setup with air operated DMA. (A) Gas Exchange Device (GED): 2 concentric tubes, separated by a porous wall. Gas molecules penetrate the walls, driven by diffusion. The particles remain in the inner tube, due to their lower diffusion rate (adapted from: Nishiguchi, Utani, & Fujimori, 2008). (B) Aerosol Particle Mass analyzer (APM): similar concept as DMA, but due to the rotation of the classifying tube, particles are fractionated according to their mass, driven by centrifugal force (adapted from: Spec sheet of APM Model 3601 from Kanomax, available on www.kanomax-usa.com). (C) Overall arrangement of DMA and APM as particle classifiers, and GED to make the aerosol ICPMS compatible (from: Suzuki, Sato et al., 2010).

ultrasonic nebulizer, generating a standard aerosol, which was added to the sample aerosol before this was introduced to the plasma. This was the only attempt found in the literature, where the aerosol could be sampled from an undefined source, independently of a primary aerosol flow rate.

With the aim to characterize aqueous suspended particles, an electrospray was used to generate airborne particles from aqueous suspensions, and a DMA to classify these particles concerning their mobility diameter, by Elzey et al. at the NIST, USA. The DMA was operated using argon as sheath gas, in order to replace most of the particle carrier gas by argon, before being introduced to an ICPMS. A GED was implemented between DMA and ICP, to increase the purity of the particle carrier argon (Elzey, Tsai et al., 2013).

1.3.3 Comparison of former coupling attempts

In Fig. 8, the explained former attempts of coupling a DMA or SMPS to a plasma spectrometer are graphically sorted by the particle size range, selectable by the used DMA, and the initial carrier gas of the particles when they were introduced to the DMA. The key data of all these couplings are composed in Table 1. The groups around Weber, Okada, and Houk were using argon as carrier gas.

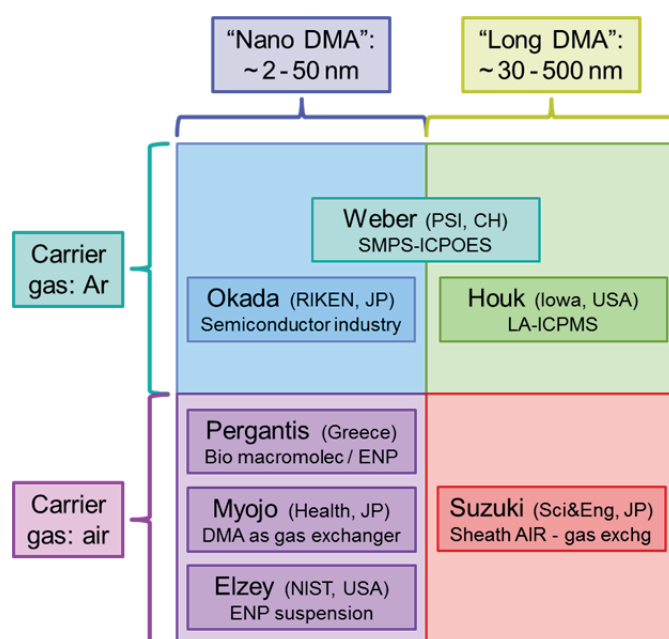


Fig. 8: Survey of all former couplings of mobility analysis and plasma spectroscopy, found in the literature.

This is advantageous since the ICP is established in an argon atmosphere anyway and the very limited oxygen tolerance of the plasma does not cause any problems. The Okada group could choose argon as carrier gas since their goal was monitoring particles occurring from a thermal process in an inert gas atmosphere in a closed volume. The Houk group added a DMA to the existing setup for LA-ICPMS, where the use of argon is obvious anyway.

Air was used as carrier gas by the groups around Myojo, Pergantis, Suzuki, and Elzey, offering the advantage that theoretically ambient aerosols could directly be introduced. Suzuki et al. also operated the DMA using air as sheath gas, reducing the argon consumption and keeping the wide particle size range of the air operated DMA, by the cost of a very low classified sample flow rate due to limitations of the GED. The others were using argon as sheath gas, to have most of the air replaced by argon behind the DMA.

Okada et al. and Pergantis et al. were using short DMA types which allow measuring very small particles, with diameters between 2 and 40 nm, since they were investigating primary metal particles from soldering processes and biological macromolecules in this size range. Weber used two different DMA types, which allowed him covering a wider size range. Myojo's and Houk's groups were measuring diameters > 30 nm. Ambient particles usually are in this size range due to the rapid agglomeration of smaller primary particles.

Since ICPMS was not as widely-used in 1992 as today, Weber et al. were using an ICPOES instrument, while all other discussed studies were done on ICPMS instruments. The *LoD* of ICPMS are usually about a factor of 100 to 1000 better than those of ICPOES.

Table 1: Overview of all DMA-ICP couplings found in literature

Laboratory (Publications)	PSI, Switzerland (Weber, 1992; Weber et al., 1991; Weber et al., 1992)	RIKEN, Japan (Okada et al., 2002)	Nat. Inst. of Industrial Health, Japan (Myojo et al., 2002)	Iowa State Univ., USA (Perdian et al., 2008; Saetveit et al., 2008)	Univ. of Crete, Greece (Carazzone et al., 2008; Kapellios & Pergantis, 2012)	Chuo Univ., Japan (Suzuki et al., 2010)	NIST, USA (Elzey et al., 2013)
Analyzed aerosol	Ag aerosol (spark discharge)	Pb and Sn particles (semicond. industry)	sample aerosol (lead particles)	laser ablated particles	biol. macromolecules, ENP suspensions	ambient air	ENP suspension
Aerosol source	spark discharge unit	flow-through furnace	nebulizer	LA chamber	nano Electropray	nebulizer	electrospray
DMA type	Hauke (≥ 5.5 nm) TSI 3071 (≥ 11 nm)	Wyckoff D1	Kawazawa Univ. type	TSI 3080L	TSI 3080C “nano DMA”	TSI 3081	TSI 3085
particle detector	CPC: TSI 3022	electrometer	CPC: TSI 3022	-	CPC: TSI 3025A	-	CPC: TSI 3776
ICPMS type	ARL 3410 (ICPOES)	Hitachi P-5000	Yokogawa PMS 2000	Thermo Element 1	Thermo X-Series	Agilent HP4500	Agilent 7700x
typ. part. size	30 nm	30 nm	100 nm	50 $\leq d_p \leq 1000$ nm	10 nm	90 nm	32 nm
part. # conc.	$4 \cdot 10^5 \text{ \#}/\text{cm}^3$ (poly)	$4 \cdot 10^5 \text{ \#}/\text{cm}^3$ (poly)	$2 \cdot 10^3 \text{ \#}/\text{cm}^3$ (mono)	no concentration info.	$3 \cdot 10^3 \text{ \#}/\text{cm}^3$ (mono)	no concentration info.	$2.3 \cdot 10^3 \text{ \#}/\text{cm}^3$ (mono)
ICPMS int.	$1 \cdot 10^3 \text{ cps}$ (^{208}Pb)	$1 \cdot 10^3 \text{ cps}$ (^{208}Pb)	$2 \cdot 10^4 \text{ cps}$ (^{208}Pb)	no concentration info.	$3 \cdot 10^4 \text{ cps}$ (^{133}Cs)	$5 \cdot 10^4 \text{ cps}$ (^{208}Pb)	$4 \cdot 10^6 \text{ cps}$ (^{197}Au)
elements/isotopes	Ag, optical spectrum	Sn, Pb, other metals	^{208}Pb	^{63}Cu , ^{64}Zn , ^{65}Cu , ^{66}Zn , ^{69}Ga , ^{238}U , ...	^{133}Cs , ^{127}I , ^{75}As	^{208}Pb	^{197}Au
Q_{poly} (gas)	0.3 L min^{-1} (Ar)	1.0 L min^{-1} (Ar)	0.6 L min^{-1} (air)	(Ar)	1.1 L min^{-1} (air)	1.0 L min^{-1} (air)	1.0 L min^{-1} (air)
Q_{sheath} (gas)	(Ar)		10.0 L min^{-1} (Ar)		6.0 L min^{-1} (Ar)	(air)	10.0 L min^{-1} (Ar)
V_{DMA}			$-160 \text{ V} \dots -2.88 \text{ kV}$		$-10 \text{ V} \dots -3 \text{ kV}$		
PSD	5.5 ... 300 nm	2 ... 40 nm	30 ... 150 nm	50 ... 1000 nm	3.5 ... 16 nm	90 nm	0 ... 40 nm
DMA mode	10 size classes	continuous	continuous	specific size classes	continuous	specific size classes	step-wise scanning
$Q_{\text{mono,CPC}}$			0.24 L min^{-1}	-	0.3 L min^{-1}	-	
$Q_{\text{mono,ICP}}$			0.36 L min^{-1}	$1.05 \dots 1.10 \text{ L min}^{-1}$	0.75 L min^{-1}	0.25 L min^{-1}	$0.25 \dots 1.0 \text{ L min}^{-1}$
Additionally coupled	epiphaniometer TEM sampler	-	-	-	-	APM (Kanomax 3600) GED (Sumitomo)	GED (SPG Technology)
limitations	inlet flow defined primary gas: argon higher LoD than ICPMS (factor 100 ... 1000)	inlet flow defined primary gas: argon specific application only particles ≤ 40 nm	inlet flow defined low aerosol flows only 1 element	inlet flow defined primary gas: argon specific application no particle detector no size scanning	inlet flow defined specific application (suspension analysis) narrow PSD	no particle detector only selected part. size low ICPMS flow due to GED limitations	inlet flow defined specific application (suspension analysis) only particles ≤ 40 nm

Explanations: (poly), concentration in the polydisperse aerosol at DMA inlet. (mono), concentration in the classified, monodisperse aerosol behind DMA.

LoD , Limits of detection. APM, aerosol particle mass analyzer. GED, gas exchange device.

Okada, Myojo, and Pergantis were using SMPS in continuous size scanning mode. Weber and Elzey chose several discrete size classes, being scanned stepwise. Weber, Myojo, Pergantis, and Elzey had a CPC, Okada an electrometer, mounted in parallel to the ICPMS. This simplifies operating the DMA in scanning mode and allows obtaining the particle concentration in parallel to the ICPMS signal. Suzuki and partially Houk were analyzing one distinct particle size at a time and had no specific particle detector attached. Their goal was not identifying PSDs, but determining chemical elements, contained in specific size classes.

Suzuki et al. were specifically focusing on lead in one distinct particle size fraction. However, this was the only attempt where the flow into the DMA was actively maintained by the measuring instrumentation, which allows investigating aerosols from undefined sources. All other coupling attempts were focusing on very specific applications and not able to determine size distribution and size resolved elemental composition of particles in aerosols from undefined sources, without particular primary aerosol flow rates, since all were relying on a defined source flow into the DMA.

1.3.4 Aim of the actual work

The technique of coupling an SMPS or DMA to an ICP spectrometer can still be seen as a novel approach for simultaneous size fractionation and determination of elemental composition of gas-borne nanoparticles, since only a few couplings have been realized up to now. These former attempts were focusing on specific applications, whereas a systematic evaluation of applicability to different aerosol types, and a detailed characterization of the instrumentation concerning sensitivity and *LoD* is missing.

This work reports on the hyphenation of an in-house modified SMPS to a commercial ICPMS instrument, combining the fast particle size analyzing capability of SMPS with the excellent sensitivity and chemical quantification capability of ICPMS. Unlike a GED, which was used in former similar coupling attempts to replace the particle carrier gas by argon, a Rotating Disk Diluter (RDD) serves to dilute the sample aerosol with argon, and at the same time acts as interface to actively introduce the diluted aerosol to the DMA.

Owing to the RDD dilution effect, the initially air-borne particles become mainly carried by argon, and the controlled dilution argon flow rate allows precisely adjusting the aerosol flow directed to the DMA and finally ICPMS. To characterize this RDD-SMPS-ICPMS arrangement, different aqueous nanoparticle suspensions are nebulized into air, followed by a water removal step in a diffusion drier. The purpose is not analyzing these commercially available suspensions, but they are used to provide nanoparticle loaded model aerosols, regardless of any particle alterations during suspension, dilution, nebulization, and drying. These aerosols are analyzed in their states at the instrumentation inlet, without respecting their provenance, in order to evaluate the capabilities of the RDD-SMPS-ICPMS instrumentation.

This setup, including the RDD, enables in-line aerosol sampling and direct elemental analysis of real samples, without being dependent on specific source flow conditions. Gas-borne particles, e.g. in process gases or from aerosol experiments, can be investigated. Achieving particle number concentration, size distribution, and chemical information, at the same time, offers an enormous potential to gain essential information in numerous research areas dealing with the investigation of engineered, combustion or mechanically generated nanoparticles, including online process control of nanoparticle genesis, release, aging, and fate. Although a number of model aerosols are used for instrument validation, the hyphenated technique allows aerosol sampling from any kind of source. It is intended to serve as a versatile instrument, applied in real-case studies like the monitoring of particles in process gases or the assessment of ENP in air environments.

The aim is to cover particles in the range up to several 100 nm. Therewith a long DMA type is used, mostly operated in continuous size scanning mode for mapping several elements in the scanned size range. The ICPMS is installed in parallel to the CPC. So the instrumentation can measure both ICPMS mass intensity and number concentration at the same time.

Since RDD and SMPS have to be operated with argon instead of air, the prospects and limitations of this modification have to be discussed. A detailed evaluation of differences in air and argon operation also includes considering important influencing parameters and standardized procedures for starting up the instrumentation and a precise adjustment of all relevant gas flows. Based on measurements on artificially generated model aerosols containing air-borne polystyrene, gold, silver, and magnetite particles, the synchronization and correlation of the data obtained by the two subsystems to each other are discussed, as well as the *LoDs* of the coupled ICPMS, depending on aerosol composition, size distribution, gas impurities, and SMPS operating conditions. The RDD-SMPS-ICPMS setup is validated by comparison to state-of-the-art techniques such as a non-modified, air operated SMPS, and particle precipitation sampling with subsequent electron microscopy analysis.

In a later period, the newly developed tool is utilized in two different application fields. As representative for the application in the field of air-borne ENP, an investigation of spray processes using nanoparticle containing consumer products is conducted, together with Sabrina Losert, PhD student at Empa/ETH Zürich (Losert, 2015). Aerosol experiments are performed in a test chamber, to assess the impact of particulate matter to the user. As a second highly prospective application field, the investigation of combustion generated nanoparticles is represented by monitoring aerosol emissions from the heat treatment of differently impregnated wood samples in a Thermogravimetric Analyzer (TGA), simulating the incineration of waste wood.

2 Setting up the instrumentation

2.1 Preliminary tests and calculations

2.1.1 Recommissioning of an old SMPS

An in-house constructed SMPS was available from former research projects at Paul Scherrer Institut (PSI), and was used as technical basis for the coupling to ICPMS. The instrument had not been used for years and had therefore to be completed and brought into service, and missing components had to be purchased. Limited access to standard replacement parts is a disadvantage of such a homemade system, but in contrast to commercial products, this setup facilitates modifications of the flow paths, and the implementation of technical components as particle filters, flow control devices, or valves. Some infrastructure had to be evaluated and furnished in order to enable aerosol measurements and method development on aerosol characterization equipment, such as flow calibration and electronic measuring and calibration instruments, aerosol generation equipment, gas and vacuum supplies, electrically conductive tubings to reduce particle loss, tube fittings, etc.

After the first initialization for standard air operation conditions, the performance of the in-house SMPS was compared to two other SMPS units. One of those was an all-in-one SMPS instrument without any measuring options to be selected by the operator (TSI 3034), the other was a modern instrument combination, consisting of separate DMA (TSI 3081) and CPC (TSI 3775). Polystyrene latex (PSL) beads with a defined diameter (50 nm Duke standard PSL beads from Fisher Scientific), suspended in ultra-pure water, were dispersed into air using a spray atomizer (TSI 3079), to generate test aerosols, which were dried in a silica gel based diffusion drier (TSI 3062), and measured by all three SMPS, connected in parallel to each other.

An example of such size distributions, measured by three different SMPS units, is displayed in Fig. 9. The straight curves with x symbols indicate the values obtained by the device under test (PSI-3010). The dashed lines with circle marks were drawn by the modern reference instrumentation (3081-3775), the dotted plots with diamond symbols show data from the older all-in-one SMPS (TSI 3034). Obviously, the 50 nm reference PSL particles were correctly identified by all devices, since the signal peaks are found at the same diameter. Therewith the three instruments show a good agreement concerning the detected particle diameter. However, the measured number concentrations diverged significantly, especially at diameters below approx. 30 nm, down to the lower limit of the measured size range.

The reason for this different weighting of the particle size classes was first not clear. The particles with sizes below 30 nm were considered as background signal, underestimated by the modern reference device, compared to the other two systems, possibly caused by different detection

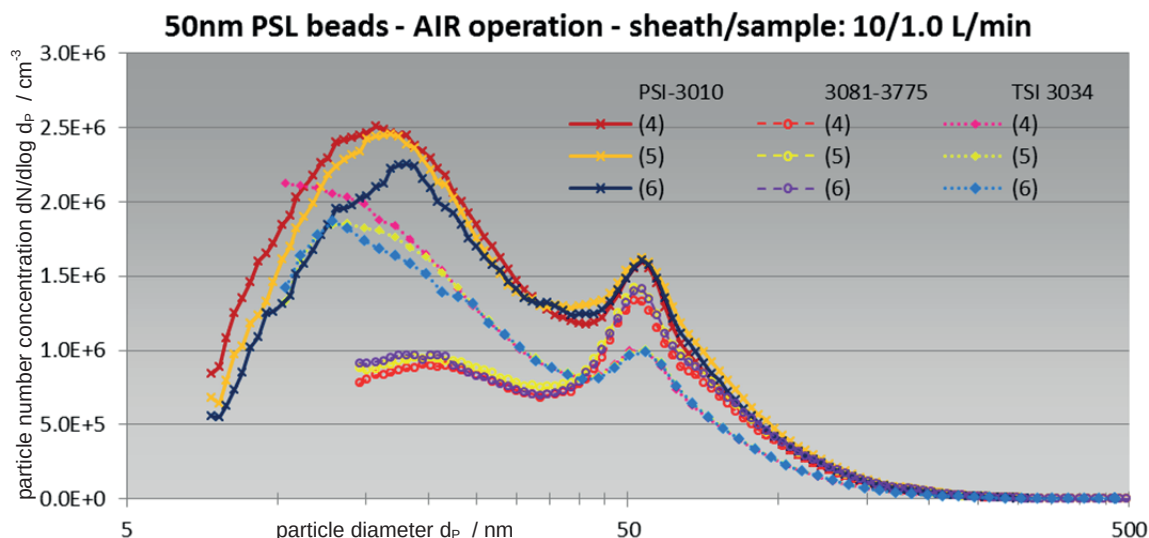


Fig. 9: Comparison of data from the SMPS instrument, intended to be hyphenated to ICPMS (PSI-3010), to data from two reference instruments (3081-3775 and TSI 3034), measuring the same test aerosol. The PSI-3010 and TSI 3034 instruments were operated with 10 L min^{-1} sheath and 1.0 L min^{-1} sample, the 3081-3775 with 3 L min^{-1} sheath and 0.3 L min^{-1} sample air flows.

efficiencies of the involved CPCs, or impurities in the particle detection laser optics of the older instruments might have provoked a virtual signal, without real particles in the detector. Since the focus was not determining absolute particle concentrations, but studying the performance of the SMPS in argon compared to air operation, it was decided not to spend more time on searching the reason for these divergent concentration measurements at very small particle diameters. Anyway, the reason was found later in an insufficient particle charge equilibrium due to outdated aerosol neutralizers in the PSI-3010 and TSI 3034 instruments.

2.1.2 Particle size range covered by argon operated DMA

The DMA is usually operated at sheath air flow rates between 3.0 L min^{-1} and 15 L min^{-1} . Higher flow rates shift the accessible size range towards smaller particles while low flow rates lead to larger particles to be selected by the DMA. In terms of the SMPS-ICPMS hyphenation, the classified particles in the monodisperse aerosol behind the DMA have to be mainly argon borne when introduced to ICPMS, due to the very limited air tolerance of the inductively coupled argon plasma. Therefore the DMA is operated using argon instead of air as sheath gas. To cover particle diameters in the same order of magnitude, classified by the argon operated DMA, similar sheath argon flow rates have to be applied as they are normally set in air operation.

The particle size classifying voltage range, applied to the used DMA type in standard air operation, is normally between 10 V and 10 kV. In argon operation, the high voltage may not reach as high values since electric arcing may occur due to the dielectric strength of argon which is lower than that of air. Arcing can cause serious damage on the power supply and insulating components, and thus needs to be avoided. Besides, the highly ionized gas molecules, resulting from arcing in the

DMA, would provoke spontaneous droplet formation in the CPC and therewith result in unwanted signals which are not related to real particles.

The DMA was run in argon operation with different maximum voltage settings, to empirically determine the applicable voltage maximum. CPC counting, caused by arcing, was observed above DMA voltages of 5.0 kV. The exact high voltage limits have not been determined, and are depending on the gas purity and the staining of insulating parts in the DMA, but arcing was not observed if the high voltage did not exceed 4.5 kV.

The particle size versus the applied DMA voltage has been calculated for several sheath gas flow rates. The diagram in Fig. 10 shows that if e.g. a sheath argon flow rate of 15 L min^{-1} is set, a voltage range of 10 V to 4.5 kV corresponds to a particle size range from about 5.5 to 120 nm. With a sheath argon flow rate of 3.0 L min^{-1} , the same voltage range allows scanning particles between 12 and 350 nm. The dotted lines show that the size ranges would reach up to 200 nm or 650 nm, respectively, if the full voltage range up to 10 kV was available in air operation. This means the upper achievable particle size limit is reduced by a factor of approx. 1.7 to 1.9 by the selection of argon as sheath gas instead of air.

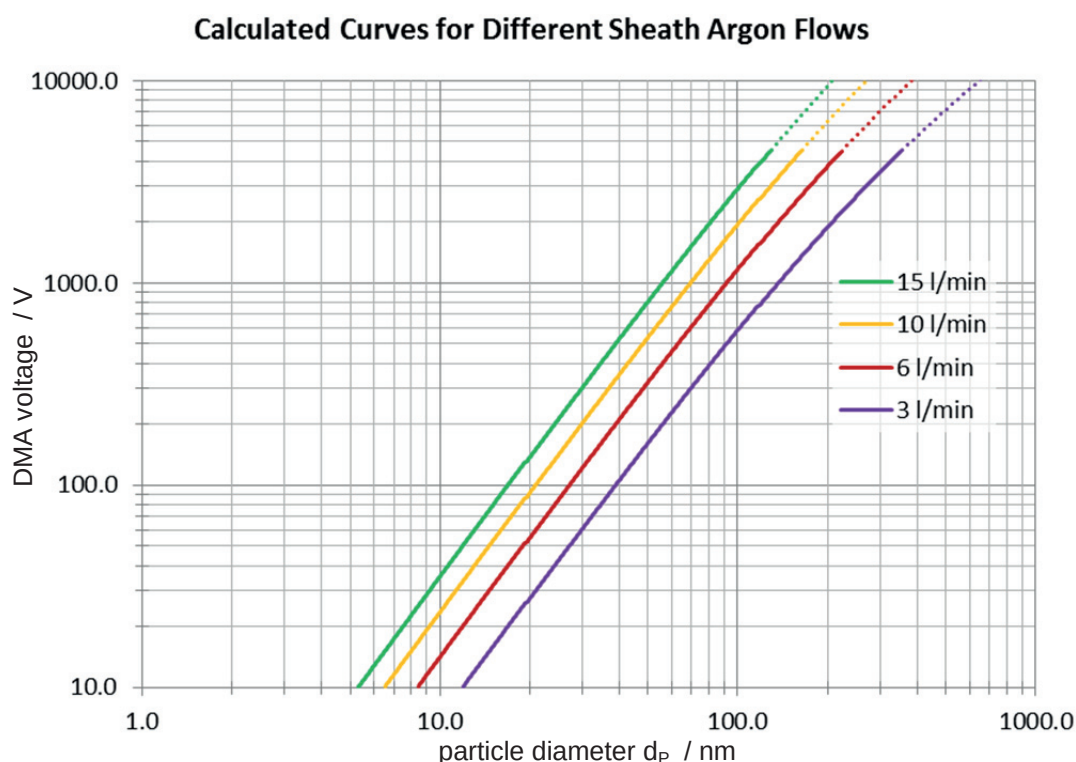


Fig. 10: Classification particle size range with argon as sheath gas, depending on available DMA voltage range, calculated for different sheath gas flows. Straight lines: Voltage limited to 4.5 kV. Dotted lines: Theoretical range if the full voltage range up to 10 kV could be utilized.

2.1.3 Argon operation validation measurements

Similar validation measurements were performed with the argon than the air operated DMA. Fig. 11 shows an example of such measuring data, comparing the argon operated SMPS (PSI-3010), to the same non-modified reference instruments as before (3081-3775 and TSI 3034). The instrumental setup and aerosol generation were equal to the tests performed with the air operated instrument, but 80 nm PSL beads were used and 3.0 L min^{-1} sheath gas and 0.3 L min^{-1} sample aerosol flow rates instead of 10.0 L min^{-1} and 1.0 L min^{-1} were applied to the DMA of the tested instrument, shifting the covered size range towards larger particles. The similarities and differences are almost the same as those observed in air operation mode. Again, all devices agree well concerning the achieved particle size, but the argon operated PSI-3010, and the TSI 3034 instruments show higher particle concentrations at very small particle sizes, due to the insufficient particle neutralization at the DMA inlet, which actually was not clear at that time.

However, the correlation of the size distributions measured by the instrument under test to those of the reference instruments was very similar in argon as in air operation, indicating that the modifications for operating the SMPS using argon as sheath gas were successful and at least the size classification of the instrument was not deteriorated by the use of sheath argon instead of air. The argon operated device generally detected higher concentrations than the other two units over the whole size range. This could be attributed to improperly set gas flows, dramatically influencing the detected particle concentrations, since small relative errors of the high sheath and excess gas flows were causing a considerable relative error of either the much smaller sample inlet flow, or the flow of classified, monodisperse particles, behind the DMA.

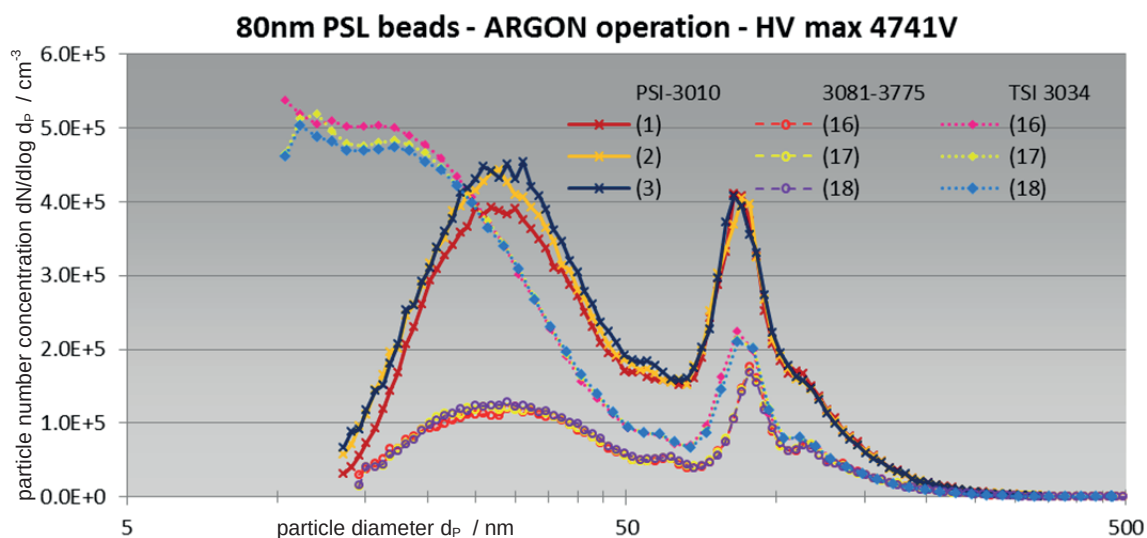


Fig. 11: Validation of argon operated SMPS (PSI-3010) by comparison to two non-modified, air operated instruments (3081-3775 and TSI 3034), measuring the same test aerosol. The PSI-3010 and 3081-3775 instruments were operated with 3 L min^{-1} sheath and 0.3 L min^{-1} sample, the TSI 3034 with 10 L min^{-1} sheath and 1.0 L min^{-1} sample air flows.

2.2 SMPS modifications and first coupling

2.2.1 Instrument arrangement and flow concept

Additional mass flow controllers (MFC) were installed to the SMPS, in order to define the flows of fresh argon blown into and used argon removed from the DMA. With these MFCs, the sheath argon flow can be varied between 0 and 16 L min^{-1} , in 0.005 L min^{-1} increments. Another mass flow controller was installed to feed clean air to the inlet of the CPC, for reducing the monodisperse sample flow taken up by the CPC from the DMA outlet, and to have the CPC operated closer to its intended purpose, i.e. with at least a certain carrier gas fraction being air. To ensure the entering gases to be particle free, additional absolute filters had to be evaluated and installed. All installed filters and MFCs were arranged in the existing rack of the SMPS setup.

The full flow concept of the SMPS-ICPMS coupling setup, including all modified SMPS gas and aerosol flows, is outlined in Fig. 12. In a normally operated SMPS, the DMA inlet flow results from the sum of the excess gas and the monodisperse aerosol consumed by the CPC (Fig. 4), subtracted by the sheath gas flow. These flows are all either defined by MFCs, or in older systems by needle valves, and by a critical orifice and a pump, integrated or connected to the CPC. Unlike the CPC, ICPMS does not attract a defined flow but the gas has to be actively introduced to the plasma. This means the classified DMA outlet flow is no longer defined unless the polydisperse flow at the DMA inlet is controlled.

Since maintaining aerosol flows by pumps and valves or flow controllers induces the risks of sample contamination and undefined particle loss, an RDD has been implemented. This allows precisely controlling the flow rate of the diluted aerosol, provided to the DMA. Therewith the flows into and out of the DMA are well-defined, but the monodisperse flow at the DMA outlet depends on the inlet flow, contrariwise to the standard SMPS arrangement, where the inlet is resulting from the monodisperse flow, attracted by the CPC.

2.2.2 First RDD-SMPS-ICPMS coupling

The first RDD-SMPS-ICPMS coupling experiments were carried out before the highly sophisticated ICPMS, evaluated and ordered for being coupled to the SMPS, was delivered and installed. The modified SMPS was therefore coupled to an existing ICPMS instrument (Perkin Elmer Elan 6000). A suspension, containing citrate covered silver particles in water (Nano Argentum Cit from NanoSys), was serving as precursor to generate the aerosol which was used for these first tests. The suspension was not a certified standard reference material, but a mean diameter of roughly 70 nm was specified by the manufacturer.

The suspension was dispersed into air, using a spray atomizer (TSI 3079 aerosol generator). The spray aerosol was then dried in a thermo denuder with three temperature zones, developed by Fierz et al. (Fierz, Vernooij, & Bartscher, 2007), resulting in dry solid air-borne silver particles. Since the flow generated by the atomizer was higher than the RDD inlet flow, it was split at the thermo

2 Setting up the instrumentation

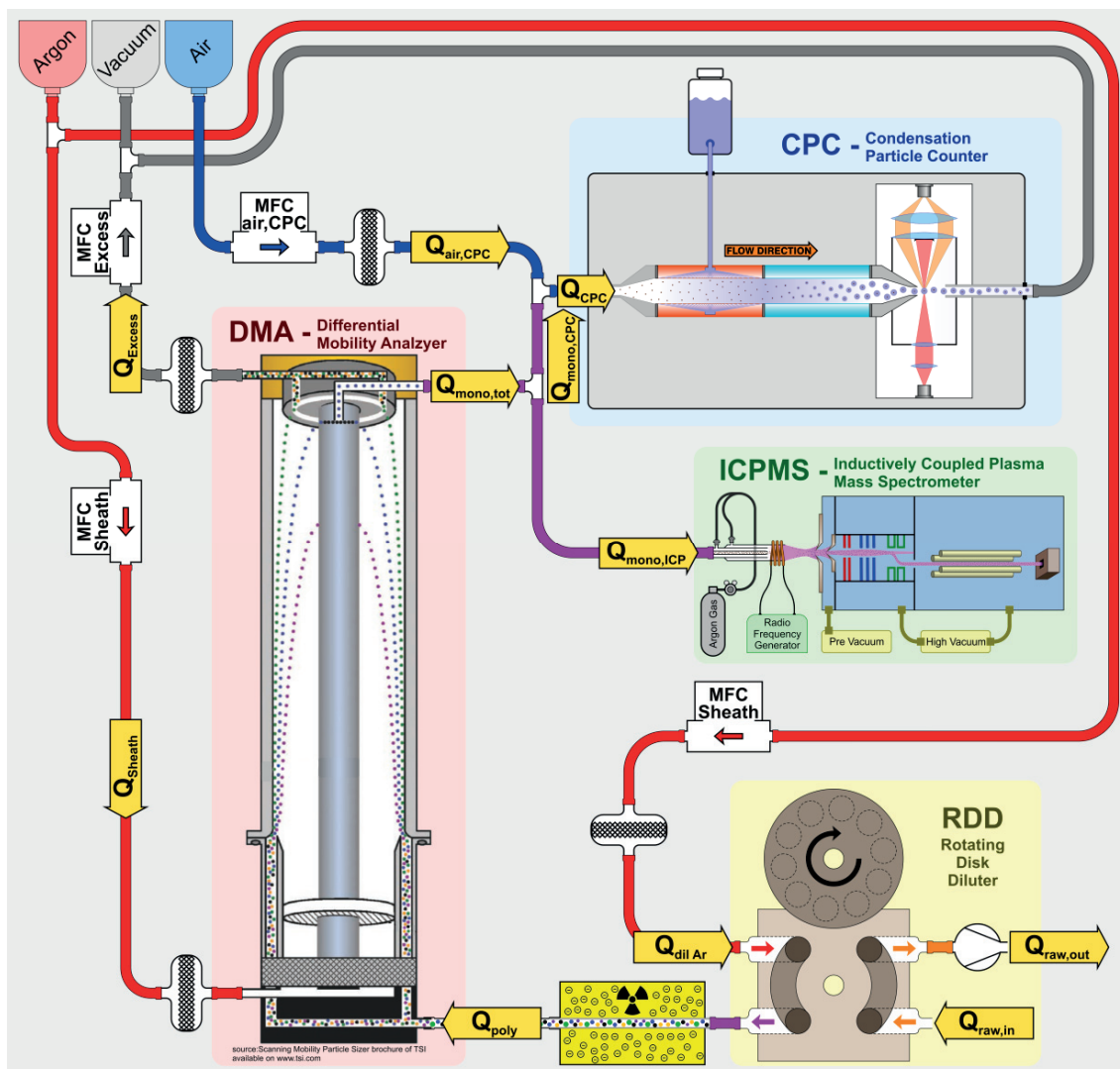


Fig. 12: Flow concept of hyphenated RDD-SMPS-ICPMS setup, including Rotating Disk Diluter (RDD), modified and argon operated SMPS, and ICPMS, with all gas and aerosol flows indicated.

denuder outlet, and the non-used fraction was filtered and released to the laboratory atmosphere as particle free air. The aerosol generation arrangement and connection to the RDD is illustrated in Fig. 13.

The actual measuring value of an integrated mass flow meter, measuring the dilution gas flow, is used to adapt the rotational speed of the diluter disk, in order to sustain the set dilution ratio. The lowest possible dilution factor was set, i.e. the disk was rotating fast and therewith adding the most possible raw aerosol to the dilution gas. By the manufacturer, the RDD was calibrated for being operated with air as dilution gas, and could reach a minimum dilution factor of 15.1 if used as intended. Since dilution argon was used instead of air, the manufacturer calibration was not valid, and the minimum dilution factor for argon operation was found to be 18.1. This was determined by

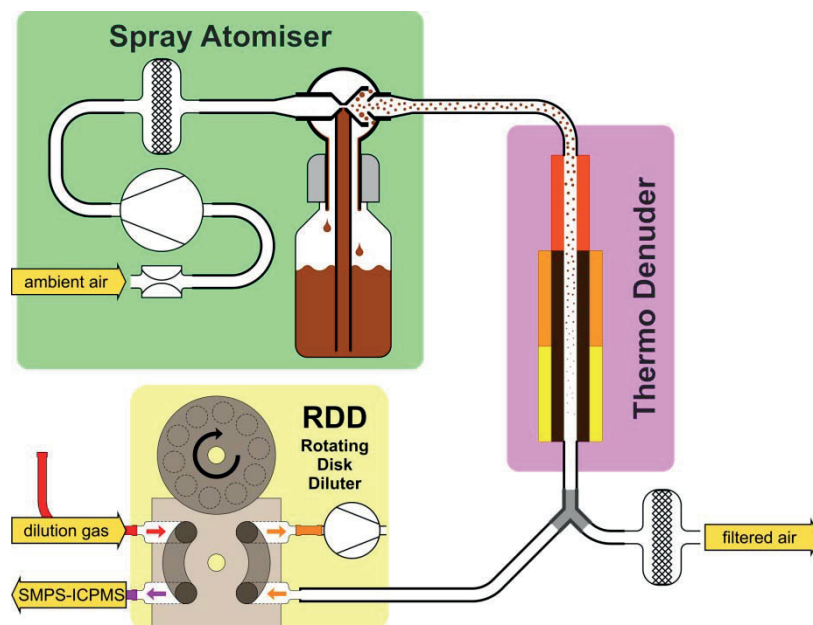


Fig. 13: Arrangement for generating a test aerosol containing dried silver particles which were used for the first experiments with the RDD and SMPS coupled to an ICPMS.

comparing concentrations, measured with the air and argon operated coupled RDD, to those obtained using another, reference RDD. The resulting particle carrier gas mixture after dilution was therefore consisting of 5.5 % air and 94.5 % argon.

The flow of the diluted polydisperse aerosol, introduced to the DMA, was 1 L min^{-1} . Both sheath and excess gas flows were adjusted to 10.0 L min^{-1} , resulting in a monodisperse aerosol flow of 1.0 L min^{-1} . This flow was split into 0.3 L min^{-1} for subsequent particle counting in the CPC and the remaining 0.7 L min^{-1} were introduced into the plasma of the ICPMS. The DMA was logarithmically scanning the voltage range from 11 V to 4.4 kV in continuous mode, corresponding to a size range between 6.8 and 151 nm. While the SMPS was scanning and recording PSDs, ICPMS signals were acquired for a few isotope masses, including both silver isotopes ^{107}Ag and ^{109}Ag .

An example of particle number concentrations, measured by the argon operated SMPS during the first coupling to ICPMS, are plotted versus the referring particle diameter in Fig. 14A. The PSD of the silver aerosol appears to be relatively wide and the size mode is between 30 and 40 nm instead of 70 nm as would be expected from the manufacturer's information. A secondary x-scale was added at the top of the diagram area, representing the approximate time progress while the size distribution was recorded.

The volume concentration of these particles was calculated using the respective function of the SMPS software (TSI AIM V9.0.0), assuming spherical particles, and plotted versus the particle diameter. This volume weighted size particle distribution (PSD_V) is displayed in Fig. 14B. Since

2 Setting up the instrumentation

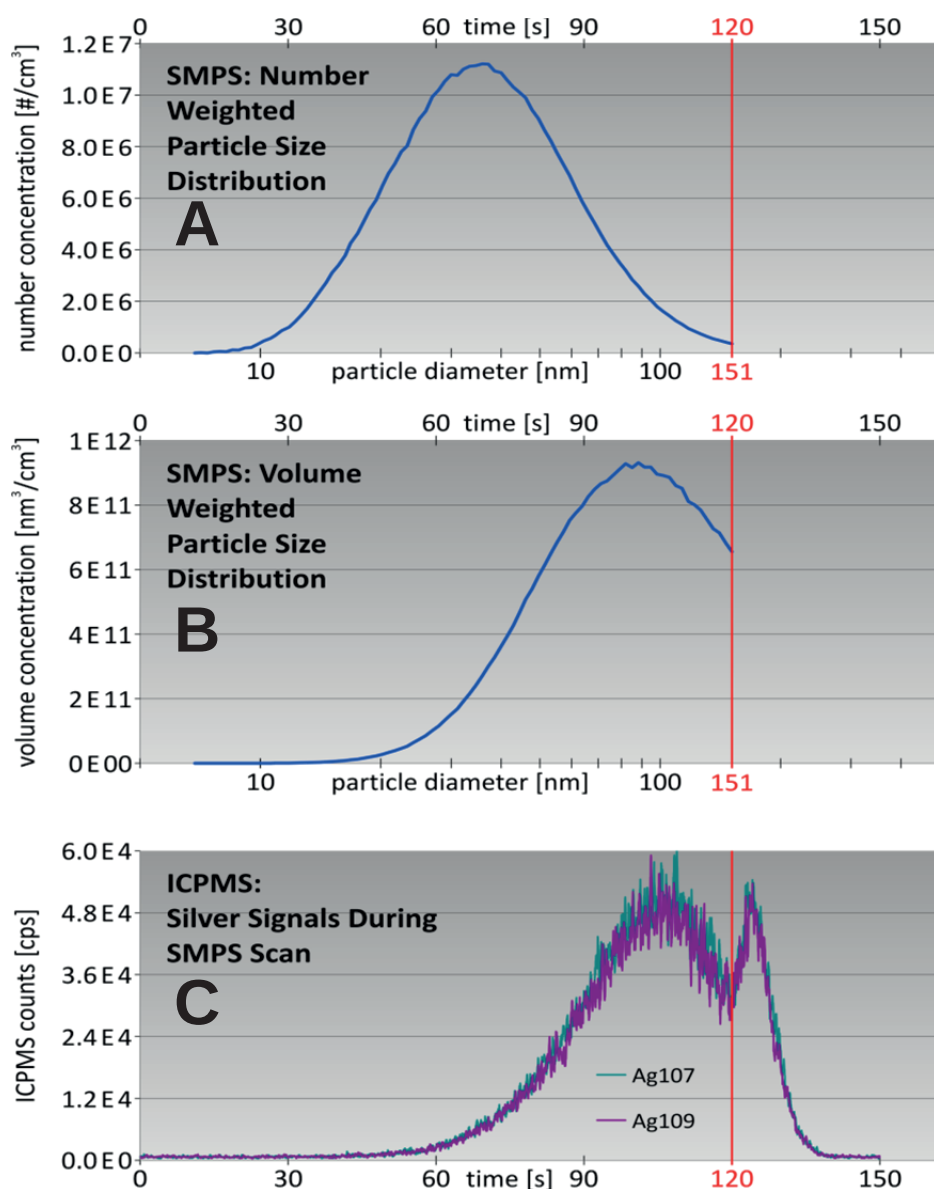


Fig. 14: Signals obtained during the first SMPS-ICPMS coupling experiment. (A) Number weighted particle size distribution, determined by SMPS. (B) volume weighted particle size distribution, calculated from the number weighted data. (C) ICPMS ¹⁰⁷Ag and ¹⁰⁹Ag intensities.

the relative contribution of larger particles to the total particle volume is higher than to their number concentration, the size distribution is significantly shifted towards larger particles. Thus, it appears that the mean particle size is indeed close to 70 nm, but only if the volume or mass instead of the number weighted PSD is considered.

The silver signals, i.e. the ICPMS intensities on $m/z = 107$ and $m/z = 109$ with the mean value of the background noise subtracted, measured while the SMPS was scanning the particle size range, are shown in Fig. 14C. In contrast to the SMPS size distributions, this signal appears with two distinguishable peaks. The first peak can be attributed to the particles fractionated in the DMA

when the size distribution was measured by the SMPS. The second peak is due to the so-called “down-scan” of the DMA. The down-scan is necessary to set voltage and electric field in the DMA back to their initial state. Number concentrations measured by the CPC during the down-scan are not processed by the SMPS software for determining size distribution, whereas the ICPMS signal represents the particulate mass concentrations during the entire measuring period. The down-scan is usually conducted in shorter time, leading to a narrower peak in the intensity versus time ICPMS signal. In fact, the durations of the up- and down-scans were set 120 s and 30 s in the SMPS operation settings.

The time elapsed between these two ICPMS intensity peaks allows determining the time relation between both SMPS and ICPMS signals: The intensity minimum between up- and down-scan can be allocated to the inflection point 120 s after the measurement start, when the SMPS reached the maximum voltage and particle diameter, i.e. when the up-scan was finished and the down-scan started. With this information, the two measuring signals can be linked to each other. The silver signals coincide quite well to the PSD_V , measured by SMPS. However, this synchronization based on the visual appearance of the ICPMS intensity was only a preliminary solution to reproducibly and reliably assess the correlation of the two signals.

Another critical factor is the signal-to-noise ratio. A contamination source might be pollutions in the RDD. However, some experiments were performed using air as dilution gas in the RDD, and argon was used as sheath gas in the DMA. This caused about 10 % air in the monodisperse aerosol, introduced to the ICPMS, leading to relatively high background signals even on the $m/z = 107$ and 109 . These were probably polyatomic interferences arising from the air and from air impurities, and by the influence of these gases onto the plasma. When the dilution air was replaced by argon, the background became significantly lower. Thus, the level of non-particulate elemental contamination in air is a critical issue and needs to be considered.

2.3. Aerosol neutralizer

The number of elemental electric charges on nanoparticles is generally not known, but this information is needed by the SMPS software to calculate the particle concentrations at the SMPS inlet from those measured by the CPC, downstream the DMA. Therefore a radioactive source, called aerosol neutralizer (Flagan, 2008), is placed at the DMA inlet. The ionizing radiation induces a gas ion cloud wherein the particles can achieve a known charge equilibrium state, the Boltzmann equilibrium.

After several measurement series, it was observed that the particle concentrations, measured by different SMPS instruments, as shown in Fig. 9 and Fig. 11, were depending on the used aerosol neutralizer. The neutralizer, used in the coupled SMPS-ICPMS, was equipped with a ^{85}Kr beta source, with an initial activity of 74 MBq, and had been manufactured at PSI more than 10 years ago. The neutralizer of the older all-in-one 3034 SMPS was a commercial product (3077A from

TSI), similarly with a ^{85}Kr source, but with an initial activity of 370 MBq, manufactured in 1997. The 3081-3775 reference instrumentation was equipped with a neutralizer of the same type, but manufactured in November 2011. By exchanging the different neutralizers, it was found that the size distributions measured by the three instruments agreed much better if the same source was used.

Considering the half-life time of ^{85}Kr , which is 10.8 years, the remaining activity of the PSI source was calculated to be below 37 MBq, that of the all-in-one instrument 168 MBq, and that of the modern 3081-3775 SMPS was about 350 MBq. Presumably all sources were not sufficient to achieve the equilibrium charge distribution on the measured model particles, since these were generated in an aqueous spray process, and such aerosols usually are strongly unipolarly charged. Probably an even stronger source would have been needed to perfectly neutralize such aerosols. Since the goal of this research project was not the improvement of the SMPS measuring arrangement in general but to characterize the SMPS-ICPMS coupling in comparison to a normally operated SMPS, it was decided to proceed using ^{85}Kr sources of the same type and production date for the coupled and reference SMPS.

However, the purchase of an alternative neutralizer was deliberated, equipped with a 370 MBq ^{241}Am source, since such alpha radiation activity would be more effective for neutralizing aerosol particles (Covert, Wiedensohler, & Russell, 1997), and the half-life of ^{241}Am , $\tau_{1/2, \text{Am}241} = 432$ years, would allow using this neutralizer for decades. Two suggestions for the design of such a neutralizer, which is not available as a standard commercial component, were obtained, one from the Leibnitz Institute for Tropospheric Research, and one from an isotope supplier, Eckert & Ziegler. Due to economic considerations and regulatory obstacles, this idea was not further pursued. Anyway, the long-term objective of the RDD-SMPS-ICPMS setup was not measuring spray generated model aerosols, but mainly particulate process emissions, and a functional ^{85}Kr neutralizer is supposed to be sufficient for such applications.

2.4 Data analysis

2.4.1 Data processing with MS Excel

A first electronic tool to correlate SMPS and ICPMS measuring data was created in Microsoft Excel. Some display details of the user interface are presented in Fig. 15. For using this tool, the measuring data from both the coupled and an air operated reference SMPS, and from ICPMS, have to be first converted into individual excel sheets. Another spreadsheet allows selecting the relevant data, recorded by all instruments during three SMPS scans.

The user can define one or two ICPMS measuring periods, which ideally have been recorded, when SMPS was not scanning, in order to determine the mean value and standard deviations of the background ICPMS intensities, on the considered m/z . Based on the clock time, recorded by all

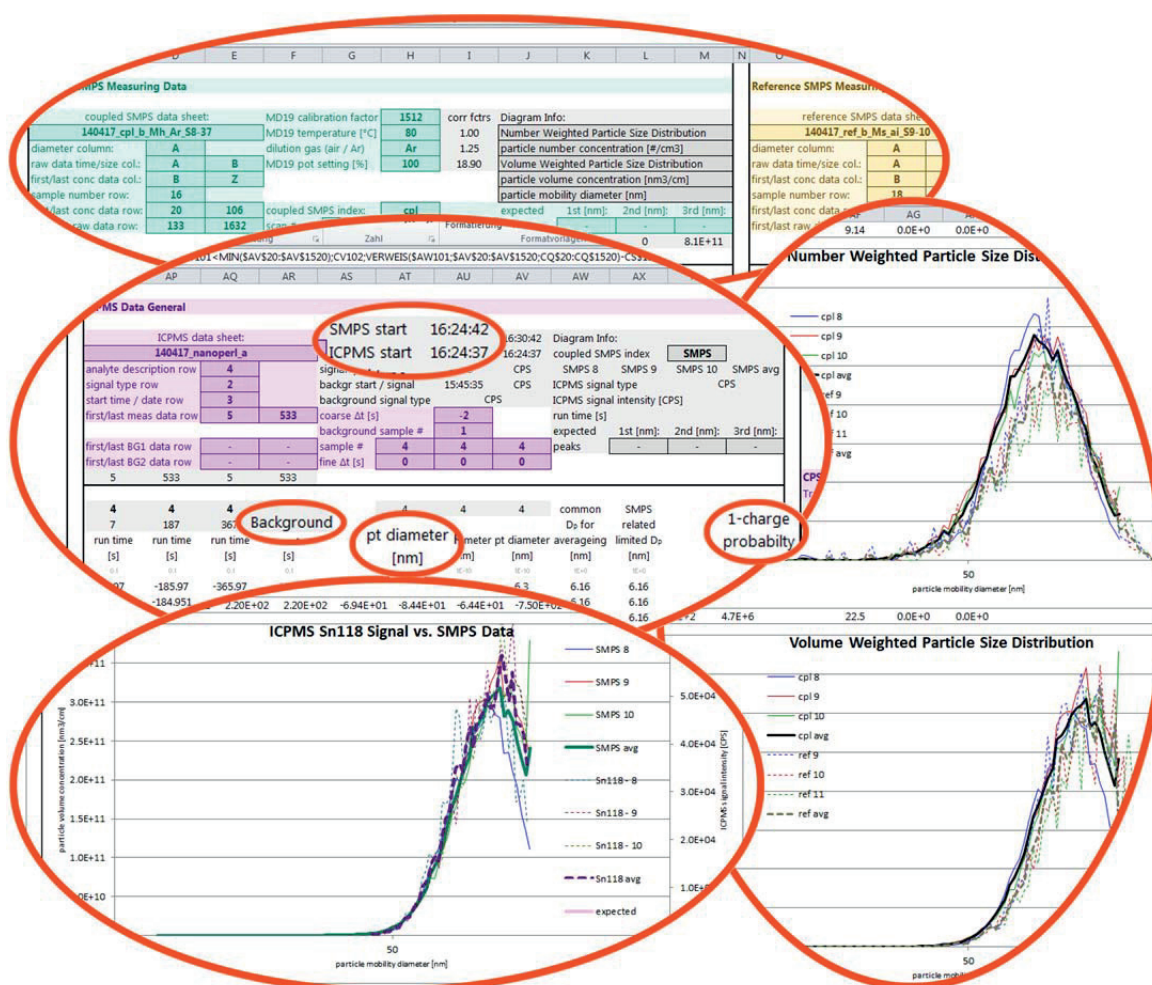


Fig. 15: User interface of the MS Excel tool, used for correlating SMPS and ICPMS measuring data.

measuring computers, a rough temporal relation between SMPS and ICPMS data is automatically determined. Besides, a coarse time delay between both signals, has to be entered manually, which is used for all processed scans, as well as individual fine time deviations, in order to obtain the best match between the size-resolved ICPMS intensities and the SMPS determined size distributions.

The mean background intensity is subtracted from all recorded ICPMS intensities, and each resulting net ICPMS value is allocated to a specific particle size class. The single charge probability for this specific size class is determined by interpolating the accordant values from the charge probability table, implemented in the SMPS evaluation software. Dividing the net intensity by the single charge probability leads to the mass related size resolved ICPMS intensity. These data of the three individual scans, and their average, are compared to the respecting PSD_v, determined by SMPS, in one diagram. Additionally, the mass related ICPMS intensity is divided by the volume of a spherical particle with the respecting diameter, resulting in a number related intensity which is compared to the originally number weighted SMPS data in a second diagram.

2 Setting up the instrumentation

The Excel tool allows determining the sensitivity of ICPMS, if the intensity on a distinct m/z can clearly be allocated to particle concentration, measured by SMPS, in a certain size range. The LoD is then calculated from the sensitivity and the standard deviation of the background signal. Up to three measuring scans can be compared, since it is not appropriate to plot more curves in a single diagram. Besides, several time-consuming calculation steps were implemented, and the tool would have become inconveniently slow if data of more than three scans were compiled in one spreadsheet.

2.4.2 Data processing with Matlab

To make use of the time resolution of a few minutes, it appeared helpful to consider more than three measuring scans in one dataset, especially when particulate emissions of thermal processes were measured during several hours. Dynamic aerosol behavior should be visualized, i.e. particle concentrations and ICPMS intensities should be represented, depending on both the experiment run time and the particle diameter. A new tool was developed in Matlab, which fulfills this requirement. The clock time of both SMPS and ICPMS measuring computers and a manually entered coarse time difference is used for roughly correlating the signals from the different sensors, similarly as in the excel tool. Size distributions, determined by SMPS, and size resolved ICPMS intensities, can be individually displayed and a fine time shift value can be set for each scan. Once these are determined, element maps can be generated. The x- and y-axes of these diagrams describe the experiment run time and the particle diameter, respectively, and span an area, filled with colors, representing particle concentration or particle related ICPMS intensities.

In contrast to the Excel tool, it is also possible to define more than two background periods, when no voltage is applied to the DMA and therewith no particles are present at the DMA outlet. Such short periods usually occur between two SMPS scans, and can be used if no background signal was measured before or after a measuring sequence. Besides, it is considered in this Matlab evaluation program that a quadrupole type ICPMS is a sequential instrument and the different m/z are not measured simultaneously. This becomes especially important if numerous elements or isotopes are monitored, or a longer signal integration time has to be selected, in order to obtain a better signal-to-noise ratio, when low concentrations are measured.

3 Final setup

(partly published in: Hess, A., Tarik, M., Ludwig, C. (2015). A hyphenated SMPS-ICPMS coupling setup: Size-resolved element specific analysis of airborne nanoparticles. *Journal of Aerosol Science*, 88, 109-118.)

3.1 Instrumentation

3.1.1 Rotating Disk Diluter

A heatable steel block, equipped with two aerosol channels, and a disk featuring several cavities are the main components of the RDD (MD19-2E from Matter Aerosol) which was used for the hyphenated instrumentation. A pump draws raw aerosol through the first channel while the second channel is rinsed with filtered dilution gas. The disk is rotating on the block surface, and every cavity transports a defined volume unit from the raw aerosol to the dilution gas channel and vice versa (Hueglin, Scherrer, & Burtscher, 1997). The diluted aerosol behind RDD is separated from the aerosol source, and the aerosol flow being introduced to subsequent instrumentation can be adjusted independently of a specific gas flow rate of the aerosol source. Therewith aerosols can be sampled from various environments, e.g. from an exhaust channel or from a glove box where spray experiments are performed. Although the argon plasma of ICPMS exhibits a low air tolerance, the sampled particles can therewith initially be carried by nearly any gas due to the dilution capabilities of the RDD, since argon was used as dilution gas.

The quantity of raw aerosol added to the dilution argon is the same like that of dilution argon transported to the raw aerosol channel. Therewith the incoming and outgoing raw aerosol flows have the same amounts ($Q_{\text{raw,in}} = Q_{\text{raw,out}}$), and also the flow rates of dilution argon and the diluted polydisperse measuring aerosol are equal ($Q_{\text{poly}} = Q_{\text{dil Ar}}$). The respecting channel must be flushed with raw aerosol but the flow rate does not have to be controlled very accurately. However, $Q_{\text{dil Ar}}$ has to be known and was therefore precisely controlled by a mass flow controller (MFC). Since the RDD, used for the coupling of SMPS to ICPMS, was operated using dilution argon instead of air, the dilution factor, DF_{cpl} , could not be set following the instrument calibration, but had been determined by comparison of size distributions obtained by the coupled and an air operated non-modified reference SMPS, in terms of a previous SMPS calibration measurement series. As dilution in the RDD is resulting from the raw aerosol amount added to the defined dilution gas flow, the maximum disk rotating frequency and the total disk cavities volume are limiting the lowest possible dilution factor. Finally, the coupled RDD was operated with the diluter block heated to 80 °C at the lowest possible dilution factor which was found to be $DF_{\text{cpl}} = DF_{\text{cpl,min}} = 18.1$. Therewith the carrier gas mixture in the diluted aerosol was containing $1/18.1 = 5.5\%$ air from the raw aerosol, and 94.5 % dilution argon.

3.1.2 Scanning Mobility Particle Sizer

The basic SMPS instrumentation, coupled to ICPMS, included a vertically installed DMA tube (similar to 3081 long DMA from TSI) with the gases and aerosols streaming upwards. The DMA had a cylinder capacitor geometry with inner and outer diameters, $d_{i,DMA} = 18.7 \text{ mm}$ and $d_{o,DMA} = 39.2 \text{ mm}$, and effective classifying length, $l_{DMA} = 444 \text{ mm}$. The classifier peripherals of the DMA were arranged in house, i.e. high voltage supply, particle filters, mass flow controllers, tubings, and connectors. The technically possible voltage range of the standard operated DMA was covering 10 V to 10 kV, with the inner electrode being negative. The CPC (3010 from TSI) was located at the top of the setup, close to the monodisperse aerosol outlet of the DMA. The aerosol flow rate through this CPC type could not be adjusted but was defined by a critical orifice behind the particle counting optics and an external pump (HN 022 AN.18 from KNF) providing at least 500 mbar vacuum to the instrument. The SMPS measuring sequence is divided into up and down scan. During up scan the DMA voltage is increased, the particle size range is scanned from small to large diameters, and the recorded CPC signal is used to calculate the PSD. During the usually shorter down scan period, the DMA voltage is reduced to the initial value, meanwhile the CPC signal is not used for size distribution calculation and therewith normally not visible to the user. The selected scan durations were 120 s for up and 30 s for down scan.

Due to the low air tolerance of the ICP, argon instead of air was used as SMPS sheath gas. This allowed the particles to be mainly argon-borne, when they were introduced to ICPMS afterwards. Based on ambient temperature and air pressure in the laboratory, the dynamic viscosity and free mean path of the used argon were calculated and entered to the measuring software (AIM 8.1 from TSI). The dielectric strength of argon is lower than that of air, meaning that electric arcing between two electrodes occurs at a lower voltage level if the volume between the electrodes is filled with argon instead of air. Therewith the voltage range of the DMA could not be fully utilized and the voltage was scanned from 10 V to 4.4 kV instead of 10 kV. The sheath argon and polydisperse sample aerosol flow rates of the coupled SMPS were $Q_{\text{Sheath}} = 10 \text{ L min}^{-1}$ and $Q_{\text{Poly}} = 1.0 \text{ L min}^{-1}$, leading to a scanned particle diameter range from 7 to 156 nm. The dependence of the particle size range on the applied voltage range has been explained above and illustrated in Fig. 10. Since the gas mixing in the DMA is nearly perfect (Myojo et al., 2002), the air content in the classified, monodisperse aerosol was further reduced by another factor of 10, resulting in >99 % argon purity, which was tolerated by the argon plasma at the ICPMS inlet.

The ^{85}Kr aerosol neutralizer (3077A from TSI) with remaining activity of 350 MBq was installed at the bottom, straight at the polydisperse aerosol inlet of the DMA tube. The charge distribution equilibrium after passing the aerosol neutralizer depends on the particle carrier gas (Wiedensohler & Fissan, 1991). If a gas molecule is ionized, the emitted electron strongly tends to attach to another gas molecule with high electronegativity, e.g. O_2 . Positive and negative ions therefore have similar properties regarding mass and mobility and their attachment coefficients to particles. Pure noble gases, however, do not form negative ions. The mobility of the remaining free electrons is by

orders higher than that of the positive gas ions, resulting in an asymmetrical particle charge distribution with charging efficiencies which are significantly different from those in air (Stober, Schleicher, & Burtscher, 1991). Hereby the charge distribution of negatively charged particles is stronger affected than that of positively charged ones. In the here presented setup, the carrier gas was not absolutely pure argon when passing the aerosol neutralizer. Since 5.5 % of the diluted gas mixture were air, the oxygen content was roughly 1.2 %, which is sufficient to provide a charge distribution equilibrium, very close to that in air, compared to that in pure argon (Franck, 1910; Wiedensohler & Fissan, 1990). The size-depending probabilities of particles to be singly or multiply charged were calculated using the Wiedensohler approximation (Wiedensohler, 1988). Since the inner DMA rod was the negative electrode, only positively charged particles were used for size classification. Due to the remaining oxygen in the carrier gas and since only positively charged particles were classified, no argon adapted calculation coefficients were utilized, but the original ones, valid for air-borne particles.

3.1.3 Inductively Coupled Plasma Mass Spectrometer

The ICPMS, used for this coupling, was a commercial instrument (8800 Triple Quad from Agilent), equipped with two quadrupole analyzers (MS/MS) and a collision/reaction cell. Since no solutions but dry aerosols were analyzed, the ICPMS was operated without conventional sampling introduction system, i.e. nebulizer and spray chamber, but the DMA outlet was directly connected to the ICP torch. A daily optimization of the ICPMS instrument was carried out before starting to measure, and main parameter settings for optimal dry plasma conditions were selected. The following plasma conditions were applied to the ICPMS instrument: RF power was tuned to 1250 W and a low sampling depth of 6.0 mm was set. The flow rate of argon as ICP dilution gas was $0.3 \text{ L}_\text{N}/\text{min}$. The auto RF matching function was used to minimize reflected power. The instrument was run in MS/MS mode. Both quadrupoles were set to the same m/z at a time. $m/z = 107$, $m/z = 109$, and $m/z = 197$ were measured with integration time 0.2 s each, in order to obtain silver and gold information with a sampling time of roughly 0.6 s. Since no significant interferences were expected, ICPMS was run without cell gas. The ICPMS signal intensity was measured during 200 s for every single measurement in time-resolved analysis (TRA) mode, and recorded in counts per second [cps].

3.1.4 SMPS-ICPMS hyphenation

The analytical setup, including all relevant parts and components, is sketched in Fig. 16, and all relevant gas and aerosol flows, included in the flow concept of the coupled SMPS setup, are indicated. The RDD was placed at the DMA inlet. The RDD raw aerosol pump was maintaining $Q_{\text{raw,in}} = Q_{\text{raw,out}} \approx 1 \text{ L min}^{-1}$. A MFC (Smart-Trak 50 from Sierra) supplied the dilution argon flow, $Q_{\text{dil Ar}}$, to the RDD. While in standard SMPS configuration, the DMA intake is resulting from all other flows into and out of the DMA, this modification of the SMPS flow concept allows precisely adjusting this polydisperse aerosol flow, $Q_{\text{poly}} = Q_{\text{dil Ar}}$, provided to the DMA. Another MFC (4850 from Brooks) was maintaining the DMA sheath argon flow, Q_{Sheath} , at fixed value. Two HEPA

3 Final setup

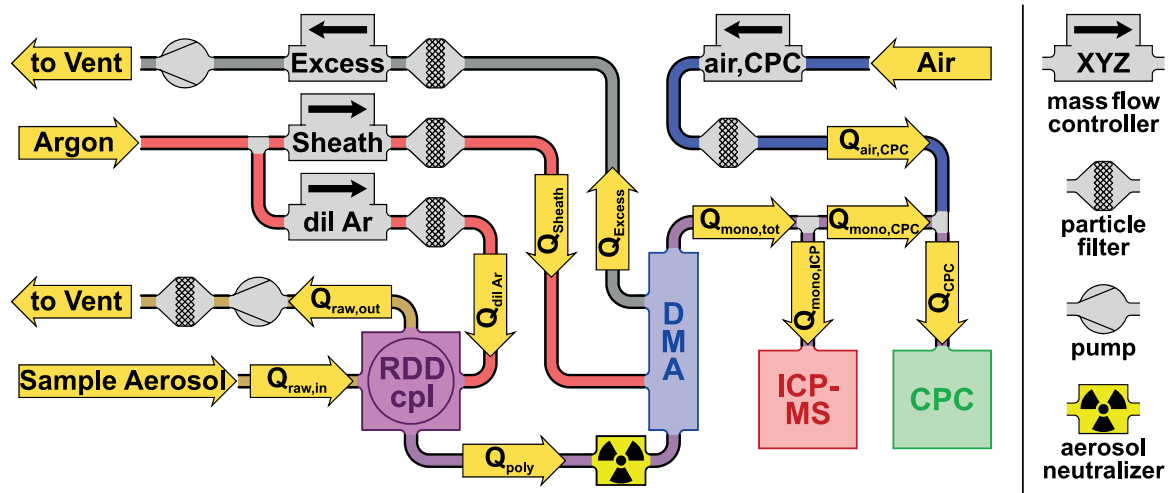


Fig. 16: Coupling instrumentation including RDD, DMA, ICPMS, CPC, and peripherals. $Q_{raw,in}$ and $Q_{raw,out}$: raw aerosol flow into and out of RDD, $Q_{dil Ar}$: dilution argon flow into RDD, Q_{poly} : diluted polydisperse measuring aerosol provided to DMA by RDD, Q_{sheath} : sheath argon flow, Q_{excess} : excess gas flow at DMA outlet, $Q_{mono,tot}$: total monodisperse flow at DMA outlet, Q_{CPC} : total flow into CPC, $Q_{air,CPC}$: air flow to reduce monodisperse aerosol fraction consumed by CPC, $Q_{mono,CPC}$ and $Q_{mono,ICP}$: CPC and ICPMS fractions of monodisperse aerosol flow.

filters (type H cartridge #95302 from MSA) were installed to ensure particle free dilution argon entering RDD and sheath argon entering DMA. The excess gas flow, Q_{excess} , was passed to an absolute filter (DIF-LN30 from Headline) before entering a further MFC (4850 from Brooks), connected to a vacuum pump (HN 035.1.2 AN.18 from KNF).

Since the total CPC flow, Q_{CPC} , was defined by a critical orifice and could not be adjusted, another MFC (Smart-Track 50 from Sierra) was adding a filtered air flow, $Q_{air,CPC} < Q_{CPC}$, to the CPC inlet, to reduce the monodisperse aerosol fraction taken in by the CPC, $Q_{mono,CPC} = Q_{CPC} - Q_{air,CPC}$. Unlike the CPC, the ICPMS does not actively aspirate a defined volume flow, and the total monodisperse flow, $Q_{mono,tot}$, is no longer defined by the sensors behind the DMA. The precisely controlled Q_{poly} allowed having $Q_{mono,tot}$ well defined anyway, enabling another modification, i.e. splitting $Q_{mono,tot}$ in $Q_{mono,CPC}$ and the remaining fraction being introduced to ICPMS, $Q_{mono,ICP} = Q_{mono,tot} - Q_{mono,CPC}$.

The different gas and aerosol flows had to be adjusted very carefully, since the low monodisperse aerosol flow rate, provided to ICPMS, $Q_{mono,ICP}$, was resulting from the much higher sheath and excess gas flows, Q_{sheath} and Q_{excess} . The used MFC's were designed to control mass flow values, given in normal liters per minute [L_N/min], while SMPS reliability bases on effective volume flows, given in real liters per minute [$L min^{-1}$]. Therefore all flows were precisely adjusted using a primary flow calibrator (Gilibrator-2 from Sensidyne). The flow calibration procedure was as follows:

1. Adjust the sheath argon flow, $Q_{sheath} = 10.0 L min^{-1}$, by tuning MFC_{sheath} .
2. Adjust the polydisperse sample flow, $Q_{poly} = 1.00 L min^{-1}$, by tuning $MFC_{dil Ar}$.

3. Set the excess gas flow, Q_{Excess} : Adjust the total monodisperse flow, $Q_{\text{mono}} = 1.00 \text{ L min}^{-1}$, by tuning $\text{MFC}_{\text{Excess}}$.
4. Set the CPC air flow, $Q_{\text{air,CPC}}$: Insert the flow calibrator between the T-pieces at ICPMS and CPC inlets. Adjust the monodisperse CPC flow, $Q_{\text{mono,CPC}} = 0.30 \text{ L min}^{-1}$, by tuning $\text{MFC}_{\text{air,CPC}}$.
5. Check and fine-adjust the monodisperse ICPMS flow, $Q_{\text{mono,ICP}} = 0.70 \text{ L min}^{-1}$, by fine-tuning $\text{MFC}_{\text{Excess}}$.

The counting efficiency values of the CPC, needed by the SMPS measuring software, were corrected by a factor of 0.3 to account for the monodisperse aerosol flow split at the DMA outlet where 0.3 L min^{-1} were allocated to the CPC and 0.7 L min^{-1} introduced to ICPMS.

3.1.5 Measuring arrangement

To validate the PSDs, determined by SMPS-ICPMS, a second SMPS setup was connected to the aerosol source in parallel to the coupled device. The complete measuring setup including both parallel arranged SMPS measuring lines is outlined in Fig. 17. To have the non-modified reference system comparable to the coupled arrangement, a separate RDD of same type, and ^{85}Kr neutralizer of the same type and age as the coupling components were implemented. The reference RDD, neutralizer, DMA (3081 from TSI), and CPC (3776 from TSI), were all operated under air atmosphere. Since there was no ICPMS, the total monodisperse flow was consumed by the CPC.

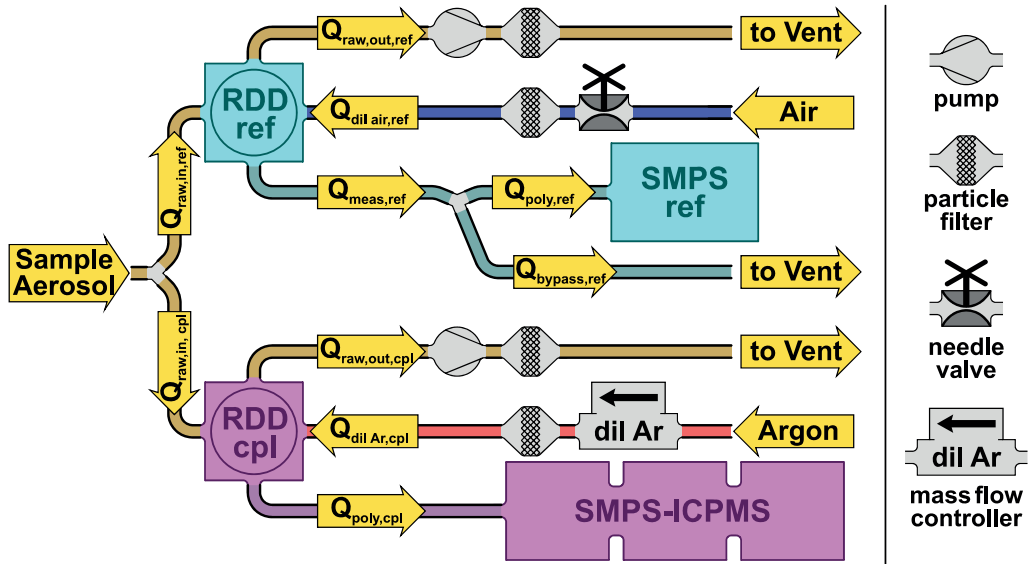


Fig. 17: Measuring setup: SMPS-ICPMS and reference SMPS including separate RDDs. $Q_{\text{raw,in}}$ and $Q_{\text{raw,out}}$: raw aerosol flow into and out of RDD, $Q_{\text{dil air}}$ and $Q_{\text{dil Ar}}$: dilution air respectively argon flow into RDD, Q_{meas} : diluted measuring aerosol exiting RDD, Q_{poly} : polydisperse flow into SMPS, Q_{bypass} : measuring aerosol bypassed before SMPS inlet. “ref” and “cpl” indicate reference SMPS and coupled SMPS

3 Final setup

Therewith the polydisperse inlet flow, $Q_{\text{poly,ref}} = 1.0 \text{ L min}^{-1}$, was equal to the CPC flow and had not to be controlled by a separate MFC.

To prevent overpressure in SMPS instrumentation, the dilution air and therewith the diluted measuring aerosol flows were set to approximately $Q_{\text{dil air,ref}} = Q_{\text{meas,ref}} \approx 1.3 \text{ L min}^{-1}$, controlled by a needle valve. The resulting slight overflow was bypassed at the DMA inlet, $Q_{\text{bypass,ref}} \approx 0.3 \text{ L min}^{-1}$. The sheath air flow of the reference SMPS was set 10 L min^{-1} and the voltage was scanned from 10 V to 9.75 kV, resulting in a particle size range from 7.5 to 305 nm. Like RDD_{cpl} , RDD_{ref} was heated to 80 °C. Due to slightly different disk geometry, the dilution factor could not be set as low as that of the coupled RDD, but was set to $DF_{\text{cpl}} = 28.1$. This was leading to lower aerosol concentration and therewith lower raw measuring values at the reference SMPS, compared to the coupled instrument.

3.1.6 Data processing

The SMPS data were multiplied by the dilution factors of the RDDs, $DF_{\text{cpl}} = 18.1$ and $DF_{\text{ref}} = 28.1$. The resulting values are therewith representing particle concentrations in aerosols at the inlet of the RDD sampling probe.

SMPS measuring data are based on number concentrations, i.e. the resulting number weighted size distributions are representing the number of particles per aerosol volume unit [$\#/\text{cm}^3$]. However, ICPMS signal represents the number of sample atoms per time which are ionized and classified according their m/z and finally reach the detector. The signal intensity is given as the number of ion counts per second [cps], and is proportional to the analyte mass concentration in the sample being introduced to ICP. This mass dependent ICPMS signal intensity correlates rather to the particle volume concentration than to the number concentration measured by SMPS. Therefore the volume concentration of every size fraction, $c_V(d_p)$, was determined by multiplying the measured number concentration, $c_N(d_p)$, by the volume of an assumed spherical particle of the referring diameter, $V_P(d_p)$:

$$c_V(d_p) = c_N(d_p) \cdot V_P(d_p) = c_N(d_p) \cdot \frac{\pi}{6} \cdot d_p^3 \quad (1)$$

The entity of these SMPS determined volume concentrations of all size fractions was the volume weighted particle size distribution, PSD_V , which could be compared to the mass-related ICPMS intensity curve.

Raw data exported from the SMPS software not only contain the finally computed size resolved concentration information, but also the raw particle counts of the CPC versus measuring run time with a time resolution of 0.1 s, including the actually scanned particle diameter at any time. To correlate the ICPMS run time to the particle diameter, this time-diameter relationship from the SMPS raw data was utilized. The coarse time adjustment between SMPS and ICPMS data was done by comparing start time and run time recorded by the two measuring computers and by

identifying the ICPMS signal inflexion point between SMPS up and down scan. Exact time correlation of ICPMS to SMPS data was carried out manually until obvious signal peaks of signal curves, recorded by both instruments during instrument startup and tuning, coincided.

The ICPMS background signal intensity, $I_{ICP,BG}$, was determined by measuring and averaging during certain seconds with no voltage applied to DMA, i.e. before or after every SMPS scan. $I_{ICP,BG}$ was then subtracted from the raw intensity, $I_{ICP,raw}(d_p)$, which had been recorded while SMPS was scanning, in order to obtain the net intensity, $I_{ICP,net}(d_p)$:

$$I_{ICP,net}(d_p) = I_{ICP,raw}(d_p) - I_{ICP,BG} \quad (2)$$

The SMPS software offers so-called multiple charge correction, which considers not only the probability of particles to carry one but also those of carrying several elemental charges. If this correction is disabled, multiply charged larger particles are not classified accurately since they behave in the electric field like singly charged smaller particles. However, multiple charges were not yet considered in the computing of ICPMS data, and therefore the correction was also disabled in the SMPS software. This simplifying assumption of only singly positively charged particles passing DMA and reaching ICPMS seems to be justifiable, since primarily the modified coupling setup should be compared to the non-modified reference instrumentation, since only particles below 160 nm were measured and multiple charges are more relevant when measuring larger particles, and finally since the observed differences between corrected and uncorrected SMPS data were small.

It was assumed that the net ICPMS intensity was proportional to the initial particle mass concentration, multiplied by the single charge probability of the actual particle diameter, $P_{1+}(d_p)$:

$$I_{ICP,net}(d_p) \sim c_m(d_p) \cdot P_{1+}(d_p) \quad (3)$$

Therewith a mass related ICPMS intensity, $I_{ICP,m}(d_p)$, could be calculated, being proportional to the mass concentration at the SMPS inlet:

$$I_{ICP,m}(d_p) = \frac{I_{ICP,net}(d_p)}{P_{1+}(d_p)} = (I_{ICP,raw}(d_p) - I_{ICP,BG}) \cdot \frac{1}{P_{1+}(d_p)} \sim c_m(d_p) \quad (4)$$

Additionally, this mass related signal was divided by the assumed particle volume, resulting in a particle number related ICPMS intensity, being comparable to the number weighted SMPS concentration:

$$I_{ICP,N}(d_p) = \frac{I_{ICP,m}(d_p)}{V_p(d_p)} = I_{ICP,N}(d_p) \cdot \frac{6}{\pi \cdot d_p^3} \sim c_N(d_p) \quad (5)$$

Three SMPS scans were performed while ICPMS intensity was recorded, and the averages of the resulting signals were calculated. The originally mass related ICPMS intensity was then

superimposed and compared to the PSD_V calculated from the SMPS data. The same was done with the calculated number related ICPMS intensity and the originally number weighted SMPS determined PSD.

3.1.7 Generation of example aerosol

A nebulizer type aerosol generator (ATM 220 from Topas) and subsequent silica gel diffusion drier (DDU 570/H from Topas) were used to generate dried sample aerosols from aqueous nanoparticle suspensions. The aerosol generation setup is sketched in Fig. 18. Dried compressed air was HEPA filtered and then fed to the aerosol generator injector nozzle. The resulting wet aerosol flow was split into a sample and an excess fraction. The water was removed from the sample fraction in the silica drier. The remaining dry air-borne nanoparticles served as a reproducible model aerosol in the laboratory, analyzed by the hyphenated SMPS-ICPMS instrumentation. The wet excess fraction was passed to another filter and finally released to the off gas. An aqueous silver particle suspension (Nano Ag 1000 Oct from NanoSys) was used to generate a model aerosol. The particles were coated by an octanoic acid layer, their mass concentration in the suspension was $1000\text{ }\mu\text{g/mL}$. The suspension was diluted 100-fold in Milli-Q water and then provided to the aerosol generator. The applied air pressure was 3.6 bar (rel), resulting in roughly 3.5 L min^{-1} generated aerosol.

3.2 Results from measuring the example silver aerosol

The purpose of the study was not analyzing the commercially available suspension, but to demonstrate the instrument's capabilities to characterize the generated silver aerosol at the RDD entrance, regardless of particle alterations during nebulization and drying. All graphs showing SMPS and ICPMS data represent the average of three scans, and PSDs determined by the coupled SMPS are drawn as grey dashed lines. In Fig. 19, the PSDs, measured by the coupled and argon operated SMPS, are validated by comparison to curves, recorded by the non-modified reference instrument, drawn as black straight curves. The PSD_V , shown in (A), has been calculated from the

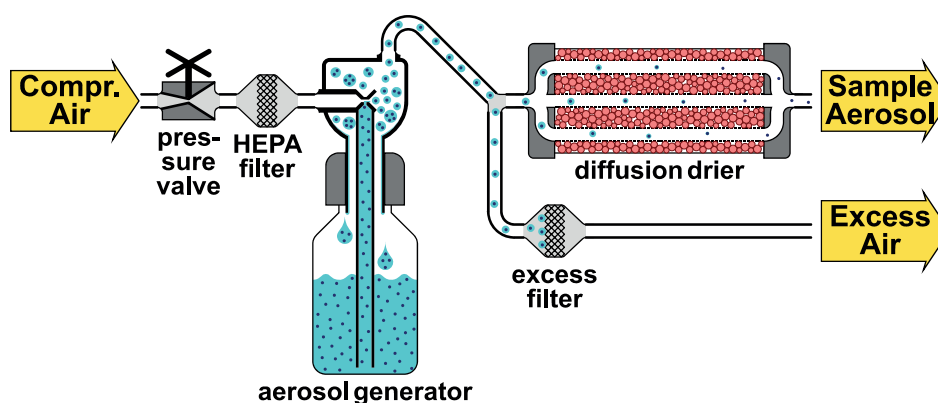


Fig. 18: Setup for generating sample aerosol, used for the characterization of the final setup.

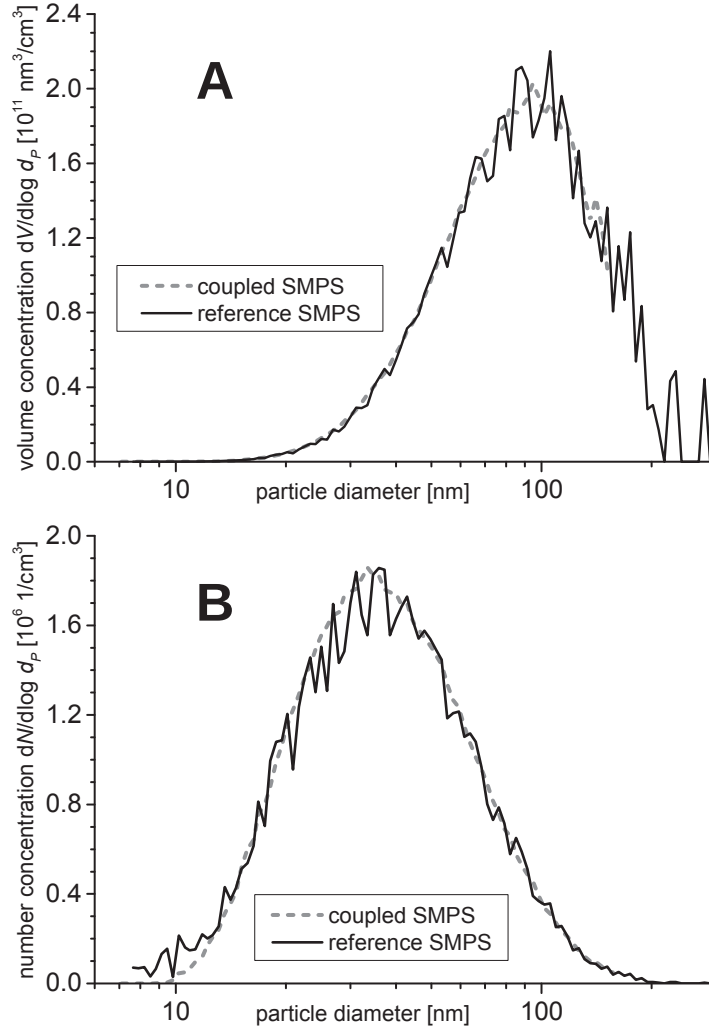


Fig. 19: Comparison of argon operated coupled and non-modified reference SMPS instrumentations. (A) PSD_V , calculated assuming spherical particles, (B) PSD_N , as originally measured by the SMPS.

number related data, PSD_N , plotted in (B). The coupled and reference SMPS signals agree well, except that the reference data is noisier than that of the coupled instrument. Three reasons can explain this difference: First, DF_{ref} was higher than DF_{cpl} , causing lower concentration at SMPS inlet. Second, CPC_{ref} was designed to measure extremely small particles, by the cost of detection efficiency. These signal reductions were corrected, resulting in an amplified curve which was as spiky as the weak primary signal. The third reason was the shorter response time of the modern reference CPC which leads to a higher signal resolution during the SMPS scans, also resulting in a less smooth curve than that stemming from the coupled instrumentation.

The size resolved ICPMS $m/z = 107$ signal is drawn as straight blue line, marked with crosses, and compared to the coupled SMPS data in Fig. 20. In (A), the initial ICPMS mass intensity, $I_{\text{ICP},m}(d_p)$, is compared to the PSD_V , computed from the originally number based SMPS data. Vice versa, (B)

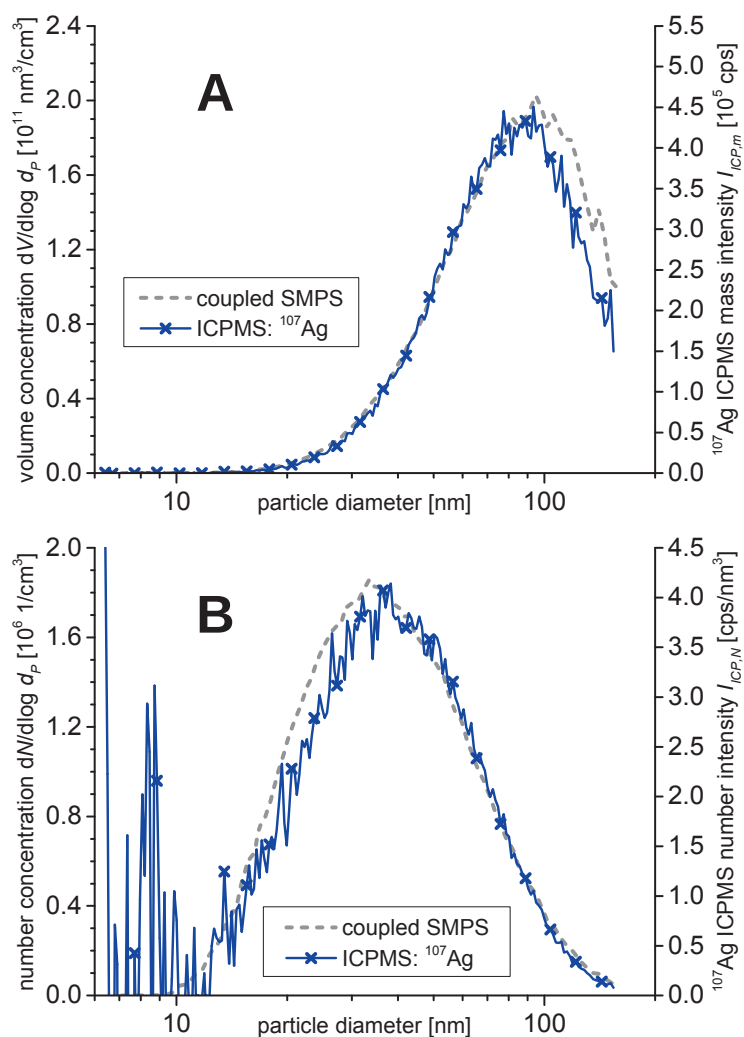


Fig. 20: PSD vs. ICPMS silver intensity at $m/z = 107$. (A) Calculated volume weighted SMPS data vs. initially mass-related ICPMS intensity. (B) Number weighted original SMPS data vs. number corrected ICPMS intensity.

shows the further calculated ICPMS number intensity, $I_{\text{ICP},N}(d_p)$, and the PSD_N , as primarily measured by the SMPS. As expected, the $m/z = 109$ signal curves on the second silver isotope were similar to those of $m/z = 107$, and no signal above background level was observed on $m/z = 197$ (data not shown). Obviously, the ICPMS and SMPS curves correlate very well in both diagrams. This indicates that assuming spherical particles for data conversion did not result in a substantial error, with respect to the used model aerosol.

The PSD_V appears being shifted towards larger particles compared to the PSD_N , since small particles contribute more to the number concentration, while larger particles do to the mass and volume concentration. For the same reason, the number related ICPMS signal becomes very weak for particles below 12 nm. Since mass concentration and therewith ICPMS signal intensity scales with the third power of the particle diameter, ICPMS precision decreases at very small particle

sizes. Besides, especially large particles are usually not spherical as was assumed for computing the PSD_V from the originally number based SMPS data, and incomplete atomization and ionization of larger particles in the plasma cannot be absolutely excluded. These effects may be responsible for the lower ICPMS than SMPS concentration signals below 40 nm and above 100 nm.

Only background noise was detected by ICPMS below 12 nm. Calculating the number related from the initially mass based ICPMS signal, by dividing the net intensity by very small assumed particle volumes, caused a strong computational amplification of this noise. The high ICPMS signal peaks below 12 nm in Fig. 20B are therewith not representing real particles, but the concentration of the measured aerosol was below the ICPMS detection limit in this size range. ICPMS information is presented as mass and number related intensities and is hence a non-calibrated signal. However, mass and number related sensitivities could be calculated from these SMPS measured concentrations and ICPMS intensities, in order to apply the instrument for real-sample investigations of particulate silver.

4 Instrument characterization

(partly published in: Hess, A., Tarik, M., Losert, S., Ilari, G., Ludwig, C. (2016). Measuring air borne nanoparticles for characterizing hyphenated RDD-SMPS-ICPMS instrumentation. *Journal of Aerosol Science*, 92, 130-141.)

Several model aerosols were generated in the laboratory, for determining the sensitivity and *LoD* of the RDD-SMPS-ICPMS setup, related to different elements, and to demonstrate the instrument's ability to distinguish between multiple elements in different particle size fractions of one aerosol. During these measurements, the size range from 7 to 156 nm was scanned, limited by the maximum voltage which should not exceed 4.5 kV, to prevent arcing in the argon operated DMA.

4.1 Model aerosol generation

Engineered nanoparticles, stabilized with a PVP coating, were purchased as dry powder or as aqueous suspensions. Information on particle diameter (d_p) and mass and number concentration (c_m and c_N) of these commercial products were inferred from the manufacturer's specification sheets. The model aerosols, used for the instrument characterization, were generated using the same setup as described in section 3.1.7 and sketched in Fig. 18.

4.1.1 Magnetite aerosol

Dry magnetite particles with $d_p = 19.6 \text{ nm}$ ($\pm 5.2 \text{ nm}$) with purity $> 97 \%$ (20 nm PVP Magnetite Nanopowder from NanoComposix) were dispersed in ultra-pure water, resulting in a suspended particle mass concentration $c_{m, \text{Mag}} = 100 \mu\text{g cm}^{-3}$, or number concentration $c_{N, \text{Mag}} = 4.9 \cdot 10^{12} \text{ cm}^{-3}$. A sample of these suspended particles was analyzed by Transmission Electron Microscopy (TEM). The majority of the observed particles were agglomerates, consisting of primary particles with diameters of about 20 nm, as can be seen in the overview and detail image in Fig. 21A.

The air pressure applied to the nebulizer type aerosol generator was $p_{\text{AG, Mag}} = 2.3 \text{ bar (rel)}$, so 2.5 L min^{-1} iron containing aerosol were generated from this suspension. ICPMS was measuring on four different m/z , including the iron isotopes ^{56}Fe and ^{57}Fe . Integration time was 0.2 s on each m/z , resulting in a total acquisition time $t_{\text{acq, ICP}} = 0.813 \text{ s}$. The measurements were first performed without any ICPMS cell gas. Then they were repeated with $1.0 \text{ mL}_N \text{ min}^{-1}$ helium as collision gas (other data than those of measuring $m/z = 56$ without and $m/z = 57$ with helium not shown in the resulting diagrams).

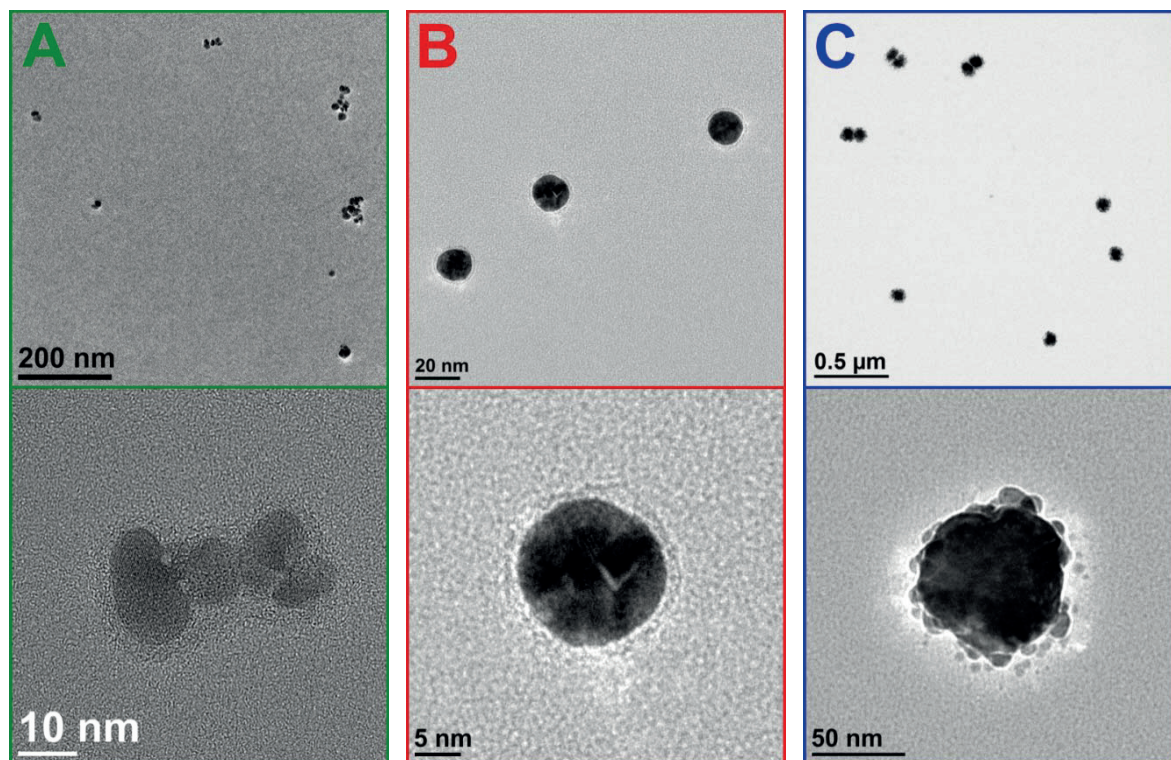


Fig. 21: Particles, sampled from all aqueous suspensions, being used for model aerosol generation. (A) TEM overview and detail image of one agglomerated magnetite particle. (B) TEM overview and detail image of one single gold particle. (C) STEM bright-field overview and TEM detail image of silver particles.

4.1.2 20 nm gold aerosol – high concentration

Gold particles with $d_p = 19.6 \text{ nm}$ ($\pm 2.1 \text{ nm}$), suspended in ultra-pure water with mass and number concentrations $c_{m,\text{Au}} = 51 \mu\text{g cm}^{-3}$ and $c_{N,\text{Au}} = 6.8 \cdot 10^{11} \text{ cm}^{-3}$ (20 nm PVP NanoXact Gold from NanoComposix), were used to generate the gold aerosols. A TEM overview and a detail image of particles from this gold suspension are shown in Fig. 21B. These nearly spherical particles were not agglomerated in the suspension and had very uniform diameters of about 20 nm.

The air pressure at the aerosol generator inlet was $p_{\text{AG,Au}} = 2.6 \text{ bar (rel)}$, resulting in 2.8 L min^{-1} generated aerosol. ICPMS was run without collision or reaction gas, and three m/z including the gold mass ^{197}Au (data of other m/z not shown in the diagrams) were measured. Integration time was 0.2 s on each m/z , resulting in a total acquisition time, i.e. temporal resolution of ICPMS signal, $t_{\text{acq,ICP}} = 0.613 \text{ s}$. For additional validation of the measuring results, an electrostatic particle precipitator (Partector TEM sampler from naneos) was connected in parallel to the SMPS-ICPMS setup during this measurement series, and aerosol particles were collected on copper grids for subsequent TEM investigation. The resulting images of aerosol particles will be shown later (Fig. 26).

4.1.3 20 nm gold aerosol – low concentration

The second gold aerosol was generated using the 100-fold diluted 20 nm NanoXact Gold suspension. The particulate gold mass and number concentrations in this suspension were $c_{m,Au} = 0.5 \mu\text{g cm}^{-3}$ and $c_{N,Au} = 6.8 \cdot 10^9 \text{ cm}^{-3}$. Aerosol generator pressure and ICPMS settings were the same as when measuring the aerosol with high gold concentration.

4.1.4 Mixed gold/silver aerosol

A mixed aerosol containing smaller gold and larger silver particles was achieved by blending the undiluted 20 nm gold suspension and a second suspension containing silver particles with $d_p = 82.1 (+/- 4.4 \text{ nm})$ (80 nm PVP NanoXact Silver from NanoComposix). The mixing ratio was 1:1, resulting in mass and number concentrations of gold particles $c_{m,Au} = 26 \mu\text{g cm}^{-3}$ and $c_{N,Au} = 3.4 \cdot 10^{11} \text{ cm}^{-3}$, those of the silver particles $c_{m,Ag} = 10 \mu\text{g cm}^{-3}$ and $c_{N,Ag} = 3.3 \cdot 10^9 \text{ cm}^{-3}$. The particles in the silver suspension were too low concentrated for direct TEM imaging. Therefore the concentration in a silver suspension sample was increased by centrifugation and 95 % water removal. Both, single primary particles and agglomerates, were then found, as shown in the Scanning Transmission Electron Microscopy (STEM) overview and the TEM detail image in Fig. 21C. The agglomerates could have been present already in the original suspension, or they might have been formed in terms of the suspension concentration and sample preparation procedure, but anyway, the shape of the primary particles was nearly spherical with a diameter of about 80 nm, and a big fraction of such non-agglomerated particles was observed.

Roughly 2.8 L min^{-1} of the mixed gold/silver aerosol were generated by applying an inlet air pressure $p_{AG,mix} = 2.6 \text{ bar (rel)}$ to the aerosol generator. ICPMS was scanning $m/z = 107$, 109 , and 197 during 0.2 s integration time each, and no cell gas was applied. So both silver isotopes ^{107}Ag and ^{109}Ag , and the gold mass ^{197}Au were measured with a total acquisition time $t_{acq,ICP} = 0.613 \text{ s}$ (only $m/z = 107$ and $m/z = 197$ signals shown in the diagrams).

4.2 Calculations

4.2.1 Signal calculations

ICPMS background mean value, $I_{ICP,BG}$, and standard deviation, $\sigma_{ICP,net}$, were calculated from the background ICPMS signal, being recorded for each measuring series during several seconds while SMPS was not scanning and therewith no particles were present at the DMA outlet. As discussed in equation (2), the net intensity related to a specific particle diameter, $I_{ICP,net}(d_p)$, was obtained by subtracting $I_{ICP,BG}$ from the raw intensity recorded during the SMPS scans, $I_{ICP,raw}(d_p)$. In equation (4), it was explained that $I_{ICP,net}(d_p)$ had to be divided by the probability of a particle to penetrate the DMA, i.e. the probability to carry one elemental positive charge after the aerosol neutralizer, $P_{1+}(d_p)$. The resulting ICPMS mass intensity, $I_{ICP,m}(d_p)$, is proportional to the particulate mass at the instrumentation inlet.

$P_{1+}(d_p)$ was calculated according to the Wiedensohler approximation (Wiedensohler, 1988), as it is done by the SMPS software to determine the PSD from CPC data. SMPS measuring data are originally based on particle number, while ICPMS intensities are proportional to the mass concentration. To compare the size resolved signals of both sensors in diagrams, the number related ICPMS intensity, $I_{ICP,N}(d_p)$, was computed by dividing $I_{ICP,m}(d_p)$ by the particle volume, assuming spherical particles with size-independent density, as calculated in equation (5). Vice versa, the number weighted SMPS determined PSD were converted into volume weighted data by multiplying the size resolved number concentrations by the assumed particle volume.

4.2.2 Instrument performance calculations

The number of particles per time, $\dot{n}_{class,CPC}(d_p)$, counted by the CPC while each of the selected size fractions was scanned, was read from SMPS measuring raw data, except for the low concentrated gold aerosol, where a reduced number was used, being the difference between the total CPC counts and the assumed lognormal distributed small non-gold particles. The number concentration of classified particles, $c_{fr,class,N}(d_p)$, was determined by dividing $\dot{n}_{class,CPC}(d_p)$ by the flow rate of the classified aerosol being allocated to the CPC, $Q_{class,CPC} = 0.3 \text{ L min}^{-1} = 5 \text{ cm}^3 \text{ s}^{-1}$:

$$c_{fr,class,N}(d_p) = \frac{\dot{n}_{class,CPC}(d_p)}{Q_{class,CPC}} \quad (6)$$

Although there is a certain dependency of the particle density on the particle size (Nanda, 2012), constant densities were assumed, since the accordance between the mass related ICPMS signals and SMPS determined PSD_V was very good, and since the influence of this variability was expected to be small compared to ICPMS signal interferences or other factors influencing the instrument performance. The material density of magnetite, $\rho_{mag} = 5.2 \text{ g cm}^{-3}$, was multiplied by the iron mass fraction of magnetite, $f_{Fe,mag} = 0.724$, to obtain the element mass density of iron in magnetite, $\rho_{elm,Fe} = 3.76 \text{ g cm}^{-3}$. The element mass densities of the gold and silver particles were assumed to be the bulk densities of the accordant materials at ambient conditions, i.e. $\rho_{elm,Au} = 19.3 \text{ g cm}^{-3}$ and $\rho_{elm,Ag} = 10.5 \text{ g cm}^{-3}$. For each particle category, ρ_{elm} was multiplied by the assumed volume of a spherical particle and by $c_{fr,class,N}(d_p)$, to obtain an estimate of the element mass concentration in the classified aerosol of the selected particle size fraction, $c_{fr,class,m}(d_p)$:

$$c_{fr,class,m}(d_p) = \rho_{elm} \cdot \frac{\pi}{6} \cdot d_p^3 \cdot c_{fr,class,N} \quad (7)$$

The sensitivity of ICPMS as isolated subsystem, related to the classified particle mass concentration, $S_{ICP,class,m}$, assumed to be independent of the particle diameter at these size and concentration levels, was then calculated by dividing the net ICPMS intensity on the dedicated m/z , $I_{ICP,net}(d_p)$, by $c_{fr,class,m}(d_p)$:

$$S_{ICP,class,m} = \frac{I_{ICP,net}(d_p)}{c_{fr,class,m}(d_p)} \quad (8)$$

With the standard deviation of the net ICPMS intensity, $\sigma_{\text{ICP,net}}$, the mass related limit of detection of ICPMS, $LoD_{\text{ICP,class,m}}$ was calculated:

$$LoD_{\text{ICP,class,m}} = \frac{3 \cdot \sigma_{\text{ICP,net}}}{S_{\text{ICP,class,m}}} \quad (9)$$

The number and mass concentrations of particles of the selected size fraction in the non-classified aerosol at the instrument inlet were calculated by dividing $c_{\text{fr,class,N}}(d_p)$ and $c_{\text{fr,class,m}}(d_p)$ by the single charge probability, $P_{1+}(d_p)$, and multiplying them by the RDD dilution factor, DF_{RDD} . To maximize signal intensity, the lowest technically possible dilution factor was selected for all measurements, i.e. $DF_{\text{RDD}} = 18.1$.

$$c_{\text{fr,inlet,N}}(d_p) = \frac{c_{\text{fr,class,N}}(d_p)}{P_{1+}(d_p)} \cdot DF_{\text{RDD}} \quad (10)$$

$$c_{\text{fr,inlet,m}}(d_p) = \frac{c_{\text{fr,class,m}}(d_p)}{P_{1+}(d_p)} \cdot DF_{\text{RDD}} \quad (11)$$

Mass related sensitivity, $S_{\text{ICP,inlet,m}}(d_p)$, and limit of detection, $LoD_{\text{ICP,inlet,m}}(d_p)$, characterizing the overall instrumentation from RDD inlet to ICPMS detection, were calculated analogously to those of only ICPMS. However, due to the size dependent single charge probability included in the calculation of the inlet concentration, these figures of merit are only valid for the selected particle diameters:

$$S_{\text{ICP,inlet,m}}(d_p) = \frac{I_{\text{ICP,net}}(d_p)}{c_{\text{fr,inlet,m}}(d_p)} \quad (12)$$

$$LoD_{\text{ICP,inlet,m}}(d_p) = \frac{3 \cdot \sigma_{\text{ICP,net}}}{S_{\text{ICP,inlet,m}}(d_p)} \quad (13)$$

Sensitivity and limit of detection, related to particle number concentration, characterizing the overall instrumentation, were determined using the particle number instead of the mass concentration:

$$S_{\text{ICP,inlet,N}}(d_p) = \frac{I_{\text{ICP,net}}(d_p)}{c_{\text{fr,inlet,N}}(d_p)} \quad (14)$$

$$LoD_{\text{ICP,inlet,N}}(d_p) = \frac{3 \cdot \sigma_{\text{ICP,net}}}{S_{\text{ICP,inlet,N}}(d_p)} \quad (15)$$

The mass related limit of detection respecting the classified aerosol was then multiplied by DF_{RDD} and divided by the single charge probability of 50 nm particles, $P_{1+}(d_p = 50 \text{ nm})$, in order to obtain the unified $LoD_{ICP,inlet,m,50}$:

$$LoD_{ICP,inlet,m,50} = \frac{LoD_{ICP,class,m}}{P_{1+}(50 \text{ nm})} \cdot DF_{RDD} \quad (16)$$

Finally, $LoD_{ICP,inlet,m,50}$ was divided by the volume of a 50 nm particle and by the element mass density, ρ_{elm} , to determine also the number related, element dependent $LoD_{ICP,inlet,N,50}$:

$$LoD_{ICP,inlet,N,50} = \frac{LoD_{ICP,inlet,m,50}}{\frac{\pi}{6} \cdot (50 \text{ nm})^3 \cdot \rho_{elm}} \quad (17)$$

4.3 Results and discussion of characterization measurements

All plotted curves illustrating SMPS and ICPMS data in the diagrams below, are representing the average of three measuring scans. Volume or number weighted particle size distributions, PSD_V or PSD_N , determined by SMPS, being normalized for the measuring bin width and scaled at the left y-axis as $dV/d\log d_p$ or $dN/d\log d_p$, with units $[\text{nm}^3 \text{cm}^{-3}]$ or $[\text{cm}^{-3}]$, are drawn as dashed grey curves. ICPMS mass or number intensities, $I_{ICP,m}(d_p)$ or $I_{ICP,N}(d_p)$, are scaled at the right y-axis in counts per second [cps] as mass or $[\text{cps nm}^{-3}]$ as number intensity unit. The scaling of the secondary y-axis was selected to fit the SMPS and ICPMS signal curves. The ratio between left and right y-axis scale was set equal within each pair of a mass/volume and a number related diagram. The standard deviation of the net ICPMS signal, $\sigma_{ICP,net}$, determined for each measuring series, underwent the same size-dependent calculation as the measuring data themselves, resulting in mass and number related standard deviations, $\sigma_{ICP,m}(d_p)$ and $\sigma_{ICP,N}(d_p)$. These curves, plotted as wide dashed lines, allow easily deciding whether displayed data really represent measuring intensity, or signal peaks arose from amplified noise.

4.3.1 Magnetite Aerosol

The ICPMS signal from measuring iron without collision gas on $m/z=56$ is suffering from polyatomic interferences. The resulting noise makes ^{56}Fe an appropriate example to discuss data processing and signal quality assessment. Therefore, a model aerosol containing air-borne magnetite nanoparticles was artificially generated and characterized by RDD-SMPS-ICPMS.

Fig. 22A shows the net ICPMS intensity, $I_{ICP,net}(d_p)$, related to the selected particle diameter, actually scanned by SMPS. The inverse single charge probability, $1/P_{1+}(d_p)$, being a size-dependent aerosol property, is drawn as a straight grey curve. Since $I_{ICP,net}(d_p)$ is obtained in equation (2) by subtracting the mean background intensity from the raw signal, negative values do occur when low concentrations were measured, i.e. at small particle diameters in the present example. The noise is

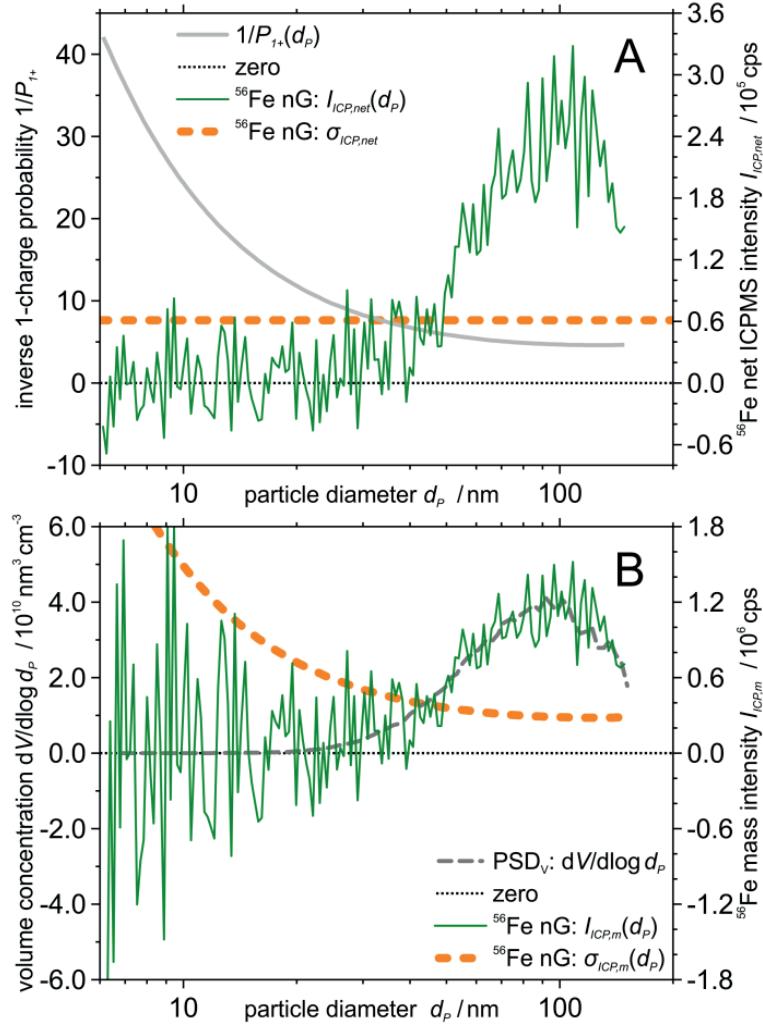


Fig. 22: Magnetite model aerosol, measured without collision gas (nG = no Gas) on isotope ^{56}Fe . (A) $I_{\text{ICP,net}}(d_p)$, net ICPMS intensity. $1/P_{1+}(d_p)$, inverse single charge probability. $\sigma_{\text{ICP,net}}$, standard deviation of net ICPMS signal. (B) $dV/d\log d_p$, volume weighted PSD, determined by the coupled SMPS. $I_{\text{ICP,m}}(d_p)$, ^{56}Fe mass intensity with negative values depicted. $\sigma_{\text{ICP,m}}(d_p)$, mass related standard deviation of ICPMS signal.

homogeneously distributed over the whole particle size range, and $\sigma_{\text{ICP,net}}$, is assumed to be constant over the whole size range. In Fig. 22B, the SMPS determined PSD_V is compared to the ICPMS mass intensity, $I_{\text{ICP,m}}(d_p)$, which was calculated in equation (4) as the product of $I_{\text{ICP,net}}(d_p)$ and $1/P_{1+}(d_p)$. Since $1/P_{1+}(d_p)$ has its minimum around $d_p = 100$ nm (Stober et al., 1991; Wiedensohler & Fissan, 1991), the noise is progressively amplified towards small particles, but, however, remains symmetrically distributed above and below the curve determined by SMPS, i.e. zero at low particle diameters. The mass related standard deviation, $\sigma_{\text{ICP,m}}(d_p)$, was calculated like $I_{\text{ICP,m}}(d_p)$ and therewith increases the same way towards small particles.

In Fig. 23A, the same PSD_V , determined by SMPS, and ICPMS mass intensity, $I_{\text{ICP,m}}(d_p)$, are plotted, but since concentrations cannot be negative, only positive values are shown. $\sigma_{\text{ICP,m}}(d_p)$

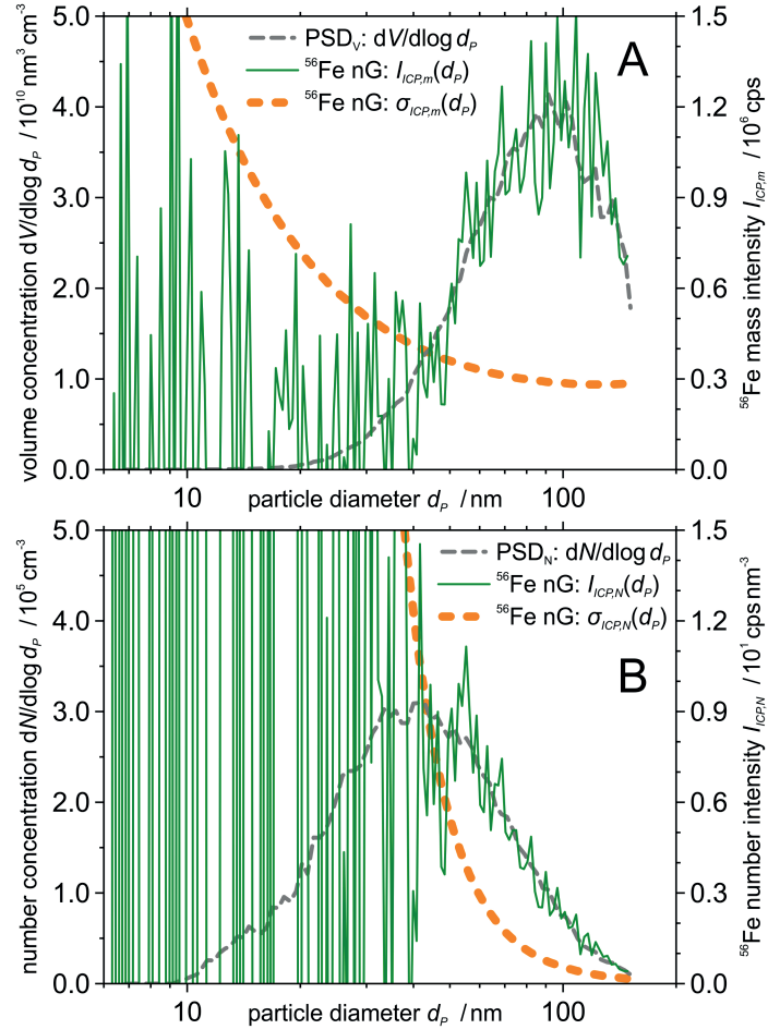


Fig. 23: Magnetite model aerosol, measured without collision gas (nG = no Gas) on isotope ^{56}Fe . (A) $dV/d\log d_p$, volume weighted PSD. $I_{ICP,m}(d_p)$, ^{56}Fe mass intensity, (only positive values displayed). $\sigma_{ICP,m}(d_p)$, mass related standard deviation of ICPMS signal. (B) The same measuring data, but related to particle number instead of volume/mass concentration.

crosses PSD_V at $d_p = 45 \text{ nm}$. At smaller diameters, the noise-dominated ICPMS signal does not provide useful information. Therewith $\sigma_{ICP,m}(d_p)$ appears to be a good criterion to decide, whether concentrations found by SMPS were high enough to induce significant ICPMS intensity, or they were too low and possible ICPMS peaks had occurred due to background noise.

SMPS primarily provides PSD_N , being often used in aerosol science. In Fig. 23B, PSD_N is compared to the number intensity, $I_{ICP,N}(d_p)$, achieved in equation (5) by dividing $I_{ICP,m}(d_p)$ by the assumed particle volume. Therewith the amplification of the ICPMS intensity in terms of conversion from mass to number related signals is inversely proportional to the third power of the particle diameter, and the noise increases even more towards small particles than regarding the mass related signal. However, above the intersection point of PSD_N and $\sigma_{ICP,N}(d_p)$ at 45 nm, the correlation between ICPMS and SMPS signals can be clearly observed on both diagrams.

To demonstrate the capabilities of the presented instrumentation to measure iron with better detection efficiency, the measurements were repeated on the less abundant isotope ^{57}Fe , using helium as collision gas to remove polyatomic interferences, and hence to reduce the background signal. This caused a decrease of the net ICPMS intensity, but at the same time the noise was reduced more drastically, leading to a better signal to noise ratio and therewith signal quality. The resulting mass/volume and number related data are presented in Fig. 24A and B, respectively. $\sigma_{\text{ICP,m}}(d_p)$ and $\sigma_{\text{ICP,N}}(d_p)$ already cross the PSD curves at $d_p = 25$ nm, where the ICPMS signals start to follow the SMPS curves.

In the manufacturer's certificate, provided with the magnetite particles which were used for aerosol generation, a mean particle diameter of 20 nm was announced. A distinctive signal peak at this diameter was not found, neither by SMPS nor ICPMS. This indicates that the 20 nm particles were

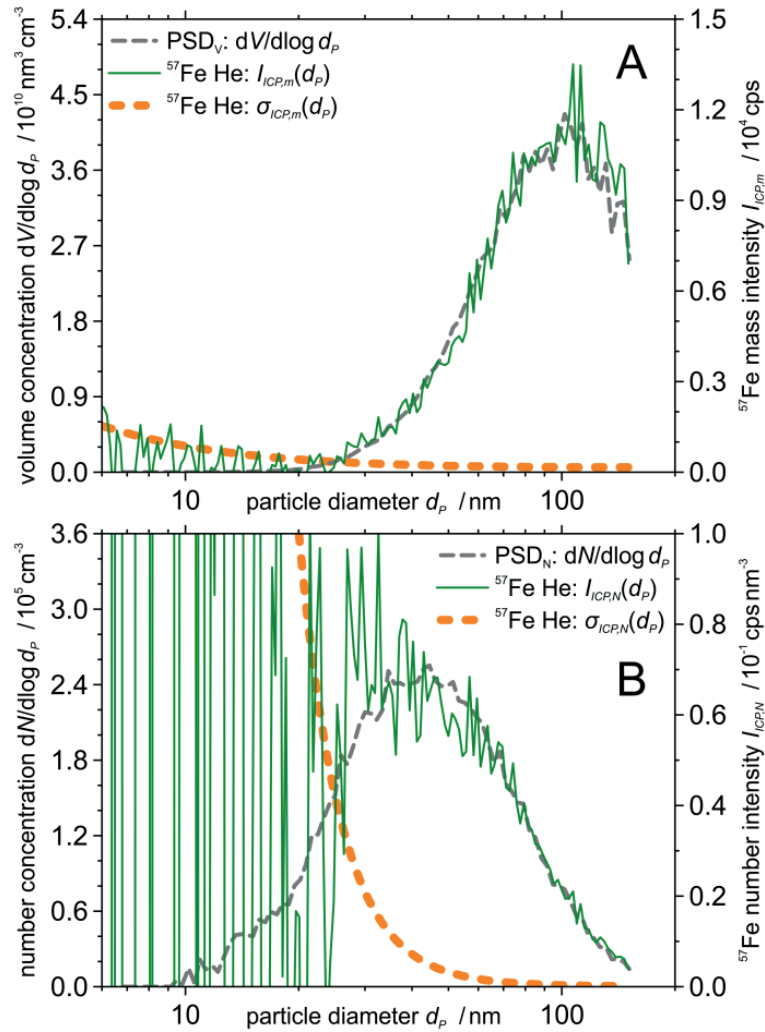


Fig. 24: Magnetite model aerosol, measured with helium as collision gas (He = helium) on isotope ^{57}Fe . (A) $dV/d\log d_p$, volume weighted PSD. $I_{\text{ICP,m}}(d_p)$, ^{57}Fe mass intensity. $\sigma_{\text{ICP,m}}(d_p)$, mass related standard deviation of ICPMS signal. (B) The same measuring data, but related to particle number instead of volume/mass concentration.

mostly agglomerated, and only a small fraction was present as primary particles. Agglomeration might have happened already in the suspension, could be driven by particle diffusion in the aerosol, or caused by several particles forming agglomerates in the shrinking suspension droplets in the diffusion drier. Since the focus was not investigating particle formation and fate, this agglomeration behavior was not further analyzed, e.g. using differently concentrated suspensions or by reducing the droplet size at the aerosol generator. Nevertheless, the good correlation of SMPS and ICPMS signals above 25 nm implies that the state of the aerosol at the RDD-SMPS-ICPMS entrance was successfully measured and characterized.

4.3.2 20 nm gold aerosol – high concentration

Since $m/z = 197$ allows measuring the monoisotopic gold without serious interferences, another aerosol was generated using an aqueous suspension containing 20 nm gold particles, and investigated to demonstrate consistent size and chemical information, obtained by RDD-SMPS-ICPMS. The volume related SMPS signal and ^{197}Au ICPMS mass intensity from measuring this aerosol, plotted in Fig. 25A, show a peak at 22.5 nm. Since SMPS and ICPMS curves correlate very well, it is obvious that this peak represents the expected nominally 20 nm sized gold particles. The more distinct ICPMS than SMPS peak was probably caused by the shorter response time of the ICPMS, which allowed reacting more quickly to concentration changes than the used CPC, while the DMA was scanning the size range.

Some wider distributed particles were found above 26 nm. RDD-SMPS-ICPMS was able to show that these particles were not caused by sample or gas impurities since they were clearly identified as gold particles due to the well correlating SMPS and ICPMS curves. $\sigma_{\text{ICP,m}}(d_p)$ remains very low in the whole size range, therewith the concentrations were high enough to ensure reliable mass related ICPMS intensities. Besides, it can be seen that a high number of small particles leads to a relatively smooth ICPMS mass intensity curve between 20 and 50 nm, compared to the spikier signal above, where similar absolute mass concentration values were detected, but these were originating from a low number of larger particles. Incomplete atomization of these larger particles in the ICP plasma, which cannot be excluded, could possibly be the reason for the slight difference in the right tail of SMPS and ICPMS curves.

Since small particles contribute much stronger to number than to mass/volume concentrations, the 22.5 nm peak is recognized more clearly with respect to the number related data, illustrated in Fig. 25B. Besides, small particles below 20 nm, detected by SMPS, become more significant in this perspective, but $I_{\text{ICP,N}}(d_p)$ did not follow the PSD in this size range. Since $\sigma_{\text{ICP,m}}(d_p)$ is far below the SMPS curve, ICPMS would have been able to detect gold at these concentrations. Therewith, these particles are identified not to consist of gold. This finding seems to be reasonable because smaller gold particles than the 20 nm sized primary ones were not expected. These particles might originate from impurities remaining in the aerosol after the water removal in the diffusion drier.

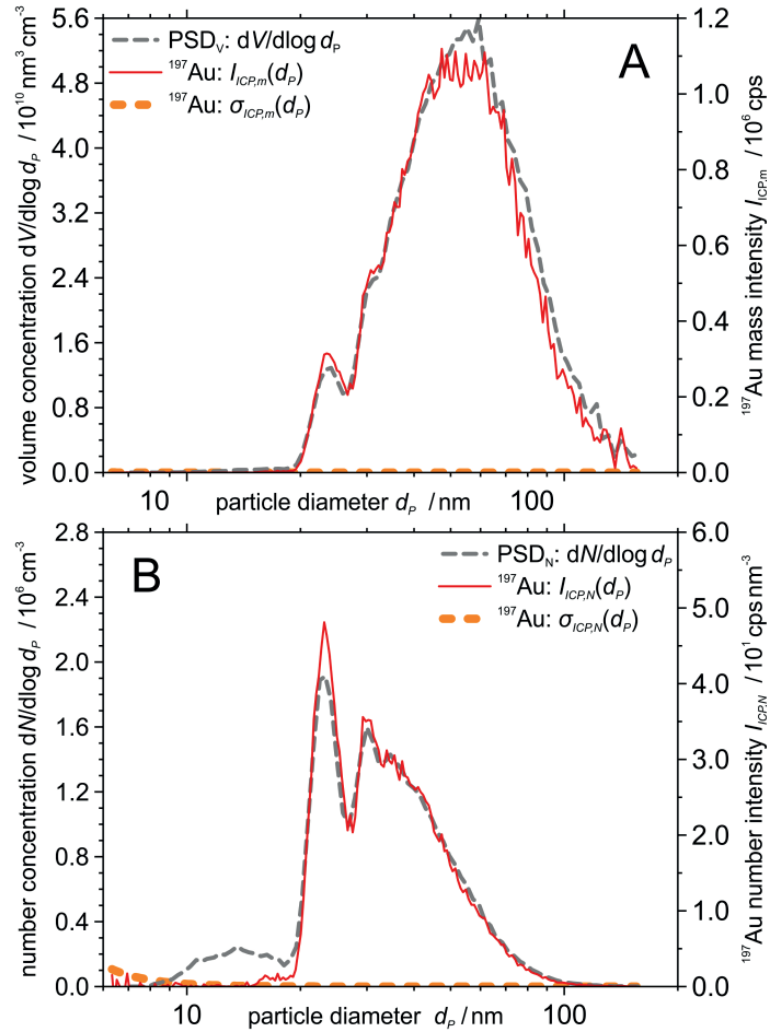


Fig. 25: Model aerosol generated from undiluted 20 nm gold suspension. (A) $dV/d\log d_p$, volume weighted PSD. $I_{\text{ICP,m}}(d_p)$, ^{197}Au mass intensity. $\sigma_{\text{ICP,m}}(d_p)$, mass related standard deviation of ICPMS signal. (B) The same measuring data, but related to particle number instead of volume/mass concentration.

To additionally validate the measuring results, aerosol particles were collected for offline analysis by TEM and STEM. Several of these particles are imaged in the STEM bright-field micrograph, one single particle in the TEM image in Fig. 26. Obviously agglomeration took place and not only primary particles were observed. The secondary particles were very compact. This explains the good agreement between SMPS and ICPMS signals which were converted assuming spherical particles in order to have them comparable to each other. Inversely, lower ICPMS than SMPS concentration curves could be an indicator for measuring loose particle agglomerates. However, in contrast to RDD-SMPS-ICPMS, electron microscopy does not allow recognizing whether the observed particle agglomerates were already present in the aerosol, or they were formed on the TEM grid during or after particle sampling. The primary particles were found to be nearly spherical, and no significantly smaller particles than 20 nm were observed. By applying electron

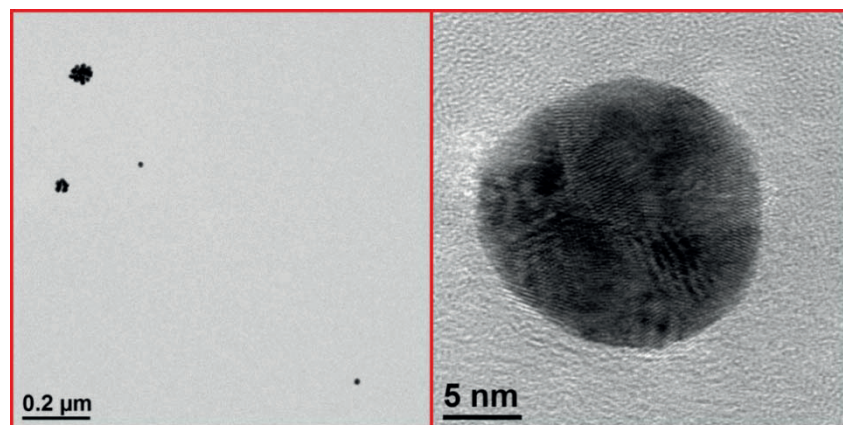


Fig. 26: Model aerosol generated from undiluted 20 nm gold suspension, offline analysis of sampled particles. Left: STEM bright-field overview image showing several collected particles. Right: TEM image of a single gold particle.

dispersive X-ray spectroscopy (EDX) it was confirmed that the particles imaged on the STEM picture were consisting of gold.

4.3.3 20 nm gold aerosol – low concentration

The high dynamic measuring range was demonstrated on a second gold aerosol, being generated using the same suspension, but 100-fold diluted. Considerably less particle agglomeration, hence a more distinct 20 nm peak, was expected with this less concentrated gold aerosol. Indeed, both SMPS and ICPMS signals in Fig. 27 clearly exhibit the expected gold peak between 20 and 40 nm, but there is no significant gold concentration found at particle diameters above 50 nm, in the mass/volume (A) as well as the number (B) related diagram. The SMPS curves indicate wider distributed particles below 20 nm with concentrations in the same order as those found in the highly concentrated aerosol. Again, ICPMS would have been able to detect gold at this level, since $\sigma_{ICP,m}(d_p)$ and $\sigma_{ICP,N}(d_p)$ were very low, compared to the SMPS measured concentrations. $I_{ICP,m}(d_p)$ and $I_{ICP,N}(d_p)$ were nearly zero below 20 nm and did not follow the SMPS curve, confirming the assumption that these were not gold particles.

Curves representing an ideal lognormal PSD with count median diameter $CMD = 14.6$ nm and geometric standard deviation $\sigma_g = 1.36$, were introduced as bright grey lines in both diagrams. The small non-gold particles were found to match very well to this lognormal PSD, which was then subtracted from the initial SMPS curves. Good correlation up to about 30 nm was found between the resulting reduced SMPS signal, represented by dark grey dotted lines, and the ICPMS ^{197}Au signal. The ratio between left and right y-axes could be kept equal to that in the diagrams with data from measuring the highly concentrated gold aerosol, since the ICPMS sensitivity to particulate gold was remaining similar, although the experiments were performed at different days but with the same operating parameters. Only particles contained in the reduced PSDs were consisting of gold and therewith contributing to the ICPMS gold intensity, hence corresponding reduced concentrations were later used to assess the instrument performance based on this measuring series.

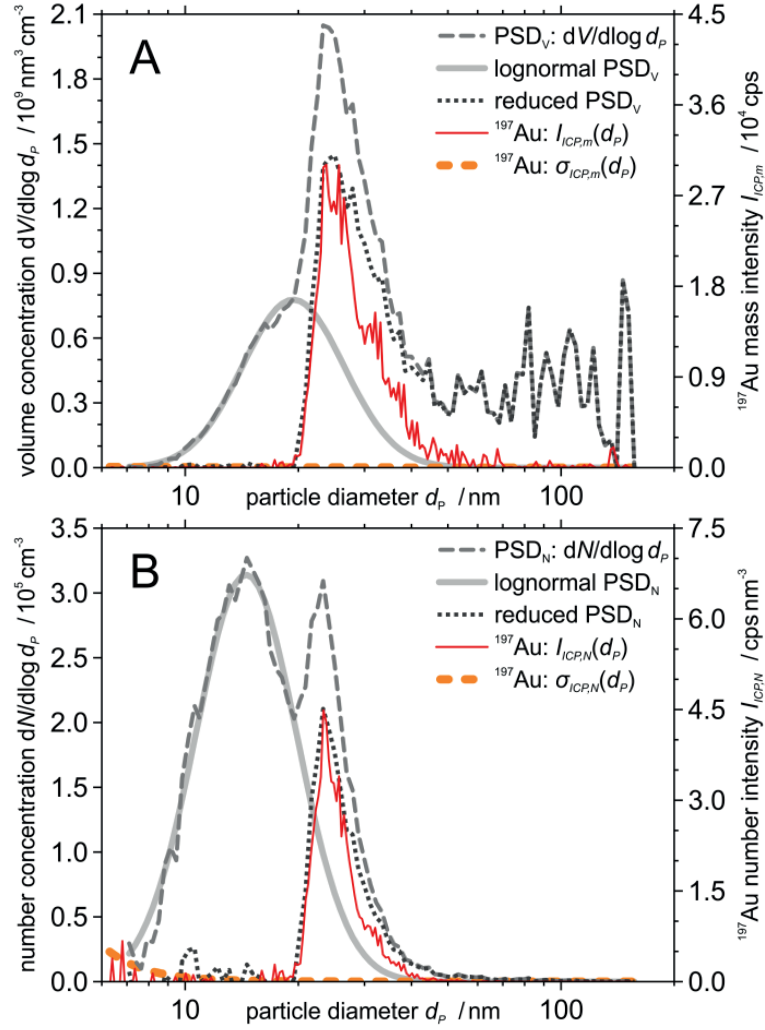


Fig. 27: Model aerosol from diluted 20 nm gold suspension. (A) $dV/d\log d_p$, volume weighted PSD, determined by SMPS. Lognormal PSD_V with $\text{CMD} = 14.6 \text{ nm}$ and $\sigma_g = 1.36$. Reduced PSD_V , difference between SMPS determined PSD_V and the lognormal PSD_V . $I_{\text{ICP,m}}(d_p)$, ^{197}Au mass intensity. $\sigma_{\text{ICP,m}}(d_p)$, mass related standard deviation of ICPMS signal. (B) The same data, but related to particle number instead of volume/mass concentration

Additionally, SMPS detected some larger particles starting at $d_p = 30 \text{ nm}$, contributing much to the volume, but only little to the number concentration. Since the volume concentration in this size range stems from a low number of large particles, the signal became very uneven. These particles were not consisting of gold; otherwise they would have induced a clear but similarly uneven ICPMS signal.

When the measuring series on the aerosol from the low concentrated gold suspension was completed, the DMA and CPC of the SMPS were replaced in order to test another instrumental setting. Due to the duration needed for this rearrangement, the suspension aged, resulting in changed size distribution and Au intensity. This observation is explicated in Appendix A.1.

4.3.4 Mixed gold/silver aerosol

To show the instruments ability to distinguish between particles with different size and composition, a suspension containing both, smaller gold and larger silver particles, was used for generating a mixed aerosol. A reference RDD-SMPS setup, installed in parallel and measuring simultaneously to the coupled, argon operated, instrument, was used to validate the PSD determined by the hyphenated RDD-SMPS-ICPMS. The voltage in the air operated reference DMA was not limited to 4.5 kV but the full voltage range up to 10 kV could be utilized, which allowed scanning from 7.5 to 305 nm. In Fig. 28A, the PSD_V of the mixed Au-Ag aerosol, determined by both SMPS, is plotted, Fig. 28B shows the number related data.

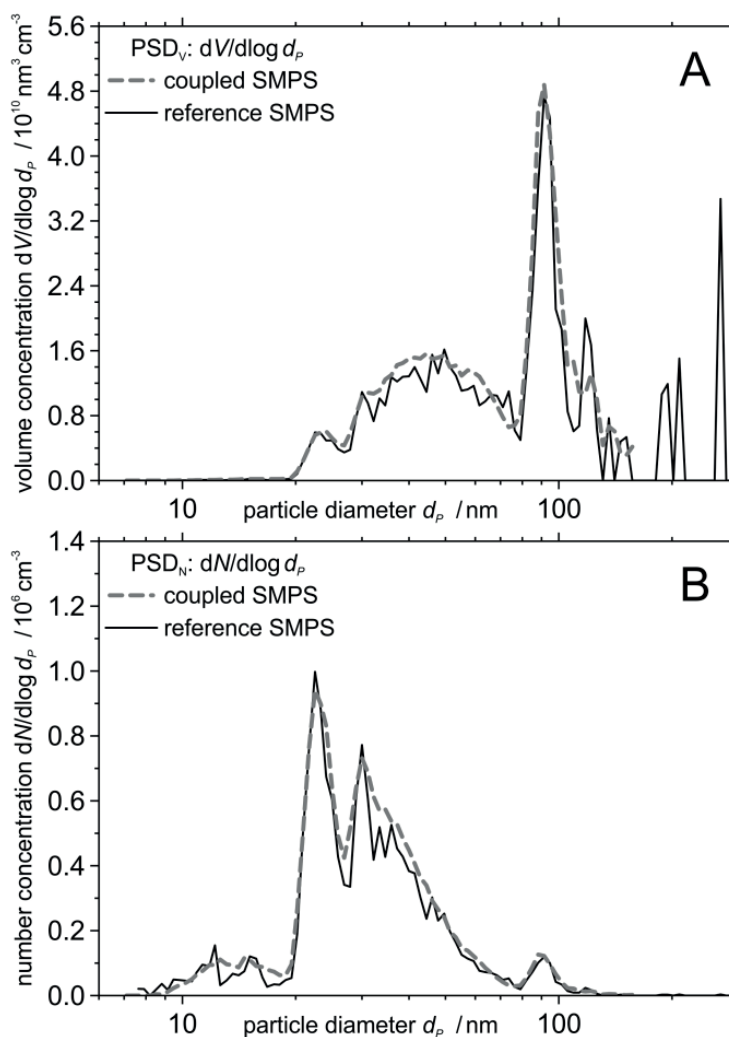


Fig. 28: Model aerosol from mixed gold/silver suspension. (A) $dV/d\log d_p$, volume weighted PSD, determined by the coupled and reference SMPS instruments. (B) The same measuring data, but related to particle number concentration, as originally determined by SMPS.

Basically, the two instruments agree well, but the same reasons as discussed in section 3.2 are causing the PSDs determined by the reference SMPS to appear more spiky, while the coupled instrumentation yielded smoother curves: First, the reference CPC was featuring a response time of 0.8 s which allowed reacting more swiftly on concentration changes during the DMA scans, while the coupled CPC needed about 5 s for 95 % response to a concentration step change. Second, the reference CPC was designed for being able to measure smaller particles and higher number concentrations, by the cost of detection efficiency, since the number of particles reaching the internal detector was only 1/9, compared to that in the coupled CPC. Third, the minimum dilution factor of the coupled RDD was $DF_{\min, \text{cpl}} = 18.1$, that of the reference RDD could not be set below $DF_{\min, \text{ref}} = 28.1$.

The expected peaks corresponding to the nominally 20 and 80 nm sized particles are clearly recognized by both SMPS as 22.5 nm and 89 nm peaks, respectively. The instruments also agree well concerning the wider distributed particles below 20 nm, only visible on the number related diagram, and those between 30 and 75 nm. Since the coupled SMPS was not measuring above 156 nm, a few larger particles were only counted by the reference CPC. In terms of conversion to PSD_v , these large particles were rated to exhibit high volume and therefore induced strong volume peaks in that size range.

While SMPS itself does not provide chemical information, the combination with ICPMS enables to discriminate online between the measured particles regarding their size and elemental composition. Fig. 29 shows the comparison of the volume/mass (A) and number (B) related SMPS-ICPMS signals, resulting from the measurements on the mixed aerosol. The ICPMS ^{197}Au and ^{107}Ag intensities are scaled at the left and right side of the secondary y-axis. The good match of the gold and SMPS curves indicates that the gold sensitivity of ICPMS was still similar to that observed before, since the ratio between the y-axes scaling these two signals was again kept equal to that in the diagrams describing only gold measurements.

The ICPMS signals obviously allow allocating the 22.5 and 89 nm SMPS peaks to the expected gold and silver particles, and the wider distributed particles between 30 and 75 nm are identified as secondary gold particles. Another silver peak, found at about 65 nm, is probably an artefact, originating from larger particles carrying two elemental charges and being therefore classified too small in the DMA (He & Dhaniyala, 2013; Stober et al., 1991). A third peak at about 120 nm might represent silver agglomerates.

Besides, enhanced gold concentration is found at or slightly above 90 nm. The presented RDD-SMPS-ICPMS instrumentation is able to distinguish between chemical elements contained in different particle size fractions. However, the results from measuring the mixed Au-Ag aerosol show a limiting factor of the technique which does not provide information about the particle structure. From the RDD-SMPS-ICPMS data it is not clear whether large gold agglomerates and separate silver particles were present at 95 nm, or if both elements were contained in the same particles. Due to the coincidence of the silver and gold peaks, agglomerates of both primary gold

and silver particles are presumed. Based on the ratio of the two measured intensities, it can be estimated that about 10 primary gold particles were attached to every silver particle, not dramatically changing the overall mobility diameter of the particle. An impression how such an agglomerate could be structured is shown in Fig. 30.

4.3.5 Instrument performance

ICPMS detection performance was assessed by comparing measured ICPMS with concentration information determined by SMPS. Particle mass (index “m”) and number (index “N”) related ICPMS sensitivity, S_{ICP} , and limit of detection, LoD_{ICP} , were calculated for several selected particle size fractions from the measurement series on the model aerosols, characterizing both, ICPMS as isolated subsystem measuring classified particles (index “class”) as well as the overall

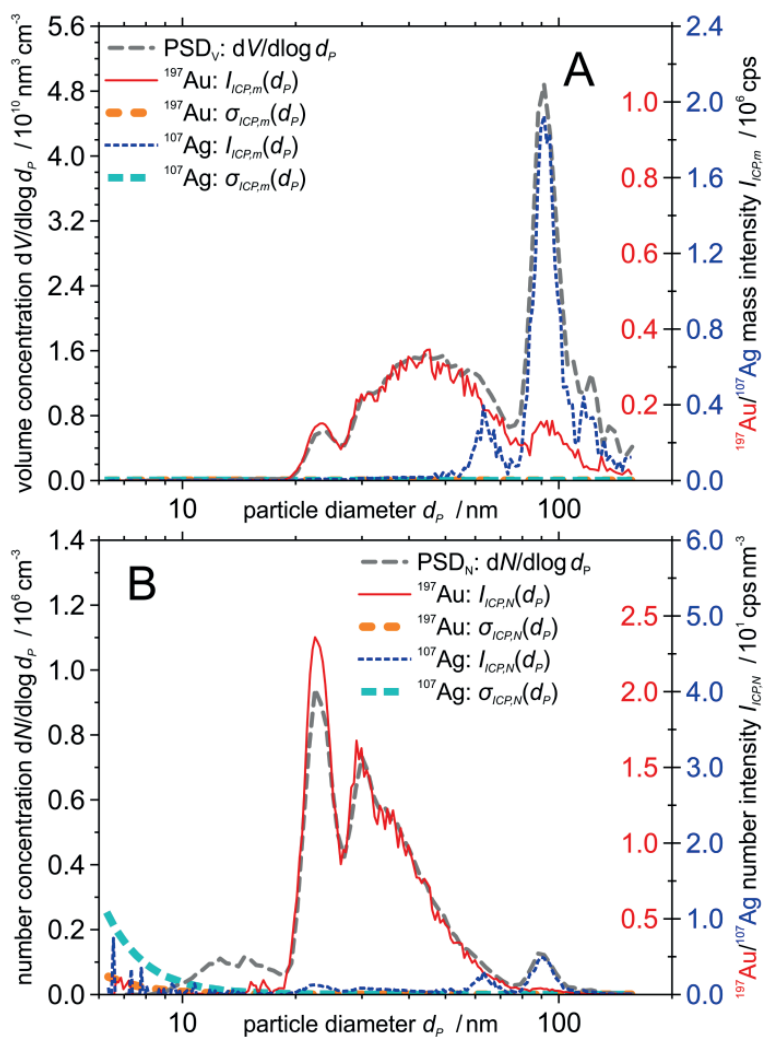


Fig. 29: Model aerosol from mixed gold/silver suspension. (A) $dV/d\log d_p$, volume weighted PSD. $I_{\text{ICP},m}(d_p)$, ^{197}Au and ^{107}Ag mass intensities. $\sigma_{\text{ICP},m}(d_p)$, mass related standard deviations of ICPMS signals. (B) The same measuring data, but related to particle number instead of volume/mass concentration.

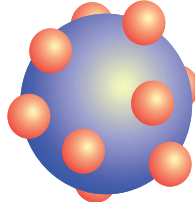


Fig. 30: Presumed structure of a mixed Ag-Au agglomerate leading to the signals at 95 nm from the measurements on the mixed Au-Ag aerosol. Blue: Primary silver particle. Red: Attached gold particles.

instrumentation from RDD inlet to ICPMS detector (index “inlet”). Besides, detection limits of virtually 50 nm sized particles, $LoD_{ICP,inlet,m,50}$ and $LoD_{ICP,inlet,N,50}$, were determined which allow comparing the SMPS-ICPMS performance for detecting different elements on a unified particle diameter, even if the characterization measurements were performed on differently sized particles. The selected size fractions, measured elements, used aerosols, measuring data, and figures of merit are compiled in Table 2.

Table 2: Figures of merit, characterizing both, ICPMS as isolated subsystem, and the complete RDD-SMPS-ICPMS

element	Fe				Au				Ag	
<i>m/z</i> (cell gas)	56 (nG)		57 (He)		197 (nG)				107 (nG)	
aerosol	Magnetite		Magnetite		Au	high	Au low	Au-Ag	Au-Ag	
$\sigma_{ICP,net}$ [cps]	61100		35.7		7.50		1.58	3.94	34.8	
<i>d_p</i> [nm]	49.5	88.0	49.0	89.0	22.7	49.8	23.0	22.9	89.6	114.4
<i>P</i> ₁₊ [-]	0.169	0.209	0.168	0.210	0.095	0.169	0.096	0.096	0.210	0.216
<i>I</i> _{ICP,net} [cps]	7.88 10 ⁴	2.12 10 ⁵	6.01 10 ²	2.26 10 ³	2.63 10 ⁴	1.78 10 ⁵	2.20 10 ³	1.40 10 ⁴	3.79 10 ⁵	7.07 10 ⁴
<i>I</i> _{ICP,m} [cps]	4.67 10 ⁵	1.02 10 ⁶	3.58 10 ³	1.08 10 ⁴	2.76 10 ⁵	1.05 10 ⁶	2.28 10 ⁴	1.46 10 ⁵	1.81 10 ⁶	3.27 10 ⁵
$\dot{n}_{class,CPC}$ [s ^{−1}]	283	148	241	136	1075	824	109	537	134	29
<i>c</i> _{fr,class,m} [fg cm ^{−3}]	13.5	39.7	11.1	37.7	25.5	206.2	2.66	12.99	134.3	28.6
<i>S</i> _{ICP,class,m} [cps fg ^{−1} cm ³]	5836	5347	53.9	60.1	1030	865	826	1076	2824	2469
<i>LoD</i> _{ICP,class,m} [fg cm ^{−3}]	31.4	34.3	1.99	1.78	0.022	0.026	0.006	0.011	0.037	0.042
<i>c</i> _{fr,inlet,m} [fg cm ^{−3}]	1.45 10 ³	3.45 10 ³	1.20 10 ³	3.26 10 ³	4.85 10 ³	2.21 10 ⁴	5.02 10 ²	2.46 10 ³	1.16 10 ⁴	2.40 10 ³
<i>S</i> _{ICP,inlet,m} [cps fg ^{−1} cm ³]	54.3	61.6	0.499	0.694	5.41	8.08	4.38	5.68	32.7	29.4
<i>LoD</i> _{ICP,inlet,m} [fg cm ^{−3}]	3376	2978	215	154	4.16	2.78	1.09	2.08	3.20	3.55
<i>c</i> _{fr,inlet,N} [cm ^{−3}]	6.08 10 ³	2.57 10 ³	5.21 10 ³	2.35 10 ³	4.10 10 ⁴	1.77 10 ⁴	4.10 10 ³	2.04 10 ⁴	2.94 10 ³	2.92 10 ²
<i>S</i> _{ICP,inlet,N} [cps cm ³]	13.0	82.7	0.115	0.964	0.64	10.10	0.54	0.69	129.0	242.0
<i>LoD</i> _{ICP,inlet,N} [cm ^{−3}]	14100	2220	928	111	35.1	2.23	8.88	17.2	0.810	0.432
<i>LoD</i> _{ICP,inlet,m,50} [fg cm ^{−3}]	3359	3666	212	190	2.33	2.78	0.62	1.17	3.96	4.52
<i>LoD</i> _{ICP,inlet,N,50} [cm ^{−3}]	13600	14900	862	773	1.85	2.20	0.49	0.93	5.76	6.59

m/z (cell gas), ICPMS isotope (“nG”, no Gas. “He”, Helium). $\sigma_{ICP,net}$, standard deviation of net ICPMS signal. d_p , diameter of selected particle size fraction. P_{1+} , single charge probability pursuant to Wiedensohler approximation. $I_{ICP,net}$, net ICPMS intensity. $I_{ICP,m}$, ICPMS mass intensity. $\dot{n}_{class,CPC}$, CPC particle counts per time. c_{fr} , concentration of particles attributed to the selected size fraction. S_{ICP} , ICPMS sensitivity. LoD_{ICP} , limit of detection. “class”, referring to classified aerosol and describing ICPMS as isolated subsystem. “inlet”, related to concentrations at the inlet and characterizing the overall setup. “m” and “N”, mass and number related data. “50”, with respect to virtually 50 nm sized particles.

Since SMPS and ICPMS were not automatically synchronized during the measurements but the data were correlated subsequently, and since ICPMS was measuring with different acquisition times, the run time points and therewith the size classes are slightly shifted, and not the exactly same but similar size fractions could therefore be selected to compare different measurements.

The observed sensitivities were in the same order of magnitude when near 23 nm gold particles were measured at three different concentrations. When $m/z = 56, 197$, and 107 signals were assessed, $S_{\text{ICP,class,m}}(d_p)$ was slightly lower for larger than for smaller particles. This might possibly be caused by incomplete ionization of larger particles in the plasma, but since this was not observed for $m/z = 57$, it could also have happened accidentally, especially since the differences were small compared to the diameter or mass ratio of the measured particles. Therewith, the influence of d_p on $LoD_{\text{ICP,class,m}}$, $LoD_{\text{ICP,inlet,m,50}}$, and $LoD_{\text{ICP,inlet,N,50}}$, was found to be very low in the measurements of all elements (Table 2). Since the analyses of the three gold containing aerosols were performed on different days and the instrument running conditions (staining of vacuum cones, tuning parameters, plasma torch alignment) were not the same, different background intensities and signal standard deviations were observed. Nevertheless, due to the high dynamic range of ICPMS, $S_{\text{ICP,class,m}}$ determined in terms of these measurements, was always in the same order, also with respect to different size classes, i.e. 23 and 50 nm. $LoD_{\text{ICP,class,m}}$, $LoD_{\text{ICP,inlet,m,50}}$, and $LoD_{\text{ICP,inlet,N,50}}$ were changing with $\sigma_{\text{ICP,net}}$ during the three experiments. The use of helium as collision gas and measuring at the less abundant isotope ^{57}Fe allowed improving the iron LoD by a factor between 15 and 20, but anyway the determined iron LoD remained two to three orders of magnitude higher than those of gold and silver.

LoD enhancement of the overall instrumentation on all elements would be achieved by directing more classified aerosol to ICPMS instead of CPC, or by setting longer ICPMS dwell times, which would entail reducing the number of measured m/z per measuring series, increasing SMPS scan duration, or reducing the size resolution of the ICPMS signal. As seen in terms of the gold measurements, not only the sensitivity but also background noise is influencing LoD . Generally, ICPMS background signals are kept on low levels by ensuring a clean sample introduction interface, and by operation in cleanest possible environment.

Although $LoD_{\text{ICP,inlet,m,50}}$ is proportional to $LoD_{\text{ICP,class,m}}$, and only the element mass density is needed to additionally calculate $LoD_{\text{ICP,inlet,N,50}}$, these size unified detection limits are helpful key figures for comparing the performance of the overall hyphenated instrumentation with respect to different elemental particle composition.

5 Consumer spray aerosol particle assessment

A first real case application of the RDD-SMPS-ICPMS instrumental setup was carried out on aerosols released by commercial consumer spray products. The highly dynamic behavior of freshly released nanoparticles cannot be monitored adequately by off-line techniques. The SMPS-ICPMS coupling could bridge this gap by offering size classified elemental composition within time spans of several minutes. Such spray experiments were conducted in a glove box, as sketched in Fig. 31. The real-time RDD-SMPS-ICPMS monitoring of these aerosol particles was conducted by Adrian Hess, while Sabrina Losert was responsible for alternative sample investigations, including offline analysis of sampled particles as well as an appraisal of the liquid borne particles in the suspensions before the spray experiment. The publication where the methodology and results of this measurement series were described (Losert, Hess et al., 2015), has been added in appendix A.3.

As an example for such a spray product, a dirt repellant pump spray was measured. In a pre-investigation, the liquid in the spray bottle was analyzed, i.e. the elements, suspended or dissolved in the bulk liquid, were determined by traditional ICPMS analysis. Mainly tin was found as metal, in terms of this pre-characterization. Then the spray experiment was performed. The spray bottle was placed in the glovebox, and three pump strokes were conducted within three seconds. Five different masses were monitored by RDD-SMPS-ICPMS, including $m/z = 118$ and $m/z = 120$, to measure the two most abundant tin isotopes, ^{118}Sn and ^{120}Sn . All m/z were measured with integration time 0.2 s. The results from measuring these aerosol particles are presented in Fig. 32.

(A) shows the particle number concentrations, detected by SMPS. The blue curve represents the PSD_N , recorded in the first scan, starting simultaneous with the first pump stroke. The red and green curves show the second and third size distributions, recorded 3 and 6 minutes after the first scan. Obviously, high number concentrations were measured directly after the spray had been

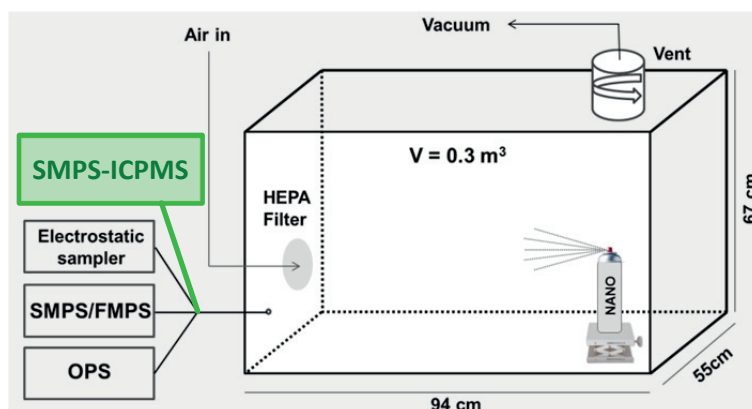


Fig. 31: Experimental setup in a glovebox, to assess the user exposition to ENPs released by spray products.

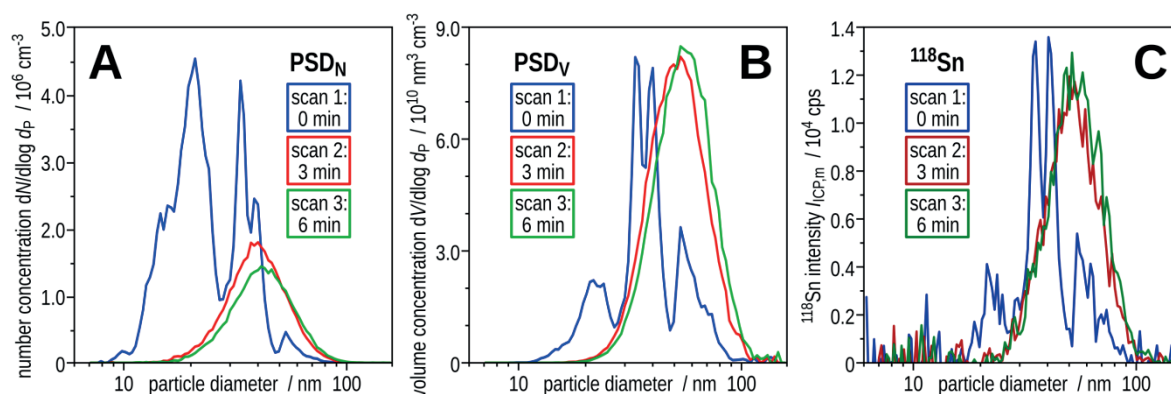


Fig. 32: Assessment of aerosol particles from a tin containing dirt repellent spray. (A) PSD_N, measured by SMPS. (B) PSD_V, calculated from PSD_N, assuming spherical particles. (C) Size-resolved ICPMS mass intensity to monitor ¹¹⁸Sn.

activated. Several concentration peaks were registered at different small particle diameters, between 10 and 50 nm. Three minutes later, the particle number concentrations were reduced to about 40 % of the earlier values, and a lognormal size distribution was established, with the mode at about 40 nm. Another three minutes later, the number concentration was further reduced to about 30 % of the initial level, and the mode was again slightly shifted towards larger particles.

(B) shows the PSD_V, calculated from the data, shown in (A), assuming spherical particles. The different size peaks, detected during the first scan, are more distinct in this perspective, at 20 nm, between 30 and 40 nm, and at about 60 nm. Again, the formation of a lognormal size distribution and a shift towards larger particles is observed on the second and third scan, but, however, the total volume concentration, recognized as the area between each curve and the x-axis, remains in the same order of magnitude.

(C) represents the ICPMS mass intensity of ¹¹⁸Sn. The other ICPMS signals are not shown, since the ¹²⁰Sn curve was very similar, and the intensities of the other measured *m/z* were remaining on the background level. The ¹¹⁸Sn signal matches very well to the PSD_V, indicating that the particles were indeed mainly consisting of tin, or at least the tin content was remaining constant over the measured size range and during all three scans. Therewith, the concentration and size distribution alterations, observed by the SMPS, were caused by particle agglomeration, and not e.g. by particle loss and simultaneous particle growth by condensation of volatile organic matter in the atmosphere.

The hyphenated technique could proof its ability to dynamically observe the nanoparticle behavior, not only with respect to size changes but also to the elemental composition. However, to obtain reliable data, the experiment should be repeated. Since it was found that the two tin isotopes yielded similar signals, and the other elements were not present in the measured particles, the number of monitored *m/z* could be set to one or two instead of five, which would allow reducing the scan duration. The development of the aerosol within the first minutes could then be investigated with higher temporal resolution.

6 Heat treatment of impregnated wood pellets

(partly submitted for publication as: Hess, A., Tarik, M., Foppiano, D., Edinger, P., Ludwig, C. Online Size and Element Analysis of Aerosol Particles Released from Thermal Treatment of Wood Samples Impregnated with Different Salts. Submitted to: *Energy & Fuels*.)

Emissions from biomass incineration and other thermal processes can be seen as aerosols, consisting of a gas mixture and gas-borne particles. Particles in the sub-micrometer size range are usually formed by condensation of evaporated matter in a supersaturated environment. In a highly supersaturated atmosphere, such particles can be formed in the absence of condensation nuclei, but the more common formation mechanism is particle growth around condensation nuclei (Hinds, 2011). Such effects occur inside a flame and after combustion processes, when the temperature decreases and supersaturation is achieved. The assessment of particulate emissions usually includes chemical analysis of the overall aerosol or filtered gases, and the number or mass concentration and size distribution of the gas-borne nanoparticles are determined. Information on the major gaseous compounds, and also on the elemental composition of such process emissions can be obtained online. Likewise, particle size distributions (PSD) are measured with time resolutions in the range of a few minutes or even less (Part, Zecha et al., 2015; Zhang & Morawska, 2002), e.g. using an SMPS.

Several groups have been investigating the effects of different parameters on the release of alkali metals and other elements from the incineration of biomass or fossil fuels (Blasing & Muller, 2012; Kowalski, Ludwig, & Wokaun, 2007). Different elements in process aerosols have been analyzed by ICPOES (Wellinger, Wochele et al., 2012). Measurements by SMPS have been combined with chemical gas and offline particle analysis (Yang, Gebremedhin, & Strand, 2013), and larger particles in industrial emissions have been analyzed offline by ion chromatography and ICPMS (Taiwo, Beddows et al., 2014). Besides, particulate emissions from zinc (Zn) impregnated wood pellets were investigated regarding the Zn content in the fraction of fine particles below 1 μm (Tissari, Sippula et al., 2015), but up to now such information was not available for narrow particle size fractions and with temporal resolutions in the range of a few minutes.

However, element information specifically on the composition of gas-borne nanoparticles emitted by thermal processes is traditionally obtained offline (Vicente, Duarte et al., 2015), especially with the focus on the elemental composition of distinct particle size fractions. Such procedures include particle sampling, sample preparation, and offline analysis, and are therefore time-consuming, entail the risk of sample contamination and other alterations. Moreover, the results of such analyses usually represent longer measuring periods and do not provide time-resolved information.

In order to measure combustion generated aerosols, the RDD-SMPS-ICPMS arrangement was equipped with an Evaporation Tube (ET), to eliminate volatile particle fractions and focus on solid particles, and connected to a Thermogravimetric Analyzer (TGA), wherein a wood pellet was treated thermally, with controlled combustion parameters as temperature, oxygen (O₂) content and other gas flows in the atmosphere surrounding the fuel sample. Using the RDD-SMPS-ICPMS setup, the emitted aerosols were analyzed online, with respect to the PSD and the size-resolved elemental particle composition, with a temporal resolution of 3 min. Differently impregnated wood samples underwent a thermal treatment and were analyzed in this arrangement, to investigate the influence of these impregnations on the formed aerosol particles.

6.1 Experimental details

6.1.1 Instrumental arrangement

A TGA (TGA/STDA851e from Mettler Toledo) had earlier been equipped by Ludwig et al. with a gas quench, named Condensation Interface (CI), to immediately cool and dilute the aerosol released by the TGA sample, to prevent further condensation and particle agglomeration and to preserve the aerosol for subsequent analysis (Ludwig, Wochele, & Jörimann, 2007). This TGA was connected to the RDD-SMPS-ICPMS instrumentation, which was similar to the recently described setup (Hess et al., 2016; Hess et al., 2015), except for the ICPMS instrument (7700 instead 8800 QQQ from Agilent), and the RDD which was further equipped with an ET (ASET15-1 from Matter Aerosol), to bring volatile components of the diluted aerosol into the gas phase, as it is mandatory e.g. for measuring particulate emissions of internal combustion engines, according to the regulation of the Swiss association for standardization (SN277206, 2011), or following the European particle measurement program (Giechaskiel, Dilara et al., 2008). The whole arrangement is sketched in Fig. 33.

6.1.2 Gas flows

All gas flows were maintained by mass flow controllers (MFC) and verified with a primary flow calibrator (Gilibrator-2 from Sensidyne). In order to apply oxidizing conditions to the sample pellet, O₂ was used as reactive gas in the TGA, with a flow of $Q_{\text{re,TGA}} = 18 \text{ mL min}^{-1}$. Argon flows served as sample carrier gas, $Q_{\text{ca,TGA}} = 63 \text{ mL min}^{-1}$, as protective gas to prevent sample aerosol and reactive gas entering the balance chamber, $Q_{\text{pr,TGA}} = 22 \text{ mL min}^{-1}$, and as quench gas in the CI, $Q_{\text{qu,TGA}}$, which was set such that a total flow of 1.0 L min^{-1} resulted at the outlet of the TGA quench interface. The sum of these gas flows was complemented by the gas and particles generated in the furnace, and provided as raw aerosol flow to the RDD head, $Q_{\text{raw,in}} \approx 1.0 \text{ L min}^{-1}$. Since this flow was well-defined, the raw aerosol pump of the RDD, which would normally maintain $Q_{\text{raw,out}}$ and $Q_{\text{raw,in}} = Q_{\text{raw,out}}$, was not used and therefore disconnected.

Argon was also used as sheath gas in the differential mobility analyzer (DMA). To cover the range of larger particles, a low sheath gas flow was set, $Q_{\text{Sheath}} = 3.00 \text{ L min}^{-1}$. Although the ideal ratio

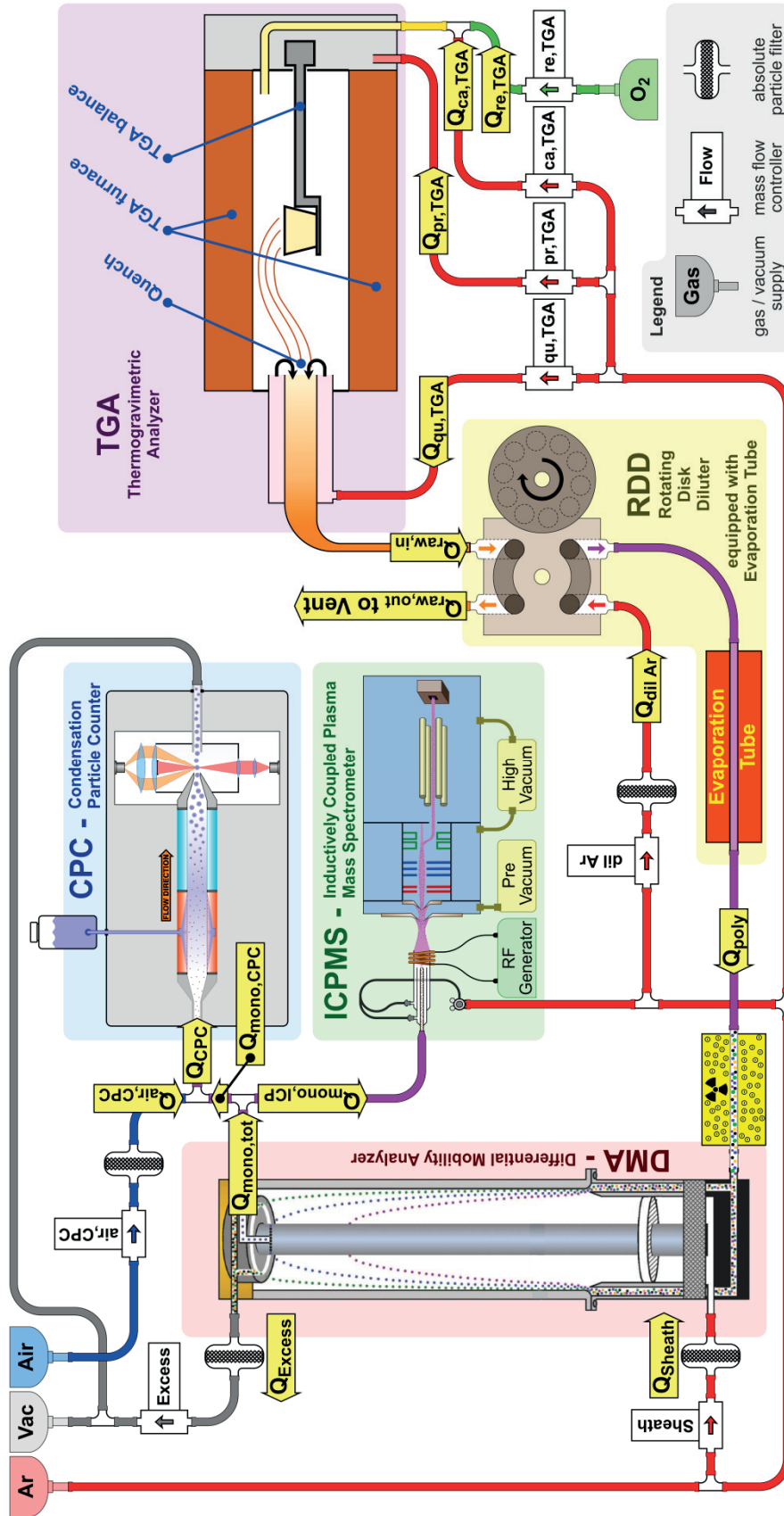


Fig. 33: Experimental TGA-RDD-SMPS-ICPMS setup, with all flows indicated. $Q_{raw,in}$: raw aerosol flow from TGA into RDD. $Q_{raw,out}$: raw aerosol flow released by RDD. $Q_{dil,Air}$: dilution argon flow into RDD. Q_{poly} : diluted polydisperse aerosol provided to DMA by RDD. Q_{sheath} : sheath argon flow. Q_{excess} : excess gas flow at DMA outlet. $Q_{mono,tot}$: total monodisperse flow at DMA outlet. Q_{CPC} : total flow into CPC. $Q_{air,CPC}$: air flow to reduce the monodisperse aerosol fraction consumed by CPC. $Q_{mono,CPC}$ and $Q_{mono,ICP}$: CPC and ICPMS fractions of monodisperse aerosol flow. $Q_{qu,TGA}$: Quench gas flow in the TGA interface. $Q_{pr,TGA}$: Protective gas flow into the TGA balance mechanics. $Q_{ca,TGA}$: Gas flow to carry the generated aerosol out of the TGA furnace. $Q_{re,TGA}$: Reactive gas flow, i.e. O_2 provided to the sample to enable controlled combustion of the wood sample. (DMA scheme adapted from: Scanning Mobility Particle Sizer Brochure of TSI, available on www.tsi.com)

between sample and sheath gas flows of the used DMA type would be 1:10, an increased polydisperse aerosol inlet flow was set, $Q_{\text{poly}} = 0.60 \text{ L min}^{-1}$, to reduce the residence time in the aerosol lines and to increase the CPC and ICPMS signals. The monodisperse flow at the DMA outlet was set equal, $Q_{\text{mono,tot}} = Q_{\text{poly}} = 0.60 \text{ L min}^{-1}$. 30 % of this flow were allocated to the CPC, $Q_{\text{mono,CPC}} = 0.18 \text{ L min}^{-1}$, and 70 % to the ICPMS, $Q_{\text{mono,ICP}} = 0.42 \text{ L min}^{-1}$.

6.1.3 Instrument settings

After introducing a sample into the TGA at room temperature, a drying period of 10 min at 105 °C was applied as first step of the TGA program. The temperature was then increased, with a constant heating rate of 5 °C min^{-1} , to 950 °C. This final temperature was kept for 30 min, so the total experiment duration was 209 min. The RDD diluter head temperature was set to $T_{\text{RDD}} = 80 \text{ °C}$. After a pre-experiment, performed without ET, large sedimented particles and sticky droplets had been observed on the impactor, installed at the inlet of the reference SMPS. To focus on the primarily emitted solid particles, volatile particle compounds were then vaporized in the ET at $T_{\text{ET}} = 350 \text{ °C}$, and no such staining was found on the impactor after the experiments performed with this arrangement. The RDD dilution factor was set to the technically possible minimum under argon operation, $DF_{\text{RDD}} = 18.1$. The DMA voltage was scanned between 10 V and 4.5 kV, covering the particle size range between 13.3 nm and 340 nm. The RF power to induce the plasma at the ICPMS inlet was set to 1350 W, the sampling depth was 8 mm, and $0.58 \text{ L}_\text{N} \text{ min}^{-1}$ argon was added to the plasma torch as dilution gas.

A non-treated natural sawdust sample was digested in acid and conventionally analyzed by ICPMS, in order to find the chemical elements potentially contained in the later emitted aerosols. Sodium (Na), magnesium (Mg), potassium (K), and a trace of copper (Cu) were found. The detected concentrations are listed in Table 3. ^{13}C , ^{23}Na , ^{35}Cl , ^{37}Cl , ^{39}K , ^{63}Cu , and ^{65}Cu were monitored in the first experiment, when a pellet from natural sawdust was treated in the TGA. In all other measurements, additionally ^{34}S was screened. Due to the high carbon concentration in the generated aerosol, the integration time of the mass-to-charge ratio $m/z = 13$ was set 0.05 s, those of all others m/z were 0.25 s each.

Since already the primary particle carrier gas was mainly argon in this application, the Wiedensohler approximation using the standard coefficients was not suitable. Adapted calculation coefficients were used to consider that argon with less than 0.1 % O_2 was used as particle carrier gas when passing the aerosol neutralizer (Wiedensohler, 1989).

Table 3: Element analysis of the non-treated sawdust

Potassium (K)	Magnesium (Mg)	Sodium (Na)	Copper (Cu)
$1327 \pm 23 \text{ } \mu\text{g g}^{-1}$	$147.2 \pm 2.5 \text{ } \mu\text{g g}^{-1}$	$2.00 \pm 0.05 \text{ } \mu\text{g g}^{-1}$	$1.20 \pm 0.01 \text{ } \mu\text{g g}^{-1}$

6.1.4 Sample Preparation

The first presented experiment was performed with natural beech wood sawdust. For each of the following experiments, a batch of 2 g sawdust was either impregnated with a salt solution, or treated with pure water. Since Cu is widely used in plant protection agents, two cupric salts were selected for impregnating the sawdust, to compare the Cu release during the thermal treatment. These salts were copper sulfate (CuSO_4) and copper chloride (CuCl_2). To see whether or not additional chlorine (Cl) would affect the Cu release, two more impregnations were applied to further sawdust batches, one with only potassium chloride (KCl), the other with both CuSO_4 and KCl. Finally, a sample was treated with pure water, to verify that the observed changes were caused by the addition of the salts and not due to osmotic effects during the impregnation.

A typical value for the Cu concentration in Swiss urban waste wood is 30 ppm (Hasler, Nussbaumer, & Bühler, 1995), and a first pre-experiment was performed with a wood pellet, impregnated with CuSO_4 to achieve this concentration. With this configuration, no particulate Cu release was detected. To see whether the Cu signal was missing due to limitations of the instrumentation or because of the thermal behavior of the fuel sample, the CuSO_4 concentration was increased, resulting in a Cu concentration of 0.3 %.

Based on previous studies, Cu is expected to evaporate as chloride (e.g. CuCl_2) (Jakob, Stucki, & Struis, 1996). Considering the stoichiometry of the chloride formation, the KCl amount in the respecting solutions was dosed to provide Cl in excess, namely $\text{Cl}:\text{Cu} = 4:1$ (mol).

The weight of each sawdust batch, before the impregnation, was $m_{\text{Wood}} = 2$ g. The amount of copper(II) sulfate pentahydrate ($\text{CuSO}_4 \cdot 5\text{H}_2\text{O}$; puriss. p.a., cryst. > 99 %, from Fluka), used for the CuSO_4 impregnation, was $m_{\text{CuSO}_4} = 23.85$ mg. With the molar masses of Cu and $\text{CuSO}_4 \cdot 5\text{H}_2\text{O}$, $M_{\text{Cu}} = 63.55 \text{ g mol}^{-1}$ and $M_{\text{CuSO}_4} = 249.68 \text{ g mol}^{-1}$, the Cu concentration in the impregnated sawdust was:

$$c_{\text{Cu}} = \frac{m_{\text{Cu}}}{m_{\text{tot}}} = \frac{m_{\text{CuSO}_4} \cdot \frac{M_{\text{Cu}}}{M_{\text{CuSO}_4}}}{m_{\text{CuSO}_4} + m_{\text{Wood}}} = \frac{23.85 \cdot \frac{63.55}{249.68}}{2000 + 23.85} = 0.003 = 0.3 \% \quad (18)$$

The copper(II) chloride dihydrate ($\text{CuCl}_2 \cdot 2\text{H}_2\text{O}$; p.a., from Merck) amount, used for the CuSO_4 impregnation, was $m_{\text{CuCl}_2} = 16.23$ mg. With the molar mass of $\text{CuCl}_2 \cdot 2\text{H}_2\text{O}$, $M_{\text{CuCl}_2} = 170.48 \text{ g mol}^{-1}$, the Cu concentration in the sawdust batch became:

$$c_{\text{Cu}} = \frac{m_{\text{Cu}}}{m_{\text{tot}}} = \frac{m_{\text{CuCl}_2} \cdot \frac{M_{\text{Cu}}}{M_{\text{CuCl}_2}}}{m_{\text{CuCl}_2} + m_{\text{Wood}}} = \frac{16.23 \cdot \frac{63.55}{170.48}}{2000 + 16.23} = 0.003 = 0.3 \% \quad (19)$$

6 Heat treatment of impregnated wood pellets

The potassium chloride (KCl) amount in the CuSO_4 -KCl impregnated sawdust batch was chosen such that a molar ratio of $\text{Cl}:\text{Cu}=4:1$ was achieved. With the molar mass of KCl, $M_{\text{KCl}} = 74.55 \text{ g mol}^{-1}$, the desired concentration was therewith:

$$c_{\text{KCl}} = c_{\text{Cu}} \cdot \frac{4 \cdot M_{\text{KCl}}}{M_{\text{Cu}}} = \frac{4 \cdot 74.55}{63.55} = 0.014 = 1.4 \% \quad (20)$$

The amounts of KCl (KCl; puriss. p.a., >99.5 %, from Fluka) and $\text{CuSO}_4 \cdot 5\text{H}_2\text{O}$, used in the mixed $\text{CuSO}_4 \cdot 5\text{H}_2\text{O}$ -KCl impregnation, were $m_{\text{KCl}} = 28.90 \text{ mg}$ and $m_{\text{CuSO}_4} = 24.20 \text{ mg}$ resulting in the desired concentrations:

$$c_{\text{KCl}} = \frac{m_{\text{KCl}}}{m_{\text{tot}}} = \frac{m_{\text{KCl}}}{m_{\text{KCl}} + m_{\text{CuSO}_4} + m_{\text{Wood}}} = \frac{28.90}{2000 + 28.90 + 24.20} = 0.014 = 1.4 \% \quad (21)$$

$$c_{\text{Cu}} = \frac{m_{\text{Cu}}}{m_{\text{tot}}} = \frac{m_{\text{CuSO}_4} \cdot \frac{M_{\text{Cu}}}{M_{\text{CuSO}_4}}}{m_{\text{KCl}} + m_{\text{CuSO}_4} + m_{\text{Wood}}} = \frac{24.20 \cdot \frac{63.55}{249.68}}{2000 + 28.90 + 24.20} = 0.003 = 0.3 \% \quad (22)$$

To impregnate a sawdust batch with only KCl, but with the same concentration as in the mixed sample, $m_{\text{KCl}} = 28.56 \text{ mg}$ were used. The resulting KCl concentration was then:

$$c_{\text{KCl}} = \frac{m_{\text{KCl}}}{m_{\text{tot}}} = \frac{m_{\text{KCl}}}{m_{\text{KCl}} + m_{\text{Wood}}} = \frac{28.56}{2000 + 28.56} = 0.014 = 1.4 \% \quad (23)$$

For each experiment with treated sawdust, the desired salt amount was dissolved in 15 ml ultrapure water. The salt solution or pure water was added to 2 g of sawdust in a beaker, later closed with paraffin film. The mixture was stirred with a magnetic stirrer for 4 hrs at room temperature and then poured into a glass dish. Residues in the beaker were rinsed with 3 ml ultrapure water and added to the sawdust slurry. The sample was heated in a drying oven for 90 min at 105°C . The dried sawdust was then stirred manually, using a spatula, and the residues at the bottom and the wall of the dish were carefully scraped off and mixed with the sawdust.

To prepare the sample fuel pellets, a stainless steel die (P0808 from msscscientific) with diameter 10 mm was filled with 200 mg of sawdust. The port at the bottom of the die was connected to a vacuum pump, and a force of 60 kN was applied to the stamp for 60 sec in order to form each pellet. The disk-shaped pellets with a diameter of 10 mm and a thickness of roughly 2.5 mm were again weighted. The sawdust batches, their treatments, and the masses of the pellets, which were finally used in the experiments, are listed in Table 4.

The residues, remaining in the TGA crucibles after the experiments with the natural and the impregnated samples, were acid digested, and the same elements were conventionally analyzed by ICPMS, as had been measured by the coupled instrumentation.

Table 4: Fuel samples used for all experiments

Sample name	Batch weight ^a	First salt	Second salt	Pellet weight ^b
Natural	no batch	no sawdust treatment, no salts added		199.8 mg
H ₂ O	2.0 g	water treatment, without salts added		200.4 mg
KCl	2.0 g	28.6 mg KCl	- -	200.9 mg
CuSO ₄	2.0 g	23.9 mg CuSO ₄ ·5H ₂ O	- -	201.2 mg
CuCl ₂	2.0 g	16.2 mg CuCl ₂ ·2H ₂ O	- -	200.0 mg
CuSO ₄ -KCl	2.0 g	24.2 mg CuSO ₄ ·5H ₂ O	28.9 mg KCl	200.9 mg

^aAmount of sawdust which underwent impregnation or water treatment.^bWeight of the pellet which was finally used for the experiment.

6.1.5 Weight information obtained by TGA

The weight recorded by the TGA balance right after the 10 min drying period at $T_{TGA} = 105\text{ }^{\circ}\text{C}$, W_{105} , was considered as start weight of each sample undergoing the thermal treatment. For all samples, the remaining weights at $T_{TGA} = 500\text{ }^{\circ}\text{C}$ and at the end of the experiment at $T_{TGA} = 950\text{ }^{\circ}\text{C}$, $W_{500,\{\text{sample}\}}$ and $W_{950,\{\text{sample}\}}$, were read from the TGA data, and the relative weight fractions at those temperatures were calculated:

$$RW_{T,\{\text{sample}\}} = \frac{W_{T,\{\text{sample}\}}}{W_{105,\{\text{sample}\}}} \quad (24)$$

The differences of the relative weights of all treated samples at these temperatures were compared to those of the natural sample, in order to recognize the influence of the treatments onto the behavior during the thermal process:

$$\Delta W_{T,\{\text{sample}\}} = RW_{T,\{\text{sample}\}} - RW_{T,\text{natural}} \quad (25)$$

6.2 Results of the heat treatment experiments

6.2.1 TGA data

The signals recorded during the TGA experiments are plotted in Fig. 34. The lower x-axis indicates the experiment run time, the top axis the corresponding TGA temperature. The sample weight is logarithmically scaled at the y-axis. In all experiments, about 60 % of the dried wood sample was converted to gas or aerosol between 38 and 52 min after the experiment start, when the temperature was increasing from $T_{TGA} = 235$ to $310\text{ }^{\circ}\text{C}$. These were probably the hemicellulose and lignin fractions of the wood (Babrauskas, 2002). After 85 min ($480\text{ }^{\circ}\text{C}$), also the cellulose fraction was oxidized, and about 0.7 % of the initial weight of the natural sample was left. Obviously, the water treatment or the subsequent drying step was influencing the behavior of the fuel samples between

6 Heat treatment of impregnated wood pellets

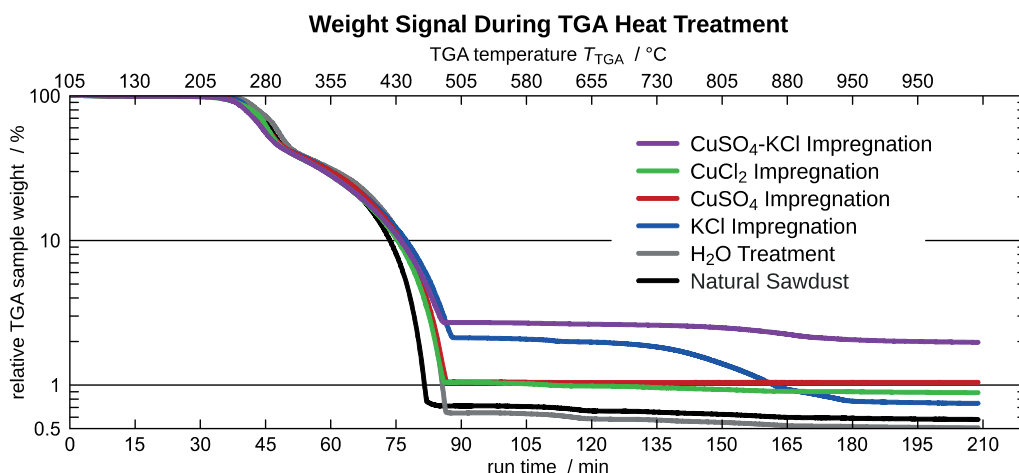


Fig. 34: TGA signal recorded during the thermal treatment of all wood sawdust pellets. Lower and upper x-axes: experiment run time and TGA temperature. The sample weight is logarithmically scaled, to represent also weight loss in the second part of the experiment. The curves are normalized, considering the weight after the initial 10 min drying period to be 100 %.

300 and 500 °C, the weight loss of the treated samples was slightly faster than that of the natural sample. After 89 min (500 °C), the combustion of the organic fraction was accomplished and a stable state was reached in all experiments.

The remaining relative weight fractions of all pellets at 500 °C (89 min) and at 950 °C (209 min), $RW_{T,\{sample\}}$, are listed in Table 5, as well as their differences to those of the natural fuel sample, $\Delta W_{T,\{sample\}}$.

$\Delta W_{500,KCl}$ was very close to the added KCl amount in the impregnation. The most part of this surplus was released later, at temperatures above 500 °C. The values of $\Delta W_{500,CuSO_4}$ and $\Delta W_{500,CuCl_2}$ match the Cu amount in the impregnations well. However, the $CuCl_2$ sample lost further weight at

Table 5: Residues of all fuel pellet samples at 500 °C and 950 °C

Sample name	RW_{500}^a	RW_{950}^b	ΔW_{500}^c	ΔW_{950}^d
Natural	0.72 %	0.58 %	-	-
H ₂ O	0.64 %	0.51 %	- 0.08 %	- 0.07 %
KCl	2.12 %	0.75 %	1.41 %	0.17 %
CuSO ₄	1.05 %	1.05 %	0.33 %	0.47 %
CuCl ₂	1.04 %	0.89 %	0.33 %	0.31 %
CuSO ₄ -KCl	2.71 %	1.98 %	1.99 %	1.40 %

^a RW_{500} , Weight fraction remaining in the TGA after 89 min, at 500 °C, relative to the start weight of the dried sample after the initial 10 min period at 105 °C. ^b RW_{950} , Final residue after experiment completion. ^c ΔW_{500} , Difference between the remaining fraction of each impregnated fuel sample after 89 min (500 °C), compared to the natural pellet. ^d ΔW_{950} , Difference between the final residue of the impregnated and the natural fuel samples.

higher temperatures, like the natural sample, while the weight of the CuSO_4 sample was remaining constant.

In the experiment with the CuSO_4 -KCl impregnated sample, $\Delta W_{500, \text{CuSO}_4\text{-KCl}}$ was higher than the sum of $\Delta W_{500, \text{CuSO}_4}$ and $\Delta W_{500, \text{KCl}}$, and the weight loss in the second period was lower than that of the KCl sample. This possibly indicates that the CuSO_4 was reacting with KCl and forming other species, such as K_2SO_4 , leading to a reduced weight loss. This appears to be consistent with the observation that in the final period at constant 950°C , the loss per time of the CuSO_4 -KCl sample was about twice as high as that of the other samples, since these secondary species might evaporate at higher temperatures. The observed values with the water treated sample were very similar to those measured with the natural one.

6.2.2 SMPS-ICPMS results

To correlate the data from SMPS and ICPMS, and to visualize the development of both, the PSD_v , determined by SMPS, and the distribution of the different elements on particle size fractions, measured by ICPMS, self-written Matlab code was used to create color map diagrams. The run time and TGA temperature are indicated on the lower and upper x-axes. The particle diameter is logarithmically scaled on the y-axis. The area, span by the x- and y-axes, is filled with colors, representing the particle concentrations or ICPMS mass intensities, related to specific particle size fractions and to the experiment run time or TGA temperature. The colors are logarithmically scaled, as indicated by the scale bar at the right of the diagram area.

Natural wood

The first particle emissions from the natural sample were observed after about 30 min, at temperatures above 200°C , as can be seen in Fig. 35, representing the development of the PSD during the TGA experiment. At about 280°C , particle volume concentrations of up to $3 \cdot 10^{14} \text{ nm}^3 \text{ cm}^{-3}$ were observed at about 100 nm in the $dV/d\log d_p$ representation. In this temperature range, the TGA had recorded the highest sample weight decrease. Another increased particle release was observed at about 460°C , when the combustion of the organic fraction was almost completed (Fig. 34). However, these particle volume concentrations were about 4 orders of magnitude lower than those at 280°C , and the mode of this size distribution was at about 30 nm. At 655°C , and when the final 950°C was reached, particle concentrations in the same order of magnitude were detected, with modes around 20 nm.

In a similar manner, the time and particle size resolved ICPMS mass intensity of the carbon isotope ^{13}C is displayed in Fig. 36. Very high carbon concentrations were found between 35 and 85 min, at temperatures between 230 and 480°C , when also the TGA had recorded the highest weight decrease, during the combustion of the organic wood fraction. The measured concentrations are nearly constant over the whole particle size range, indicating that the intensity mainly arose from gaseous and not particulate carbon, since otherwise certain particle diameters would be emphasized. A gradual decrease from 10^6 cps at 13 nm to about $2 \cdot 10^5$ cps at 100 nm appears in the

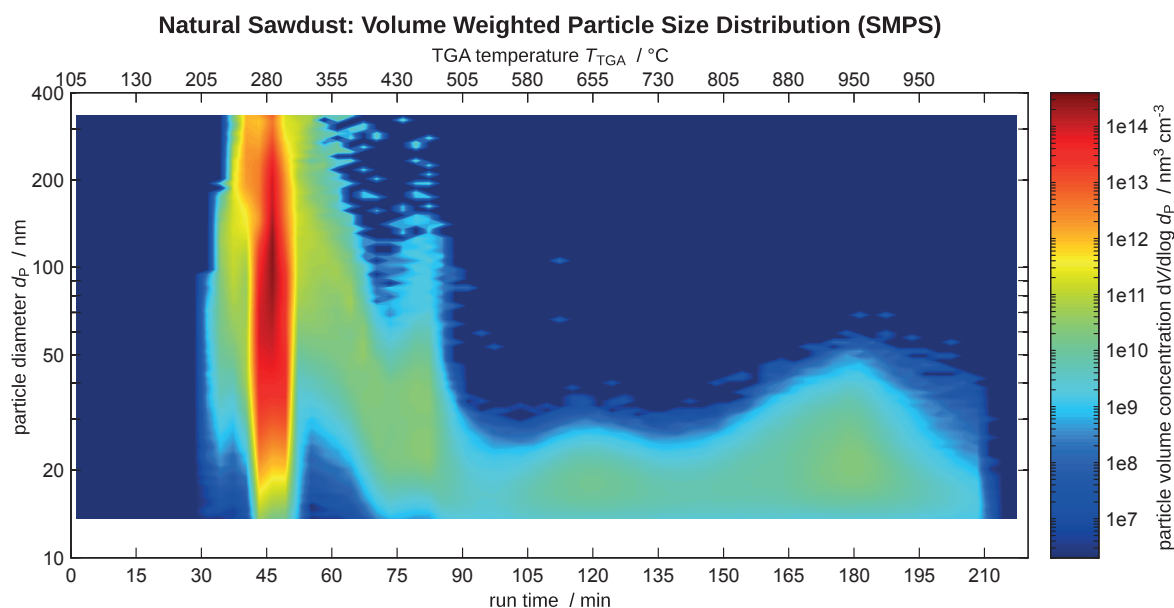


Fig. 35: Development of the volume weighted PSD of aerosol particles, emitted by the pellet, pressed from natural sawdust, during the TGA experiment, measured by SMPS. Lower and upper x-axes: run time and TGA temperature. Diagram y-axis: Logarithmically scaled particle diameter. The colors represent the logarithmically scaled particle volume concentrations, as indicated on the color bar at the right side.

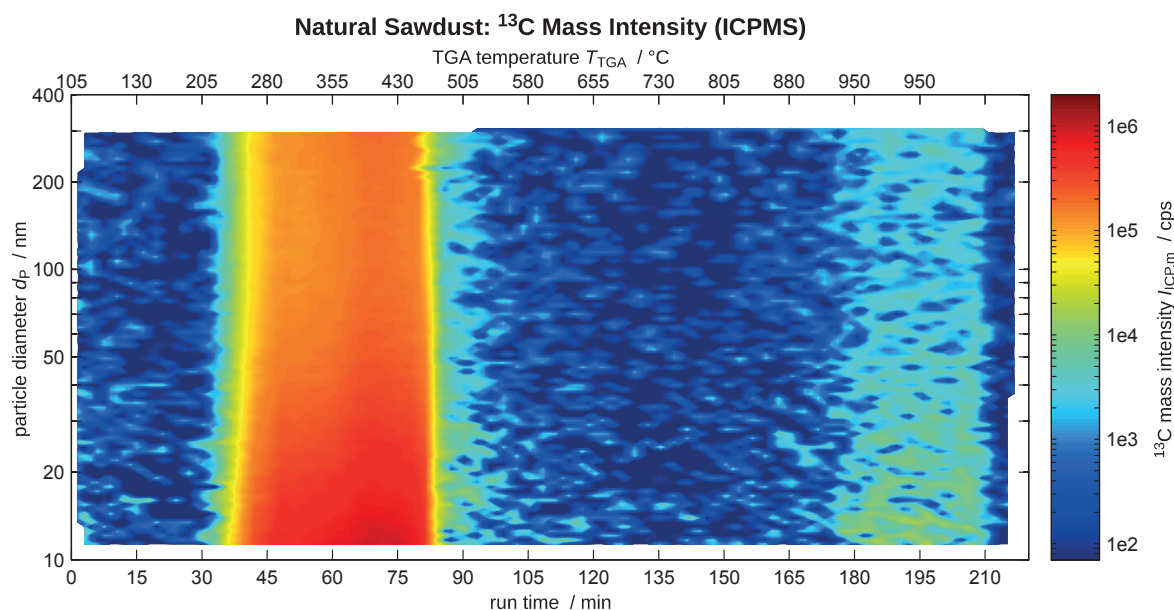


Fig. 36: Particle size related ICPMS mass intensity on $m/z = 13$, given in counts per second (cps). The data are presented the same way as the volume weighted PSD measured by SMPS, and allow a qualitative observation of the carbon release during the TGA experiment with the pellet from natural sawdust.

diagram since not the raw or net ICPMS intensity is visualized, but a signal which was converted to correctly reflect particulate element mass concentrations. The correction factor used for this conversion considers the probability of particles to carry one elemental charge, and is a size-dependent particle property (see Fig. 22A).

The particulate carbon fraction in this period would have been higher if no ET had been used to convert volatile matter into the gas phase, and volatile particles far above the classifying range of the DMA were expected. However, the ET allowed focusing on solid particles, and hardly reproducible effects like uncontrolled particle growth due to condensation were avoided. The weak ^{13}C signal at 950°C had also been observed in the blank measurement, and hence did not originate from the sample itself, but from carbonaceous impurities in the TGA furnace.

The sample weight loss rate determined by the TGA at 280°C was about $\dot{m}_{\text{wood}} = 10 \text{ mg min}^{-1}$. As an approximation, the stoichiometric wood composition was assumed to be $\text{CH}_{1.4}\text{O}_{0.7}$ (Behrendt, Neubauer et al., 2008). With the molar masses of C, H, and O, $M_{\text{C}} = 12 \text{ g mol}^{-1}$, $M_{\text{H}} = 1 \text{ g mol}^{-1}$, and $M_{\text{O}} = 16 \text{ g mol}^{-1}$, the carbon content in the dried wood mass can be estimated:

$$f_{\text{C}} = \frac{M_{\text{C}}}{M_{\text{CH}_{1.4}\text{O}_{0.7}}} = \frac{12}{12 + 1.4 \cdot 1 + 0.7 \cdot 16} = 0.49 \quad (26)$$

Hence, the carbon release in this period was roughly $\dot{m}_{\text{C}} = f_{\text{C}} \cdot \dot{m}_{\text{wood}} = 4.9 \text{ mg min}^{-1}$. The integrated particle volume concentration measured at the same time by the SMPS was $c_{\text{part,V}} = 1.2 \cdot 10^{14} \text{ nm}^3 \text{ cm}^{-3}$. With the total aerosol flow, $Q_{\text{raw,in}} \approx 1.0 \text{ L min}^{-1} = 10^3 \text{ cm}^3 \text{ min}^{-1}$, the particulate volume flow, $\dot{V}_{\text{part}} = 1.2 \cdot 10^{17} \text{ nm}^3 \text{ min}^{-1}$, can be estimated. With an assumed particle density, $\rho_{\text{part}} = 1 \text{ g cm}^{-3} = 10^{-18} \text{ mg nm}^{-3}$, the particulate mass flow is estimated to be in the order of $\dot{m}_{\text{part}} = 0.12 \text{ mg min}^{-1}$, which is 2.5 % of the total carbon mass. Only about 10 % of all particles were classified in the DMA due to the probability of particles to carry one elemental charge, i.e. the probability to be correctly classified in the SMPS, and only a narrow fraction of the remaining particles was passing the DMA at a particular time, due to the size scanning procedure. Therefore the contribution of the classified particles to the total ^{13}C intensity was far below the standard deviation of the ICPMS background signal. This calculation is based on a number of assumptions and rough estimations. However, it explains why no carbon intensity could be allocated to particles, since the signal was dominated by gaseous carbon.

Fig. 37 shows the visualization of the ^{35}Cl signal. Increased $m/z = 35$ intensities were measured at about 260°C , when the combustion process started, and above 805°C during about 30 min. Since these enhanced Cl concentrations also span the whole particle size range, they can again be allocated to gaseous emissions. There is a certain probability that these $m/z = 35$ intensities were due to interferences, e.g. from carbonaceous compounds generated by the wood incineration and the plasma-surrounding atmosphere, such as $^{16}\text{C}^{18}\text{C}^1\text{H}$ (May & Wiedmeyer, 1998). Since for this case a similarly wide pattern as in the ^{13}C map (Fig. 36) would be expected, it appears more probably that indeed Cl was emitted at the beginning of the main combustion period. Together with

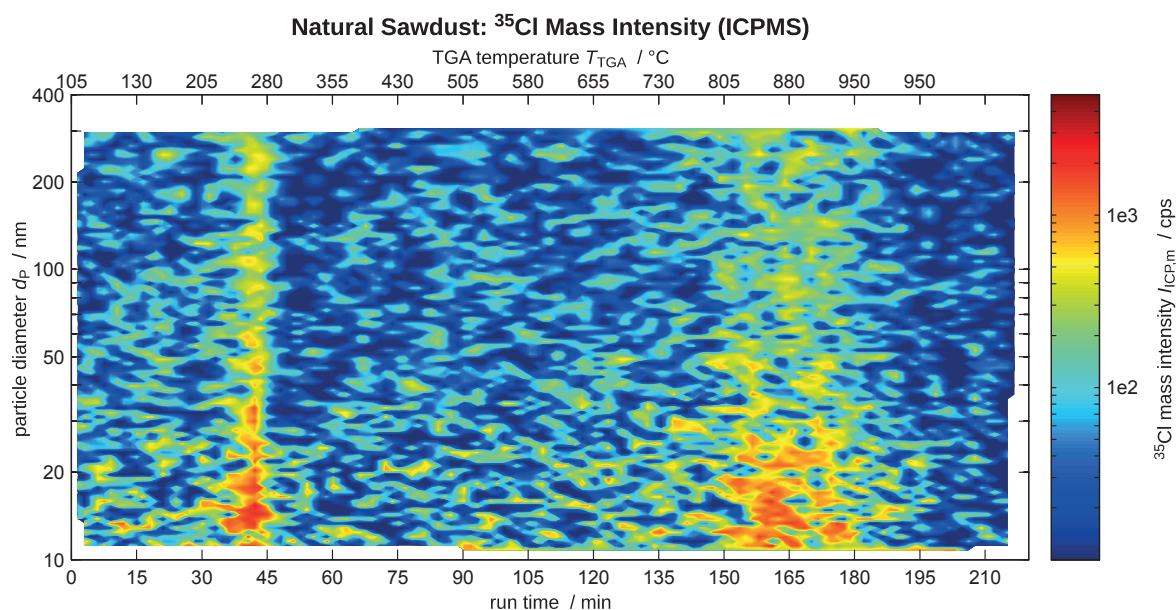


Fig. 37: Particle size related ICPMS mass intensity on $m/z = 35$, given in counts per second (cps): Cl release during the TGA experiment with the pellet from natural sawdust.

some hydrogen released by the wood decomposition, it might have formed HCl and passed through the SMPS as a gas. The enhanced intensity between 800 and 950 °C is not clearly explained. Neither K nor Na emissions were detected in this experiment, so this signal is not related to KCl or NaCl. The $m/z = 35$ intensity could represent another gaseous compound containing Cl, or be caused by an interference.

On the Na, K, and Cu maps, no enhanced intensities were observed during the experiment with the natural wood (data not shown). In a real combustion situation, where the fuel usually does not experience a constant heating rate but is rapidly heated up and combusted, Na and K would probably be released together with Cl, as salt particles. However, in the here presented TGA experiment, Cl was released at lower temperatures and not available for later salt formation.

Water treatment

No obvious differences were observed between the SMPS and ICPMS signals from analyzing the emissions from the water treated sawdust pellet, to those of the natural sample, except the ^{13}C intensity, which lasted about 6 min longer, corresponding to the TGA signal. Therefore no diagrams from this experiment are shown, except the ^{34}S map, which is shown in Fig. 38, since no S information was available from the first experiment. Weak $m/z = 35$ intensity of gaseous matter was recorded in the beginning of the main combustion period, between about 250 and 350 °C. These signals might have arisen from S, but it cannot be excluded that they were partially caused by polyatomic oxygen and nitrogen interferences.

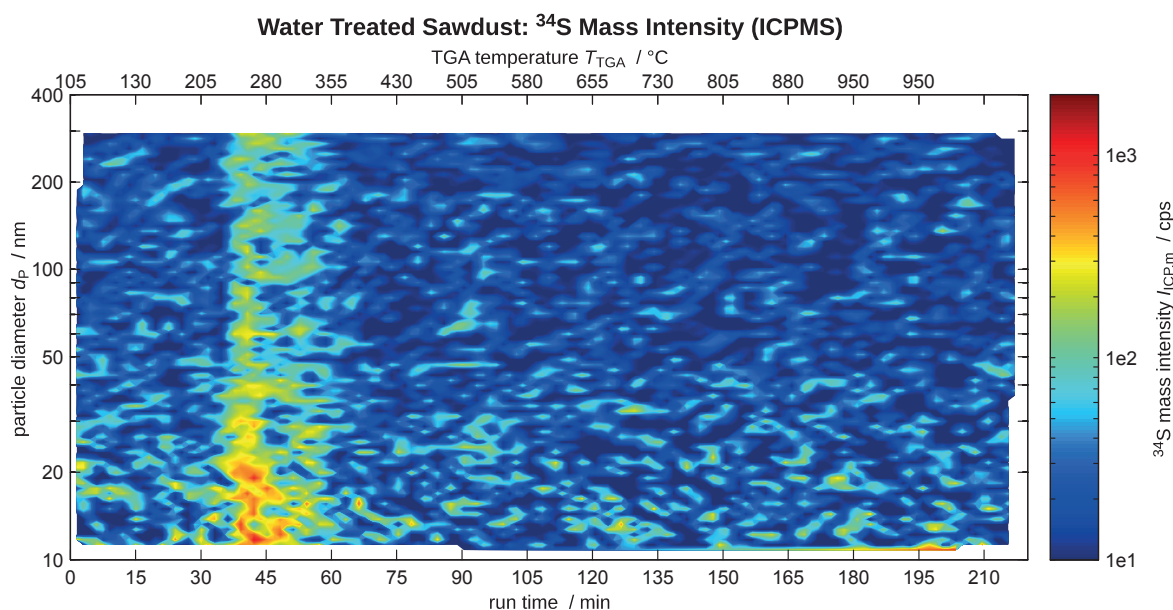


Fig. 38: Particle size related ICPMS mass intensity on $m/z = 34$, given in counts per second (cps): S release during the TGA experiment with the pellet from water treated sawdust.

KCl impregnation

The time dependent PSD_V , measured by the SMPS during the heat treatment of the KCl impregnated sawdust pellet, is visualized in Fig. 39. In the period with the highest particle emissions, around 280 °C, the mode of the PSD was about 50 nm, while it had been close to 100 nm in the experiment with the natural sawdust (Fig. 35). The most obvious difference between the SMPS signals of these two experiments was found above 655 °C, where concentrations between 10^{12} and $10^{13} \text{ nm}^3 \text{ cm}^{-3}$ in the $dV/d\log d_p$ representation were measured with the modes of the size distribution first increasing from about 50 to above 300 nm and then returning to about 150 nm, at 950 °C. Unlike in the experiment with the pellet from natural sawdust, no PSDs with modes around 20 nm were found. Possibly, the primarily generated particles were in the same size range, but due to their much higher concentration, they rapidly disappeared by agglomeration, forming bigger particles.

While no particulate K emissions above background level had been observed in the experiment with the natural sample, the ^{39}K map of the KCl impregnated sample in Fig. 40 shows an obvious time and size correlation to the SMPS signal in the temperature range above 650 °C. Thus, the RDD-SMPS-ICPMS instrumentation reveals that the detected SMPS particles are K compounds. Since no distinct particle diameters are emphasized below 400 °C it can be excluded that the enhanced intensities on $m/z = 39$ in this period were caused by particulate matter. Again, the intensity is slightly amplified at small particle diameters due to the correction for the single particle charge probability. The enhanced signal did probably not arise from K. It could be a polyatomic

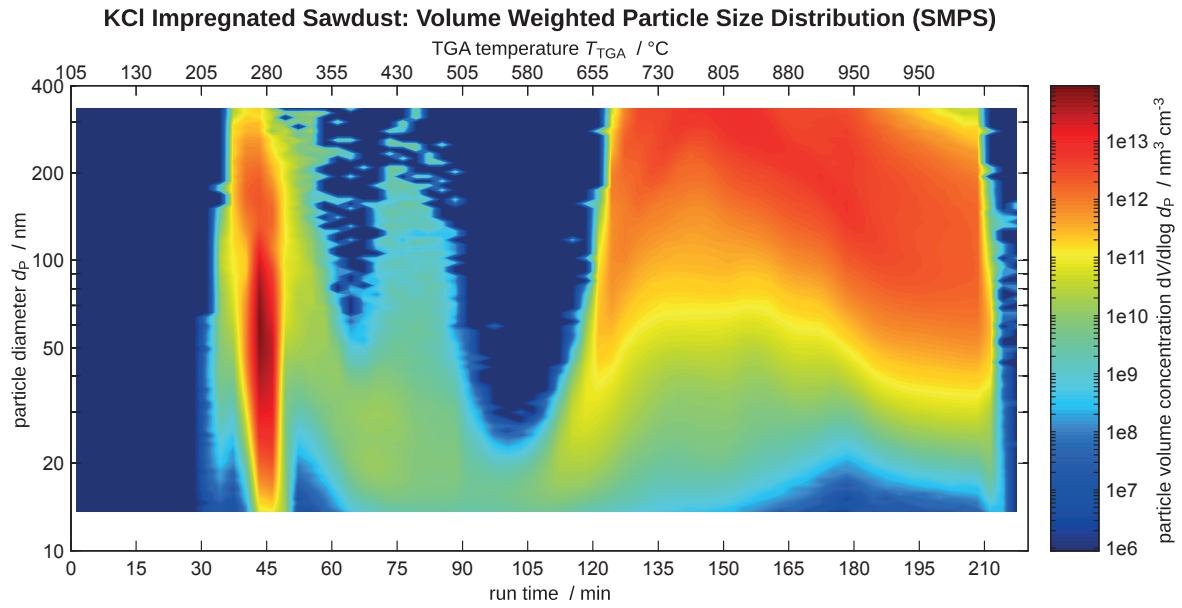


Fig. 39: Development of the volume weighted PSD of aerosol particles, emitted by the pellet from KCl impregnated sawdust.

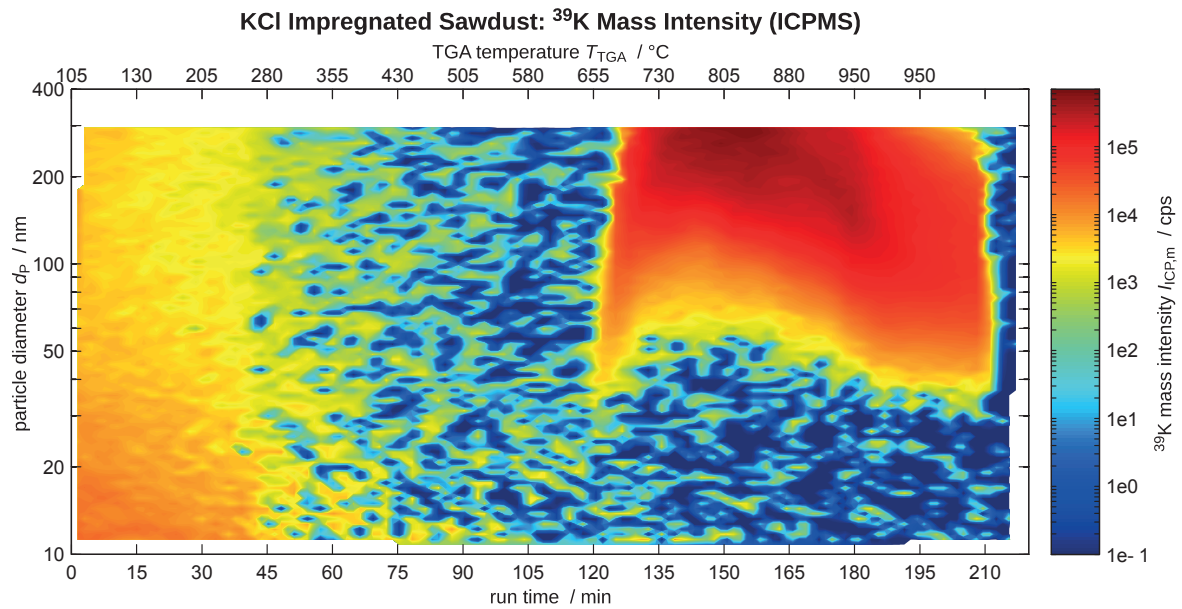


Fig. 40: Particle size related ICPMS mass intensity on $m/z = 39$, given in counts per second (cps): K release during the TGA experiment with the KCl impregnated sample.

interference, e.g. from $^{38}\text{Ar}^1\text{H}^+$, arising from water released in this period, or it might be caused by contaminations at the ICPMS inlet, dissipating during the first hour of operation.

Over a wide temperature range, the KCl in the fuel sample was stable. This was verified using thermodynamic equilibrium calculation software (HSC 7.1 from Outotec; data not shown). At moderate temperatures, KCl can only decompose if complex mechanisms allow the release of Cl (e.g. as HCl), and more stable K species are formed. The ^{35}Cl map in Fig. 41 shows both gaseous and particulate Cl in the same diagram. Gaseous Cl was detected around 280 °C. This was probably HCl, formed by Cl^- ions from the impregnation, and H^+ ions, released in terms of the wood decomposition. The ^{35}Cl signal decreased to the background level after 90 min when the first weight decrease was accomplished, as seen in the TGA curve of the KCl impregnated sample (Fig. 34). In the same temperature and size range as K, also particulate Cl was detected. At 805 °C, ^{35}Cl intensities above $2 \cdot 10^3$ cps were recorded, when those of ^{39}K were around $7 \cdot 10^5$ cps. Since usually 2 to 3 orders of magnitude are between the ICPMS sensitivities on these elements, it seems reasonable that the K and Cl intensities were caused by particles consisting of at least partially of KCl.

When particulate K was detected, also Na was found, with different concentrations but a similar distribution over the particle size range, as can be recognized in the ^{23}Na map in Fig. 42. Such emissions had not been observed in the experiment with the natural sample. Since the KCl impregnation did not contain Na, it appears that the naturally present Na^+ ions in the wood and the K^+ ions were competing for the additional Cl^- ions in the KCl impregnation, allowing a considerable formation and release of particulate NaCl. RDD-SMPS-ICPMS was able to show that

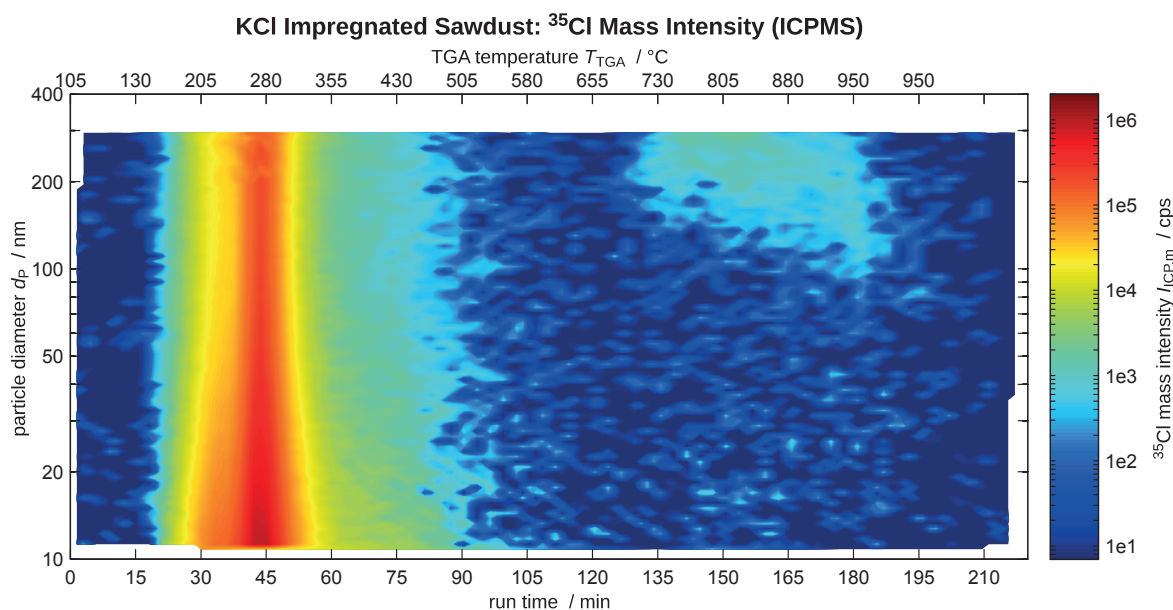


Fig. 41: Particle size related ICPMS mass intensity on $m/z = 35$, given in counts per second (cps): Cl release during the TGA experiment with the KCl impregnated sample.

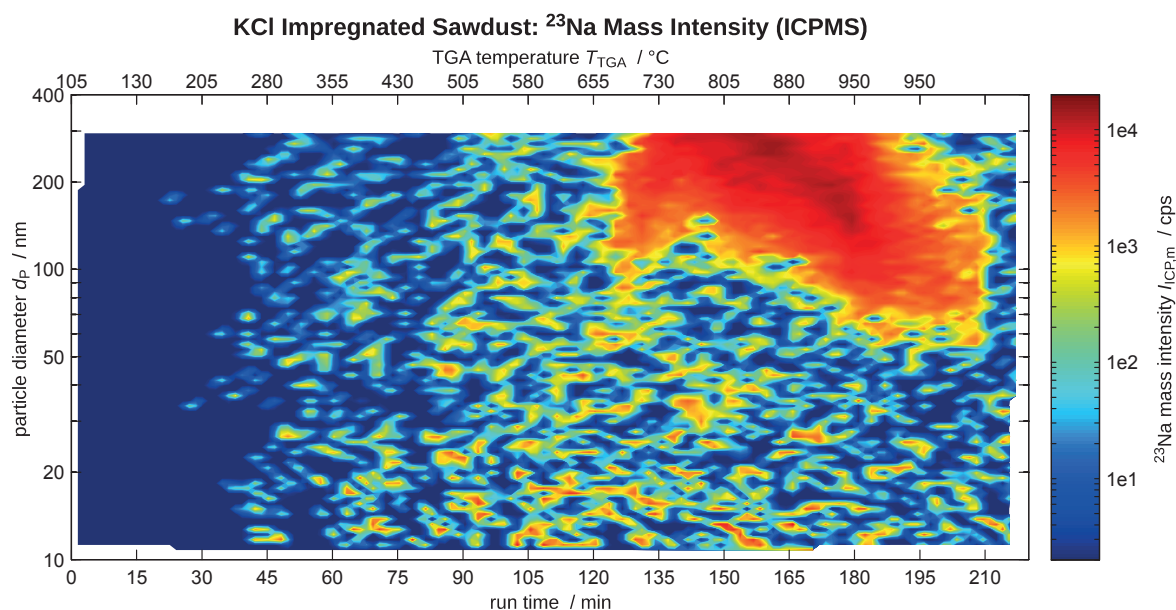


Fig. 42: Particle size related ICPMS mass intensity on $m/z = 23$, given in counts per second (cps): Na release during the TGA experiment with the KCl impregnated sample.

^{23}Na , ^{35}Cl , and ^{39}K were contained in the same particle size fractions. Since these signals coincide well regarding their distribution in the relevant size classes, they were probably not induced by separate NaCl and KCl particles but both salts were contained in the same particles.

In the period with the highest particulate Na, K, and Cl emissions, also an increase of the ^{63}Cu signal was detected on the same particle diameters, as shown in Fig. 43. A similar signal was neither recorded during the experiments with non-impregnated wood samples, nor during the blank measurement, performed before the KCl experiment. The KCl impregnation seems to have provoked a release of Cu, contained in the natural wood, which had also been detected in the wet chemistry analysis of the sawdust.

The ^{13}C map was similar to that of the natural sample, except that the release of gaseous carbon during the main combustion period was about 6 min longer, like observed with the water treated sample. Also ^{34}S map was not affected by the KCl impregnation (diagrams not shown).

CuSO₄ impregnation and CuCl₂ impregnation

During the treatment of the CuSO₄ impregnated sample, the carbon emitting period was longer, corresponding to the TGA signal. No Cu release was detected, and the only obvious difference to the experiment with the natural sample was that a gaseous S compound was found in the first combustion period around 280 °C, as shown in Fig. 44. In the heating period below 250 °C, most of the water, including the hydration water of the CuSO₄·5H₂O, was evaporated. Under oxidizing conditions, CuSO₄ is thermodynamically stable below 400 °C. However, HSC calculations were made to check whether the formation of gaseous sulfur compounds was thermodynamically

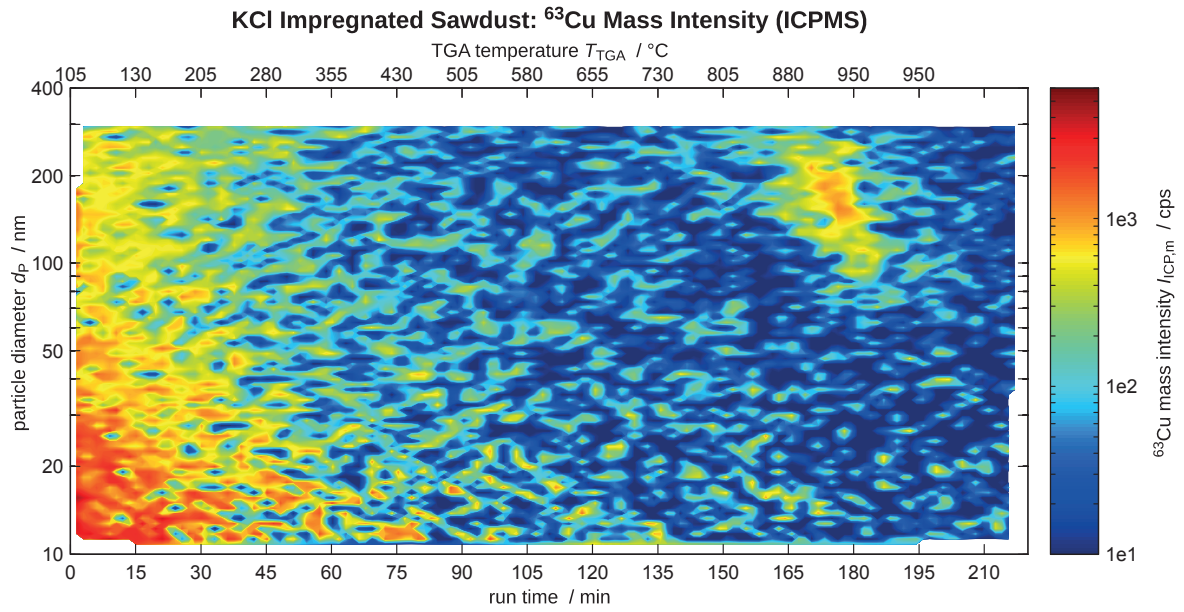


Fig. 43: Particle size related ICPMS mass intensity on $m/z = 63$, given in counts per second (cps): Cu release during the TGA experiment with the KCl impregnated sample.

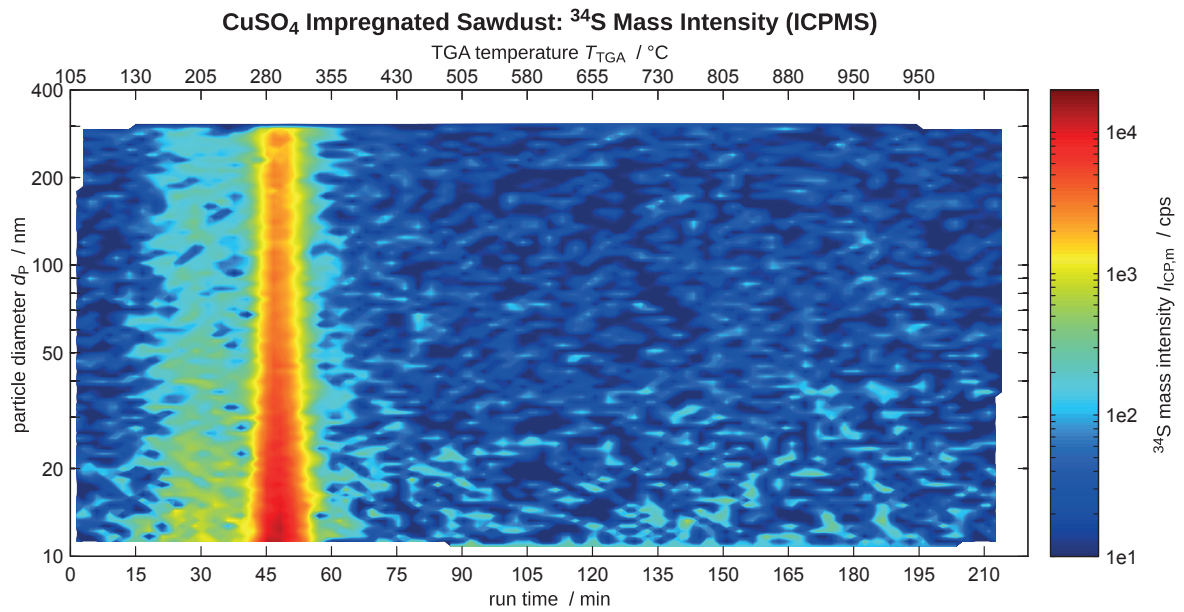


Fig. 44: Particle size related ICPMS mass intensity on $m/z = 34$, given in counts per second (cps): S release during the TGA experiment with the CuSO_4 impregnated sample.

avored under these conditions. They confirmed that sulfur dioxide (SO_2) can be formed under slightly reducing conditions (see Appendix; Fig. A2), and hydrogen sulfide (H_2S) can immediately arise under highly reducing conditions (see Fig. A3). It seems that locally reducing conditions were obtained during the prompt combustion of wood, possibly resulting in the formation of H_2S .

Below 500°C , similar gaseous Cl emissions were measured from the CuCl_2 as from the KCl impregnated sample. In the HSC calculation, it was confirmed that Cl_2 and HCl species are stable under oxidizing conditions above 200°C (Fig. A4) Probably, the most Cl was released in the period below 500°C as HCl , and no Cl was later available to form chlorides. Hence, no Cl containing particles were detected at high temperatures, as shown in Fig. 45.

No particulate Cu was detected during both experiments with CuSO_4 and the CuCl_2 impregnated samples. Also the other signals were similar to those recorded during the experiment with the natural sample, and hence are not shown.

CuSO_4 -KCl Impregnation

The PSD map recorded by the SMPS during the heat treatment of the CuSO_4 -KCl impregnated sample is shown in Fig. 46. Compared to the KCl sample, the PSD between 600 and 800°C was narrower and less particles above 100nm were measured. This is consistent with the TGA signals, where a stronger weight decrease was observed in this period from the KCl than from the CuSO_4 -KCl sample, since possibly the CuSO_4 and KCl were reacting to other stable species, resulting in reduced evaporation. At 880°C and above, the particle concentrations were in the same order of magnitude, when also the weight loss rates were comparable. The relation of

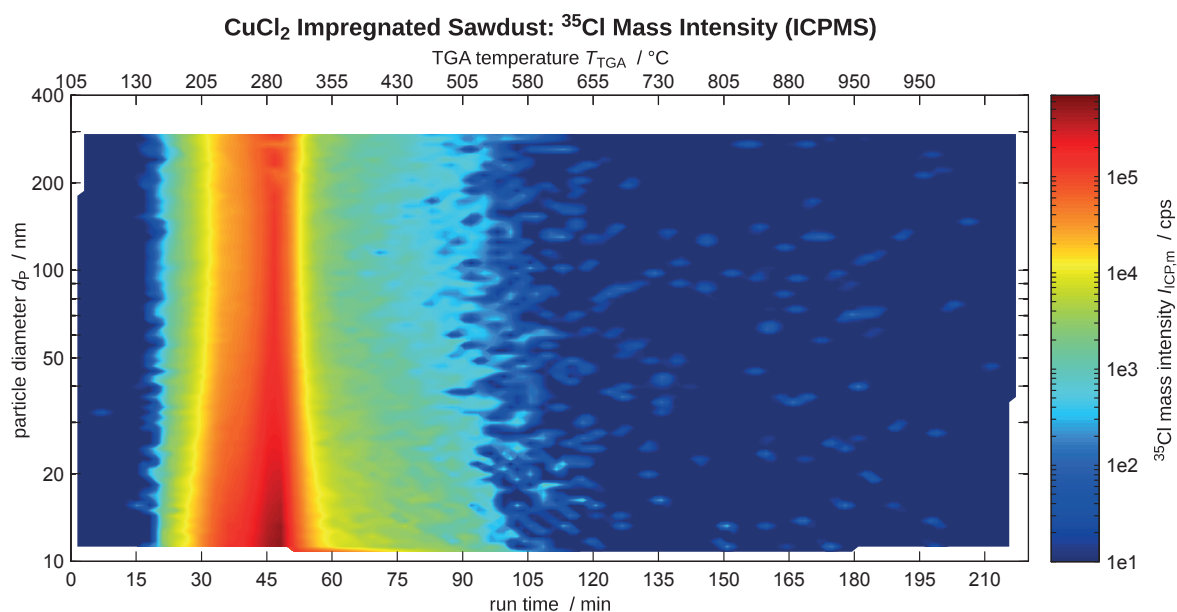


Fig. 45: Particle size related ICPMS mass intensity on $m/z = 35$, given in counts per second (cps): Cl release during the TGA experiment with the CuCl_2 impregnated sample.

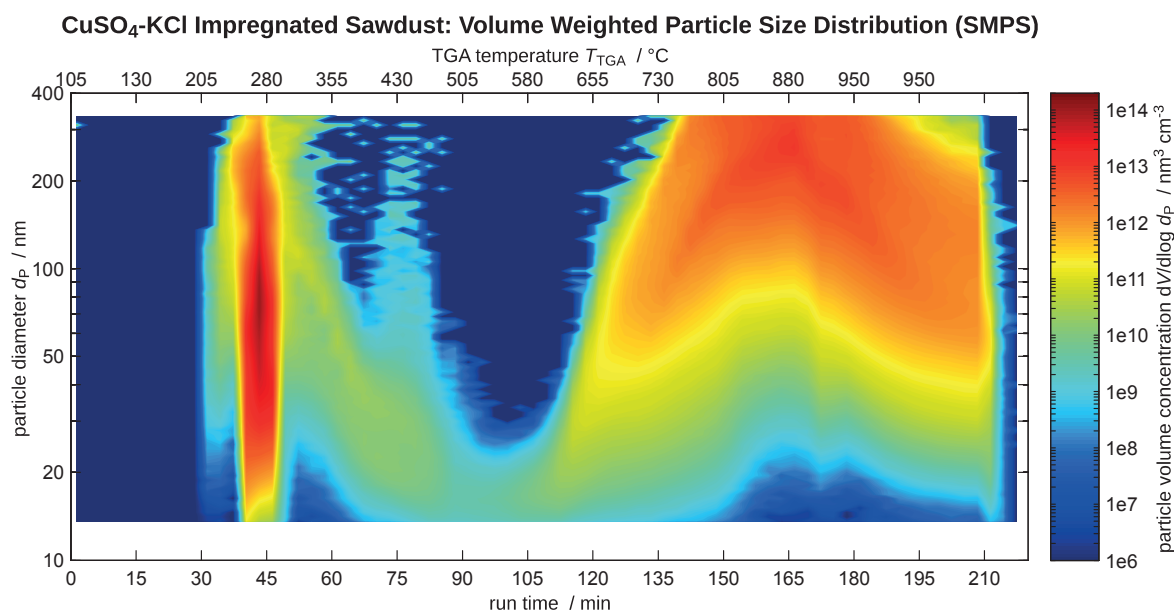


Fig. 46: Development of the volume weighted PSD of aerosol particles, emitted by the pellet from CuSO₄-KCl impregnated sawdust.

the K (Fig. 48), Na (Fig. 47), and Cl (Fig. 49) maps to the PSD map was very similar to that observed with the KCl sample.

When the CuSO₄-KCl impregnated sample was treated in the TGA, gaseous S was emitted between 200 and 300 °C. Unlike those from the sample with only CuSO₄ impregnation, these emissions were spread uniformly over the period when the temperature was increasing from 160 to 310 °C, as can be seen in the ³⁴S map in Fig. 50. Similar to the case with the CuSO₄ impregnated sample, S species are supposed to arise under reducing conditions. Possibly, SO₂ was continuously formed (Fig. A2) in this experiment, while the more rapid H₂S formation mechanism (Fig. A3) was taking place with the CuSO₄ sample. This could explain the difference between the S signals below 350 °C in Fig. 50 and Fig. 44.

Even the ⁶³Cu map was not remarkably different to that from the KCl experiment, although the sample contained Cu with a very high concentration of 0.3 %. Hence, Cu seems to feature a very low tendency to be evaporated in such a thermal process, if no Cl is available to form cupric chlorides. The ⁶³Cu map is shown in Fig. 51.

6.3 Analysis of residues from the TGA experiments

The elements which were found in the final analysis of all residues are compiled in Table 6. These values allow appraising the results from the aerosol experiments. The remaining K was in the same order of magnitude for all samples except the CuSO₄-KCl impregnated pellet, where a substantially

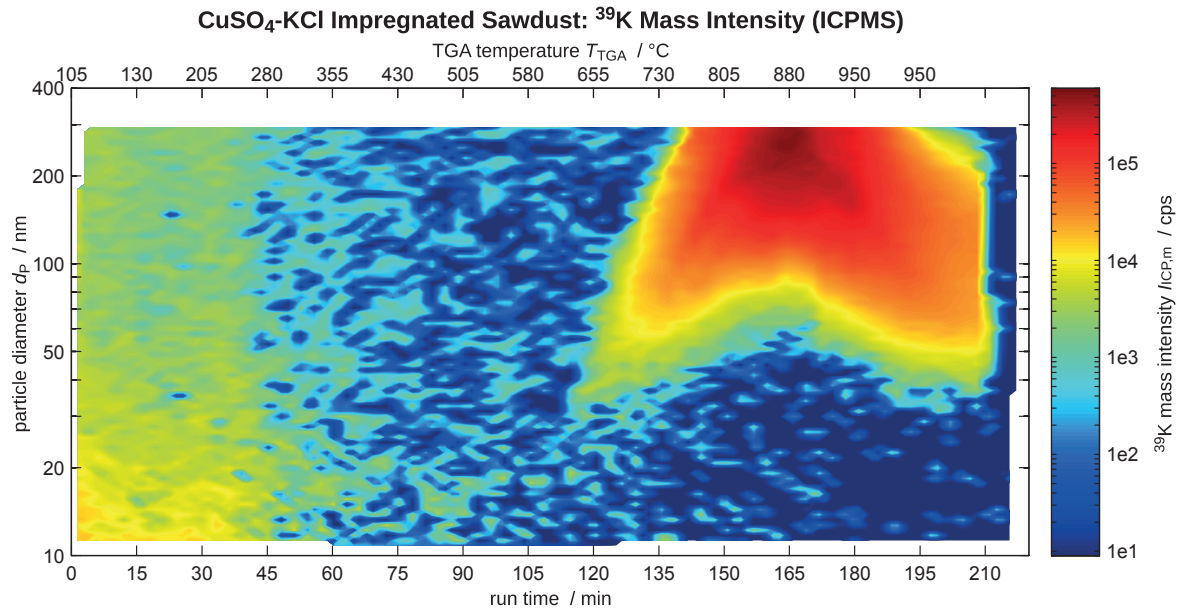


Fig. 48: Particle size related ICPMS mass intensity on $m/z = 39$, given in counts per second (cps): K release during the TGA experiment with the CuSO₄-KCl impregnated sample.

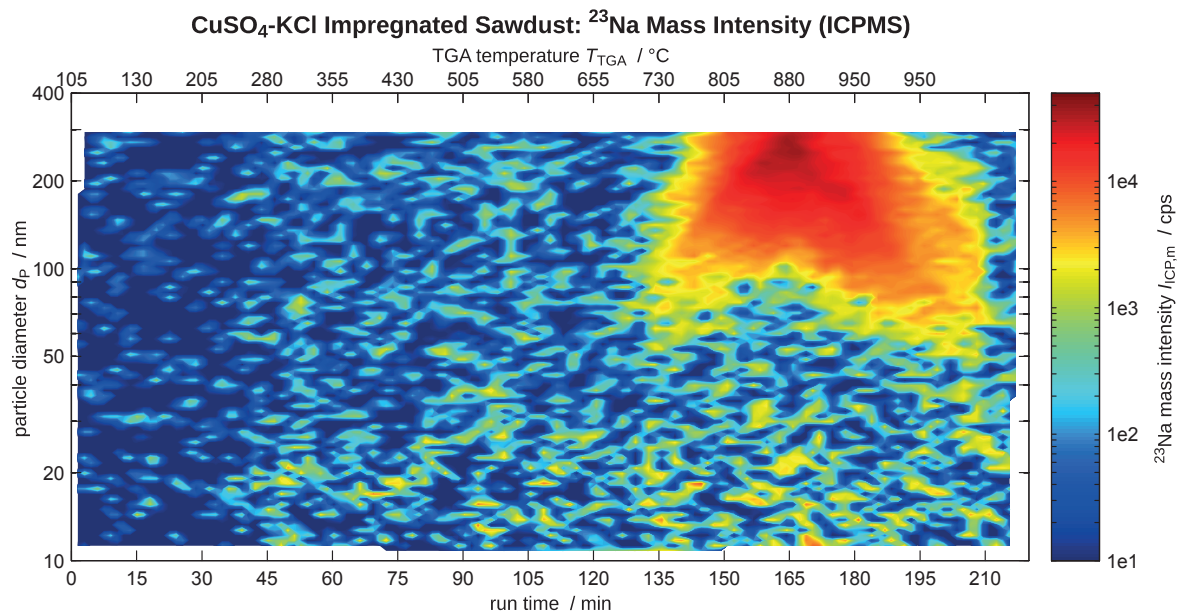


Fig. 47: Particle size related ICPMS mass intensity on $m/z = 23$, given in counts per second (cps): Na release during the TGA experiment with the CuSO₄-KCl impregnated sample.

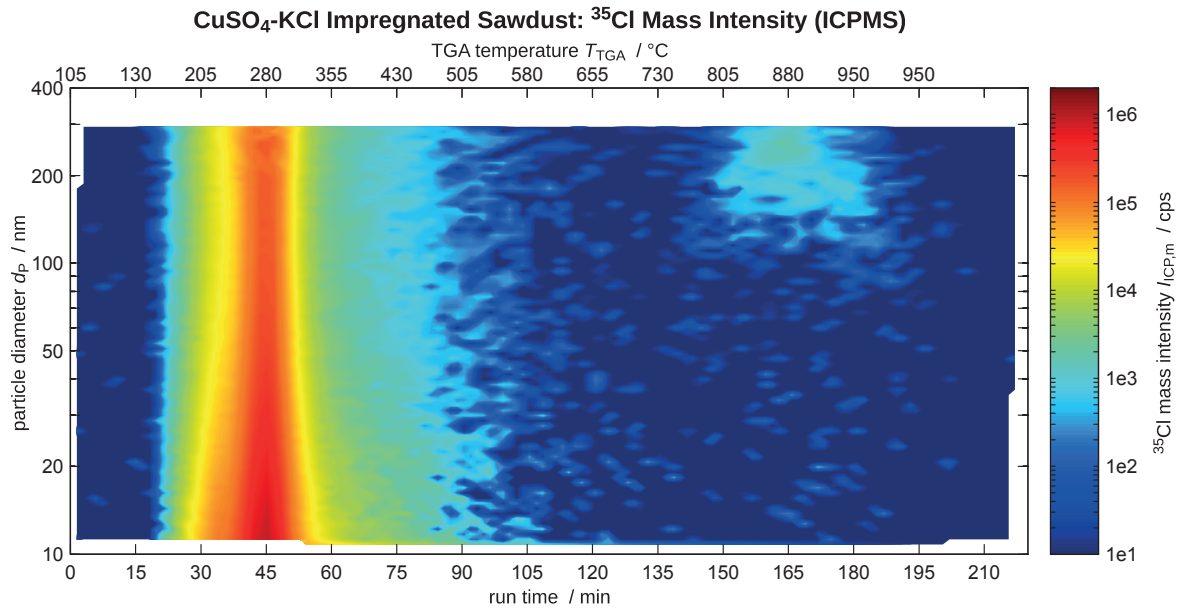


Fig. 49: Particle size related ICPMS mass intensity on $m/z = 35$, given in counts per second (cps): Cl release during the TGA experiment with the CuSO₄-KCl impregnated sample.

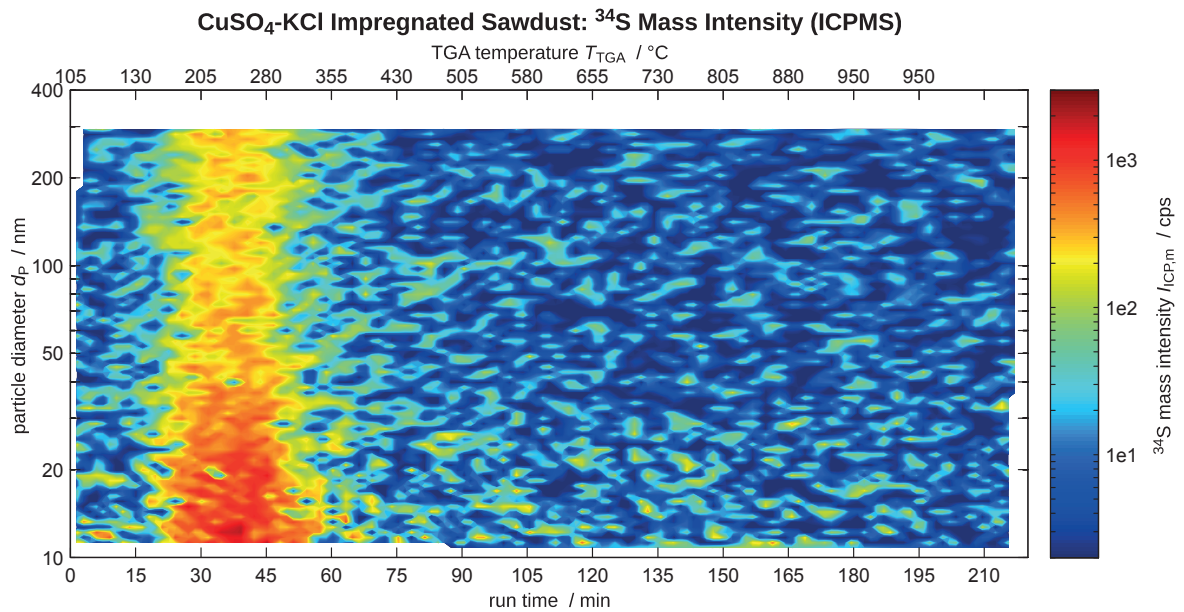


Fig. 50: Particle size related ICPMS mass intensity on $m/z = 34$, given in counts per second (cps): S release during the TGA experiment with the CuSO₄-KCl impregnated sample.

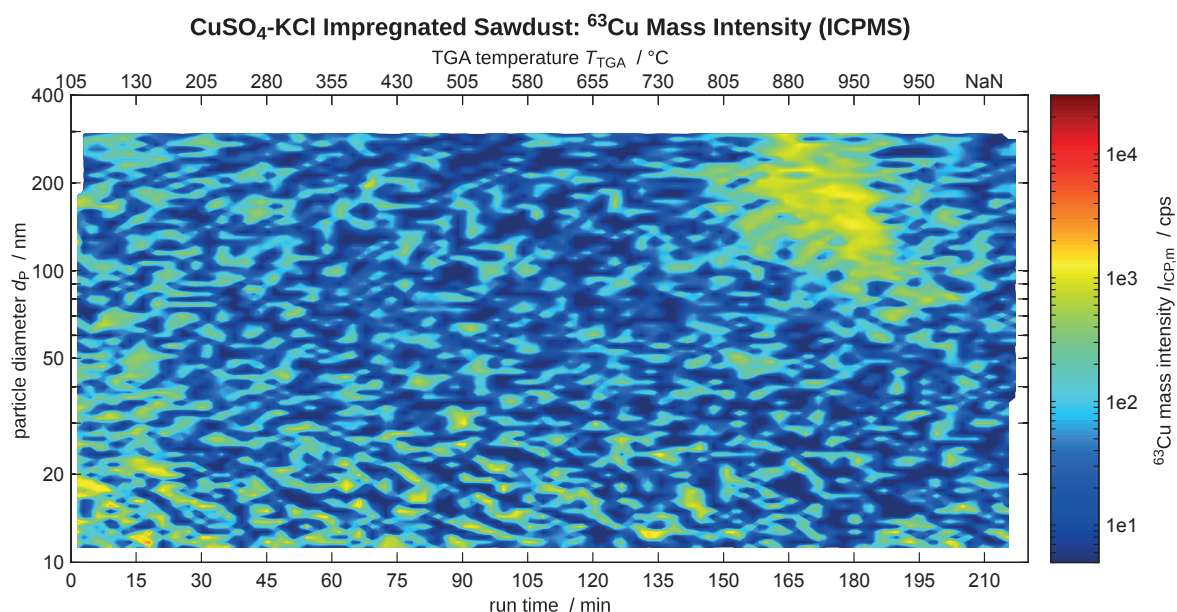


Fig. 51: Particle size related ICPMS mass intensity on $m/z = 63$, given in counts per second (cps): Cu release during the TGA experiment with the CuSO₄-KCl impregnated sample.

Table 6: Element analysis of sample residues

Sample name	Added K	Remaining K	Added Cu	Remaining Cu	Added Cl	Remaining Cl
Natural	-	0.27 mg	-	<0.01 mg	-	<0.01 mg
KCl	1.50 mg	0.42 mg	-	<0.01 mg	1.34 mg	<0.01 mg
CuSO ₄	-	0.33 mg	0.60 mg	0.59 mg	-	<0.01 mg
CuCl ₂	-	0.23 mg	0.60 mg	0.52 mg	0.67 mg	<0.01 mg
CuSO ₄ -KCl	1.50 mg	1.43 mg	0.60 mg	0.64 mg	1.34 mg	<0.01 mg

higher K amount was found in the residue. This supports the supposition that the CuSO₄ was impeding the KCl evaporation and therewith the K release. The remaining Cu quantities detected in all residues from the samples impregnated with cupric salts are close to the added Cu amounts, considering a certain error, caused by the procedure of removing the residues from the crucibles and digesting them in acid, before measuring the concentration by ICPMS and calculating the listed amount. Therewith the Cu was mainly found in the residues in all cases. No Cl was found in the residues. This is consistent with the RDD-SMPS-ICPMS data.

7 Conclusions and outlook

7.1 Setting up the instrumentation

The concept of using an RDD as sample introduction interface to SMPS-ICPMS was proven. Several m/z were simultaneously measured by the ICPMS, and the measured intensities were sufficient to achieve signal integration times, which allow similar size resolutions like the SMPS, at least with the particulate silver concentrations applied for these pilot tests.

Although the use of air as dilution gas, leading to 10 % air in the particle carrier gas of the classified monodisperse aerosol, was provoking an increase of the background noise, the argon plasma was persisting and silver particles could be measured even under these conditions. However, the use of dilution argon in the RDD is preferred, since reducing the background noise means improving the signal quality and the limits of detection (*LoD*). To reduce the argon consumption of the instrumentation, rather a partial or complete recirculation of the used excess gas and re-introduction as sheath gas after filtration should be considered. With a recirculation of the total excess gas flow, the expected air content in the carrier gas of the classified particles would be around 5.5 % in this configuration, and not only reduce the argon consumption of the SMPS by 90 %, but also simplify the startup procedure of the instrumentation, since the sheath and excess gas flows were forced to be equal. Therewith, the monodisperse flow would no longer be affected by the difference of these two flows.

The SMPS is a powerful aerosol characterization technique, based on the principle of particle number measurements. However, ICPMS is a mass related measuring technique. To correlate the signals of both CPC and ICPMS, either the number concentrations obtained by the CPC have to be converted to mass or volume PSDs, or number based data have to be calculated from the initially mass related ICPMS intensities. The simplest approach to do this conversion is assuming spherical particles, neglecting different particle shapes or the formation of secondary particles which usually are not spherical. If an ICPMS intensity curve coincides well with the PSD, determined by SMPS, at smaller particles, but is lower at larger particles, this can be an indicator for loosely formed agglomerates, comprising less mass than expected for a dense sphere.

If thorough aerosol neutralization becomes crucial, e.g. if the nebulizer-RDD-SMPS-ICPMS setup is applied for the characterization of aqueous particle suspensions, or if other highly unipolarly charged aerosol particles are analyzed with high concentration accuracy, the sufficient efficiency of the neutralizer should be verified. This could be done e.g. by comparing measuring results obtained using an even stronger neutralizer, or arranging two or more of the actual ^{85}Kr neutralizers in series.

7.2 Instrumental setup

A hyphenated SMPS-ICPMS coupling setup was successfully realized. The gas flow concept between an in-house modified SMPS and a commercial ICPMS instrument was re-designed and adapted to match the requirements of both instruments. These modifications include replacing the normally used air flows in SMPS by argon. An implemented RDD allows precisely controlling the particle carrier argon flow, and directing a defined sample aerosol flow into the DMA. This enables in-line sampling of aerosols from undefined environments. Moreover, particles can be investigated which initially have been carried by nearly any gas, due to the argon dilution, effected by the RDD. The hyphenated SMPS-ICPMS instrumentation, including RDD, serving as sample introduction interface, was explained in detail.

To demonstrate the feasibility of this technical concept, a model aerosol containing dried silver nanoparticles was generated and analyzed by the developed setup. The parallel arrangement of a non-modified reference SMPS setup allowed easily validating the SMPS data recorded by the argon operated hyphenated instrumentation. The concentrations and particle size distributions, measured by both SMPS instruments, were in good agreement, and the ICPMS signal was found to correlate very well with the PSD_V , measured by the SMPS. Although the *LoDs* of the hyphenated setup were not yet investigated in detail after these first measurements, it was observed that the signal-to-noise ratio became very small below $d_p = 12$ nm, and no reliable ICPMS data were obtained in this particle size range.

7.3 Instrument characterization

RDD-SMPS-ICPMS allows determining size distribution and size resolved elemental composition of air-borne nanoparticles with very high sensitivity, enabling low *LoDs*. Moreover, the RDD opens the possibility to sample nanoparticles in different carrier gases, such as fuel and process gases, for SMPS-ICPMS analysis. Newly defined size related mass and number related ICPMS intensities allow clearly allocating chemical elements to specific particle size fractions, and distinguishing between differently sized and composited aerosol particles. Besides, the degree of correlation between number based SMPS and mass related ICPMS curves is an indicator for the density of the particles and the compactness of particle agglomerates.

The standard deviation of the ICPMS signal, undergoing the same size-depending calculations as ICPMS measuring intensities, is helpful to decide whether the measured concentrations were high enough to induce reliable intensities, or the signal consists of amplified background noise, while real concentrations were below the instruments detection limits. Particle mass and number related *LoD* are determined for different elements on selected particle size fractions, and unified detection limits for virtual 50 nm particles, determined on differently sized real particles, allow assessing the

instrument's sensitivity for different elements, and comparing instrumentations and settings among each other.

7.4 Heat treatment of impregnated wood pellets

In the TGA, the O₂ content and furnace temperature can be controlled, which allows repeating a defined thermal treatment with differently impregnated fuel samples, and studying the influence of these treatments onto the combustion process. Coupling this equipment to the RDD-SMPS-ICPMS particle analyzing instrumentation enables simultaneous size-resolved online-measurement of the elemental composition of gaseous and particulate emissions, depending on fuel properties and TGA parameters.

Short SMPS scan durations in the range of a few minutes allow generating particle concentration maps, representing the time and size resolved particle concentration during such an experiment. Similar element maps, generated from the measured ICPMS intensities of a number of elements, with the same time and similar size resolution as the SMPS data, representing time- and size-resolved particle concentration and elemental composition of gas-borne particles in the nanometer size range, allow visually distinguishing between gaseous and particulate nature of the detected elements.

The instrumentation was able to show that the KCl impregnation facilitated the release of particles, containing Cu which was originally present in the natural wood. Even very high concentrations of cupric salts in the wood sawdust impregnation did not lead to a substantial additional Cu release in terms of the applied heat treatment. Obviously the addition of KCl has led to the formation of Na and Cu containing particles, confirming that adding Cl to the fuel provokes the release of alkali and heavy metals.

7.5 General Conclusions

The developed technique opens new analytical possibilities and applications in many fields. Simultaneous determination of size distribution and size-resolved chemical composition with a temporal resolution of a few minutes, combined with in-line aerosol sampling, allows real-time assessment of material depending behavior of gas-borne nanoparticles. For instance, the fate of nano objects in incineration processes can be traced, i.e. whether they are lost, or if they form new structures or simply go through. Additionally, newly formed nano objects resulting from incineration can be identified. Moreover, the instrumentation could be used, in combination with the model aerosol generation hardware, for the characterization of nanoparticles being suspended in liquids, although SMPS-ICPMS is primarily intended for aerosol analysis.

Individual particles cannot be characterized by RDD-SMPS-ICPMS. Analyzing the particle structure is not possible, and particles with the same mobility diameter but different elemental composition, contained in the same aerosol, will yield the same signals as uniform particles, composed of the same different elements. However, RDD-SMPS-ICPMS enables quantitative online size-resolved elemental analysis of aerosol particles with time resolutions of a few minutes, and alterations in terms of sample preparation and storage are avoided. This makes the technique highly valuable for applications like aerosol exposure studies or monitoring of particulate emissions from thermal processes.

7.6 Outlook

7.6.1 Particle charge corrections

Corrections for multiple charges on particles are available and usually implemented in standard SMPS measuring software. In the Boltzmann equilibrium state, particles with diameters around 50 nm start to carry more than one elemental charge, and this effect becomes more important towards larger particles. The most urgent improvement of the coupled instrumentation is therefore the implementation of such a correction into the ICPMS intensity correction calculations. This would increase the measuring accuracy, especially if particles above 100 nm are investigated, and artefacts like the 65 nm silver peak in Fig. 29 could be avoided.

Another aspect is that the charges on the particles were assumed to be in the Boltzmann equilibrium behind the aerosol neutralizer. It was observed that the use of weak neutralizers led to different measuring values, calculated with this assumption. Possibly the neutralizer with the strongest ^{85}Kr source was sufficient to indeed achieve the equilibrium state, but this has to be confirmed, before highly unipolarly charged particles like those from liquid sprays are characterized with high accuracy. To ensure the charges to reach the equilibrium state, the use of a more efficient neutralizer, e.g. based on a ^{241}Am alpha source, should be considered.

Related to particle charges, also the carrier gas has to be considered. Up to now, it was assumed, based on literature research, that the oxygen content of an initially air based but argon diluted aerosol was still sufficient to obtain a similar charge equilibrium state as in air. Contrariwise, the Wiedensohler coefficients for pure argon were used for the TGA measurements where already the primary carrier gas was mainly argon, although a very low oxygen flow and the gases emitted by the heat treated sample were contained. These assumptions should be validated.

7.6.2 Gas recirculation

Further instrument improvement includes the reduction of argon consumption. This would allow reducing operational costs, which is mandatory, if such a coupling can become a tool for praxis relevant analysis of nanoparticle containing aerosols. For applying a partial or total recirculation of the used sheath gas, a gas recirculation pump, an additional MFC, and a flow component to avoid

pump pulsations entering the DMA have to be implemented, as sketched in Fig. 52. These components are available, since the SMPS had been recirculating the total sheath air flow in its original configuration. Negative aspects of such a recirculation might be gas impurities which could negatively influence the argon plasma, or increase the background noise of the ICPMS intensities, deteriorating the *LoDs*.

A partial argon recirculation would entail a more delicate flow adjustment during instrument startup, and maybe the monodisperse aerosol flow directed into the ICPMS may become more fluctuating. On the other hand, a total sheath gas recirculation would reduce exactly these obstacles, since the sheath gas inlet and excess gas outlet flows were enforced to be equal. The flow of the classified, monodisperse aerosol was no longer depending on the difference of these flows, but directly related to the polydisperse sample inlet flow, provided by the RDD.

7.6.3 Distinguish between particulate and gaseous matter

With the actual instrumentation, the ICPMS intensity on the specified elements can only be allocated to particulate or gaseous matter by comparison to the size distributions, determined by the SMPS. This appraisalment has to be done as a discussion of the measuring results, and the instrumentation is not able to distinguish between gas and particles, if only a distinct particle size

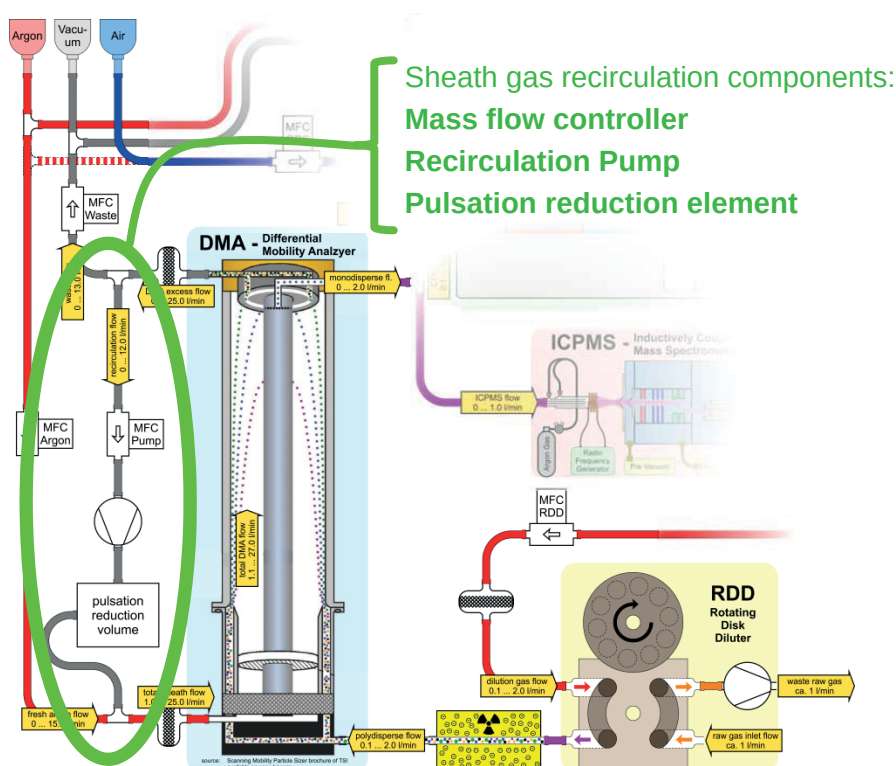


Fig. 52: Arrangement of additional flow components, enabling partial or complete recirculation of used excess gas, and re-introduction to the DMA as sheath gas.

class is analyzed and not a certain size range is scanned. Two technical approaches were found, which could solve this problem:

The first approach is introducing a Gas Exchange Device (GED) between DMA and ICPMS, to replace the particle carrier gas by argon. With this additional component, the measuring setup would become more complex, and the rate of the classified aerosol, provided to the ICPMS, was limited by the maximum gas exchange rate of the GED. On the other hand, this would allow operating the DMA with air, the covered particle size range would no longer be limited by the use of argon, and air could be assumed for the particle charge probabilities.

The second approach consists of installing a conventional Mass Spectrometer (MS) in parallel to the RDD-SMPS-ICPMS setup. This would allow detecting gaseous compounds, and signals which are caused by gases could be subtracted from the intensities, detected by the ICPMS, resulting in separate signals for gaseous and particulate matter, provided by the MS and the RDD-SMPS-ICPMS instrumentation, respectively.

7.6.4 Considering particle shape

Spherical particles were assumed for linking the mass related ICPMS intensities and the number concentration, determined by the CPC, to each other. This is a simplifying assumption. However, the coincidence between SMPS and ICPMS signals was good, indicating that the particles in the presented experiments were either nearly spherical, or their agglomerates were at least very dense. If more complex structures, as e.g. fractal-like agglomerated real particles are investigated, more sophisticated approximations could be applied, considering such a particle configuration, in order to correlate number based SMPS and mass based ICPMS data.

7.6.5 Applications

Future applications of the RDD-SMPS-ICPMS setup will include investigations of process gases, released by impregnated and real waste samples which can undergo different heat treatments. The next steps may include experiments with different model and real samples, treated in the TGA, as well as going a step further towards real incineration investigations, e.g. in a one-pellet oven, where a single sample pellet is introduced into a hot environment, or in a tube furnace, where different real and model waste samples are moved through different temperature zones, as it is typical for waste which undergoes a heat treatment in an incineration facility.

Apart from incineration related research, this versatile technique can be applied in different fields where online information on the composition of aerosol particles is desired. Such an application can be the monitoring of emissions from combustion processes, as it is needed for combustion research, risk assessment, engine or process development, emission control, and the evaluation of measures to reduce particulate emissions, like e.g. particle filters. Other applications could be in the quality control of ENP fabrication, and in the appraisal of inhalation risks, related to thermal

processes, or to processes and devices emitting nanoparticles, e.g. the release of toner powder by office printers.

ICPMS sensitivities may be determined for different particulate elements and SMPS-ICPMS operating conditions, and collected in a database. This would allow not only to allocate certain elements to distinct particle size fractions but also to determine their concentrations in those particles.

In the actual state, the RDD-SMPS-ICPMS is limited to laboratory applications, which means that only aerosols can be assessed which are generated or released close to an installed ICPMS instrument. Mounting the ICPMS in a container or on a vehicle, would enable mobile applications, e.g. measuring on real emissions from waste incineration plants or from airplane engines on a test bench, or aerosol assessment in industrial facilities.

Appendix

A.1 Observation of suspension aging

When the measuring series on the aerosol from the low concentrated gold suspension was completed (section 4.3.3), the DMA of the SMPS was exchanged by a Nano-DMA (3085 from TSI), and another CPC was installed (3776 from TSI). The goal was to get experience with these components, since they allow measuring smaller particles, down to 2.5 nm. The reference SMPS, running in parallel to the coupled instrument, was not changed, in order to have a proper control on the detected size distributions.

The aerosol generator was not interrupted during the rearrangement of the SMPS components, and the suspension in the container was not changed, since the idea was to measure the same aerosol, under the same conditions, with both instrument configurations, in order to finally compare the results. Four hours after the first experiment, the modified instrumentation was ready, and the next PSDs and size-resolved ICPMS intensities were recorded.

While it was observed in earlier experiments that the highly concentrated gold suspension was very stable, even if it had been used for several measuring days or even weeks, the gold particles in the diluted suspension turned out to be lost over time, and only very moderate ICPMS intensities were measured after four hours of aerosol generation. The measuring data are presented in Fig. A1. A distinct peak, between 20 and 30 nm is recognized in the volume/mass (A) and the number (B) related diagrams, representing the aerosols generated from the fresh suspension, measured by both the coupled and the reference SMPS, at the same position where ICPMS had recorded the highest intensity. The axes of the volume/mass (C) and number (D) based diagrams, showing the later recorded data, have the same scaling. No clear peak was detected anymore by the SMPS instruments, and less than 10 % of the initial ICPMS intensity was still measured.

At the same time, the PSD_N and PSD_V were shifted towards larger particles, and especially the volume concentrations had increased. It was not further investigated if the increase of the particle concentrations, recorded by both SMPS instruments, was caused by impurities, e.g. from the compressed air which was steadily passing the aerosol generator, or if initially dissolved matter was precipitating and causing particle growth, and partially the formation of new particles. However, this accidental observation demonstrates the ability of the RDD-SMPS-ICPMS instrumentation to characterize also aqueous suspended particles and to observe their time-dependent behavior.

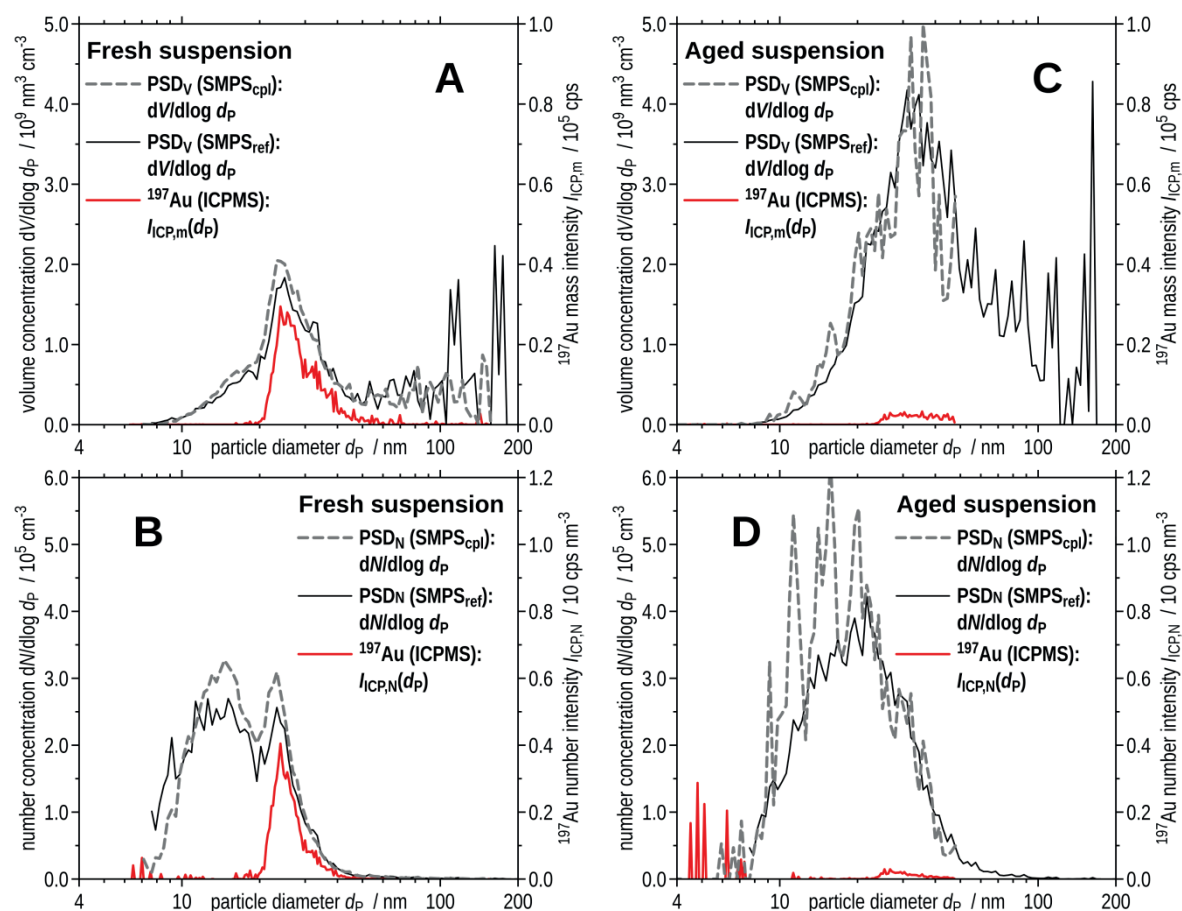


Fig. A1: Aging demonstration of the diluted 20 nm gold suspension. (A) volume/mass and (B) number related SMPS and ICPMS ^{197}Au signals, recorded when the fresh suspension was used to generate an aerosol. (C) volume/mass and (D) number related data, measured after 4 hours of suspension use. “SMPS_{cpl}” and “SMPS_{ref}” indicate data recorded by the coupled and by the non-modified reference SMPS, “ ^{197}Au ” the size-resolved ICPMS intensity, recorded on $m/z = 197$.

A.2 Thermodynamic equilibrium calculations

In section 6.2.2, the release of gaseous compounds during the thermal treatment of impregnated wood samples was discussed. The formation of these gases was verified using thermodynamic equilibrium calculation software (HSC 7.1 from Outotec), to estimate whether or not the signals indicating gaseous emissions were realistic, and which compounds could be involved.

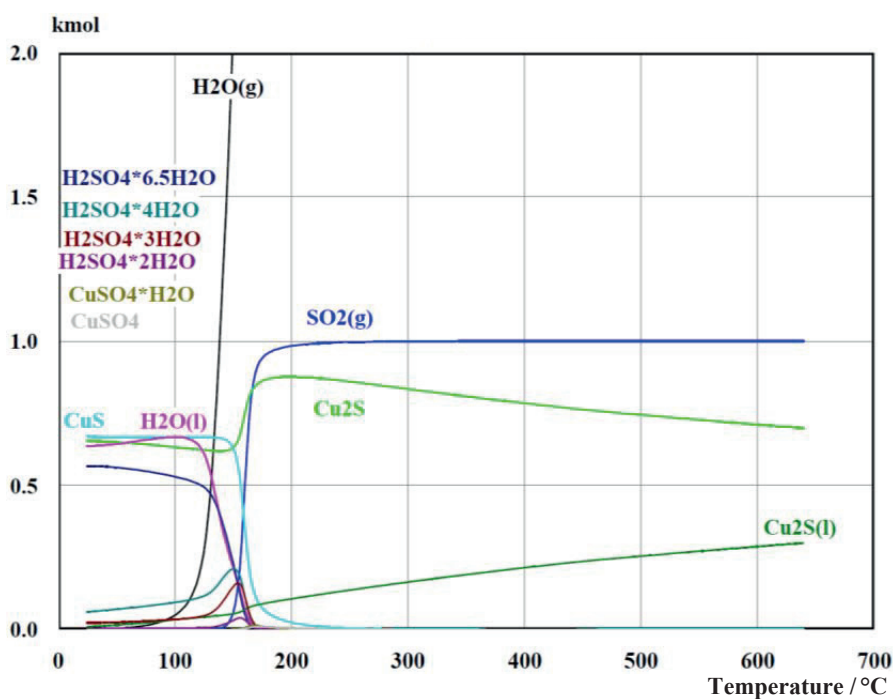


Fig. A2: HSC calculation of the thermodynamic equilibrium of CuSO_4 , undergoing a temperature increase from 25 to 640 °C under slightly reducing conditions, in the presence of water, at an absolute pressure of 1.0 bar. The input compounds, considered for the calculation, were: 0.1 mol N_2 , 6 mol H_2 , 2 mol CuSO_4

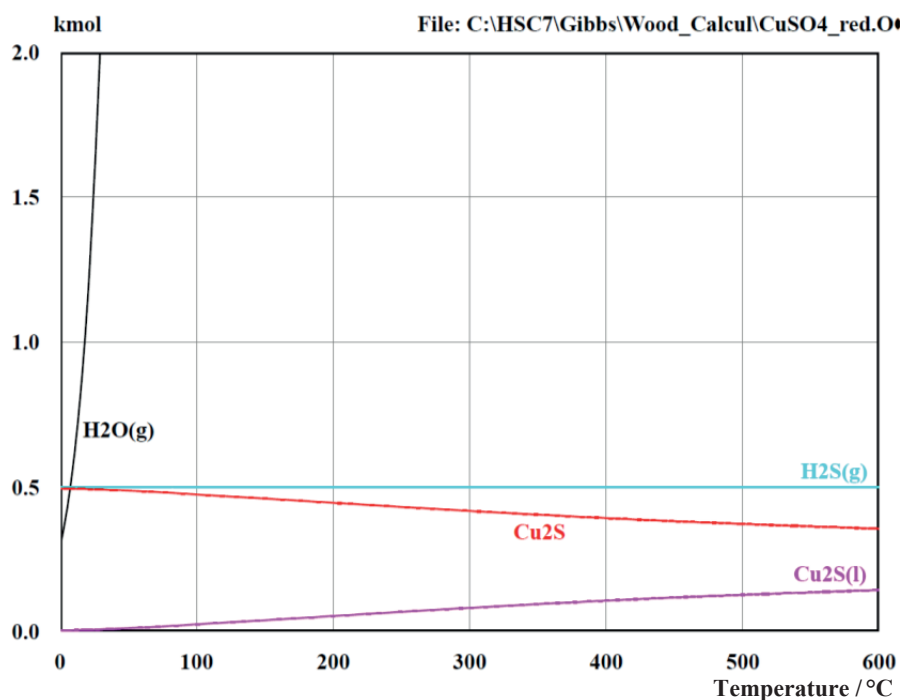


Fig. A3: HSC calculation of the thermodynamic equilibrium of CuSO_4 , undergoing a temperature increase from 25 to 1000 °C under highly reducing conditions, in the presence of water, at an absolute pressure of 1.0 bar. The input compounds, considered for the calculation, were: 0.1 mol N_2 , 200 mol H_2 , 1 mol $\text{CuSO}_4 \cdot 5\text{H}_2\text{O}$

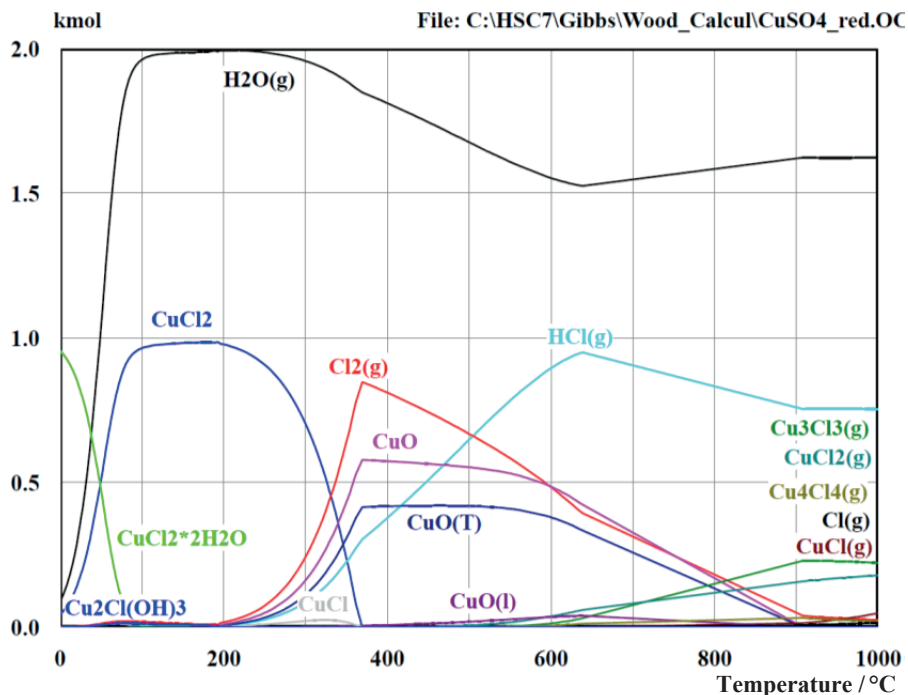


Fig. A4: HSC calculation of the thermodynamic equilibrium of CuCl_2 , undergoing a temperature increase from 25 to 1000 °C under oxidizing conditions, at an absolute pressure of 1.0 bar. The input compounds, considered for the calculation, were: 0.1 mol N_2 , 100 mol O_2 , 1 mol $\text{CuCl}_2 \cdot 2\text{H}_2\text{O}$

A.3 Characterization of ENP containing sprays

(published in: Losert, S., Hess, A., Ilari, G., von Goetz, N., Hungerbuehler, K. (2015). Online characterization of nano-aerosols released by commercial spray products using SMPS-ICPMS coupling. *Journal of Nanoparticle Research*, 17(7), 293.)

Nanoparticle-containing sprays are a critical class of consumer products, since human exposure may occur by inhalation of nanoparticles (NP) in the generated aerosols. In this work, the suspension and the released aerosol of six different commercially available consumer spray products were analyzed. Next to a broad spectrum of analytical methods for the characterization of the suspension, a standardized setup for the analysis of aerosol has been used. In addition, a new online coupling technique (SMPS-ICPMS) for the simultaneous analysis of particle size and elemental composition of aerosol particles has been applied. Results obtained with this new method were confirmed by other well-established techniques. Comparison of particles in the original suspensions and in the generated aerosol showed that during spraying single particles of size less than 20 nm had been formed, even though in none of the suspensions particles of size less than 280 nm were present (Aerosol size range scanned: 7–300 nm). Both pump sprays and propellant gas sprays were analyzed and both released particles in the nm size range. Also, both water-based and organic solvent-based sprays released NP. However, a trend was observed that spraying an aqueous suspension contained in a pump spray dispenser after drying resulted in bigger agglomerates than spraying organic suspensions in propellant gas dispensers.

A.3.1 Introduction

The number of nanoparticle-containing consumer products increased over the last 10 years from a few to several hundreds and their number is expected to further increase in the future (nanotechproject.org, 2011). Market surveys identified silver (Benn, Cavanagh et al., 2010; X. Chen & Schluesener, 2008; Kaegi, Sinnet et al., 2010), zinc oxide (Graf, Chaney et al., 2013), titanium dioxide (Skocaj, Filipic et al., 2011), carbon and silica (Zhu, Zhao et al., 2010) as the species that are most frequently used as nanoparticles (NP) in consumer products such as textiles, food and food storage, cosmetics (e.g., sprays), household chemicals (e.g., paints, sprays), or sports equipment (Al-Kattan, Wichser et al., 2013; Brzeziński, Malinowska et al., 2012; Hall, Tozer et al., 2007; Lorenz, Windler et al., 2012; von Goetz, Fabricius et al., 2013; Xue, Chen et al., 2012).

Sprays that contain NP were identified as the most critical class of consumer products due to their direct exposure pathway via lungs, which implies an enhanced health risk (Krug & Wick, 2011; Norgaard, Larsen et al., 2010; Schneider, Brouwer et al., 2011; Sung, Ji et al., 2008). During the last years, first studies on nanoparticle-containing sprays and associated nanoparticle exposure were published (B. T. Chen, Afshari et al., 2010; Hagendorfer et al., 2010; Lorenz et al., 2011; Oomen, Bennink et al.). In some of these studies, the original spray suspensions were investigated (Hagendorfer et al., 2010; Lorenz et al., 2011). Information was collected about the following four important properties: particle size, chemical composition (of the particles and the whole

suspension), particle number concentration, and shape. However, thus far, no analytical technique is available that informs about all these parameters at the same time. Particle shape, size, and chemistry can be determined offline via electron microscopy (SEM/TEM), which is very time consuming and costly. Size can also be determined online via dynamic light scattering (DLS), which, however, is not very precise for polydisperse samples, as the larger particles are overestimated and measured particle size is always larger than it really is. Bulk analysis of the chemical composition and concentration can be done by inductively coupled plasma mass spectrometry (ICPMS) after the digestion of a sample, which is very time consuming and requires a high level of sample preparation.

New promising techniques for suspension analytics investigate at least two or three of the desired four parameters. Via single-particle inductively coupled mass spectrometry (spICPMS), particle size and number concentration can be measured, if the elemental composition is known and spherical particles can be assumed. This technique is extremely fast (a few seconds) and can be performed with most of the conventional ICPMS instruments (older instruments, however, may not have the adequate acquisition time). Second, asymmetric flow field-flow fractionation (A4F) can provide information on the particle size distribution (PSD), coating of the particles and, when coupled to ICPMS, also on the chemistry and the concentration.

For the analysis of the nanosized particle fraction generated by sprays, analytical techniques need to be used that are different from the techniques used for the suspension. To date the following techniques have been used for nanoparticle analysis in aerosols: PSD and number concentration have been measured online by scanning mobility particle sizer (SMPS) (Hagendorfer et al., 2010; Lorenz et al., 2011; Quadros & Marr, 2011) or fast mobility particle sizer (FMPS) for particles in the size range of 10–500 nm (B. T. Chen et al., 2010; Losert et al., 2014; Norgaard, Jensen et al., 2009; Oomen et al.). However, with SMPS or FMPS, it is not trivial to differentiate between droplets and solid particles, and in many studies only droplet sizes have been determined. Size and shape of particles have been identified offline by prior sampling on TEM grids and analysis by TEM (Bekker, Brouwer et al., 2014; Hagendorfer et al., 2010; Lorenz et al., 2011; Quadros & Marr, 2011), and the aerodynamic diameter of larger particles between 300 nm and 20 μm online by aerodynamic particle sizer (Norgaard et al., 2009). The chemical identity of particles was determined by EDX coupled to TEM or SEM. Currently no technique is available that provides information on all properties simultaneously. Instead, properties of a sample have to be determined with online and offline techniques at the same time, which means that the sampled aliquot may differ between techniques. For example, PSD and number concentration can be measured online and time-resolved, whereas shape and chemistry need to be identified offline with TEM–EDX after sampling on a TEM grid over a longer period of time.

In this work, a new promising coupling technique, SMPS–ICPMS, was used to analyze the aerosol of six commercially available sprays concerning PSD, number concentration, and elemental composition. Simultaneously, these properties were determined by other established methods in

order to assess the performance of the new coupling technique. Furthermore, spICPMS was applied for characterizing the suspensions and compared to conventional methods such as DLS and scanning electron microscopy (SEM).

A standardized spray setup was employed that simulates worst-case consumer exposure. To meet worst-case conditions, particle number concentration and the PSD of pump and propellant gas sprays were monitored at a defined position inside a spray chamber. This position had been identified to be the worst case for most spray applications. For good comparability among the experiments, the duration and direction of spraying had been predefined.

A.3.2 Experimental section

Selection of products

The aim was that the selection be most representative of the range of consumer spray products with NP on the market. The first criterion was that the manufacturer should have labeled the product with “nano”. Second, since the composition of the aerosol depends on the spraying device and the formulation, we considered different vessel types, different solvents, and different intended uses (Losert et al., 2014). Thus, a broad spectrum of sprays was covered that included cosmetic sprays as well as impregnation sprays (used to render a material dirt or water repellent), and different types of NP. The six different spray products, which were selected for this study, are listed in Table A1.

Standardization of exposure experiments

Spray experiments were conducted in a spray chamber with a volume of 0.33 m^3 , representing the near breathing zone of a consumer. Spray vessels were always positioned at a distance of 30 cm to the outlet of the chamber. The average arm length of a Swiss resident was calculated to be 57 cm (woman and man) (Bammes, 2001; COMPASS, 2007; destatis, 2013; Ruehli, Henneberg, & Woitek, 2008). As some sprays are applied with outstretched arms and others with bent arms, the chosen distance of 30 cm should represent a reasonable worst-case scenario.

Table A1: Selected consumer sprays

	Vessel type	Solvent	Application	Target medium	NP type
Spray I	Pump	Water	Cosmetic spray	Human skin	Ag
Spray II	Pump	Water	Impregnation spray	Glass	n.m.
Spray III	Propellant	Water	Impregnation spray	Glass, Ceramic	n.m.
Spray IV	Propellant	Alcohols	Impregnation spray	Textiles	n.m.
Spray V	Propellant	Silicones (I)	Antiperspirant	Human skin	Ag
Spray VI	Propellant	Alcohols	Sunblock	Leather, Textiles	n.m.

n.m. NP type not mentioned on the label; but labeled as a “nano product”

Spraying was directed toward the outlet. The spray duration was always the same for each spray. Propellant gas sprays were sprayed for 3 s; 3 pump strokes were applied for pump spray dispensers.

Experimental setup

The six nanoparticle-containing consumer sprays were analyzed for their chemical composition and PSD. The suspension was analyzed by ICPMS, spICPMS, DLS, and SEM. The aerosol was released by spraying inside a modified glove box setup with integrated analytical devices (Hagendorfer et al., 2010). Based on the considerations by Losert et al. (2014), the spray direction, spray duration, and the distance of the vessel to the measurement device were precisely defined for the spraying procedure.

Before each experiment, the background of the chamber was measured and after each experiment, the chamber was flushed with fresh air. The next experiment was performed when the background was again at the same level as at the beginning of the preceding experiment.

Throughout the measurements, the relative humidity and the temperature were monitored. Humidity did not exceed 50 and 60 % for propellant gas sprays and pump sprays, respectively. During the experiment, an almost constant temperature of 21 °C was measured. The spray chamber was connected to a modified SMPS coupled to a commercial ICPMS to determine online the size distribution and size-resolved elemental composition. The SMPS, consisting of a differential mobility analyzer (DMA) followed by a condensation particle counter (CPC), first selected one particle size fraction from the heterogeneous aerosol and then determined the number concentration of particles contained in this fraction by condensation-driven particle growth and subsequent optical detection. By varying the selected size fraction, a particular particle size ratio was scanned for 120 s and the instrument was ready for the next scan another 60 s later. The ICPMS ionized the particles and detected the mass-to-charge ratio. Thus, the elemental composition of the particles of each size class could be identified. A detailed explanation of this technique is given by Hess et al. (2015).

The shapes of the particles were determined by applying electron microscopy: a TEM sampler was connected to the spray chamber to collect samples for these offline analysis techniques. Also a non-modified reference SMPS was connected to the spray chamber to validate the results obtained by the coupled instrument. A rotating disk dilutor (RDD) was positioned at the inlet of each SMPS instrument and served as sample introduction interface and heated dilution unit (see Fig. A5). The RDDs were heated to 80 °C, so that the solvent droplets were evaporated and only the solid particles could enter the measuring instrumentation. Conductive tubing was used for all connections from the spray chamber to the instruments and also within the instruments to minimize electrostatic particle losses at the tubing walls.

Chemicals

Nitric acid (65 % w/w) and hydrochloric acid (30 % w/w) were purchased in suprapure quality and hydrogen peroxide (31 % w/w) in pro-analysis quality from Merck. ICPMS multi-element standard

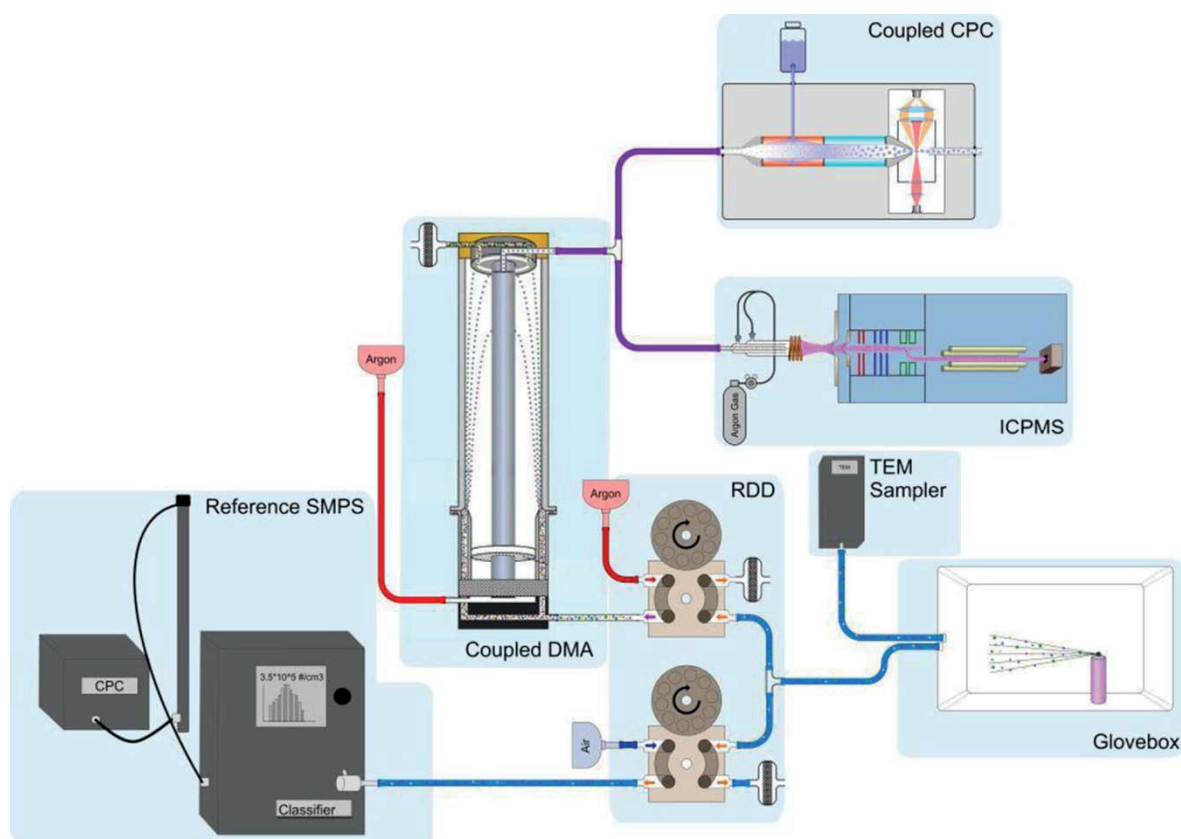


Fig. A5: Experimental setup for aerosol analysis. *Right to left* spray chamber connected to the TEM sampler and two RDDs – one leading to the reference SMPS, one to the coupled DMA. After the DMA, the stream is split between CPC and ICPMS

Merck VI (110580 from Merck) and single element standards of 1 g/L Au, P, Pt, S, Si, Sn, Ti (Specpur, Alfa Aesar) were freshly diluted with deionized water before each measurement. For the production of deionized water (18 M Ω cm), a Millipore, Milli-Q A-10 water unit was used. The single element and multi-element standards were always freshly diluted before each measurement.

Suspension analysis

For the suspension analysis, the spray cans were cooled with liquid nitrogen for 15 min. Then they were opened and left over night to let the organic solvent and the expanding propellant gas evaporate. The next day one part of the suspension was digested completely by microwave digestion for subsequent total elemental analysis and another part was diluted for nanoparticle analysis. The digestion method was adapted to each spray product depending on its labeled composition and observations during the digestion process. For the digestion of product I, 6 mL nitric acid and 2 mL hydrochloric acid were added to an aliquot of 200 μ L. For products II and IV, 2 mL nitric acid and 6 mL hydrochloric acid were added to an aliquot of 200 μ L. For products III, V, and VI, 3 mL nitric acid and 1 mL hydrogen peroxide were added to an aliquot of 50 μ L. After microwave digestion (220 $^{\circ}$ C, 30 min), a clear solution was obtained. The digests were transferred

to PE vessels and filled up with DI water to 50 mL. Suspension ICPMS analysis was carried out on an Agilent 8800 ICPMS using an external calibration adjusted against Scandium, Germanium, and Rhodium as internal standards. The instrument was equipped with two quadrupole analyzers (MS/MS) and a collision/reaction cell. The limit of detection was calculated as three times the standard deviation of the background signal.

The diluted, non-digested samples were analyzed via batch DLS. Measurements were carried out on a Malvern Zetasizer NanoZS. Before analysis, all samples were warmed in the batch cell to 25 °C (1 min).

For SEM analysis, the suspensions were centrifuged on “FORMVAR carbon-coated mesh 200 copper TEM grids” (#3420C from SPI). Imaging was done on a Nova NanoSEM 230 (FEI). Particles were counted using image analysis software (ImageJ, National Institutes of Health, USA).

Single-particle ICPMS measurements were carried out on the same Agilent 8800 ICPMS as the suspension analysis. A dwell time of 5 ms and a flow rate of 0.24 mL/min were applied.

Aerosol analysis

A commercially available Poly(methyl methacrylate) PMMA glove box (Meca Plex) with dimensions of 94 × 55 × 67 cm was modified as described by Hagendorfer et al. (2010). The basic SMPS instrumentation used for coupling to ICPMS included a DMA 3081 (TSI) and a CPC 3010 (TSI). The aerosol flow rate directed to the CPC was accurately defined with 0.3 L/min (Hess et al., 2015). A radioactive source (Kr 85 aerosol neutralizer 3077A from TSI) was installed at the inlet of the DMA to generate a known charge equilibrium state of the particles. In addition to the coupled SMPS, a reference instrument was used to determine the PSD and particle number concentration. The instrument contained an electrostatic classifier 3080L (TSI) and an ultrafine condensation particle counter 3776 (TSI). The modified coupled SMPS was able to scan a particle size ranging from 7.5 to 156 nm, the reference instrumentation from 7 to 300 nm.

The same Agilent 8800 ICPMS was used for the SMPS–ICPMS coupling. The sampling introduction system was removed. The DMA was operated with 1.0 L/min sample flow, being split at the DMA outlet, and a 0.7 L/min fraction was directed to the ICP torch.

Aerosol samples were collected on TEM grids using a portable nanoparticle detector, which were sampled on standard TEM grids by electrostatic precipitation (Partector TEM sampler from naneos). TEM images were acquired on a JEOL 2200 microscope operated at 200 kV.

A.3.3 Results

Suspension

Total chemical analysis

Fig. A6 shows the concentration of metals determined after digestion and total elemental analysis of the spray suspensions. All suspensions showed peaks for Al and Fe. These most probably originate from the spray cans. Apart from these, suspension I contained only silver (18.1 µg/L) and zinc (52.6 µg/L) in higher concentrations. In suspension II, tin was found in the highest concentration of all investigated elements (395 µg/L). Suspension III contained high concentrations of zinc (224 µg/L) and tin (9.5 µg/L). In suspension IV, tin (413 µg/L) and zinc (52.8 µg/L) were found. Suspension V contained the highest concentration of metals: In addition to a high concentration of aluminum (185 300 µg/L), iron (392 µg/L), titanium (27.9 µg/L), and silver (27.2 µg/L) were present. Suspension VI contained a high concentration of zinc (73 000 µg/L).

Particle analysis

DLS measurements showed that in suspension I, particles of the size 320 ± 39 nm were present. In suspension II, particles of 555 ± 120 nm were found. For suspension III, the size of the particles was outside the effective range, which was between 0.3 nm and 10 µm (Malvern, 2004). Suspension IV contained particles of size 373 ± 73 nm. For suspension V, DLS analysis was not possible since the residue resisted to dilution after evaporation of the organic solvent. For suspension VI, the size of the particles was outside the effective range.

spICPMS detected Ag particles of 303 ± 12 nm for suspension I, and tin particles of 263 ± 10 and 244 ± 37 nm for suspensions II and IV, respectively. For suspension III, no particles in the nano-

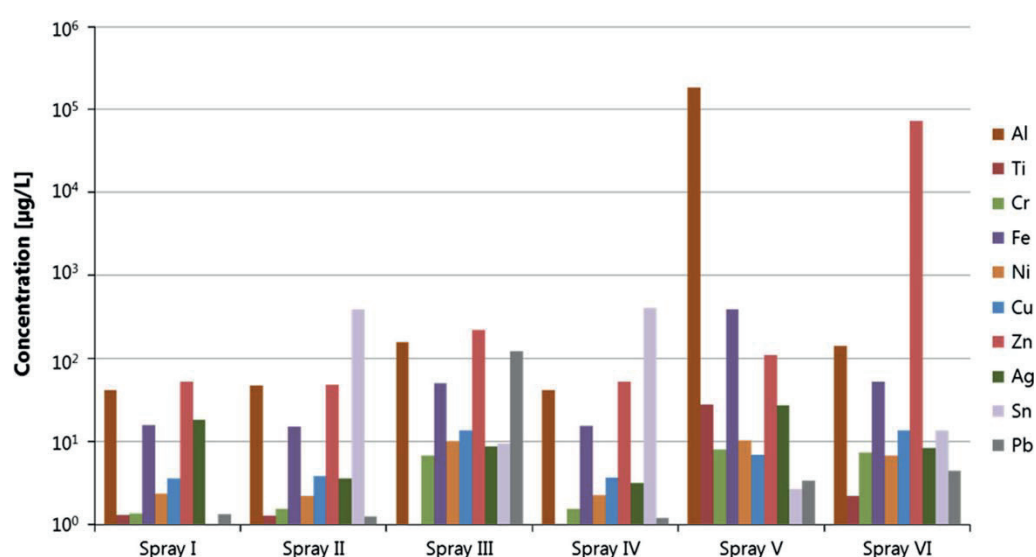


Fig. A6: Metal concentrations in the investigated commercial spray suspensions

range were detected. Consequently, either dissolved tin and zinc ions or very big agglomerates were present in suspension III. The same can be supposed for suspension VI.

SEM images of particles/agglomerates in the original spray suspensions (see left column of Fig. A7) show huge agglomerates of particles in the μm size range for all tested suspensions. For suspension I (Fig. A7a), a three-dimensional agglomerate with the dimensions $6\mu\text{m} \times 3\mu\text{m}$ was observed consisting of single particles of size $369 \pm 87\text{ nm}$. Also for suspensions IV and VI, similarly structured agglomerates were found (Fig. A7d,e). The agglomerate in suspension IV had the dimensions $6.8\mu\text{m} \times 4.3\mu\text{m}$, and single particles were of size $205 \pm 31\text{ nm}$. The agglomerate of suspension VI was $26\mu\text{m} \times 24\mu\text{m}$; the single particles were as large as $1700 \pm 250\text{ nm}$. Particles found in suspension II and III (Fig. A7b,c) were also agglomerated, but the layer of agglomerates on the TEM grid was less thick than for the other three suspensions. Primary particles found in suspension II were $600 \pm 143\text{ nm}$; primary particles in suspension III were $1000 \pm 400\text{ nm}$. EDX analysis (see right column of Fig A7) agrees well with bulk ICPMS results, with the exception of suspension I (no silver was found with EDX).

In all of the analyzed samples, aluminum was detected with EDX. A comparison of all results for suspension analysis can be found in Table A2.

Aerosol

Validation of SMPS-ICPMS data

With an SMPS being hyphenated to ICPMS (SMPS-ICPMS) and an additional, non-modified reference SMPS, particle concentrations above the measured particle background signal were measured for all tested sprays apart from sample I. Generally, both instruments agreed well, but the particle sizes measured by the reference SMPS were slightly larger than the sizes measured by the coupled instrument, because the instruments have different delay times due to different tubing

Table A2: Characteristics of the investigated spray products (suspensions and aerosols) as determined with different analytical methods

	Suspension					Aerosol				
	Identity		Particle size (nm)			Identity		Particle size (nm)		Particle number
	ICPMS	EDX	DLS	spICPMS	SEM	ICPMS	EDX	SMPS	TEM	
Spray I	Ag	Al	320 ± 39.5	303 ± 12	agg	-	Ag, Cl	-	1350 ± 270	-
Spray II	Sn, Zn	Al, Zn, F	555 ± 120	263 ± 10	agg	Sn	Sn, F	85 ± 3	1057 ± 590	$(5.5 \pm 0.4) 10^5$
Spray III	Zn, Sn	Al, Si, F	agg	agg	agg	Sn	Sn, F	24 ± 1	330 ± 20	$(2.4 \pm 0.12) 10^5$
Spray IV	Sn, Zn	Al, Sn, F	373 ± 73.1	244 ± 37	agg	Sn	Sn, F	85 ± 0	124 ± 25	$(5.6 \pm 0.45) 10^5$
Spray V	Al	n.m.	n.m.	n.m.	n.m.	-	Al	24 ± 1	-	$(3.7 \pm 0.1) 10^5$
Spray VI	Zn	Al, Zn, F	agg	agg	agg	Zn	Zn, F	19 ± 1	25 ± 4	$(4.7 \pm 0.15) 10^5$

For SMPS results the number PSD was used to determine the mean size
agg agglomerate

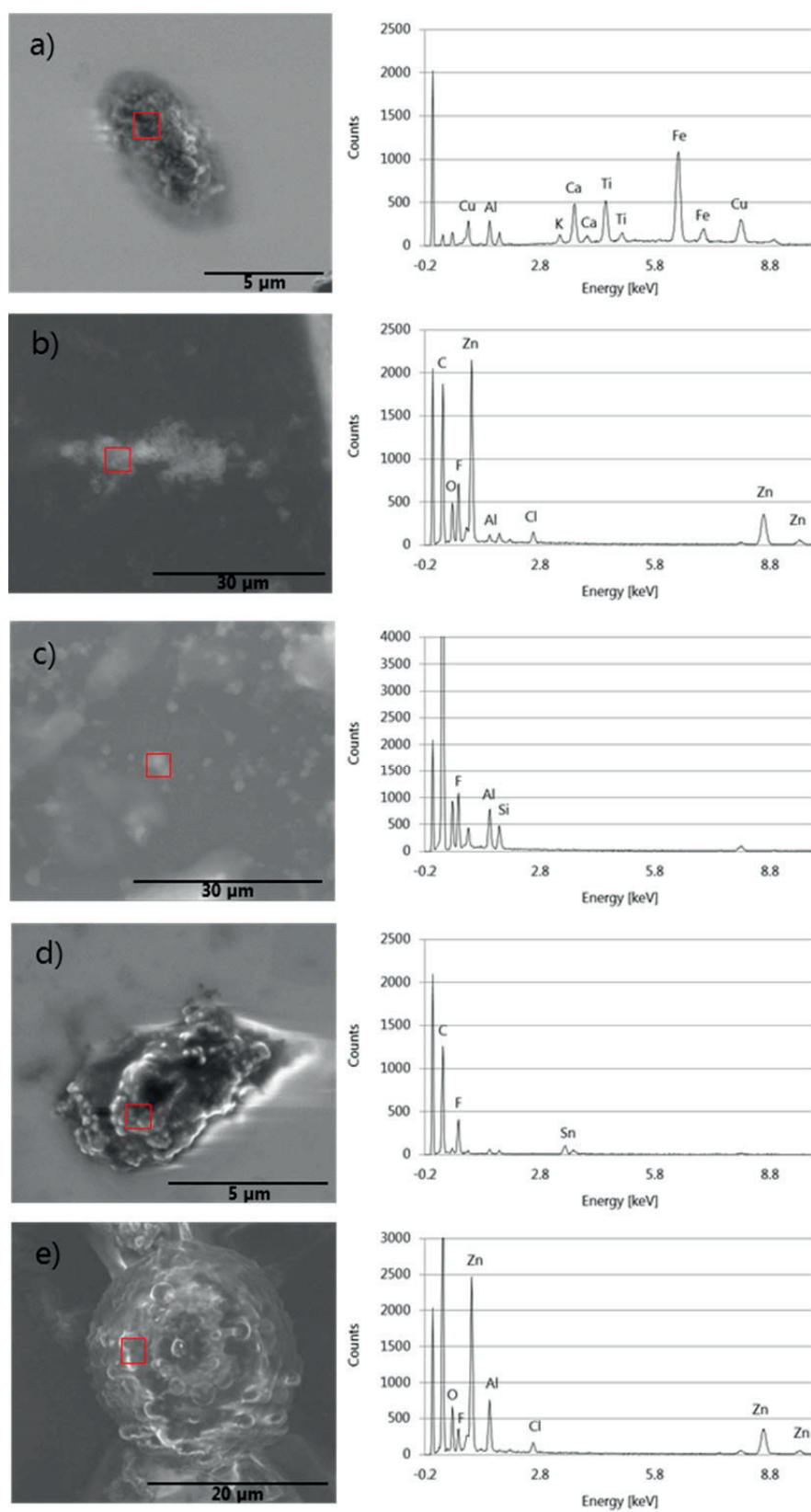


Fig. A7: SEM/EDX images of nanoparticles present in the spray suspensions (a= spray I, b= spray II, c= spray III, d= Spray IV, e= spray VI). Red-shaded areas were investigated by EDX.

lengths (the delay time describes the time a particle needs to travel from the outlet of the DMA to the inlet of the CPC (see Fig. A5). The particle number concentrations in most cases agreed well for the coupled SMPS, if compared to the reference SMPS.

SMPS-ICPMS setup

Based on the results from the conventional suspension measurements with ICPMS, sample-specific elements were selected for SMPS–ICPMS aerosol analysis. Since for the coupled device the scanning time of the SMPS needs to match the acquisition time of the ICPMS (Hess et al., 2015), only 5 metals could be measured simultaneously and the ICPMS was adjusted to the masses of the metals found in the suspensions.

No increased particle concentrations, in comparison to the background level, were recorded by SMPS after spraying of spray I, which was one of the two pump sprays (see diagram in Fig. A8a). The particles found in the second pump spray, spray II, had the highest mean diameter of all investigated products. Nevertheless, we could observe a release of NP also from pump spray dispersers. Among propellant sprays, the mean particle diameter in spray IV was about 3.5 times higher than those in the other three sprays. The originally number-weighted PSD determined by SMPS was transformed into a volume-weighted curve, in order to be comparable to the mass-related ICPMS data. As an approximation, spherical particles were assumed for this data conversion.

Figure A9a–c illustrates on the left the volume-weighted PSD, and the size-resolved ICPMS signal intensity, and on the right the number-weighted PSD, determined by the hyphenated SMPS–ICPMS instrumentation. SMPS data are represented as gray-dashed lines, scaled at the left, ICPMS intensities as straight black curves, scaled at the right.

Since the ^{118}Sn ICPMS curve agrees very well with the PSD determined by SMPS (see Fig. A9a,b), SMPS–ICPMS demonstrated that the particles found in sprays II and IV were mainly consisting of tin.

Fig. A9c illustrates the average SMPS signal of spray VI and the zinc ICPMS signal of the same spray. The SMPS signal of spray VI and the zinc ICPMS show a similar trend for the volume-weighted PSD: an increase in the zinc concentration can be observed for sizes above 80 nm. Around this size (70–90 nm), the curves of the number-based SMPS and the corresponding ICPMS signal fit quite well. This observation hazards the guess that particles present in sample VI consist not only of zinc but also of another element, which could not be identified by the coupled device. Note that after the conversion of volume-weighted (Fig. A9c, left side) to number-weighted concentration (Fig. A9c, right side, conversion equation, see Fig. A7), the smaller particle sizes are emphasized. Since health effects are mostly associated with single particles, for NP often the number-based concentrations are the preferred unit.

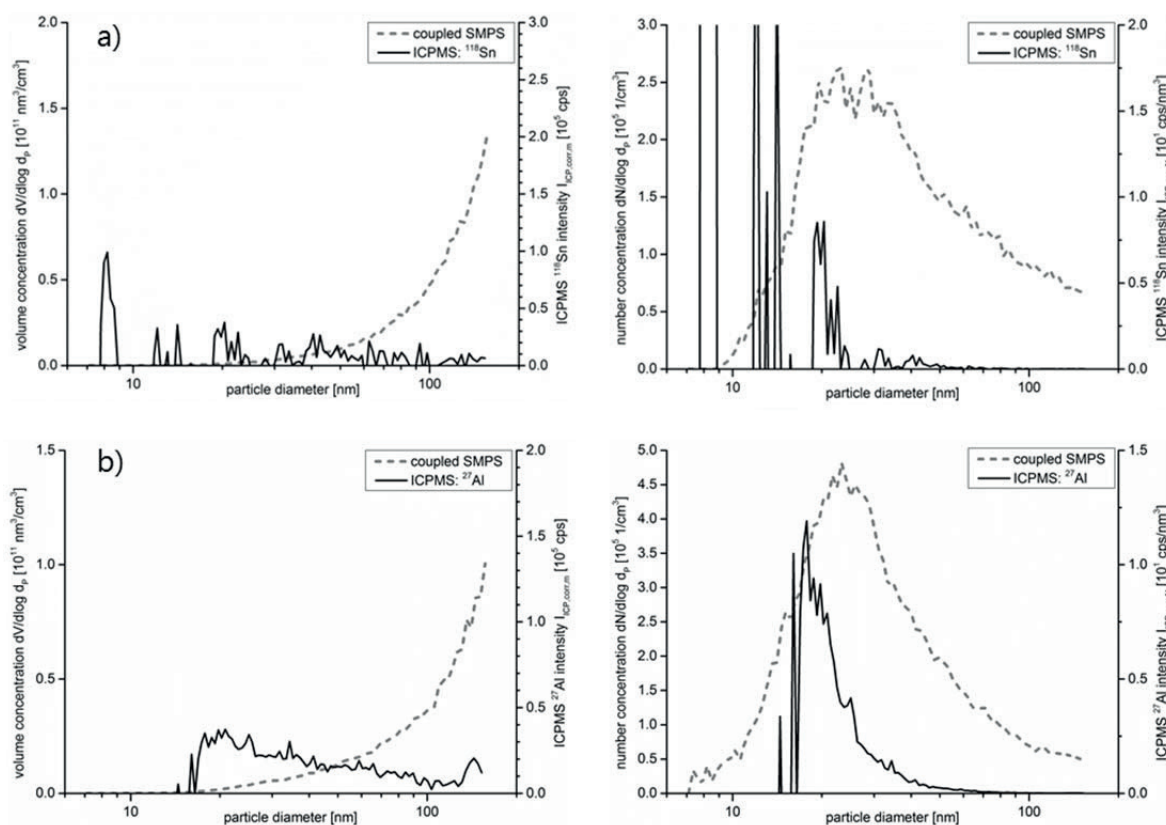


Fig. A7: Volume-weighted (left) and number-weighted (right) SMPS-IPCMS signals a = spray III, b = spray V. SMPS signal does not fit to the corresponding ICPMS signal. For conversion from volume concentration to number concentration the following formula is used: $c_N = c_V / (\pi/6 \cdot d_p^3)$ with c_N : number concentration; c_V : volume concentration and d_p : particle diameter.

Also for sprays III and V, SMPS signals were found, which could not completely be matched to an ICPMS signal (see Fig. A7). Therefore, the TEM–EDX measurements were consulted to identify the chemical identity of the aerosol. Spray I did not evoke an SMPS and the corresponding ICPMS signal, but with bulk ICPMS Ag was found in the suspension. Therefore, with EDX it was further investigated, whether Ag in particular form was present in the aerosol (see below).

Comparison of online measurements with TEM

TEM images of NP released from the different sprays are displayed in Fig. A8 (red squares = area of EDX).

No nanometer-sized particles had been detected in the aerosol of spray I by SMPS. This was confirmed by TEM analysis, but a 1.35- μm agglomerate was detected, consisting of primary particles with a size of about 30 nm. Smaller particles were observed, which are arranged in a ring-shaped area surrounding the big particle. These smaller particles did not contain metals, but organic compounds (see EDX results in Fig. A10). The primary particles inside the agglomerate were identified as silver particles. Summing up, there were primary silver particles in the nm size range.

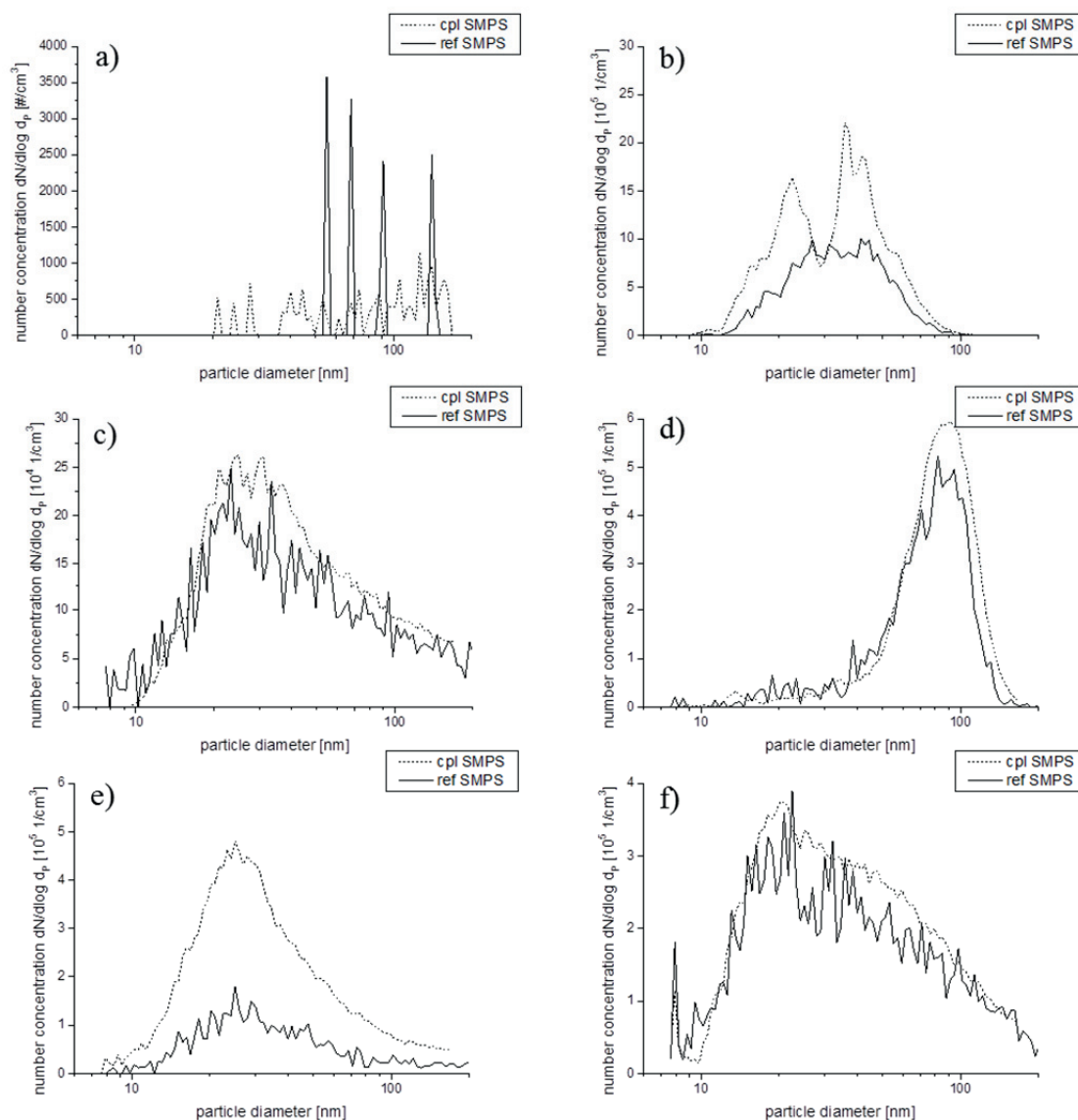


Fig. A8: SMPS signals for tested spray products (a= spray I, b= spray II, c= spray III, d= Spray IV, e= spray V, f= spray VI).

These were agglomerating very fast and the resulting structures were above the SMPS–ICPMS measuring range, and/or the primary particles were shielded by organic compounds and therewith not ionized and detected in ICPMS. No single particles were found from spray II, but two agglomerates of 0.5- and 1.5- μm diameter, respectively, were observed by TEM, with primary NP of around 30 nm building up these big agglomerates. SMPS, however, produced a signal between 80 and 90 nm. Most probably this finding indicates a shortcoming of TEM analysis, being an offline technique, which requires aerosol sampling over a longer period of time. For most of the analyzed products, 3–6 spray experiments were necessary to deposit enough particles on the TEM grids, especially long sampling times were needed for collecting pump spray aerosol particles.

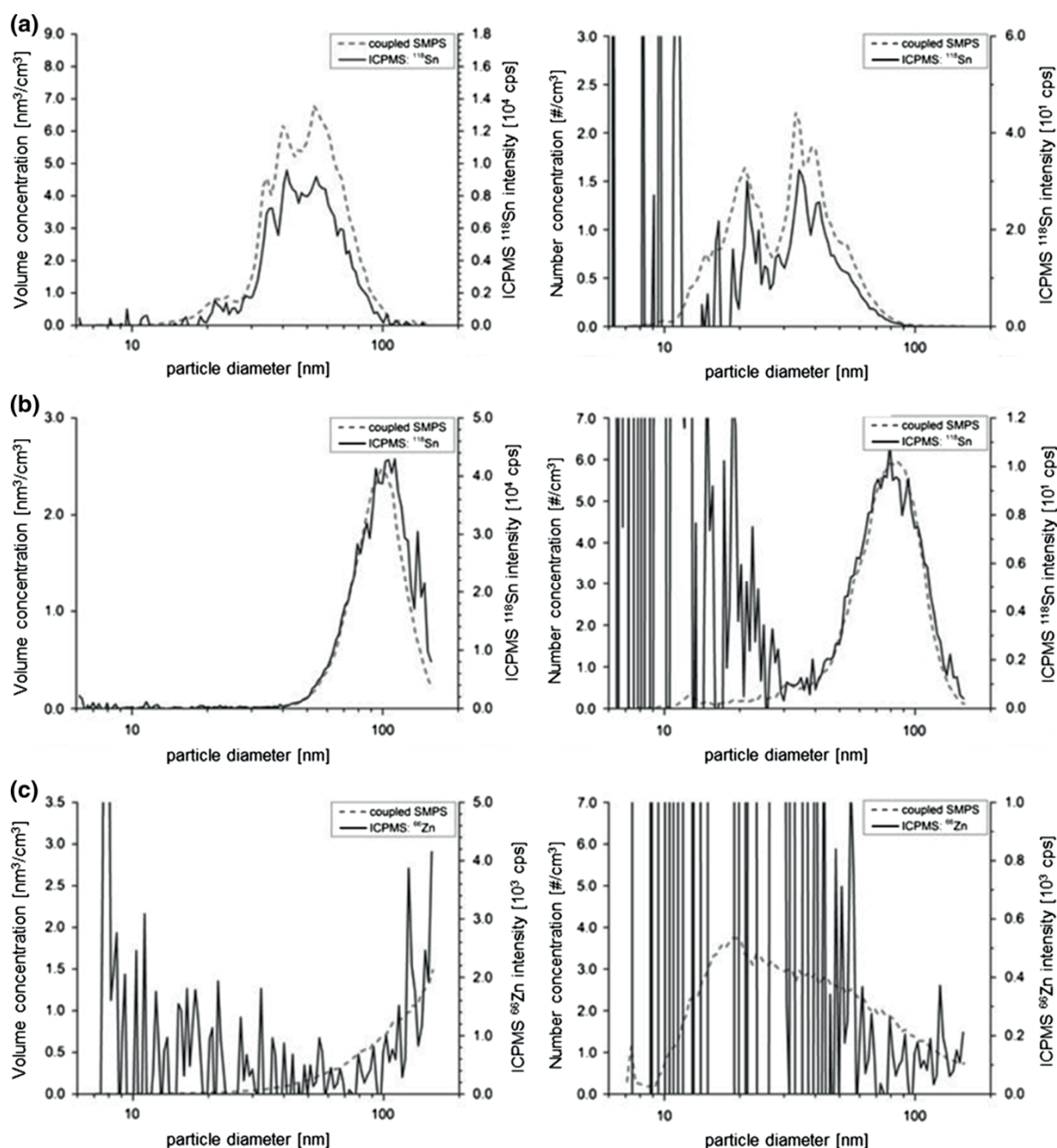


Fig. A9: SMPS-ICPMS results for **a** spray II, **b** spray IV, and **c** spray VI; *left* volume-weighted PSD, *right* number-weighted PSD.

During the time on the grid, the primary particles from spray II may have agglomerated (Hagendorfer et al., 2010; Lorenz et al., 2011). Furthermore, the TEM images show that the bigger agglomerate from spray II was consisting of a tin core and a light shell around the core, which mostly consisted of fluorine. For sprays III, IV, and VI, primary particles with mean diameters of 25, 85, and 20 nm (in the number-weighted PSD), respectively, were found by SMPS. This result could be verified by TEM (Fig. A10c,d,f): All TEM images show primary particles, but

Appendix

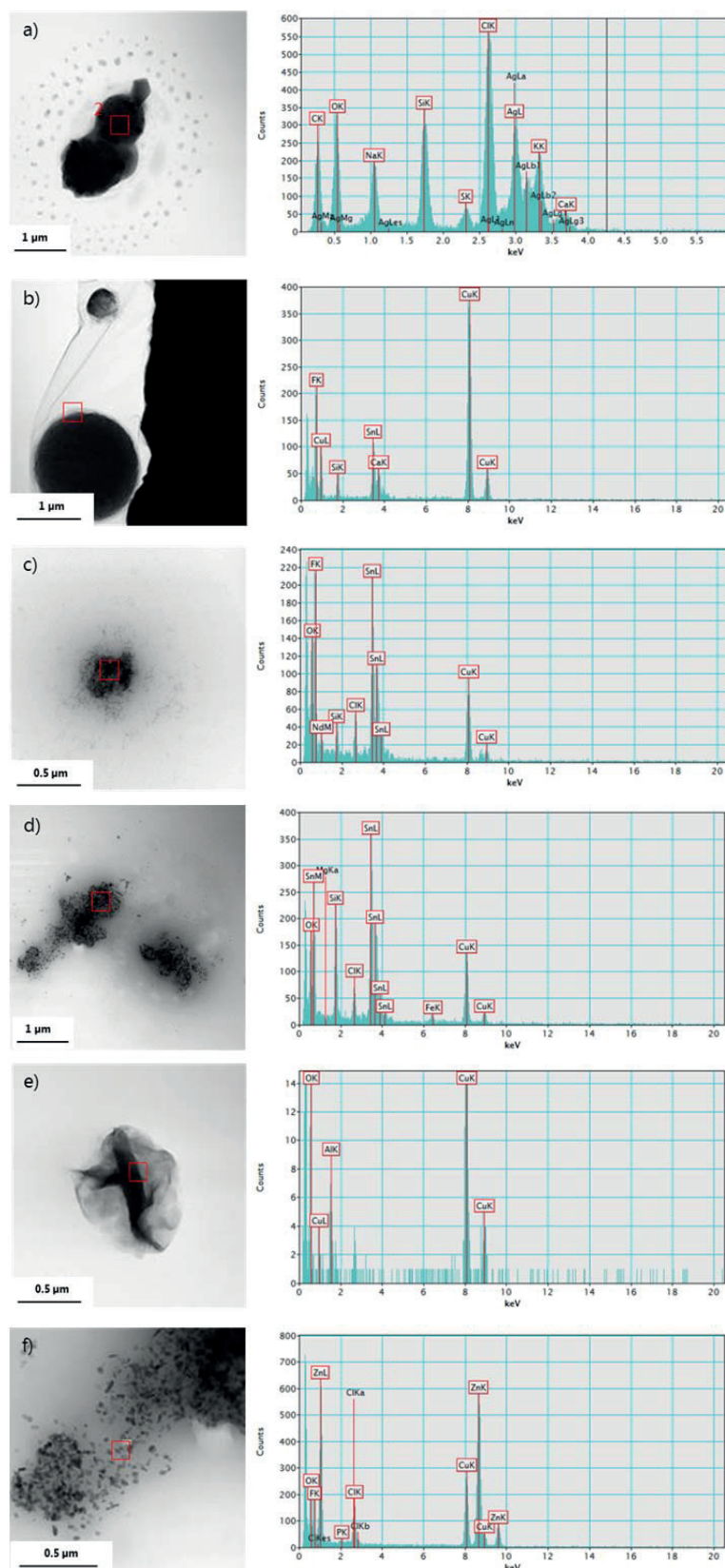


Fig. A10: TEM/EDX images of nanoparticles collected from the aerosol (a= spray I, b= spray II, c= spray III, d= Spray IV, e= spray V, f= spray VI)

agglomeration was observed as well. Via EDX the composition of the particles was analyzed. NP detected in sprays III and IV contained tin and fluorine. Particles present in spray VI contained also zinc. For spray V, no particles in the nm size range were detected by TEM: the PSD determined by SMPS and the size-resolved ICPMS intensities recorded in terms of the SMPS–ICPMS online measurements did not match. The particles mainly contain aluminum (determined by EDX).

Summary of suspension and aerosol measurements

For all investigated products, particle sizes changed due to spraying. With the exception of spray V, all aerosols contained primary particles of size less than 50 nm (Table A2), even though particles in the suspensions had been larger.

A.3.4 Discussion

Standardized setup for spray experiments

Using a standardized spray setup, good reproducibility was achieved. Although a larger number of sprays with different applications were tested, results could easily be compared, marking an improvement over previous studies (Berger-Preiss, Boehncke et al., 2005; Norgaard et al., 2009).

Suspension analysis

Elemental composition

Product I was labeled with a content of 50 mg/L silver, but only 18 µg/L Ag was found with ICPMS analysis of the diluted and digested suspension. As product I is an aqueous cosmetic spray to be applied on the skin, presumably no acid had been added to the formulation and without acid silver is not stabilized. Hence, the contained Ag may actually have been adsorbed to the vessel walls, so that it was not detectable in the suspension.

In suspensions II, III and IV, tin was found. Tin is typical for impregnation sprays, since they often contain organotin compounds, which are used as accelerators (for faster hardening of the other ingredients) (BgVV, 2000). The high aluminum concentration in product V can be explained by the fact that this was an antiperspirant spray. These sprays usually contain high amounts of aluminum to prevent perspiration. According to the product label, the aluminum had been added to the product in the form of aluminum chlorohydrate, which had the highest concentration of all product ingredients, apart from the solvents (in Europe ingredients with a concentration >1 % are listed on the product label in descending order relative to their concentration). The same suspension also contained small concentrations of iron and titanium, which were not labeled, but those elements can be part of so-called alums, being chemical compounds with the formula $AM(SO_4)_2 \cdot 12H_2O$, where A is a cation and M is a metal-like iron or titanium. Alums have antiperspirant and antibacterial effects. For those compounds, no labeling is required, because their concentration is below 1 %.

Particle sizes

Sizes obtained with different methods fit well. Particle diameters determined by spICPMS were smaller than those determined by DLS and SEM, which can be explained by matrix effects: As all samples were simply diluted for spICPMS analysis and the matrix was not removed, probably interferences with the matrix occurred, causing higher background and therewith lower net signal intensity, and finally resulting in smaller calculated particle sizes. Additionally, sprays II and IV contain high amounts of fluorine, which covers the metal NP. As fluorine cannot be ionized in the plasma and subsequently be detected by ICPMS, the calculated particle size is smaller than that obtained from methods that are able to detect fluorine. For sprays III and VI, no particles were found with DLS and spICPMS, whereas SEM allowed observation of agglomerates of 1.0 and 1.7 μm . Possibly the respective particles got dissolved during the sample preparation for spICPMS and for DLS measurements.

Particle composition

Silver was found by ICPMS analysis of suspension I, but not via SEM–EDX of the particles, which were sampled from the suspension. This is presumably due to the lower detection limit of the ICPMS, compared to SEM–EDX.

Aerosol measurements

The slight discrepancy between particle number concentrations obtained by coupled SMPS and reference SMPS can be explained with the use of two different rotating disk diluters (RDD). The sampling line included a flow splitter, and each RDD was absorbing about 1 L/min raw aerosol. In the RDD, heated to 80 °C, a defined amount of raw aerosol was added to 1.0 L/min dilution air in the case of the conventional SMPS, resulting in a dilution factor of 28 (reference RDD), or with argon in the case of SMPS–ICPMS, resulting in a dilution factor of 18 (coupled RDD). The difference of the resulting dilution factors was caused by geometrical differences of the disks of the two RDD devices (Hueglin et al., 1997).

SMPS–ICPMS and conventional SMPS curves correlate very well for both volume-weighted and number-weighted distributions. The number-weighted distributions appear to be shifted a little toward smaller particles compared to the volume-weighted curves, since small particles contribute more to the number concentration and larger particles contribute more to the mass and volume concentration. This is also the reason for the high intensity of the number-related ICPMS signal for particles below 15 nm. As mass concentration and thereby ICPMS signal intensity scales with the third power of the particle diameter, ICPMS intensity is much higher for very small particle sizes.

Large agglomerates were found in TEM images of aerosol particles. However, such offline imaging of previous collected particles does not allow distinguishing whether the agglomerates were already present in the aerosol, or if they were formed during particle sampling on the TEM grids, or during sample preparation and storage. Online sampling and SMPS–ICPMS analysis is

better suited for characterizing the size-resolved elemental composition of particles in the aerosol, when they enter the measuring instrumentation directly after spraying. Besides, transient aerosol behavior also becomes visible since the size range scans were repeated every 180 s.

Comparison of suspension and aerosol

For some products, the metals found in the suspension were not detected in the SMPS–ICPMS aerosol measurements, but with TEM–EDX. Fluorine can generally not be detected by ICPMS, because its first ionization energy is higher than that of argon so that it cannot be ionized with argon plasma. For aluminum, which was not detected in the aerosol of spray V, the ICPMS has a relatively low intensity due to the use of a collision cell to eliminate mass-based interferences. In spray VI, NP consisting of zinc were detected with TEM–EDX. With the SMPS–ICPMS coupling, this finding was confirmed. Nevertheless, larger particles found by SMPS were not correlated to the ICPMS zinc signal. As discovered by EDX, at larger sizes, the zinc particles were imbedded in fluorine, which apparently shielded them from the ICPMS.

Particle sizes found in the released aerosol were always smaller compared to the particle sizes in the suspensions. This means that during spraying the agglomerates decrease in size or are fully broken to release the primary particles. This result was confirmed by different analytical methods. Spray IV and VI showed the biggest agglomerates in suspension, which broke up into the NP found in the aerosol. In the TEM, these agglomerates looked like raspberries with single particles on the surface, which may be a structure that is easily cleaved during the spray process.

For three products (Spray I, II, and III), large agglomerates containing small primary particles were detected by TEM. The SMPS could not detect these agglomerates as their sizes were exceeding the SMPS measuring range.

After spraying, the aluminum, which had been detected in all six suspensions by SEM–EDX, was only detected in the aerosol of spray V via TEM–EDX. With the SMPS–ICPMS instrumentation, an increase of the aluminum background signal was observed after spraying sprays III, IV, V, and VI, which remained stable on this elevated level for several minutes. So far we have no explanation for the observation of aluminum after spraying. As we observed no corresponding SMPS signal, it is not likely that the ICPMS signal was caused by Al NP in or above the size range scanned by SMPS (bigger particles would not stay in the aerosol phase). A mass interference is not supposed, as Al was measured in the collision mode of the ICPMS. One possible reason could be that this signal was caused by particles <3 nm, but it is expected that these would have been detected with TEM.

With TEM we found that some of the primary particles were not spherical, which is a phenomenon that had already been observed by Bekker et al. (2014). Since online methods always simplify the calculations by assuming spherical particles for size calculation, it has to be kept in mind that for nonspherical particles the dynamic shape factor has to be determined before calculating the size (Scheuch & Heyder, 1990).

A.3.5 Conclusion and outlook

The purpose of this paper was to define a standard for nanoparticle characterization in sprays and to test different methods for nanoparticle analysis in suspension and in sprays. New methods were tested for both media: spICPMS for suspension analysis and SMPS–ICPMS coupling for aerosol analysis. Despite the fact that also in future experiments a combination of several methods will be necessary, since there is no perfect single method, spICPMS can be highly recommended for suspension analysis, because it is a fast method and delivers reproducible results, compared to conventional methods such as TEM and DLS. For aerosol analysis, SMPS–ICPMS coupling is a very promising technique. Compared to the conventional methods, it is very fast and delivers the most important data during one online measurement. A drawback, however, is the low detection efficiency of ICPMS for elements with high ionization energy, which is unfavorable e.g. for sprays containing fluorine.

With the new online coupling method, small primary particles can be monitored online and their chemistry can be identified without the generation of artificial agglomerates due to sampling on a TEM grid. Thus, our project is the first to characterize online nanosized aerosols regarding particle size and corresponding composition (Bekker et al., 2014; B. T. Chen et al., 2010; Hagendorfer et al., 2010; Lorenz et al., 2011; Norgaard et al., 2009; Quadros & Marr, 2011). The shape of the particles still can only be determined using offline techniques like electron microscopy, so that TEM–EDX should support the method.

To prove the new technique, also suspensions were analyzed with known particle size and concentrations. However, this work has been published elsewhere (Hess et al., 2016).

In general, a release of NP was observed for all sprays apart from spray I. Hence, not only propellant gas, but also pump sprays can release NP. Therefore, the assumption of Hagendorfer et al. (2010) and Lorenz et al. (2012) that only propellant gas sprays can release NP has to be revisited.

The final size and the agglomeration state of the released particles seem to depend on different factors such as the solvent and the formulation. Metals found in the suspensions are the main component of the NP in the released aerosol. Some particles, especially the ones released from impregnation sprays, had a metal core covered by a fluorine–carbon shell. This had already been observed by Lorenz et al. (2012). During the spray process, the size of the initial particles that were present in the suspension decreased: Particles/Agglomerates present in the suspensions were about 10 times larger than the ones released after application of the sprays. Consequently, also sprays, which are not labeled as nano, may release particles in the nanometer size range. This confirms the results published by Bekker et al. (2014).

For the moment it is difficult to judge if the released particle/metal concentrations pose a real health risk for the consumer, because the toxicological relevance of the nanoform is still under

debate. A comparison of the metal concentrations determined in the spray suspension can be done with the concentrations given by the International Conference on Harmonization for elemental impurities in inhalable drugs, which are 0.7 µg/g for Ag and 6 µg/g for Sn (ICH, 2014). In comparison to these guidance values for bulk material, the concentrations detected in this study are low: The highest detected Ag concentration in suspension was 0.03 µg/g and the highest Sn concentration 0.4 µg/g.

A.4 Instrument and sample manufacturers

The manufacturers or suppliers of all instruments, technical components, and particle products, mentioned in this work, were the following:

Agilent	Agilent Technologies Santa Clara, USA	Mettler Toledo	Mettler Toledo GmbH Greifensee, Switzerland
Alfa Aesar	Alfa Aesar GmbH & Co KG Karlsruhe, Germany	Millipore	Merck Millipore Schaffhausen, Switzerland
Brooks	Brooks Instrument Ede, Netherlands	MSA	Mine Safety Appliances Pittsburgh, USA
Eckert & Ziegler	Eckert & Ziegler AG Braunschweig, Germany	msscscientific	msscscientific GmbH Berlin, Germany
FEI	FEI Corporate Hillsboro, USA	naneos	naneos particle solutions Windisch, Switzerland
Fisher Scientific	Fisher Scientific AG – Reinach, Switzerland	NanoComposix	NanoComposix Inc. San Diego, USA
Fluka	Fluka / Sigma-Aldrich Buchs SG, Switzerland	NanoSys	NanoSys GmbH Wolfhalden, Switzerland
Headline	Headline Filters Aylesford, UK	Outotec	Outotec Espoo, Finland
JEOL	JEOL (Germany) GmbH Freising, Germany	Perkin Elmer	Perkin Elmer Office Basel, Switzerland
KNF	KNF Neuberger AG Freiburg, Germany	Sensidyne	Sensidyne St. Petersburg, USA
Malvern	Malvern Instruments GmbH Herrenberg, Germany	Sierra	Sierra Instruments Inc. Monterey, USA
Matter Aerosol	Matter Aerosol AG Wohlen, Switzerland	SPI	SPI Inc. West Chester, PA, USA
Meca Plex	Meca Plex, Grenchen Switzerland	Topas	Topas GmbH Dresden, Germany
Merck	Merck GmbH Darmstadt, Germany	TSI	TSI Inc. Shoreview, USA

A.5 References

- Agarwal, J. K., Sem, G. J. (1980). Continuous flow, single-particle-counting condensation nucleus counter. *Journal of Aerosol Science*, 11(4), 343-357.
- Al-Kattan, A., Wichser, A., Vonbank, R., Brunner, S., Ulrich, A., Zuind, S., et al. (2013). Release of TiO₂ from paints containing pigment-TiO₂ or nano-TiO₂ by weathering. *Environmental Science-Processes & Impacts*, 15(12), 2186-2193.
- Babrauskas, V. (2002). Ignition of wood: A review of the state of the art. *Journal of Fire Protection Engineering*, 12(3), 163-189.
- Baltensperger, U., Gaggeler, H. W., Jost, D. T. (1988). The Epiphaniometer, a New Device for Continuous Aerosol Monitoring. *Journal of Aerosol Science*, 19(7), 931-934.
- Bammes, G. (2001). *Studien zur Gestalt des Menschen : eine Zeichenschule zur Künstleranatomie mit Arbeiten von Laienkünstlern, Kunstpädagogen und Kunststudenten* (3rd ed.). Leipzig: Seemann.
- Baron, P. A., Willeke, K. (2001). *Aerosol Measurement: Principles, Techniques, and Applications* (2 ed.). New York: John Wiley and Sons, Inc.
- Behrendt, F., Neubauer, Y., Oevermann, M., Wilmes, B., Zobel, N. (2008). Direct Liquefaction of Biomass. *Chemical Engineering & Technology*, 31(5), 667-677.
- Bekker, C., Brouwer, D. H., van Duuren-Stuurman, B., Tuinman, I. L., Tromp, P., Fransman, W. (2014). Airborne manufactured nano-objects released from commercially available spray products: temporal and spatial influences. *Journal of Exposure Science and Environmental Epidemiology*, 24(1), 74-81.
- Benn, T., Cavanagh, B., Hristovski, K., Posner, J. D., Westerhoff, P. (2010). The Release of Nanosilver from Consumer Products Used in the Home. *Journal of Environmental Quality*, 39(6), 1875-1882.
- Berger-Preiss, E., Boehncke, A., Konnecker, G., Mangelsdorf, I., Holthenrich, D., Koch, W. (2005). Inhalational and dermal exposures during spray application of biocides. *International Journal of Hygiene and Environmental Health*, 208(5), 357-372.
- BgVV. (2000). *Organozinnverbindungen in Imprägniermitteln für Lederwaren und Textilien*. Retrieved 07.01.2016, from http://www.bfr.bund.de/cm/343/organozinnverbindungen_in_impraegniermitteln_fuer_lederwaren_und_textilien.pdf
- Blasing, M., Muller, M. (2012). Investigations on the influence of steam on the release of sodium, potassium, chlorine, and sulphur species during high temperature gasification of coal. *Fuel*, 94(1), 137-143.
- Brem, B. T., Durdina, L., Siegeris, F., Beyerle, P., Bruderer, K., Rindlisbacher, T., et al. (2015). Effects of Fuel Aromatic Content on Nonvolatile Particulate Emissions of an In-Production Aircraft Gas Turbine. *Environmental Science & Technology*, 49(22), 13149-13157.
- Brzeziński, S., Malinowska, G., Kowalczyk, D., Kaleta, A., Borak, B., Jasiorski, M., et al. (2012). Antibacterial and Fungicidal Coating of Textile-polymeric Materials Filled with Bioactive Nano- and Submicro-particles. *Fibres & Textiles in Eastern Europe*, 90(1), 70-77.
- Buha, J., Mueller, N., Nowack, B., Ulrich, A., Losert, S., Wang, J. (2014). Physical and chemical characterization of fly ashes from swiss waste incineration plants and determination of the ash fraction in the nanometer range. *Environmental Science & Technology*, 48(9), 4765-4773.

- Burtscher, H. (2005). Physical characterization of particulate emissions from diesel engines: a review. *Journal of Aerosol Science*, 36(7), 896-932.
- Carazzone, C., Rami, R., Pergantis, S. A. (2008). Nanoelectrospray ion mobility spectrometry online with inductively coupled plasma-mass spectrometry for sizing large proteins, DNA, and nanoparticles. *Analytical Chemistry*, 80(15), 5812-5818.
- Chen, B. T., Afshari, A., Stone, S., Jackson, M., Schwegler-Berry, D., Frazer, D. G., et al. (2010). Nanoparticles-containing spray can aerosol: characterization, exposure assessment, and generator design. *Inhalation Toxicology*, 22(13), 1072-1082.
- Chen, X., Schluesener, H. J. (2008). Nanosilver: A nanoparticle in medical application. *Toxicology Letters*, 176(1), 1-12.
- COMPASS. (2007). *Swiss Health Survey 2007 (SHS)*. Retrieved 07.01.2016, from http://compass-data.unil.ch/webview/index/en/compass/Data-from-the-swiss-public-statistic.c.COMPASS/Health-Survey.d.11/Swiss-Health-Survey-2007-SHS-.s.ESSSGB-2007-072012/Gesundheitszustand.h.7/K-rpermasse--Schwanger.h.29/K-rpergr-sse-cm-/fVariable/ESSSGB-2007-072012_V760
- Covert, D., Wiedensohler, A., Russell, L. (1997). Particle charging and transmission efficiencies of aerosol charge neutralizers. *Aerosol Science and Technology*, 27(2), 206-214.
- DeCarlo, P. F., Slowik, J. G., Worsnop, D. R., Davidovits, P., Jimenez, J. L. (2004). Particle Morphology and Density Characterization by Combined Mobility and Aerodynamic Diameter Measurements. Part 1: Theory. *Aerosol Science and Technology*, 38(12), 1185-1205.
- destatis. (2013). *Körpermaße nach Altersgruppen und Geschlecht*. Retrieved 07.01.2016, from <https://www.destatis.de/DE/ZahlenFakten/GesellschaftStaat/Gesundheit/GesundheitszustandRelevantesVerhalten/Tabellen/Koerpermasse.html>
- Elzey, S., Tsai, D.-H., Yu, L., Winchester, M., Kelley, M., Hackley, V. (2013). Real-time size discrimination and elemental analysis of gold nanoparticles using ES-DMA coupled to ICP-MS. *Analytical and Bioanalytical Chemistry*, 405(7), 2279-2288.
- Fierz, M., Vernooij, M. G. C., Burtscher, H. (2007). An improved low-flow thermodenuder. *Journal of Aerosol Science*, 38(11), 1163-1168.
- Flagan, R. C. (2008). Differential mobility analysis of aerosols: A tutorial. *Kona Powder and Particle Journal*, 26, 254-268.
- Franck, J. (1910). Über die Ionenbeweglichkeit in Argon und den Einfluss geringer Mengen Sauerstoffs auf diese Grösse. *Verhandlungen der Deutschen Physikalischen Gesellschaft*, 12, 291-298.
- Gaggeler, H. W., Baltensperger, U., Emmenegger, M., Jost, D. T., Schmidtt, A., Haller, P., et al. (1989). The Epiphaniometer, a New Device for Continuous Aerosol Monitoring. *Journal of Aerosol Science*, 20(5), 557-564.
- Gehrig, R., Hill, M., Lienemann, P., Zwicky, C. N., Bukowiecki, N., Weingartner, E., et al. (2007). Contribution of railway traffic to local PM10 concentrations in Switzerland. *Atmospheric Environment*, 41(5), 923-933.
- Gianini, M. F. D., Gehrig, R., Fischer, A., Ulrich, A., Wichser, A., Hueglin, C. (2012). Chemical composition of PM10 in Switzerland: An analysis for 2008/2009 and changes since 1998/1999. *Atmospheric Environment*, 54, 97-106.

- Giechaskiel, B., Dilara, P., Sandbach, E., Andersson, J. (2008). Particle measurement programme (PMP) light-duty inter-laboratory exercise: comparison of different particle number measurement systems. *Measurement Science & Technology*, 19(9), 16.
- Gonzalez, J. J., Liu, C., Wen, S. B., Mao, X., Russo, R. E. (2007). Glass particles produced by laser ablation for ICP-MS measurements. *Talanta*, 73(3), 577-582.
- Graf, B. W., Chaney, E. J., Marjanovic, M., De Lisio, M., Valero, M. C., Boppart, M. D., et al. (2013). In vivo imaging of immune cell dynamics in skin in response to zinc-oxide nanoparticle exposure. *Biomedical Optics Express*, 4(10), 1817-1828.
- Hagendorfer, H., Lorenz, C., Kaegi, R., Sinnet, B., Gehrig, R., Goetz, N. V., et al. (2010). Size-fractionated characterization and quantification of nanoparticle release rates from a consumer spray product containing engineered nanoparticles. *Journal of Nanoparticle Research*, 12(7), 2481-2494.
- Hall, B., Tozer, S., Safford, B., Coroama, M., Stelling, W., Leneveu-Duchemin, M. C., et al. (2007). European consumer exposure to cosmetic products, a framework for conducting population exposure assessments. *Food and Chemical Toxicology*, 45(11), 2097-2108.
- Hasler, P., Nussbaumer, T., Bühler, R. (1995). Vergasung von belasteten Brennstoffen zu Synthesegas. *Bundesamt für Energiewirtschaft, Villigen, Bern*.
- He, M., Dhaniyala, S. (2013). A multiple charging correction algorithm for scanning electrical mobility spectrometer data. *Journal of Aerosol Science*, 61(0), 13-26.
- Heeb, N. V., Ulrich, A., Emmenegger, L., Czerwinski, J., Mayer, A., Wyser, M. (2005). Secondary Emissions Risk Assessment of Diesel Particulate Traps for Heavy Duty Applications. *SAE Technical Paper*, 2005-26-014, 329-338.
- Heringa, M. F., DeCarlo, P. F., Chirico, R., Lauber, A., Doberer, A., Good, J., et al. (2012). Time-resolved characterization of primary emissions from residential wood combustion appliances. *Environmental Science & Technology*, 46(20), 11418-11425.
- Hess, A., Tarik, M., Losert, S., Ilari, G., Ludwig, C. (2016). Measuring air borne nanoparticles for characterizing hyphenated RDD-SMPS-ICPMS instrumentation. *Journal of Aerosol Science*, 92, 130-141.
- Hess, A., Tarik, M., Ludwig, C. (2015). A hyphenated SMPS-ICPMS coupling setup: Size-resolved element specific analysis of airborne nanoparticles. *Journal of Aerosol Science*, 88, 109-118.
- Hewitt, G. W. (1957). The charging of small particles for electrostatic precipitation. *American Institute of Electrical Engineers*, 76(3), 300-306.
- Hinds, W. C. (1999). *Aerosol Technology* (2nd ed.). New York: John Wiley and Sons, Inc.
- Hinds, W. C. (2011). Physical and Chemical Processes in Aerosol Systems. In *Aerosol Measurement* (pp. 31-40): John Wiley & Sons, Inc.
- Hueglin, C., Gehrig, R., Baltensperger, U., Gysel, M., Monn, C., Vonmont, H. (2005). Chemical characterisation of PM_{2.5}, PM₁₀ and coarse particles at urban, near-city and rural sites in Switzerland. *Atmospheric Environment*, 39(4), 637-651.
- Hueglin, C., Scherrer, L., Burtscher, H. (1997). An accurate, continuously adjustable dilution system (1:10 to 1:104) for submicron aerosols. *Journal of Aerosol Science*, 28(6), 1049-1055.

- ICH. (2014). *Guideline for Elemental Impurities*. Retrieved 07.01.2016, from http://www.ich.org/fi/leadmin/Public_Web_Site/ICH_Products/Guidelines/Quality/Q3D/Q3D_Step_4.pdf
- Jakob, A., Stucki, S., Struis, R. (1996). Complete heavy metal removal from fly ash by heat treatment: Influence of chlorides and evaporation rates. *Environmental Science & Technology*, 30(11), 3275-3283.
- Kaegi, R., Sinnet, B., Zuleeg, S., Hagendorfer, H., Mueller, E., Vonbank, R., et al. (2010). Release of silver nanoparticles from outdoor facades. *Environmental Pollution*, 158(9), 2900-2905.
- Kapellios, E. A., Pergantis, S. A. (2012). Size and elemental composition of nanoparticles using ion mobility spectrometry with inductively coupled plasma mass spectrometry. *Journal of Analytical Atomic Spectrometry*, 27(1), 21-24.
- Knutson, E. O., Whitby, K. T. (1975). Aerosol classification by electric mobility: apparatus, theory, and applications. *Journal of Aerosol Science*, 6(6), 443-451.
- Koch, J., Walle, M., Dietiker, R., Gunther, D. (2008). Analysis of laser-produced aerosols by inductively coupled plasma mass spectrometry: Transport phenomena and elemental fractionation. *Analytical Chemistry*, 80(4), 915-921.
- Kowalski, T., Ludwig, C., Wokaun, A. (2007). Qualitative evaluation of alkali release during the pyrolysis of biomass. *Energy & Fuels*, 21(5), 3017-3022.
- Krug, H. F., Wick, P. (2011). Nanotoxicology: An Interdisciplinary Challenge. *Angewandte Chemie-International Edition*, 50(6), 1260-1278.
- Kulkarni, P., Baron, P. A., Willeke, K. (2011). *Aerosol Measurement*: John Wiley & Sons, Inc.
- Laborda, F., Jimenez-Lamana, J., Bolea, E., Castillo, J. R. (2011). Selective identification, characterization and determination of dissolved silver(I) and silver nanoparticles based on single particle detection by inductively coupled plasma mass spectrometry. *Journal of Analytical Atomic Spectrometry*, 26(7), 1362-1371.
- Lee, S., Bi, X. Y., Reed, R. B., Ranville, J. F., Herckes, P., Westerhoff, P. (2014). Nanoparticle size detection limits by single particle ICP-MS for 40 elements. *Environmental Science & Technology*, 48(17), 10291-10300.
- Limbach, L. K., Wick, P., Manser, P., Grass, R. N., Bruinink, A., Stark, W. J. (2007). Exposure of engineered nanoparticles to human lung epithelial cells: Influence of chemical composition and catalytic activity on oxidative stress. *Environmental Science & Technology*, 41(11), 4158-4163.
- Lorenz, C., Hagendorfer, H., von Goetz, N., Kaegi, R., Gehrig, R., Ulrich, A., et al. (2011). Nanosized aerosols from consumer sprays: experimental analysis and exposure modeling for four commercial products. *Journal of Nanoparticle Research*, 13(8), 3377-3391.
- Lorenz, C., Windler, L., von Goetz, N., Lehmann, R. P., Schuppler, M., Hungerbuehler, K., et al. (2012). Characterization of silver release from commercially available functional (nano)textiles. *Chemosphere*, 89(7), 817-824.
- Losert, S. (2015). *Dissertation: Analytical Strategies for a Systematic Characterization of Nanoparticle Release from Commercial Spray Products for Exposure Quantification and Risk Assessment*. PhD thesis, ETH, Zürich, Switzerland.
- Losert, S., Hess, A., Ilari, G., von Goetz, N., Hungerbuehler, K. (2015). Online characterization of nano-aerosols released by commercial spray products using SMPS-ICPMS coupling. *Journal of Nanoparticle Research*, 17(7), 293.

- Losert, S., von Goetz, N., Bekker, C., Fransman, W., Wijnhoven, S. W., Delmaar, C., et al. (2014). Human exposure to conventional and nanoparticle-containing sprays-a critical review. *Environmental Science & Technology*, 48(10), 5366-5378.
- Ludwig, C., Wochele, J., Jörimann, U. (2007). Measuring evaporation rates of metal compounds from solid samples. *Analytical Chemistry*, 79(7), 2992-2996.
- Malvern. (2004). *Zetasizer Nano Series User Manual*: Malvern Instruments.
- May, T. W., Wiedmeyer, R. H. (1998). A table of polyatomic interferences in ICP-MS. *Atomic Spectroscopy*, 19(5), 150-155.
- Mayer, A., Czerwinski, J., Kasper, M., Ulrich, A., Mooney, J. J. (2012). Metal oxide particle emissions from diesel and petrol engines. *SAE Technical Paper*, 2012-01-0841.
- Meier, R., Eeftens, M., Aguilera, I., Phuleria, H. C., Ineichen, A., Davey, M., et al. (2015). Ambient Ultrafine Particle Levels at Residential and Reference Sites in Urban and Rural Switzerland. *Environmental Science & Technology*, 49(5), 2709-2715.
- Mitrano, D. M., Dasilva, Y. A. R., Nowack, B. (2015). Effect of variations of washing solution chemistry on nanomaterial physicochemical changes in the laundry cycle. *Environmental Science & Technology*, 49(16), 9665-9673.
- Mohr, C., DeCarlo, P. F., Heringa, M. F., Chirico, R., Richter, R., Crippa, M., et al. (2015). Spatial Variation of Aerosol Chemical Composition and Organic Components Identified by Positive Matrix Factorization in the Barcelona Region. *Environmental Science & Technology*, 49(17), 10421-10430.
- Myojo, T., Takaya, M., Ono-Ogasawara, M. (2002). DMA as a gas converter from aerosol to "Argonsol" for real-time chemical analysis using ICP-MS. *Aerosol Science and Technology*, 36(1), 76-83.
- Nanda, K. K. (2012). Size-dependent density of nanoparticles and nanostructured materials. *Physics Letters A*, 376(45), 3301-3302.
- nanotechproject.org. (2011). *Nanotech-enabled Consumer Products Continue to Rise*. Retrieved 07.01.2016, from <http://www.nanotechproject.org/news/archive/9231/>
- Nishiguchi, K., Utani, K., Fujimori, E. (2008). Real-time multielement monitoring of airborne particulate matter using ICP-MS instrument equipped with gas converter apparatus. *Journal of Analytical Atomic Spectrometry*, 23(8), 1125-1129.
- Norgaard, A. W., Jensen, K. A., Janfelt, C., Lauritsen, F. R., Clausen, P. A., Wolkoff, P. (2009). Release of VOCs and Particles During Use of Nanofilm Spray Products. *Environmental Science & Technology*, 43(20), 7824-7830.
- Norgaard, A. W., Larsen, S. T., Hammer, M., Poulsen, S. S., Jensen, K. A., Nielsen, G. D., et al. (2010). Lung Damage in Mice after Inhalation of Nanofilm Spray Products: The Role of Perfluorination and Free Hydroxyl Groups. *Toxicological Sciences*, 116(1), 216-224.
- Okada, Y., Yabumoto, J., Takeuchi, K. (2002). Aerosol spectrometer for size and composition analysis of nanoparticles. *Journal of Aerosol Science*, 33(6), 961-965.
- Oomen, A., Bennink, M., van Engelen, J., Sips, A. Nanomaterial in consumer products : Detection, characterisation and interpretation, *Nanomateriaal in consumentenproducten : Detectie, karakterisatie en interpretatie*: National Institute for Public Health and the Environment, The Netherlands.

- Part, F., Zecha, G., Causon, T., Sinner, E. K., Huber-Humer, M. (2015). Current limitations and challenges in nanowaste detection, characterisation and monitoring. *Waste Management*, 43, 407-420.
- Perdian, D. C., Bajic, S. J., Baldwin, D. P., Houk, R. S. (2008). Time-resolved studies of particle effects in laser ablation inductively coupled plasma-mass spectrometry. *Journal of Analytical Atomic Spectrometry*, 23(3), 325-335.
- Petrović, V. S., Janković, S. S., Tomić, M. V., Jovanović, Z. S., Knežević, D. (2011). The possibilities for measurement and characterization of diesel engine fine particles: A review. *Thermal Science*, 15(4), 915-938.
- Pisonero, J., Fernandez, B., Gunther, D. (2009). Critical revision of GD-MS, LA-ICP-MS and SIMS as inorganic mass spectrometric techniques for direct solid analysis. *Journal of Analytical Atomic Spectrometry*, 24(9), 1145-1160.
- Pratt, K. A., Prather, K. A. (2012). Mass spectrometry of atmospheric aerosols - Recent developments and applications. Part II: On-line mass spectrometry techniques. *Mass Spectrometry Reviews*, 31(1), 17-48.
- Quadros, M. E., Marr, L. C. (2011). Silver Nanoparticles and Total Aerosols Emitted by Nanotechnology-Related Consumer Spray Products. *Environmental Science & Technology*, 45(24), 10713-10719.
- Ruehli, F., Henneberg, M., Woitek, U. (2008). Variability of Height, Weight, and Body Mass Index in a Swiss Armed Forces 2005 Census. *American Journal of Physical Anthropology*, 137(4), 457-468.
- Saetveit, N. J., Bajic, S. J., Baldwin, D. P., Houk, R. S. (2008). Influence of particle size on fractionation with nanosecond and femtosecond laser ablation in brass by online differential mobility analysis and inductively coupled plasma mass spectrometry. *Journal of Analytical Atomic Spectrometry*, 23(1), 54-61.
- Scheuch, G., Heyder, J. (1990). Dynamic Shape Factor of Nonspherical Aerosol-Particles in the Diffusion Regime. *Aerosol Science and Technology*, 12(2), 270-277.
- Schlagenhauf, L., Chu, B. T. T., Buha, J., Nuesch, F., Wang, J. (2012). Release of Carbon Nanotubes from an Epoxy-Based Nanocomposite during an Abrasion Process. *Environmental Science & Technology*, 46(13), 7366-7372.
- Schmid, K. (2010). *Dissertation: Assessment of the occurrence of nanoparticles in Swiss industry and evaluation of the appropriateness of the measurement devices to determine the workforce exposure*. PhD thesis, I.S.T, Universite de Lausanne.
- Schneider, T., Brouwer, D. H., Koponen, I. K., Jensen, K. A., Fransman, W., Van Duuren-Stuurman, B., et al. (2011). Conceptual model for assessment of inhalation exposure to manufactured nanoparticles. *Journal of Exposure Science and Environmental Epidemiology*, 21(5), 450-463.
- Setyan, A., Song, C., Merkel, M., Knighton, W. B., Onasch, T. B., Canagaratna, M. R., et al. (2014). Chemistry of new particle growth in mixed urban and biogenic emissions - insights from CARES. *Atmospheric Chemistry and Physics*, 14(13), 6477-6494.
- Sinclair, D., Hoopes, G. S. (1975). A continuous flow condensation nucleus counter. *Journal of Aerosol Science*, 6(1), 1-7.

- Skocaj, M., Filipic, M., Petkovic, J., Novak, S. (2011). Titanium dioxide in our everyday life; is it safe? *Radiology and Oncology*, 45(4), 227-247.
- SN277206. (2011). *Internal Combustion Engines – Exhaust Gas After-treatment – Particle Filter Systems – Testing Method*: SNV Swiss Association for Standardization.
- Solomon, P. A., Fraser, M. P., Herckes, P. (2011). Methods for chemical analysis of atmospheric aerosols. In P. Kulkarni (Ed.), *Aerosol Measurement* (pp. 153-177): John Wiley & Sons, Inc.
- Steiner, S., Czerwinski, J., Comte, P., Heeb, N. V., Mayer, A., Petri-Fink, A., et al. (2015). Effects of an iron-based fuel-borne catalyst and a diesel particle filter on exhaust toxicity in lung cells in vitro. *Analytical and Bioanalytical Chemistry*, 407(20), 5977-5986.
- Stober, J., Schleicher, B., Burtscher, H. (1991). Bipolar diffusion charging of particles in noble-gases. *Aerosol Science and Technology*, 14(1), 66-73.
- Sun, Z., Huang, Z., Wang, J. S. (2007). Experimental and modeling studies on number and size spectrum evolutions of aerosol particles within a chamber. *Chinese Science Bulletin*, 52(10), 1302-1306.
- Sung, J. H., Ji, J. H., Yoon, J. U., Kim, D. S., Song, M. Y., Jeong, J., et al. (2008). Lung function changes in Sprague-Dawley rats after prolonged inhalation exposure to silver nanoparticles. *Inhalation Toxicology*, 20(6), 567-574.
- Suzuki, Y., Sato, H., Hikida, S., Nishiguchi, K., Furuta, N. (2010). Real-time monitoring and determination of Pb in a single airborne nanoparticle. *Journal of Analytical Atomic Spectrometry*, 25(7), 947-949.
- Suzuki, Y., Sato, H., Hiyoshi, K., Furuta, N. (2012). Quantitative real-time monitoring of multi-elements in airborne particulates by direct introduction into an inductively coupled plasma mass spectrometer. *Spectrochimica Acta Part B: Atomic Spectroscopy*, 76(0), 133-139.
- Taiwo, A. M., Beddows, D. C. S., Shi, Z. B., Harrison, R. M. (2014). Mass and number size distributions of particulate matter components: Comparison of an industrial site and an urban background site. *Science of the Total Environment*, 475, 29-38.
- Takaya, M. (2004). Novel characterization method for airborne particulate matter in workplace-chemical speciation method for heavy metals and real time size classified analysis. *Bunseki Kagaku*, 53(10), 1193-1194.
- Thomas, R. (2013). *Practical Guide to ICP-MS: a Tutorial for Beginners* (3rd ed.): Taylor & Francis.
- Tissari, J., Sippula, O., Torvela, T., Lamberg, H., Leskinen, J., Karhunen, T., et al. (2015). Zinc nanoparticle formation and physicochemical properties in wood combustion - Experiments with zinc-doped pellets in a small-scale boiler. *Fuel*, 143, 404-413.
- Ulrich, A., Wichser, A. (2003). Analysis of additive metals in fuel and emission aerosols of diesel vehicles with and without particle traps. *Analytical and Bioanalytical Chemistry*, 377(1), 71-81.
- Vicente, E. D., Duarte, M. A., Calvo, A. I., Nunes, T. F., Tarelho, L. A. C., Custodio, D., et al. (2015). Influence of operating conditions on chemical composition of particulate matter emissions from residential combustion. *Atmospheric Research*, 166, 92-100.
- von Goetz, N., Fabricius, L., Glaus, R., Weitbrecht, V., Guenther, D., Hungerbuehler, K. (2013). Migration of silver from commercial plastic food containers and implications for consumer exposure assessment. *Food Additives and Contaminants Part a-Chemistry Analysis Control Exposure & Risk Assessment*, 30(3), 612-620.

- Wang, S. C., Flagan, R. C. (1990). Scanning Electrical Mobility Spectrometer. *Aerosol Science and Technology*, 13(2), 230-240.
- Wang, Z. M., Wagner, J., Wall, S. (2011). Characterization of laser printer nanoparticle and VOC emissions, formation mechanisms, and strategies to reduce airborne exposures. *Aerosol Science and Technology*, 45(9), 1060-1068.
- Weber, A. P. (1992). *Dissertation: Characterization of the geometrical properties of agglomerated aerosol particles*. PhD thesis, PSI and ETH, Zürich, Switzerland.
- Weber, A. P., Baltensperger, U., Gaggeler, H. W., Tobler, L., Keil, R., Schmidtott, A. (1991). Simultaneous insitu measurements of mass, surface and mobility diameter of silver agglomerates. *Journal of Aerosol Science*, 22, S257-S260.
- Weber, A. P., Keil, R., Tobler, L., Baltensperger, U. (1992). Sensitivities of inductively coupled plasma optical-emission spectrometry for dry and wet aerosols. *Analytical Chemistry*, 64(6), 672-677.
- Wellinger, M., Biollaz, S., Wochele, J., Ludwig, C. (2011). Sampling and online analysis of alkalis in thermal process gases with a novel surface ionization detector. *Energy & Fuels*, 25(9), 4163-4171.
- Wellinger, M., Wochele, J., Biollaz, S. M. A., Ludwig, C. (2012). Online elemental analysis of process gases with ICP-OES: A case study on waste wood combustion. *Waste Management*, 32(10), 1843-1852.
- Wiedensohler, A. (1988). An approximation of the bipolar charge distribution for particles in the submicron size range. *Journal of Aerosol Science*, 19(3), 387-389.
- Wiedensohler, A. (1989). *Dissertation: Die bipolare Diffusionsaufladung von Partikeln in chemisch trägen Reinstgasen*. PhD thesis, Univ. Gesamthochschule Duisburg.
- Wiedensohler, A., Fissan, H. J. (1990). Bipolar ion and electron diffusion charging of aerosol particles in high purity argon and nitrogen. *Particle & Particle Systems Characterization*, 7(1-4), 250-255.
- Wiedensohler, A., Fissan, H. J. (1991). Bipolar charge distributions of aerosol particles in high-purity argon and nitrogen. *Aerosol Science and Technology*, 14(3), 358-364.
- Wochele, J., Ludwig, C., Lau, H.-J., Heep, W. (2006). Heavy Metal Partitioning in a Nuclear Waste Treatment Plant. *China Particuology*, 04(02), 86-89.
- Xue, C.-H., Chen, J., Yin, W., Jia, S.-T., Ma, J.-Z. (2012). Superhydrophobic conductive textiles with antibacterial property by coating fibers with silver nanoparticles. *Applied Surface Science*, 258(7), 2468-2472.
- Yang, J. J., Gebremedhin, A., Strand, M. (2013). Characterization of particles and inorganic vapors through high-temperature extraction in a biomass-fired grate boiler. *Energy & Fuels*, 27(10), 5915-5922.
- Zhang, J. F., Morawska, L. (2002). Combustion sources of particles: 2. Emission factors and measurement methods. *Chemosphere*, 49(9), 1059-1074.
- Zhu, R., Zhao, W., Zhai, M., Wei, F., Cai, Z., Sheng, N., et al. (2010). Molecularly imprinted layer-coated silica nanoparticles for selective solid-phase extraction of bisphenol A from chemical cleansing and cosmetics samples. *Analytica Chimica Acta*, 658(2), 209-216.

A.6 Outreach and publications

A.6.1 Peer-reviewed journal publications

Hess, A., Tarik, M., Ludwig, C. (2015). A hyphenated SMPS-ICPMS coupling setup: Size-resolved element specific analysis of airborne nanoparticles. *Journal of Aerosol Science*, 88, 109-118.

Losert, S., Hess, A., Ilari, G., von Goetz, N., Hungerbuehler, K. (2015). Online characterization of nano-aerosols released by commercial spray products using SMPS-ICPMS coupling. *Journal of Nanoparticle Research*, 17(7), 293.

Hess, A., Tarik, M., Losert, S., Ilari, G., Ludwig, C. (2016). Measuring air borne nanoparticles for characterizing hyphenated RDD-SMPS-ICPMS instrumentation. *Journal of Aerosol Science*, 92, 130-141.

Edinger, P., Tarik, M., Hess, A., Testino, A., Ludwig, C. (2016). Online Detection of Selenium and its Retention in Reducing Gasification Atmosphere. *Energy & Fuels*, 30(2), 1237-1247.

Hess, A., Tarik, M., Foppiano, D., Edinger, P., Ludwig, C. Online Size and Element Analysis of Aerosol Particles Released from Thermal Treatment of Wood Samples Impregnated with Different Salts. Submitted to: *Energy & Fuels*.

A.6.2 Conference contributions

Oral presentations

On-Line SMPS-ICPMS Coupling for Simultaneous Analysis of Nanoparticles Concerning Size Distribution and Elemental Composition.

18th Conference on Combustion Generated Nanoparticles, June 22-25, 2014, ETH Zürich.

On-Line Analysis of Airborne Nanoparticles Concerning Size Distribution and Elemental Composition Using SMPS-ICPMS Coupling.

International Aerosol Conference 2014, August 31 - September 5, 2014, Busan, Korea.

Posters

Hess, A., Ludwig, C., Ulrich, A. *Size-Resolved Element-Specific Analysis of Nanoparticles using an Online SMPS-ICPMS Coupling.*

CCMX Annual Meeting, April 25, 2012, Berne.

Hess, A., Ludwig, C., Ulrich, A. *Simultaneous Analysis of Size Distribution and Elemental Composition of Airborne Nanoparticles Using an Online-Coupling of SMPS and ICPMS.*

16th Conference on Combustion Generated Nanoparticles, June 24-27, 2012, ETH Zürich.

This poster achieved the first best poster award of the conference.

Hess, A., Ludwig, C., Ulrich, A. *Online Size Distribution and Elemental Composition Analysis of Airborne Nanoparticles Using a Novel SMPS-ICPMS Coupling.*

Empa PhD symposium, October 13, 2012, Dübendorf.

Hess, A., Ludwig, C., Ulrich, A. *Novel SMPS-ICPMS Coupling Allows Simultaneous Analysis of Size Distribution and Elemental Composition of Airborne Nanoparticles.*

European Winter Conference on Plasma Spectrochemistry, February 10-15, 2013, Krakow, Poland.

Hess, A., Ulrich, A., Ludwig, C. *Physical and Chemical Characterization of Nanoparticles by SMPS-ICPMS Coupling.*

CCMX Annual Meeting, April 30, 2013, Berne.

Hess, A., Wichser, A., Tarik, M., Ludwig, C. *Size Distribution and Elemental Composition of Airborne Nanoparticles Measured On-Line by SMPS-ICPMS Coupling Technique.*

17th Conference on Combustion Generated Nanoparticles, June 23-26, 2013, ETH Zürich.

This poster achieved the third best poster award of the conference.

Tarik, M., Hess, A., Ludwig, C. *Online Determination of Size Distribution and Elemental Composition of Nanoparticle Aerosols by a Scanning Mobility Particle Sizer Coupled to an Inductively Coupled Plasma Mass Spectrometer (SMPS-ICPMS).*

presented at the following conventions:

CCMX Annual Meeting, May 8, 2014, Berne.

Swiss Nano Convention, May 21-22, 2014, Windisch

18th Conference on Combustion Generated Nanoparticles, June 22-25, 2014, ETH Zürich.

Hess, A., Tarik, M., Foppiano, D., Ludwig, C. *Size-Resolved Element-Specific Analysis of Nanoparticles using RDD-SMPS-ICPMS.*

CCMX Annual Meeting, April 30, 2013, Berne.

This poster achieved one of three equivalent best poster awards of the conference.

Losert, S., Hess, A., Ilari, G., von Goetz, N., Hungerbühler, K. *Analytical Strategies for Characterization of Nanoparticle Release from Commercial Spray Products.*

BNASS 2014, August 31 - September 4, 2014, Aberdeen, Scotland, UK.

Hess, A., Tarik, M., Foppiano, D., Schuler, A., Ludwig, C. *Particulate Metal Emissions from Wood Incineration Measured Online Using RDD-SMPS-ICPMS.*

19th Conference on Combustion Generated Nanoparticles, June 28 - July 1, 2015, ETH Zürich.

Hess, A., Tarik, M., Foppiano, D., Schuler, A., Ludwig, C. *Particulate Metal Emissions from Wood Incineration Measured Online Using RDD-SMPS-ICPMS.*

EDMX Research Day, November 23, 2015, EPF Lausanne.

Conference Proceedings

Hess, A., Ludwig, C., Ulrich, A. *Simultaneous Analysis of Size Distribution and Elemental Composition of Airborne Nanoparticles Using an Online-Coupling of SMPS and ICPMS.*

16th Conference on Combustion Generated Nanoparticles, June 24-27, 2012, ETH Zürich.

Hess, A., Wichser, A., Tarik, M., Ludwig, C. *Size Distribution and Elemental Composition of Airborne Nanoparticles Measured On-Line by SMPS-ICPMS Coupling Technique.*

17th Conference on Combustion Generated Nanoparticles, June 23-26, 2013, ETH Zürich.

Hess, A., Losert, S., Tarik, M., Ludwig, C. *On-Line SMPS-ICPMS Coupling for Simultaneous Analysis of Nanoparticles Concerning Size Distribution and Elemental Composition.*

18th Conference on Combustion Generated Nanoparticles, June 22-25, 2014, ETH Zürich.

A.6.3 Media

Report in the PSI News, written by Leonid Leiva, in May 2013.

Kehrichtverbrennung: Der Reinheit letzter Schluss?

available online: <https://www.psi.ch/media/kehrlichtverbrennung-der-reinheit-letzter-schluss>

Report in the CCMX News, written by Carey Sargent, in March 2014.

Innovative Instrument Developed by Empa and PSI Analyses Airborne Nanoparticles.

available online: <http://www.ccmx.ch/news-amp-events/news-single/article/228/185/>

A.7 Curriculum Vitae

Personal data

Name	Adrian Hess
Date of birth	21. April 1979
Nationality	Swiss
Address	Rennweg 10, 8001 Zürich
Telephone	+41 76 386 96 67
E-mail	hessa@alumni.ethz.ch
Marital status	married, 2 children



Education and professional activities

Period	Activity
Dec 2011 - Apr 2016	PhD thesis: “Time-resolved size and element analysis of gas-borne nanoparticles”
2015 - 2016	Second part at Paul Scherrer Institut (Villigen, CH)
2011 - 2015	First part mainly at Empa (Dübendorf, CH)
Feb 2014	Training course at Empa Academy: “Basics in Management”
Mar 2012	Radiation protection course (SPG) at Suva (Luzern, CH)
2007 - 2011	Research and Service Engineer at Matter Aerosol AG (Wohlen, CH): <ul style="list-style-type: none"> - Aerosol measurements (laboratory, test bench, field measurements) - Collaborations with the AFHB engine test center (BFH, Bienne, CH) - Measurement reports and technical documentations - Representation on exhibitions and international conferences - Technical customer support
Oct 2010 - Feb 2011	Project leader course at University of Applied Sciences Northwestern Switzerland: „Projekte erfolgreich leiten – Projektmanagement und Systems-Engineering“
Apr - Oct 2010	Foreign consulting assignment at Testo AG (Lenzkirch, Germany): Development of a dilution unit for an exhaust measuring system
Feb 2008	Refresher course at University Erlangen: „Grundlagen und moderne Anwendungen der Verbrennungstechnik“
2000 - 2007	Studies in Mechanical Engineering at ETH Zürich: Focus 1: Aerothermochemistry and Combustion Systems (www.lav.ethz.ch) Focus 2: Nanotechnology (www.nanotechnology.ethz.ch)
Winter 2006/2007	Diploma thesis (Aerothermochemistry and Combustion Systems): „Optimization of an Existing Soot Generator Burner and Development of Measures to Reduce Pulsations in the Flame”

Period	Activity
Mar - Oct 2005	Industrial placement at Verenum (Zürich, CH): time and size resolved particle measurements on flue gas from wood combustion
Winter 2004/2005	Semester thesis (Bioenergy and Catalysis Laboratory at PSI): „Mass and Energy Balance of a Pilot Wood Gasifier Plant as Basis for System Optimization”
Summer 2004	Semester thesis (Nanotechnology): „Microfluidic Channels for Electrostatic Particle Assembly“
2001	Assistant at the Center for Product Design at ETH Zürich
Feb - Mar 2001	Practical trainee course at Gretag Imaging AG (Regensdorf, CH): Basic knowledge in mechanical and electronic workshops
1999 - 2000	First professional experience at Radio Hess (Zürich, CH): Electric installations, stock management, customer service
1992 - 1999	Grammar School: Kantonsschule Zürich-Oerlikon (classical profile)

Memberships

since 2016	Organizing Committee of the ETH-Conference on Combustion Generated Nanoparticles
since 2011	Member of the Saint Nicholas Society of Zürich (www.chlaus-zuerich.ch)

Leisure, Hobbies

Hobbies	- Do-it-yourself (create furniture, installation and repair works) - since June 2013: father duties
Journeys	- Tandem bike tours: Some thousands of kilometers in Switzerland, Germany, Eastern Europe - Railway and flight trips: Europe, Malaysia
Feb 2015	Birth of the second son: Tamaro
Jun 2013	Birth of the first son: Malvin
2005 - 2006	Volunteering at „Nightline Zürich“ (www.nightline.ch): confidential listening and information service for students of university and ETH Zürich
1994 - 2008	Voluntary social engagement at Cevi Switzerland, being part of the global YMCA movement: Scouting activities with children and education of teenagers.